POWER SYSTEM STABILIZER AND CONTROLLED SERIES CAPACITOR SMALL-SIGNAL STABILITY PERFORMANCE ANALYSIS

By

Gert Fourie

Thesis presented in partial fulfilment of the requirements for the degree of Masters of Science (Engineering) at the University of Stellenbosch

Supervisor: Dr. H.J. Beukes

December 2002

DECLARATION

I, the undersigned, hereby declare that the work contained in this thesis is my own original work and that I have not previously in its entirety or in part submitted it at any university for a degree.

SUMMARY

This thesis presents results of a study on the small-signal stability of a single-machine infinite-bus power system. Conditions of generator loading and network impedance are identified that require additional stability support. Two methods of stability enhancement are investigated, namely the power system stabilizer and the controlled series capacitor. Both stabilizers employ the conventional (classic) control structure, and parameters are evaluated for optimum performance using an integral-of-the-squared-error-based method. Results for damping capability versus generator loading and system impedance were generated. The ability of the power system stabilizer and controlled series capacitor to provide stability support is compared. This comparison is based on (a) the ability to provide more damping torque when needed, and (b) the amount of damping torque contributed by the stabilizer.

OPSOMMING

Hierin word die resultate van 'n studie op die klein-sein stabiliteit van 'n enkel-masjien oneindige-bus kragstelsel weergegee. Kondisies van generator belasting en netwerk impedansie waar dempings-ondersteuning benodig word, word geïdentifiseer. Twee metodes van stabiliteits-verbetering word ondersoek, naamlik die kragstelstel stabiliseerder en die beheerde serie kapasitor. Beide stabiliseerders maak gebruik van die konvensionele (klassieke) beheerstruktuur, waarvan parameters geëvalueer word deur gebruik te maak van 'n integraal-van-die-vierkant-fout-gebaseerde metode. Resultate vir dempingsvermoë teenoor generator belasting en stelsel impedansie word verkry. Die vermoë van die kragstelsel stabiliseerder en beheerde serie kapasitor om stabiliteits-ondersteuning te verskaf, word vergelyk. Hierdie vergelyking is gebasseer op (a) die vermoë om meer dempingswrinkrag te voorsien wanneer benodig, en (b) die hoeveelheid dempingswrinkrag deur die stabiliseerder bygedra.

TABLE OF CONTENTS

LIST OF FIGURES

LIST OF TABLES

ACKNOWLEDGEMENTS

I would like to thank the following persons and institutions:

To NamPower and PEG, for giving me the opportunity to work on this project.

To my study leader, Dr. H.J. Beukes, for his guidance throughout the duration of this investigation, for the late nights and weekends he had to work because of me. Thank you Johan, your effort does not go unnoticed.

To the members of the power electronics group, who never neglected to correct me when I was mistaken.

To my family and friends, whose support and prayers helped me complete this report.

And last, but most importantly, my Creator, who used the prayers and blessed me indeed. To You be all the glory.

GLOSSARY

Abbreviations

AGC	Automatic Generation Control
AR	Armature Reaction
AVR	Automatic Voltage Regulator
CSC	Controller Series Capacitor
FACTS	Flexible Alternating Current Transmission Systems
GCSC	GTO Thyristor-Controller Series Capacitor
GTO	Gate Turn-Off
HVDC	High Voltage Direct Current
Im	Imaginary part of
PAR	Phase Angle Regulator
PSS	Power System Stabilizer
Re	Real part of
SMES	Superconducting Magnetic Energy Storage
SMIB	Single-Machine Infinite-Bus
SS	Steady-state
SVC	Static Var Compensator
TCR	Thyristor Controlled Reactor
TCSC	Thyristor-Controller Series Capacitor
TGR	Transient Gain Reduction
TSR	Thyristor Switched Reactor
TSSC	Thyristor-Switched Series Capacitor
UPFC	Unified Power Flow Controller

System model parameters

H	Inertia constant of the machine
ω_0	Nominal rotor angular velocity
δ	Angular position of rotor with respect to a synchronously rotating reference
T_m	Turbine mechanical power
T_e	Air-gap electrical torque
t	Time
K_D	Damping torque coefficient
ω_r	Rotor speed
X_C	Series compensation capacitive reactance
X_L	Circuit inductive reactance
L	Circuit inductance
C	Series compensation capacitance
ω_n	Circuit inductance and capacitance natural frequency
Δ	Perturbed value, deviation from nominal
p	Differential operator d/dt
s	Laplacian operator
$\dot{}$	Embellishment representing differentiation with respect to time

Classic model parameters

P_e	Air-gap electrical power
E'	Classic machine model internal voltage
E_B	Infinite bus voltage
E_t	Machine terminal (bus) voltage
X'_d	Generator transient reactance
X_E	External system equivalent reactance
X_T	Total machine and system reactance
K_X	Controlled series reactance coefficient
K_{DX}	CSC damping torque coefficient
K_S	Synchronizing torque coefficient

$\mathbf{A}$	System state matrix
$\mathbf{x}$	State vector
$\mathbf{\Gamma}$	Perturbation matrix
$\mathbf{p}$	Perturbation vector
λ	Eigenvalue from system state matrix
σ	Real part of λ
ω	Actual or damped frequency
ζ	Damping ratio
ω_n	Undamped natural frequency
$K_\omega \Delta\omega_r$	Damping torque due to stabilizer
$K_\delta \Delta\delta$	Synchronizing torque due to stabilizer

System model – generator by higher order model

Rotor and stator quantities

Ψ_{fd}	Rotor flux linkage
L_{fd}	Rotor field inductance
R_{fd}	Rotor field winding resistance
Ψ_d, Ψ_q	*d*- and *q*-axis stator flux linkages
Ψ_{ad}, Ψ_{aq}	*d*- and *q*-axis air-gap (mutual) flux linkages
e_{fd}	Rotor field voltage
L_d, L_q	*d*- and *q*-axis stator inductances
L_{ad}, L_{aq}	*d*- and *q*-axis mutual inductances
L_l	Stator leakage inductance
L_{ffd}	$L_{ad} + L_{fd}$
L'_{ad}	$L_{ad} \| L_{fd}$
X'_d	*d*-axis transient reactance
X_q	*q*-axis stator (synchronous) reactance
e_d, e_q	*d*- and *q*-axis stator (machine terminal) voltages
i_d, i_q	*d*- and *q*-axis stator currents

i_{fd}	Field current
R_a	Stator resistance
E_q	Effective internal machine voltage
K_3	Field circuit transfer function gain
T_{3fd}	Field circuit transfer function time constant
T'_{d0}	Transient open-circuit time constant

Generator parameters

E_{Bd}, E_{Bq}	d- and q-axis components of infinite bus voltage E_B
δ_i	Internal machine angle
X_{Td}, X_{Tq}	d- and q-axis components of system total reactance
R_T	Total system resistance
D	$R_T^2 + X_{Td}X_{Tq}$
E_{fd}	Exciter output voltage
$G_{ex}(s)$	Excitation system transfer function
K_A	Excitation system gain
T_A	Exciter time constant
v_s	PSS output voltage
V_{ref}	Voltage regulator reference voltage
V_{err}	Generator terminal voltage deviation from V_{ref}

Sensitivity coefficients

m_1	Sensitivity of d-axis stator current to variations in rotor angle
m_2	Sensitivity of d-axis stator current to variations in field flux
n_1	Sensitivity of q-axis stator current to variations in rotor angle
n_2	Sensitivity of q-axis stator current to variations in field flux linkage
K_1	Sensitivity of electrical torque to variations in rotor angle
K_2	Sensitivity of electrical torque to variations in field flux linkage

K_4	Accounts for the demagnetising action of a change in angle
K_5	Sensitivity of terminal voltage to variations in rotor angle
K_6	Sensitivity of terminal voltage to variations in field flux linkage
m_3	Sensitivity of *d*-axis stator current to variations in compensation reactance
n_3	Sensitivity of *q*-axis stator current to variations in compensation reactance
K_P	Sensitivity of electrical torque to variations in compensation reactance
K_q	Accounts for the demagnetising action of a change in compensation reactance
K_V	Sensitivity of terminal voltage to variations in compensation reactance

System parameters

R_E	External series resistance
X_E	External series reactance
P_{load}	Local load active power consumption
R_{load}	Local load resistance
X_{line}	External reactance in system with local load
P_t	Sending-end (generator output) active power
Q_t	Sending-end (generator output) reactive power
P_B	Receiving-end (infinite bus) active power
Q_B	Receiving-end (infinite bus) reactive power
I_t	Sending-end current
f_T	Terminal voltage frequency

Torque coefficient expressions

$K_{S(SS)}$	Steady-state synchronizing torque coefficient
$K_{D(*)}$	Damping torque coefficient due to specific system element. * may be AVR, PSS, etc.
$K_{S(*)}$	Synchronizing torque coefficient due to specific system element. *

	may be AVR, PSS, etc.
K_D	Total (net) damping torque coefficient. Not to be confused with K_D of damper windings, which is set to zero in investigation
K_S	Total (net) synchronizing torque coefficient

Damping controllers and parameter optimisation parameters

K_C	Controller gain
$G_{PSS}(s)$	PSS controller washout and phase compensation transfer function
$G_{CSC}(s)$	CSC controller washout and phase compensation transfer function
T_W	Signal washout time constant
$T_1 \ldots T_4$	Lead-lag block time constant
P_{s1}, P_{s2}	PSS controller intermediate state variables
$GEP(s)\|_{\text{PSS}}$	"Plant" transfer function for system with PSS
C_{s1}, C_{s2}	CSC controller intermediate state variables
$GEP(s)\|_{\text{CSC}}$	"Plant" transfer function for system with CSC
$\hat{\mathbf{x}}$	Error of $\mathbf{x}(t)$ from the steady-state value
e	Error function
T_s	Settling time of error function $e(t)$
J	Performance index
α	Relative weighting factor
$\mathbf{Q}$	A diagonal matrix
$\mathbf{P}$	Solution to Lyapunov equation
$J_{\min}$	Minimum of J

1 INTRODUCTION

1.1 The Small-Signal Stability Problem

The stability of an interconnected power system is a topic that has raised many questions and has been the focus of much research. The aim has always been to improve the stability of the system more. Even to this day the solution to this question is not entirely understood due to complexity of the problem, which goes hand-in-hand with the complexity of the systems considered.

Distributed energy resources are becoming a more attractive option to increase generation capacity as large-scale generation installations reach capacity. These resources are often not close to the rest of the network, particularly in developing countries with limited power system infrastructure. Stability is an important consideration to keep in mind when implementing new generation, particularly when such generation are connected at the lowest possible cost option using weak radial lines. *This investigation focuses on the stability of generation connected to a large system via radial lines.*

"Stability" can take on many forms. Small-signal (or steady-state) stability is concerned with the ability of the oscillations of the synchronous machine rotor angle following a small disturbance to reduce to zero. Transient stability concerns the generator rotor angle response following a large disturbance such as a 3-phase line fault. Voltage stability is concerned with the ability of the system to maintain acceptable voltage levels at all buses of the system. Frequency stability deals with the ability of the power system to maintain the system frequency within a nominal range following a severe system upset or disturbance.

Small disturbances in the system include changing of loads or switching of shunt reactors or capacitors into or out of the system. The generator response to a small disturbance is an oscillation of the angle of the rotor relative to the rotor angle of another generator or group of generators, at a certain frequency. Typically the oscillatory response to a small disturbance is small, and for a single disturbance may be deemed insignificant. However, the system is subject to many small disturbances all the time. To ensure the oscillations do not build up in amplitude and eventually lead to a loss of stability, it is important to quench these oscillations following even a small disturbance.

It is possible for the generators of one part of the system to oscillate against generators of another part of the system at the same frequency. This is known as inter-area oscillations. This problem is very complex in nature due to the complexity of power systems.

The scenario of a generator oscillating relative to another close-by generator, or a single generator against the rest of the system, is known as local small-signal stability. *This investigation considers the problem of rotor oscillations of a single generator against a large system.* The single-machine versus infinite-bus (SMIB) model is ideal for investigating the small-signal stability of a local nature.

A synchronous machine is rotor angle stable if the electrical air-gap torque of the machine contains both a positive synchronizing and positive damping torque component [2]. Lack of sufficient synchronizing torque may cause an aperiodic drift in the rotor angle following small disturbances. Lack of sufficient damping torque may cause the oscillations following small disturbances to increase in amplitude until the rotor angle steps out of synchronism with the rotor angle of the other generator (or generators, in the case of oscillations relative to a large system). *It is the lack of damping torque that is more often the cause of small-signal instability* ([60] pp. 25).

1.2 Solutions to the Small-Signal Stability Problem

Because of this ability of a system to be unstable under certain system conditions, researchers have devised methods to introduce damping torque to the generator, to ensure the oscillations following disturbances are damped and the system is stable. Installing a power system stabilizer (PSS) is the solution most often employed. It can be a very effective and yet low-cost option. Another method, which in recent years has begun to receive more attention, is the controlled series capacitor (CSC). Other options include adding supplementary control to a static var compensator (SVC) or high voltage direct current (HVDC) converter, should these be present in the system. Lately the use of a Unified Power Flow Controller (UPFC) or Superconducting Magnetic Energy Storage (SMES) system to damp oscillations has been proposed and investigated.

According to research to date ([3] – [11]), PSS and CSC are the two more effective methods of stability control. Both work to modulate the generator air-gap torque, but by different mechanisms. PSS controls generator excitation, while CSC controls the external reactance. *In this investigation, the ability of PSS and CSC to provide stability to possible generator rotor oscillations is researched.*

1.3 Research Focus

Two questions that may be asked are:

1. When is it necessary to add stability support to a SMIB system to ensure small-signal stability?
2. Which method of stability support is more appropriate, given the loading on the generator, strength of the connecting radial line, etc.?

This report aims to provide insight into these questions. In a SMIB system configuration, conditions that may affect the choice of stabilizer include the active power loading of the generator under consideration or the reactance as seen at the terminals of the generator. The latter is an indication of the strength of the system into which the generator operates. If the generator is connected to a large "stiff" system, this reactance is predominantly that of the connecting radial line. Other factors include the presence of significant resistance in the connecting radial line, or a load local to the generator in question. *The investigation considers these factors, and how each factor influences the stability of the system as well as the choice of stabilizer.*

The comparison between the ability of a PSS and a CSC to enhance stability focuses firstly on trends. Here the focus is on the ability of the controller to introduce more damping torque when more is required. Damping torque is a measure of the effectiveness of the controller to enhance stability. This research considers a range of generator loading and external impedance conditions, and evaluates how the inherent stability of the system and the damping support of the stabilizers vary as the conditions vary.

Secondly, the comparison focuses on the amount of damping torque the stabilizers introduce into the system, and which is able to introduce more. To evaluate the damping and synchronizing torques, use is made of the Phillips-Heffron block diagram model [1]. Heffron and Phillips developed this model in 1952, and in 1969 DeMello and Concordia [2] used this model to assess and discuss concepts regarding the stability of a SMIB system. The Phillips-Heffron model is used to this day in investigations of small-signal stability of a SMIB system.

1.4 Structure of this Report

The thesis is sectioned as follows:

Chapter 2 provides theoretical background on system stability, with main emphasis on the small-signal stability of a SMIB system. The concepts of damping and synchronizing torques are introduced. A discussion on the block diagram approach focuses on previous research in this regard, and the importance of understanding the behaviours of the parameters of the model. An overview of the methods to enhance system dynamic stability highlights the superiority of PSS and CSC to enhance stability.

Chapter 3 investigates the need for stability support, and aims to identify conditions of system loading and impedance that require the implementation of an oscillation stabilizer. Much of this has been done in previous research (Refs [2], [12] and [13]), although under different modelling assumptions. Also, the influence of significant system resistance and local load on overall system stability has not been considered, and these are included in this investigation.

The influence of both the rotor field winding and the excitation system on stability is discussed. The expressions for the damping and synchronizing torques are functions of parameters in the Phillips-Heffron block-diagram model known as the K-parameters. Results obtained for the torques are analysed and discussed in terms of these K-parameters. It is therefore deemed important to understand the behaviours or trends of these K-parameters for various network structure and loading conditions. Results for the K-parameters themselves are interpreted in terms of changes in the generator rotor angle. A detailed discussion on the trends and the influence of field voltages, currents, etc. on the K-parameter results is beyond the scope of this research.

Chapter 4 discusses the ability of a PSS to enhance the system stability. The focus is mainly on how this ability varies with changes in system conditions. Performance is measured in its ability to provide damping torque to the system without aggravating the synchronizing torque. Again, results are analysed and discussed in terms of the K-parameters presented in chapter 3.

Chapter 4 also presents the conventional (classic) controller scheme, and a method for evaluating the controller parameters for optimum performance. This method is applied to both the PSS and CSC cases, to assure a common base for comparison of abilities to enhance stability. For each condition of generator loading, system reactance, etc., the controller parameters are evaluated for optimal performance. The damping and synchronizing torque results reflect such optimal performance. This is similar to obtaining performance trends for

an adaptive stabilizer, with parameters such that the performance remains optimal as system conditions vary.

Chapter 5 discusses the ability of a CSC to enhance the stability of the SMIB system, in a similar fashion to the PSS chapter. Again, focus is mainly on the variation of this ability with changes in system conditions. The control scheme and optimisation methodology employed is similar to the PSS case. The block diagram model to accommodate a CSC differs somewhat from the Phillips-Heffron model as it incorporates additional K-parameters. This chapter presents this model and the trends of these K-parameters. The CSC performance results are discussed in terms of the K-parameters of the system model.

Chapter 6 presents a summary of the results of chapters 4 and 5. This summary is in the form of a comparison between the need for damping support and the ability of each controller to supply the needed damping torque.

Chapter 7 concludes the thesis with an overview of the main results, and suggestions for further research.

2 BACKGROUND INFORMATION

2.1 Introduction

This chapter presents a theoretical background on system stability, concepts of system stability, and methods used to improve the dynamic stability of a system. Focus is on the small-signal stability of a simple SMIB system model.

Section 2.2 provides an overview of the various stability phenomena present in a power system. The discussion focuses on the principles governing the particular stability issues, as well as factors that influence stability.

Section 2.3 introduces the concepts of damping and synchronizing torque, and how these relate to the stability of the system. A discussion on the block diagram approach (section 2.4) focuses on previous research in this regard, and the importance of understanding the behaviours of the parameters of the model.

Section 2.5 discusses various methodologies in use today to damp system oscillations, with main emphasis on the PSS and CSC, the two methods investigated. The discussion gives a comparative overview of previous research on these methods of stability.

2.2 System Stability

Ref. [60] pp. 17 defines *Power system stability* broadly as that *property of a power system that enables it to remain in a state of operating equilibrium under normal operating conditions and to regain an acceptable state of equilibrium after being subjected to a disturbance.*

Stability may be classified as (a) angle stability, (b) voltage stability, or (c) frequency stability. The following sections discuss each of these in more detail. Focus is on the governing principles and the factors that influence loss of stability.

2.2.1 Small-signal stability

According to the IEEE [23],

A power system is steady-state stable for a particular steady-state operating condition if, following any small disturbance, it reaches a steady-state operating condition which is identical or close to the pre-disturbance operating condition.

Steady-state stability is a property only of the power system and its steady-state operating condition. The terms *small-disturbance*, or *small-signal*, *stability* are sometimes used [60][63]. A *small disturbance* is one for which the equations that describe the dynamics of the power system may be linearized for the purposes of analysis. Small-signal stability implies that the power system, as described by the set of differential equations linearized about the steady-state operating point, is stable.

Governing principles

System stability depends on the existence of both synchronizing and damping torque components for each of the synchronous machines in a power system [2]. Section 2.3 discusses these concepts in more detail. The fundamental equation that describes rotor dynamics in small-signal and transient stability studies, is the per unit swing equation ([60] pp. 128-135, [63] pp. 141-144),

$$\frac{2H}{\omega_0}\frac{d^2\delta}{dt^2} = T_m - T_e - K_D\Delta\omega_r . \tag{2.1}$$

H is the inertia constant of the machine in seconds, ω_0 the nominal rotor angular velocity in rad/s (equal to $2\pi f$), and δ the angular position (measured in electrical radians) of the rotor with respect to a synchronously rotating reference. T_m and T_e are the per unit turbine mechanical and air-gap electrical torques, respectively. Time t is measured in seconds. $K_D\Delta\omega_r$ represents a component of damping torque not accounted for in the calculation of T_e, such as provided by the machine damper windings.

The swing equation describes swinging in rotor angle δ during disturbances. Small-signal stability requires that δ-oscillations following small disturbances damp out to a steady-state value equal or close to the pre-disturbance value. Under normal operating conditions the power system is subject to numerous random disturbances due to the application or removal of loads ([64] pp. 54). Such disturbances lead to power swings that, if sufficiently damped, remain suitably low in amplitude. Insufficient damping cause these power swings to build up on one another and grow in amplitude until the rotor angles of one or more machines exceed the stability limit and synchronism is lost.

Factors that influence stability

For small deviations in rotor speed, the damper windings produce a damping power that is proportional to the rotor speed deviation. The field winding provides a similar damping action to the damper windings, but much weaker. The combined effect of the two damping mechanisms helps to return the rotor quickly to the equilibrium point. It is even possible to achieve an aperiodic rotor motion (without oscillations) if the damping effect is large. The opposite, unfortunately, is also possible. At large values of network resistance as seen by the generator, negative damping may be introduced into the system [13]. This may happen when a generator operates in a medium-voltage distribution network. If this negative damping is larger than the positive damping introduced by the damper windings, the generator may lose stability. Section 3.8 investigates the conditions for such negative damping in more detail.

The amount of damping is dependent on the initial loading of the system [13]. As loading increases, so does the damping coefficient K_D; the undamped natural frequency ω_n decreases as the initial value of δ increases ([63] pp. 169). Consequently, the rotor oscillations become slower and more heavily damped with increased initial loading. Fig. 2.1 illustrates this concept.

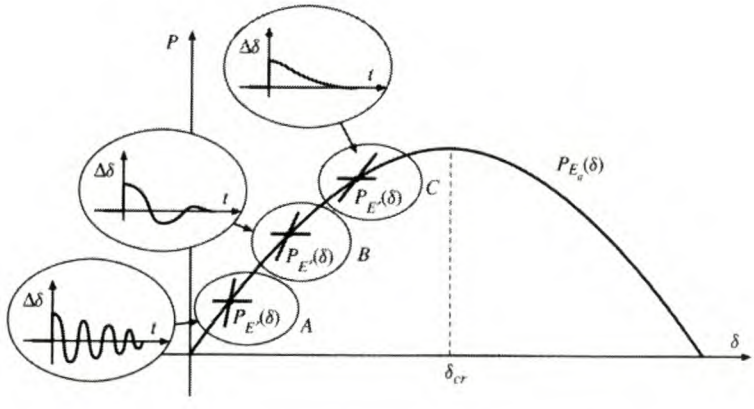

Fig. 2.1: Examples of rotor swings for three cases of stable equilibrium points [63]

Synchronous machine excitation control comprises an automatic voltage regulator (AVR) and exciter, with additional compensator and protective circuits. The purpose of excitation control is to keep the generator terminal voltage E_t constant by controlling the excitation current. If the AVR is slow acting, then for a small disturbance the AVR will not react during the transient state, and the regulated system behaviour will be similar to that of the unregulated system. If the AVR is fast acting, stability is dependent on the system and AVR

parameters [2][12]. A fast acting AVR may introduce a net negative damping into the system that is enhanced by:

1. A large generator load
2. A large gain in the AVR controller
3. A large network reactance

This may lead to an oscillatory loss of stability if this negative damping exceeds the positive damping of the damper and field windings. Section 3.8 of this report investigates the influence of network structure and loading conditions on these damping components and the net system damping. Section 2.5 discusses different methods in use to improve the system steady-state stability.

Classification of the problem

It is convenient to classify small-signal stability problems as being either local or global in nature ([60] pp. 817-818). Local problems involve only a small part of the system. Certain distinctions can be made on the nature of oscillation:

1. *Local plant mode oscillations* involve the swinging of a single generator or plant against the rest of the power system. This is similar to the single-machine infinite-bus case and is the most encountered small-signal stability problem. *This report focuses on this type of oscillation mode.*
2. *Intermachine* or *interplant mode oscillations* involve oscillations between rotors of a few generators close to each other.
3. *Control modes* are associated with generating units and their controls, HVDC converters, and static var compensators. The problems associated with control modes are mainly due to control devices being inadequately tuned.
4. The above-mentioned controls may interact with the dynamics of the turbine-generator shaft system rotational components, causing instability of *torsional mode oscillations*. Section 2.2.3 elaborates more on this instability problem.

Global small-signal stability problems are a result of interactions among large groups of generators. The effects are widespread and complex. The problem involves oscillations of a group of generators in one part of the system swinging against a group of generators in other parts. Weak interconnection ties are normally the cause of this type of oscillation.

2.2.2 Transient stability

Transient stability is the ability of a power system that enables it to maintain synchronism when subjected to a severe transient disturbance, such as a fault on the transmission circuit, loss of generation or load, or loss of a tie line. The formal definition according to the IEEE [23] is:

A power system is transiently stable for a particular steady-state operating condition and for a particular disturbance if, following that disturbance, it reaches an acceptable steady-state operating condition.

The concept of synchronizing torque and the swing equation, discussed in section 2.2.1, apply. Generally, transient instability manifests itself as a steady increase ([60] pp. 26) in rotor angle until synchronism is lost, a phenomenon called *first-swing* instability.

The IEEE definition of transient stability [23] indicates that transient stability is a property of the power system, its steady-state operating condition **and** the disturbance itself. For a system that remains stable beyond the first swing, the oscillations would damp out if such a system is small-signal stable.

Governing principles

The conditions necessary for such a stable condition to be reached following a disturbance can be graphically explained using the *equal-area criterion*. The equal-area criterion is a helpful aid in evaluating stability for one machine connected to an infinite bus, or for two machines connected by radial line.

The fault clearing time is a major factor in determining the stability of the generator. The relative difference between the critical clearing time and the actual clearing time can be used to define the *transient stability margin*, which is a measure of "instability proximity".

Factors that influence stability

Factors that influence the stability of the system following a severe fault include ([63] pp. 184-189, [66] pp. 743-745):

1. The severity of the fault and the clearing time of such a fault
2. The pre-fault load – a more heavily loaded generator reduces the stability margin
3. The distance to the fault – the further the distance to the fault, the less severe the fault

4. The generator reactance, inertia, as well as the generator internal voltage magnitude as influenced by the field excitation (the characteristics of which also has significant influence on transient stability)

In the SMIB case, the infinite bus voltage magnitude also influences the stability following a disturbance.

Section 2.2.1 explains how the AVR may reduce damping of rotor swings following a small disturbance. The AVR behaves similar in the case of large disturbances ([63] pp. 193). However, immediately after the fault is cleared, a strong acting AVR may prevent loss of synchronism. Refs [63] pp. 193-197 and [65] pp. 562 explain this in more detail.

2.2.3 Subsynchronous oscillations

In analysing the effects of large and small disturbances on power system dynamic performance, the rotor of the turbine generator is assumed to consist of a single, very stiff mass. This representation accounts for the oscillations of the turbine-generator rotor with respect to other generators. These oscillation modes are generally in the frequency range of 0.1 to 3.0 Hz ([60] pp. 1133). In reality however, the rotor of a turbine-generator has a very complex mechanical structure consisting of several predominant masses (such as rotors of turbine sections, generator rotor, couplings, and the exciter rotor) connected by shafts of finite stiffness. Therefore, whenever the generator is perturbed, torsional oscillations result between different sections of the turbine-generator rotor.

The rotor system of a generator-turbine shaft has many torsional vibration modes both above and below the rated frequency. However, the problem due to interaction between the electrical system and the rotor mechanical system is mainly in the frequency range below synchronous frequency (the *subsynchronous* frequency range). The torsional oscillations in the subsynchronous range could, under certain circumstances, interact with the power system in an adverse manner. The following are problems particular to torsional oscillations:

- Torsional interaction with power system controls.
- Subsynchronous resonance with series capacitor-compensated transmission lines.
- Torsional fatigue duty due to network switching.

It is interesting to note that the torsional characteristics of hydro units are such that interaction with power system controls or transmission network has not been a source of concern. On the other hand, large generators with multistage steam turbines are most

susceptible to subsynchronous resonance with series capacitor compensated transmission lines ([70] pp.215).

Subsynchronous resonance

The phenomenon of *subsynchronous resonance* (SSR) occurs mainly in series capacitor-compensated transmission systems ([60] pp. 1050). Consider the radial system illustrated in Fig. 2.2.

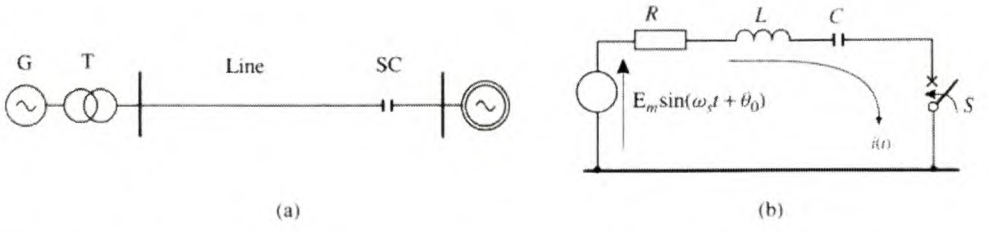

Fig. 2.2 Series compensated transmission line: (a) schematic diagram; (b) equivalent circuit when shorting the line [63]

The natural frequency of the circuit inductance and capacitance is

$$\omega_n = \frac{1}{\sqrt{LC}} = \omega_0 \sqrt{\frac{X_C}{X_L}} \tag{2.2}$$

where ω_0 is the synchronous frequency in radians per second (ω_s in Fig. 2.2). In the case of a fault, instead of the dc component of fault current, the offset transient current is also alternating current, of frequency equal to ω_n. Generator stator current components at this frequency induce rotor currents (and torque) of slip frequency $(\omega_0 - \omega_n)$.

If the complement of the natural frequency $(\omega_0 - \omega_n)$ of the network is close to one of the torsional frequencies of the turbine-generator shaft system, torsional oscillations can be excited. This condition is commonly called *subsynchronous resonance*. Should these conditions be present, a small voltage induced by rotor oscillations can result in large subsynchronous currents; this current will produce an oscillatory component of rotor torque such that rotor oscillation is enhanced. Should this torque be larger than that resulting from mechanical damping, the coupled electromechanical system will experience growing oscillations.

The consequences of SSR can be disastrous (e.g. the turbine-generator shaft could break), should the torsional oscillations be allowed to build up. Even if the oscillations are not

unstable, system disturbances can result in shaft torques of high magnitude, the result being a loss of fatigue life of the shaft.

2.2.4 Voltage stability

Voltage stability is concerned with the ability of a power system to maintain acceptable voltages at all buses in the system ([60] pp. 959-1024). This should hold for normal operating conditions, as well as after the system has been subjected to a disturbance. A state of voltage instability is reached when a change in the system causes a progressive and uncontrollable decline in voltage. The "change" may be an increase in load demand, a disturbance, or a change in system condition.

Voltage stability problems were once thought only a problem in weak systems or systems with long lines. Nowadays, voltage problems are also a source of concern in highly developed networks as a result of heavier loadings as systems are being stretched to their limits due to financial and geographical constraints.

Governing principles

Fig. 2.3 shows a traditional method of illustrating the phenomenon. Here the relationship between the receiving (load) -end voltage and power, V_R and P_R, is plotted for different load power factor values, with E_S assumed constant. Only the operating points above the critical points represent satisfactory operation.

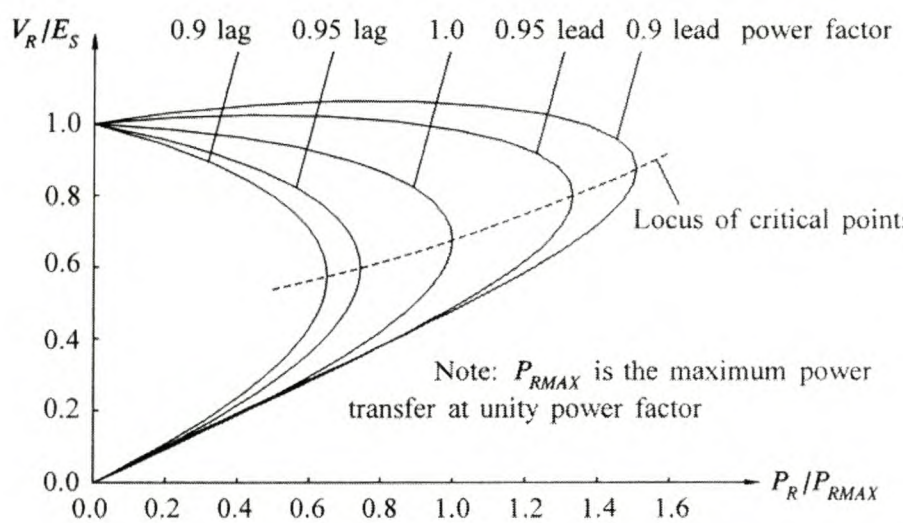

Fig. 2.3: V_R-P_R characteristics of the system in [60]

Operation at or near the stability limit is impractical and a satisfactory operating condition is ensured by allowing sufficient "power margin". From a power system security point of view, the operating power, and voltage, at the system nodes should be kept as far away as possible from their critical values.

All reactive devices are designed to operate satisfactorily when an increase in Q is accompanied by an increase in V. The inability to meet the demand for reactive power is the main factor causing voltage instability. The classic voltage stability criterion is based on this concept.

Enhancing voltage stability

Generator AVRs are the most important means of voltage control in a power system. Another "method" is the series capacitor. Series capacitors are self-regulating. The reactive power supplied is proportional to the current squared and independent of voltage, which has a favourable effect on voltage stability. Series capacitors effectively shorten line lengths, reducing both the characteristic impedance and electrical length of the line. This improves both voltage regulation and stability significantly.

Contributing factors to voltage collapse

The main factors that contribute to voltage collapse are:

- The stiffness of the load characteristics.
- Control of tap-changing transformers.
- Limited ability for reactive power control by generators.

2.2.5 Frequency stability

Frequency stability is the ability to maintain the system frequency within a nominal range following a severe system upset, which may or may not result in the system being divided into subsystems ([63] pp. 259-290).

Governing principles

Momentary disturbances, as discussed in the sections on electromechanical dynamics, are normally cleared without the need to reduce the generated or consumed power. However, in the case of a severe disturbance, such as the sudden connection or disconnection of a large load, or when a generating unit is suddenly disconnected from the system by protection equipment, there is a long-term distortion in the power balance between that generated by the

turbines, and that consumed by the loads. As a result, the frequency in the system will change.

Automatic generation control (AGC) is fundamental in determining the way in which the frequency will change in response to a load change. The aims of this control mechanism are:

- To maintain frequency at the scheduled value (frequency-control).
- To maintain the net power interchanges with neighbouring control areas at the scheduled values (tie-line control).
- To maintain power allocation among the generating units in accordance with area despatching needs (economic, security or emergency).

Should the total generation equal the total system demand (including losses), the system frequency would remain constant.

Normally medium-sized units are used for frequency control, while larger base load units operate independently of any frequency control action and only at their prescribed generation values.

Factors that influence frequency stability

Stability in frequency depends on the system's ability to restore the balance between system generation and load with minimum loss of load. Generally, stability problems are associated with inadequacies in equipment response, poor coordination of control and protection equipment [60]. Sufficient spinning reserve is also essential to ensure the system frequency remains stable.

2.3 Synchronizing and damping torques

The concept of synchronizing and damping torque [2] forms the basis of this investigation on small-signal stability. The advantage of this approach is that is provides both engineering insight and understanding of the influence of system elements (such as AVR) on stability, and the action of the stabilizers in enhancing the damping performance of the system [3].

At any given oscillation frequency, braking air-gap electrical torques are developed in phase with the machine rotor angle (synchronizing torque) and speed (damping torque), respectively. The torque developed by any particular means can be broken down into these components for an insight to their effect on stability.

Synchronizing torque is that component in phase with the machine rotor angle. Positive synchronizing torque assures restoring of the rotor angle of the machine following an arbitrary small displacement of this angle.

Damping torque is the braking torque developed in phase with the machine rotor speed deviation (from the nominal). Damping torque is therefore only present in the event of system oscillations or power swings. Positive damping torque is essential to damp out any oscillations due to any perturbation.

Stability is only assured if both these torque components are present in the system, and positive. This condition is sufficient and necessary ([12], [60] pp. 22-25).

2.4 Block Diagram Approach to Stability Investigation

This investigation is based on the block diagram approach, first used by Heffron and Phillips [1] in 1952. deMello and Concordia [2] first used the block diagram to analyse the small-signal stability of synchronous machines. This approach is useful in gaining physical insight into the effects of field circuit dynamics and in establishing the basis for methods of enhancing stability through excitation (PSS). Also, consideration of the system in this manner allows the application of the methods of feedback control system analysis, a powerful tool developed expressly for determination of stability and transient performance.

Fig. 2.4 shows the block diagram model with thyristor-type excitation system. The relations describing the parameters in the block diagram applies to a 2-axis machine representation with a field circuit in the d-axis but without amortisseurs (damper windings).

Ref. [44] presents an extended block diagram model of the synchronous machine that has one damper winding along the d-axis in addition to the field winding, and two damper windings along the q-axis. Results show the influence of the q-axis representation on generator damper winding performance is most significant at low values of rotor angle. The q-axis then contributes significantly to the damping power. This shows representation of the q-axis can significantly affect performance prediction with respect to system damping. However, in this investigation the focus is on the need of damping, and a worse case scenario is desired. As a result the representation of Fig. 2.4 is used, even though its application may be limited to only certain machine types [44].

The block diagram model can greatly simplify the explanation and analysis of fundamental generator dynamic characteristics. Its form lends itself readily to the assessment of the

dynamic contribution of individual generation elements (field circuit, excitation) and the influence of standard controllers on overall generator dynamic behaviour and stability. The way in which controller performance is influenced by generator loading conditions and external reactance can readily be determined.

The representation of Fig. 2.4 indicates the following [1]:

- Machine angle has a direct effect $(K_5\Delta\delta)$ on terminal voltage.
- The magnitude of the field flux linkage has a direct influence $(K_6\Delta\delta)$ on terminal voltage.
- Torque output of the machine depends on the machine angle and field flux linkages
- Presence of time lags indicates machine angle affects the field flux linkage, but only after a delay.

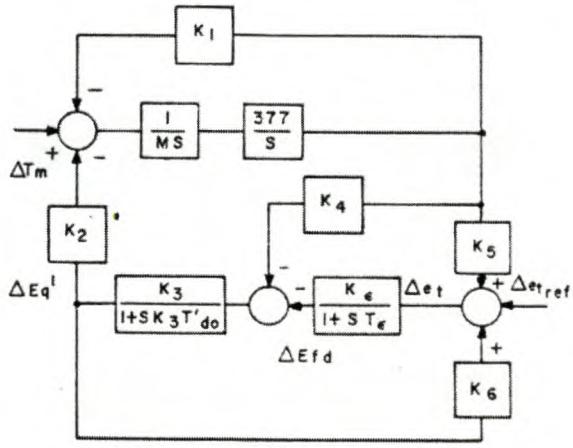

Fig. 2.4: Phillips-Heffron block diagram model with excitation system [2]

The *K*-parameters in this model are functions of machine and system impedances as well as the loading condition of the system. The system dynamic behaviour can be expressed in terms of these parameters. Because the parameters change with loading, the dynamic behaviour of the machine can be quite different at different operating points. Understanding the behaviours of the *K*-parameters for different operating conditions helps understanding the dynamic behaviour of the machine at such conditions.

Research into the influence of system impedances and loading conditions on the values of the *K*-parameters reveal the following [1][2][12][13]:

1. The coefficient K_1 is positive for most conditions, and decreases with increase in system and machine reactance. In the case of very long ties and relative high loading

K_1 can be negative. K_1 shows no definite trend with respect to loading as a result of transient saliency effects. In a system with local load, K_1 can turn negative as reactive power loading on the generator increases and/or the power factor decreases.

2. The coefficient K_2 is positive for all conditions. K_2 increases with increase in generator active power loading and system strength [16].
3. K_3 is also positive for all conditions, and is a function only of the ratio of impedances. K_3 is independent of generator loading.
4. K_4 is mostly positive and increases with increase in generator active power loading. K_4 can be negative when the generator supplies part of a local load that is partly supplied by the remote system, or the generator is connected through considerable external resistance to the remote system.
5. K_5 is positive for low to medium external impedance and loadings, and negative for moderate to high transfer impedances and heavy loadings. The latter is more often the case. K_5 also decreases with increase in reactive power loading of the generator. For a system with local load K_5 is always positive.
6. K_6 is always positive, although the magnitude reduces with increase in loading and with small external impedances. In a system with local load, K_6 increases with increase in generator loading.

For a system without excitation voltage control, the parameter K_1 has the dominant influence on the system synchronizing torque. As this parameter is mostly positive, so the system is transiently stable under most conditions.

Losses in the field circuit contribute positive damping as long as the parameter K_4 is positive [13]. Whenever K_4 is negative then the field circuit introduces negative damping to the system, aggravating stability. Damping by the field circuit is negative when generation approaches synchronous condenser operation (reduced active power loading and increased reactive loading). This tendency increases with increase in external reactance. Hence the machine itself (without regulator) can exhibit negative damping, for certain system structures and operating conditions.

The influence of a thyristor excitation system on the damping and synchronizing stability of the system is primarily influenced by the parameter K_5 and the AVR and exciter transfer

characteristic. When K_5 is negative, the exciter contributes positive synchronizing torque but negative damping torque to the system. The opposite is the case when K_5 is positive. As K_5 is more often negative than positive [2], the excitation system contributes to oscillation instability. The effect of a negative K_5 on system damping stability becomes more pronounce as the exciter response increases (higher gain).

The above is for a thyristor excitation system. Ref. [12] also discusses the influence of a type-1 excitation system [19] on system stability. In this case the exciter introduces negative damping and the system is unstable, regardless of whether K_5 is positive or negative.

Previous research on small-signal stability of a SMIB system using the block diagram approach, made the following assumptions:

- Saturation effect was neglected.
- Armature resistance was neglected.
- Amortisseur effects were assumed negligible.

The latter assumption is already dealt with. Neglecting armature resistance is appropriate as inclusion significantly complicates the relations describing the K-parameters, and the influence on results is minimal (the effort not justified).

Neglecting saturation does influence the relations, but to a lesser degree. Ref. [45] attempts to study the effect of saturation on system stability, and obtains the following results:

- Saturation has no effect on the synchronizing torque at low frequencies, but at higher frequencies the synchronizing torque is increased (for system without regulator).
- For a system with thyristor exciter, the influence of saturation on synchronizing torque at higher frequencies depends on the sign of the parameter K_5.
- Saturation effect improves the damping torque coefficient at low frequencies in the system without regulator.
- For the system with thyristor exciter, at low frequencies the influence on damping torque depends on the sign of K_5. At higher frequencies the damping torque is decreased, whether an AVR is implemented or not.

In the investigation reported in Ref. [45], saturation is assumed to influence only the parameters K_2, K_3 and K_6 in the block diagram by a constant m. This constant is the same for all parameters. A closer look at the relations describing the K-parameters reveals these

parameters are a complex function of, amongst others, the machine inductances (see Appendix D for expressions for the parameters). Also, machine inductances do not appear in these expressions in any same way, and also in other parameters than those mentioned above. It is the opinion of the author of this report that the results reported in Ref. [45] are not entirely valid. For this reason the influence of saturation effect (or rather the neglecting thereof) on results is also considered in this investigation.

Swift *et al.* [14][15] extended the block diagram of Fig. 2.4 to include parameters (K_P, K_q and K_V) essential to incorporate Flexible AC Transmission Systems (FACTS) devices, such as CSC, SVC and phase angle regulator (PAR). This present section considers only results from previous work done in this regard. Section 5.4 derives the extended model in question as well as expressions for these added parameters (see Fig. 5.5).

The parameter K_P is shown to have dominant influence on generator behaviour in Refs [14][15]. Results show K_P increases with increase in generator loading and system strength.

Refs [14] and [15] do have some drawbacks:

- Relations for the K-parameters developed are not presented.
- The variation of K_q and K_V with respect to generator loading and system reactance is not presented, as the influence of damping torque through these parameters is assumed negligible.
- The influence of external resistance are not investigated.

For these reasons, the block diagram model to incorporate FACTS devices is derived in this report (section 5.4), and the parameters K_P, K_q and K_V investigated under various conditions of generator loading and network impedance.

2.5 Methods to Improve Stability

Section 2.2 discussed the various forms of system stability. Special emphasis was placed on small-signal stability, particularly the problem of local mode oscillations.

Oscillations of small magnitude and low frequency may persist for long periods of time and in some cases present limitations on power transfer capability [16]. Insufficiently damped oscillations may build up in amplitude, causing rotor swings of significant amplitude until synchronism is lost. Power system stabilizers and other methods of stability enhancement

were developed to damp out oscillations following a disturbance (small or large) and ensure stable operation of the system. This section presents these methods, and provides an overview of research already done in the field of angle stability enhancement.

2.5.1 Power System Stabilizer

The PSS is one of the most cost-effective and common methods of enhancing small-signal stability and extending the stability limits of the system ([16], [63] pp. 182, 291-296). It is a device that provides additional supplementary control loops to the generator AVR system, modulating the generator excitation to provide damping to the oscillations of generator rotors relative to one another. Section 2.3 discusses the concepts of oscillation damping and damping torques in more detail.

The overall excitation system (with PSS) is designed with the following aims in mind [25][29]:

- To maximize the damping of both local and interarea mode oscillations without adversely affecting other modes of oscillations, such as torsional oscillations or control modes such as "exciter modes" associated with the excitation system and the field circuit.
- To enhance the system transient stability.
- Not to adversely affect system performance during major system upsets which cause large excursions in system frequency.
- To minimize the consequences of possible excitation system malfunction due to component failures.

Factors to consider when implementing a PSS [32] include (a) the location of the generating unit where a PSS is to be installed, (b) the type of excitation system employed, and (c) the voltage characteristics of system loads. The system loads and location of the PSS affects only the damping of inter-area oscillations. The damping of local mode oscillations are unaffected by these factors.

The structure of a PSS consists of low- and high-pass filters, lead-lag elements to obtain the required phase shift, a signal amplifier and output limiters. A phase shift is required to compensate for the phase lag between the exciter input and the electrical torque. This is explained mathematically in section 4.4. Section 4.2 explains the various components in the PSS control structure in more detail. An important design consideration is the input signal

employed; this has significant influence on the way the PSS is constructed. Input signals typically employed are (a) shaft speed deviation from the nominal, (b) ac bus frequency and (c) a combination of power and speed ([16], [18], [63] pp. 14, 291-296). Factors to consider when deciding on an input signal include torsional interactions, the presence of power system noise, and mechanical power variations. Each of these input signals is discussed briefly below.

PSS based on $\Delta\omega_r$: The oldest type of PSS uses a measurement of the speed deviations of the generator shaft. A disadvantage to this type of PSS is that the stabilizer gain is constrained by the influence of the PSS on torsional oscillations. Also, selecting a measurement position on the shaft that properly represents the speed deviation is another obstacle. A solution is to measure the speed at a number of points along the shaft and calculate the average speed deviation.

PSS based on $\Delta\omega_r$ and P_e: This type of PSS calculates the average speed deviation from measured electrical quantities, avoiding the need to measure speed deviation at a number of points. This has the added advantage that a large gain can be used so that good damping of the power swings can be obtained.

PSS based on f_T: In this type of PSS, the terminal voltage frequency f_T is used as input to the PSS. The advantage to this solution is that the PSS is more sensitive to inter-area oscillations than the previously mentioned methods. Hence the damping of inter-area oscillations in interconnected power systems is improved. However, there is a disadvantage. Terminal voltage waveform can contain noise produced by large industrial arc furnaces. Also, as in the case of a PSS with speed deviation as input, the stabilizer gain is limited by the effect on shaft torsional oscillations.

Some practical considerations regarding PSS design and implementation [25]: A thorough knowledge of the regulator and its parameters is required. A badly designed PSS can be a source of undesired oscillations. Voltage control on one generator also influences the dynamic response of all generators in the power system. As a result, a PSS that improves the damping of one generator does not necessarily add to the positive damping of other generators in the system. Also to consider is the sensitivity of the PSS performance to its parameters [72].

Previous research on PSS performance [16][25] indicate the following:

- Excitation gain, generator loading and system strength strongly influences the performance of a PSS on generator damping.
- For PSSs with speed and/or electrical power as input, PSS performance increases with generator loading and system strength.
- For PSS with ac bus frequency as input, PSS performance decreases with increase in system strength.
- Increase in stabilizer gain improves the damping of both local and interarea modes of oscillations.
- If no transient gain reduction (TGR) is employed on the excitation system, the PSS also increases the transient stability of the system.

The problem of interaction with other oscillation modes in the system and possible adverse effect is the focus of much research. One possible solution is investigated in [56]. The turbine-governor is utilised for the damping of local and inter-area oscillations, instead of the generator excitation system. This is similar to adding a PSS to the excitation system. Phase compensation is also needed, since time constants in the turbine-governor introduce a phase shift between oscillations in $\Delta\omega_r$ and the turbine mechanical power.

The advantage to this solution lies in the fact that turbine-governor dynamics are weakly coupled with those of the rest of the system. Consequently, the parameters of the PSS do not depend on the network parameters. Although not in current use, this solution should receive more attention in the future.

Some advantages of PSS over other forms of stability enhancement:

- Cost. PSS are very low cost [48], particularly in the case of new installations or excitation system modernization [49]. Other means of compensation enhancement need added (and costly) protection equipment.
- PSS provide robust damping control [49]. Outage or maltuning of a few PSSs does not significantly influence the damping of low frequency oscillations.

Ref. [50] states a disadvantage to the use PSS. In the case of low frequency oscillations, a large external reactance between groups of generators is usually involved. Such a high reactance cause a low damping effect, which the PSS may not sufficiently damp. In such cases a more costly alternative may need to be considered.

Also, the ability of the PSS to provide damping to transient oscillations following a large disturbance is impaired if the generator operates at such a loading that the exciter voltage is close to or at its physical limit [7]. Only a small margin is available for excitation system adjustments via the action of the PSS controller. The PSS controller may not be able to ensure stability if this is the case.

2.5.2 The FACTS option

Traditionally, AVR and PSSs have been used for the damping of transient and dynamic oscillations in power systems [7]. The introduction of FACTS provides several novel techniques for this purpose.

The concept of FACTS was developed to make the transmission and distribution of electricity more reliable, more controllable and more efficient [59]. The technology, based on power electronic switches, offers utilities five opportunities for increased efficiency:

- Greater control of power flow on prescribed transmission routes.
- Secure loading of transmission lines to levels nearer the thermal limits.
- Greater ability to transfer power between areas, so that generation reserve margin may be reduced.
- Prevent cascading outages by limiting the effects of faults and equipment failure.
- Damp power system oscillations, which could damage equipment and/or limit usable transmission capacity [16].

The electric power transmission network is essential for reliable, low-cost power. Inadequate transmission will result in less reliable, more costly power. This is one of the main reasons for interconnecting networks. FACTS technology opens up new options for controlling power and enhancing the usable capacity of present lines.

The following sections discuss various FACTS devices that have been developed and implemented in power systems, as well as some new concepts. The focus is on the ability of the device to damp electromechanical oscillations.

2.5.3 Static Var Compensator

The SVC can be described as dynamic shunt reactive power compensation. An SVC adjusts its reactive power output to that required by the system. It is a flexible and continuous scheme that operates in both the capacitive and inductive regions (depending on the design).

It utilizes thyristor-switched and/or thyristor-controlled shunt elements. A variety of combinations of fixed and controlled elements are possible.

The main function of an SVC is the control bus voltage by adjusting the reactive power output to that required by the system. A voltage regulator that attempts to keep busbar voltage constant usually controls the thyristor firing circuits.

An SVC has no ability to control active power flow [59]. The reason is that, at a predefined transmission voltage, line series impedance and the angle between the line end voltages ultimately determine active power flow ([70] pp. 209). An SVC controls neither of these parameters.

It has been found that the SVC voltage control does little to help the oscillation stability of the power system [42]. To improve power system damping and increase oscillation stability, supplementary control can be super-imposed on the regulator. This forms an extra damping loop and provides positive damping to the power system (if properly designed).

Research on the use of an SVC to damp power system oscillations (local and inter-area mode) ([8], [9], [15] and [42]) found the performance to increase with transmission line power transfer. This is a favourable trend, as more damping is needed in a more heavily loaded system. However, damping at low load conditions is negative and hence there exists a "dead-point" where the SVC damping function is lost (damping torque zero). A possible solution to this is to use an adaptive controller to change the sign of the SVC damping controller gain according to the loading. Results from Ref. [8] show this can result in positive damping of the inter-area oscillation mode at all loadings. However, control of inter-area mode oscillations cannot at the same time guarantee a positive damping for the local oscillation mode.

Usually, the SVC damping control is more effective when the power system is working at a weak system connection with higher transmission line impedance [15][42]. Again, this is a favourable characteristic, since damping is needed more in a weaker system.

Results from Refs [15] and [42] indicate the damping torque contribution of the SVC damping control is linear to the controller gain. Hence for more effective damping control following a large disturbance the gain should be set as high as possible. Physical limitation would however not allow continuous control with a very high gain, and "bang-bang" control appears one of the best control strategies to curb transient stability. Continuous control is a more favourable approach for small-signal stability.

The damping effect (effectiveness) of the SVC is sensitive to its location on the intertie [9][48]. It must be remembered that the SVC influences the phase angle rather than the magnitude of the line current [10]. Bus voltage and line power flow depends on the impedance between the point of connection of the SVC and the sources; the location of the SVC equipment thus has a significant impact on its characteristics and capability. Ref. [48] suggests the SVC to have greatest influence when located near the midpoint of the electrical distance from the two power systems, or two machines that oscillate against each other.

The presence and nature of bus load near the SVC location also has significant influence on the effectiveness of SVC damping. It is even possible for the damping to be negative altogether, depending on the load characteristics. To avoid such negative damping an "inverted" control algorithm may be necessary if the SVC is placed close to the receiving end bus, and this bus carries substantial passive load [10].

A disadvantage to the SVC is that the reactive power capability reduces steeply as a function of the square of the voltage. Thus, when the SVC is most needed for voltage control (its main function) it may not be able to provide the required reactive power support. The Static Compensator is a shunt device that overcomes this obstacle.

2.5.4 Static Compensator

Another form of dynamic shunt compensation is the Static Compensator (STATCOM), also called an Advanced-SVC or Gate Turn-Off (GTO) -SVC ([63] pp.34-35), or Static Condenser [59]. The STATCOM provides shunt compensation in a similar way to the SVC, but utilises a voltage source converter rather than shunt capacitors and reactors. The STATCOM incorporates a high content of power electronics, but conventional components are reduced to only a transformer and capacitor. This has the advantage that the construction is modular and compact, making shipping, assembling and even possible relocation simple. The STATCOM can also be used to help damp electromechanical oscillations.

An advantage of a STATCOM over a SVC is that, if the voltage is depressed, the STATCOM can still deliver high levels of reactive power by using its overcurrent capability [59]. The most reactive power that can be delivered equals the voltage times the current.

Since the STATCOM is a relatively new concept, research on its ability to enhance system stability is limited. Ref. [57] shows the dc voltage regulator of a STATCOM is a source of negative damping to system oscillations. A stabilizer superimposed on the AC voltage

regulator is able to counterattack this negative influence and provide positive damping to system oscillations.

Other possible application for a STATCOM is the damping of subsynchronous oscillations [58].

2.5.5 Controlled Series Compensation

A CSC can be described as dynamic series reactance compensation. The primary purpose of applying series compensator is to solve power flow problems. A CSC adjusts its degree of series capacitive compensation to (a) increase/decrease the transmittable power, (b) control power flow in the lines, and (c) prevent loop flows in the system ([70] pp. 209-265). Series capacitive compensation can be effectively used to reduce underutilization of power systems.

Series capacitors are one of most cost-effective and economical methods to raise stability limits [9]. Kimbark [47] in 1969 proposed the concept of switching series capacitors to improve the transient stability of a simple SMIB power system. It was found the use of switched series capacitors also reduces the fluctuation of load voltage, and that the MVAr rating of shunt capacitors or reactors is 3 to 6 times the rating of switched series capacitors for the same increase in stability limit. Hence switched series capacitors is more effective than their shunt counterpart to improve transient stability.

The work by Kimbark set the stage for research in series capacitor control for stability enhancement. With the advent of high-power thyristors, control of series capacitors in a more economical and effective manner could be realized.

Series capacitive compensation can also be employed to minimize the receiving-end voltage variation (at load end) and hence the possibility of voltage collapse. It does so more effectively than a SVC ([70] pp. 212). Series compensation can also be used to effectively damp electromechanical oscillations, which is does by the following working principle:

- The applied compensation is varied so as to counteract the accelerating and decelerating swings of the disturbed machine(s).
- When the oscillating generator accelerates and δ increases, the electric power transmitted must be increased to compensate for the excess mechanical input power.
- Conversely, when the generator decelerates and δ decreases, to balance the insufficient mechanical input power the electric power transmitted must be decreased.

Analytically, damping control by CSC action is similar to the direct addition of damping torque to each generator in a power system [43]. The effectiveness of the CSC to provide damping for a certain generator depends on the sensitivity of that generator to CSC action. This has significant influence for the CSC location and ratings needed for effective performance.

The following topologies of variable impedance series compensators exist ([70] pp. 209-265):

- GCSC – GTO Thyristor-Controller Series Capacitor
- TSSC – Thyristor-Switched Series Capacitor
- TCSC – Thyristor-Controller Series Capacitor

A GCSC is based on the GTO thyristor valve, that has ability to turn on and off upon command. Thyristors are the most rugged power semiconductors available, with the highest current and voltage ratings, and highest surge current capability. GTO thyristors presently have lower voltage and current ratings, and considerably lower short-term surge current rating. This limits the application of the GCSC to date, and thyristor-type topologies have more favour with researchers.

A TSSC consists of a number of capacitors, each shunted by reverse parallel-connected thyristors. The degree of series compensation is controlled in a step-wise manner by increasing or decreasing the number of series capacitors inserted. Although a TSSC can control the degree of series compensation, a sufficiently high degree of compensation could cause subsynchronous resonance problems just as well as an ordinary capacitor. Its use is therefore limited to applications where a high degree of compensation is not required and the danger of subsynchronous resonance is not present. The TSSC finds application in power flow control and oscillation damping where the required speed of response is moderate.

The TSSC configuration has the added disadvantage that a strong amount of active power loss arises by valve conduction, when the system condition is such that a higher compensation level is not required [51].

The TCSC consists of a series capacitor shunted by a thyristor-controlled reactor (TCR). The basic principle is to provide a continuously variable capacitor by means of cancelling the effective compensating capacitance by the TCR. The TCSC design is complicated by the fact that the internally generated harmonics aggravate the limit conditions ([70] pp. 234). Harmonic currents cause additional losses and corresponding temperature increase in both the thyristor valve and the reactor.

For the TCSC a wider control range of the compensation degree is allowed, compared to the TSSC configuration [51]. Better first-swing stability and system damping is also achieved. Other advantages of the TCSC configuration are:

- Load flow control by continuous control in the TCR mode
- Overvoltage protection of the series capacitor by step-wise control in the thyristor switched reactor (TSR) mode
- Reduction of capacitor overvoltages at reinsertion by point of wave control

CSC performance in oscillation damping [8][9][14][15][46]

Regardless of network structure or loading condition, a CSC with appropriate damping control is able to contribute positively to the damping of oscillations, whether local or inter-area in nature. Also, there exists a linear relationship between the gain of the damping controller and its damping torque contribution. Hence for more effective damping control the gain should be set as high as possible. Physical limitation would however not allow continuous control with a very high gain, and "bang-bang" control appears one of the best control strategies. This is suitable to ensure stability following a large disturbance (transient stability). However, to damp relatively small power oscillations, continuous variation of the degree of compensation, in sympathy with the generator angle or power, may be a better alternative ([70] pp. 214).

CSC damping control is more effective in a heavier load condition. This is an advantageous feature, since damping of the system normally is lower at heavily loaded lines. However, CSC damping control is less effective in a weaker system configuration with same load transfer, when more damping torque is needed.

CSC damping control also benefits transient stability.

Another advantage to system stability enhancement by a CSC is the fact that CSC damping effect is not sensitive to the system load characteristics [9]. Also, the location of the CSC along a tie-line has little influence on its ability to damp power swings [10][48]. Damping of a particular oscillation mode in a large complex power system by CSC damping is a bit more complicated. Results from Ref. [43] indicate the CSC damping controller should be installed close to the generator most sensitive to the system oscillation so as to achieve better damping control. The optimum location for a CSC installation depends on the system operating condition.

Results from Ref. [8] show CSC damping control, when designed for damping inter-area oscillations, positively influences local mode oscillations but to a smaller extent.

Implementation considerations

Compensating a transmission line by fixed series compensations increases the steady-state limit. Also, damping action is stronger compared to the case of the non-compensated line [10]. Adding a controllable segment with the appropriate damping control topology improves the damping action even more. Hence the most advantageous way of implementing the damping equipment in a CSC form, seems to provide a larger fixed series capacitor with a few controllable segments having suitable power ratings. This is to counter the system constraints at least cost [59]. Typically a trade-off exists between the transient performance required, which is influenced by the amount of adjustable capacity available, and the cost of the equipment [7]. Increasing the adjustable range means better transient performance, but also an increase in cost.

Advantages of CSC over other forms of stability enhancement

- A CSC is more effective in terms of damping effect per Mvar installed equipment than shunt compensation, even with the 'SVC located at the location of maximum influence [48] or several CSCs installed in parallel transmission paths, and compared to one SVC [50][52]. Ref. [10] states the ratio of Mvar for similar performance between CSC and SVC to be on the order of 10.
- A CSC is more efficient in terms of damping effect per Mvar installed equipment than a PAR (section 2.5.6), particularly when the transmission line is heavily loaded [9].
- The impact of switched series capacitors and CSC operation on bus voltage amplitude fluctuation is lower than is the case with SVC [10][47].
- CSC control causes much less voltage variation at the machine terminal than does a PSS [7].
- The CSC damping effectiveness is less sensitive to location and loading conditions than the corresponding SVC damping system [10][50]. The CSC is more robust in this regard.
- A CSC is more effective than a SVC at damping inter-area oscillation modes [8].

- In the case of two large systems interconnected by a series-compensated transmission link, the extension of the series capacitor with some controllable segments [50] or one or a few appropriately located CSCs [48], may offer an alternative to providing PSSs for large number of machines.

When the CSC is used to damp oscillations, generator output is controlled mainly by varying the transmission line reactance, and not by varying the exciter output (as in the case of a PSS). Hence the CSC control action can still be in force even when the field voltage is close to its physical limit (exciter saturated) [7]. The CSC is then able to provide damping to the system oscillations following a disturbance when the PSS is not, and the CSC superior in this regard.

The discussion in [7] considers only transient stability. Of course, damping small-signal oscillations by a PSS will be less influenced by margin of field voltage available. However, if no margin is available and the exciter saturated, the PSS is also not able to provide the needed damping to small oscillations.

2.5.6 Phase Angle Regulator

A PAR works by adding or subtracting a variable voltage component that is perpendicular to the phase voltage of the line to accomplish the phase shift [59]. Similar to the CSC, a PAR (also called "phase shifter") can be used for power flow control, with possible application in power system stability enhancement [9]. There is an added benefit for the use of a PAR over a CSC: use of a PAR does not contribute to subsynchronous resonance [59].

As with the CSC, there is a linear relationship between the gain of the controller and its damping torque contribution [15]. This suggests for most effective damping control, the gain should be set as high as possible. Physical limitation would not allow continuous control with a very high gain, and "bang-bang" control appears the most effective option. In practice, as is the case with CSC, this is more appropriate for curbing transient stability; continuous control ought to be utilized to enhance small-signal stability.

The damping effect of a PAR decreases with increase in line loading [9]. This is an unfavourable trend, as damping is needed more in a more heavily loaded system.

Other than is the case for a CSC, the damping effect of a PAR is influenced by the load characteristics, but to a lesser degree than the SVC.

A PAR is able to provide positive damping torque regardless of network configuration or system loading [15]. Also, the PAR damping control is less effective in a weaker system, which is unfavourable as more damping torque is then needed. The location of a PAR along a tie-line does not influence its ability to damp power swings [48].

Even though theoretically a PAR can be used to damp electromechanical oscillations, it shows unfavourable trends with respect to both generator loading and system strength. Also, it is more sensitive to load characteristics and hence not as robust in that regard as a CSC. The advantage of using a PAR is the fact that it does not contribute to subsynchronous resonance and as a result no special control mechanism needs to be implemented.

2.5.7 Unified Power Flow Controller

The UPFC controls bus voltage in both magnitude and phase ([63] pp. 37-38) by use of GTO thyristors. Through this action, a UPFC is able to control the flow of real and reactive power in the network, as well as damp electromechanical oscillations.

The primary function of a UPFC is power flow control. The UPFC power flow and voltage controller have little influence on system oscillation damping [54]. For continuous and effective operation of the UPFC, the dc voltage across the UPFC link capacitor must be kept constant. This can be achieved by installing a dc voltage regulator in the UPFC. Ref. [54] found this dc voltage regulator is a source of negative damping torque and reduces the damping of rotor angle oscillation mode. A damping controller added to damp system oscillations is able to counterattack this problem. The damping of low-frequency oscillations is one of the secondary functions of the UPFC.

Research into the influence of system loading and network characteristic on the UPFC damping performance [55] found UPFC performance increases with loading. This is favourable, and a result of the forward path of the UPFC damping controller. This "plant" transfer function varies with power system operating condition as well as choice of input control signal. The variation of the "plant" transfer function with respect to the system or external reactance (resistance not considered) is dependent on the input control signal chosen. The four input control signals are the amplitude modulation ratio and phase angle of the control signal of each voltage source converter.

2.5.8 Superconducting Magnetic Energy Storage

A SMES ([63] pp. 35-36) can be seen as a controllable current source whose magnitude and phase can be changed within one cycle; the upper limit of this source is imposed by the dc current in the superconducting coil. Converter firing angles are determined by a PQI controller (referring to the control of active power (P), reactive power (Q), and current (I)) so as to control the output real and reactive power and the dc current in the coil. The modulation controller determines control strategy in such a way as to damp power swings in the network.

A SMES can constitute a powerful tool for transient stability enhancement as well as support primary frequency regulation.

2.6 Summary

Chapter 2 provided background information on system stability. The focus fell on small-signal stability, as the investigation of this report considers this type of stability. In particular the problem of local mode oscillations are considered, and for that purpose the SMIB system is ideal in developing concepts.

The block diagram that describes the SMIB system is presented. The damping and synchronizing torque expressions can be obtained using this diagram, and are functions of the K-parameters in this diagram. An understanding of the behaviours of these parameters is essential in understanding the torques of the system. Previous research investigated the K-parameters, but in that research the infinite bus voltage was not constant for all conditions and allowed to vary. For this reason this report (chapter 3) also investigates the behaviours of the parameters, but for the case of a generator connected to a large and "stiff" external system (infinite bus constant).

An extension of the block diagram to incorporate FACTS devices is also mentioned. In the references that describe this block diagram, relations for the K-parameters are not given. Also, only the parameter K_P is investigated and that also only for the system with no external resistance. Chapter 5 derives expressions for the K-parameters in this block diagram model, and these are investigated for conditions of loading, reactance and resistance.

Section 2.5 presented an overview of methods to use (or can be used) to enhance stability of a power system. Of all the methods so far researched, the PSS and the CSC appear the most effective at damping system oscillations. The PSS has cost in its favour, whereas the CSC is

more effective per MVAr rating than other FACTS devices. Chapters 4 and 5 investigate the performance of the PSS and the CSC for various different operating conditions, respectively. Chapter 6 provides a comparison of the results. The discussion focuses on which controller is more able to improve system stability, when more damping torque is needed.

3 REQUIREMENT FOR STABILITY SUPPORT

3.1 Introduction

This chapter introduces the state-space and block diagram models of the SMIB system without oscillation stabilizer, and investigates and discusses scenarios of possible system instability.

The concept of system eigenvalues are of much importance. The classic model generator versus infinite bus system is presented to illustrate the role eigenvalues play in evaluating the stability of the system. Section 3.3 discusses the system model used in this and subsequent chapters for stability analysis. This model comprises the state-space model, from which the eigenvalues are obtained, and the block diagram model, useful to evaluate torque expressions used in the investigation.

The concepts of damping and synchronizing torques are used to evaluate the stability condition of the system. These torque expressions are functions of parameters known as the system model K-parameters. The stability of the system can be related to the signs of the K-parameters. It is therefore deemed important to understand the behaviours or trends of these K-parameters for various network structure and loading conditions. The characteristics and conditions under investigation are: (a) generator load; (b) system reactance as seen by the generator; (c) the amount of external (line) resistance relative to reactance; (d) load local to the generator (sending-end) side of the SMIB system. The influence of machine saturation on results is also examined.

Both the influence of armature reaction and the excitation system on system stability are investigated for the characteristics and conditions mentioned above. In addition to these, the influence of AVR gain on results is also considered. Emphasis is placed on identifying scenarios of possible system instability, to determine when it is required to provide stability enhancement.

3.2 Classic Model Representation

The classic generator model is a simplified version of the machine model of section 3.3. A simple voltage source of fixed magnitude behind an effective transient reactance describes the classic generator model. In the SMIB configuration, a constant infinite bus voltage and reactance represents the external system. The simplicity of this model helps to understand the effects of synchronizing and damping torques on the stability and frequency of system oscillations.

3.2.1 Small perturbation equations

Fig. 3.1 shows the SMIB configuration. E' and E_B are the machine and infinite bus voltages, respectively; X'_d is the generator transient reactance, and X_E the equivalent reactance of the external system.

The scenario considered in this report is that of a generator connected to a large system via a power line. This has the following implications on the investigation performed in this research:

- The external system is modelled by the infinite bus, and assumed to be relatively strong or stiff. As a result the voltage E_B is constant at a pre-determined value regardless of generator loading or line impedance.
- The power line may be of low voltage (this option not excluded), so that neglecting resistance in the line may influence results erroneously ([67] pp. 415). Throughout this report, seperate sections present the influence of resistance on results.

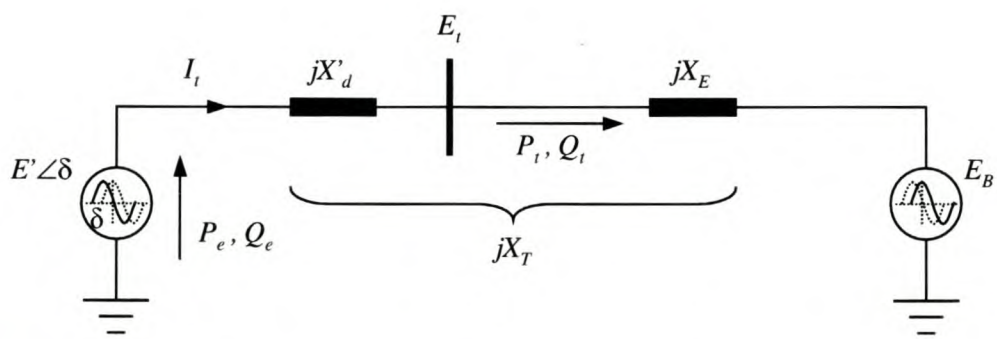

Fig. 3.1: SMIB system with generator represented by classic model

The configuration of Fig. 3.1 does not include line resistance or local load, to simplify the basic analysis presented in this present section. Section 3.4 discusses the modelling of line resistance or local load in the SMIB system.

Section 2.2.1 describes the governing principle behind rotor dynamics, namely the swing equation. Eq. (2.1) expresses the per unit swing equation, which is a second order differential equation. For the purpose of investigating the dynamic performance of the SMIB system, component models are expressed in state-space and block diagram form. This requires the component models to be expressed as a set of first order differential equations. The swing equation of (2.1) can be expressed as:

$$p\Delta\omega_r = \frac{1}{2H}(T_m - T_e - K_D\Delta\omega_r) \tag{3.1}$$

$$p\delta = \omega_0\Delta\omega_r \tag{3.2}$$

These are a set of two first-order differential equations. p is the differential operator d/dt, with time t in seconds. δ is evaluated with respect to a synchronously rotating reference, in this case E_B.

A note on symbology usage. The subscript 0 refers to the steady-state or predisturbance condition. So is δ_0 the nominal or steady state value of δ. Also, the prefix Δ implies a perturbation or small deviation of the variable from the pre-disturbance value. So does $\Delta\omega_r$ imply the deviation of the rotor speed ω_r from its steady state value.

In per unit, the air-gap torque is equal to the air-gap power P_e, and can be expressed as:

$$T_e = P_e = \frac{E'E_B}{X_T}\sin\delta \tag{3.3}$$

X_T is the total system reactance depicted in Fig. 3.1. To obtain the state-space and block diagram models, this expression for T_e is substituted into Eq. (3.1) and linearised about the initial condition represented by $\delta = \delta_0$. The following expression results:

$$p\Delta\omega_r = \frac{1}{2H}(\Delta T_m - K_S\Delta\delta - K_D\Delta\omega_r) \tag{3.4}$$

K_S is the synchronizing torque coefficient

$$K_S = \frac{E'E_B}{X_T}\cos\delta_0 . \tag{3.5}$$

Eqs (3.4) and (3.2) describe the system in small perturbation form. These expressions combined give the system state-space and block diagram models.

3.2.2 System state-space model and block diagram

Eqs (3.2) and (3.4) can be combined in matrix format to give

$$\frac{d}{dt}\begin{bmatrix}\Delta\omega_r \\ \Delta\delta\end{bmatrix} = \begin{bmatrix}-\frac{K_D}{2H} & -\frac{K_S}{2H} \\ \omega_0 & 0\end{bmatrix}\begin{bmatrix}\Delta\omega_r \\ \Delta\delta\end{bmatrix} + \begin{bmatrix}\frac{1}{2H} \\ 0\end{bmatrix}\Delta T_m . \tag{3.6}$$

This is the state-space model of the SMIB system, and is of the form $\dot{\mathbf{x}} = \mathbf{A}\mathbf{x} + \mathbf{\Gamma}\mathbf{p}$. $\mathbf{A}$ is the state matrix of the system, $\mathbf{x}$ and $\mathbf{p}$ are the state and perturbation vectors respectively, and $\mathbf{\Gamma}$ is the perturbation matrix.

The eigenvalues $\lambda = \sigma \pm j\omega$ of the state matrix are a useful indication of the stability of the system. The damping ratio,

$$\zeta = \frac{-\sigma}{\sqrt{\sigma^2 + \omega^2}}, \tag{3.7}$$

determines the rate of decay of the amplitude of the oscillation ([60] pp. 711-712). To ensure such oscillation is positively damped, the real part of the eigenvalue, σ, must be negative. From the eigenvalues of Eq. (3.6), the damping ratio can also be written as

$$\zeta = \frac{1}{2}\frac{K_D}{\sqrt{K_S 2H\omega_0}} . \tag{3.8}$$

ω represents the actual or damped frequency. The undamped natural frequency is

$$\omega_n = \frac{\omega}{\sqrt{1-\zeta^2}} = \sqrt{K_S \frac{\omega_0}{2H}} . \tag{3.9}$$

Observation: increasing K_D increases the damping ratio (as might be expected), whereas increasing K_S increases the natural frequency but decreases the damping ratio.

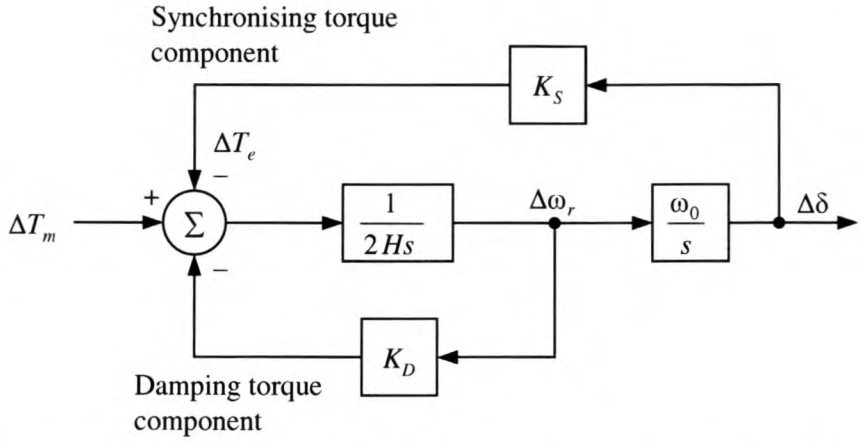

Fig. 3.2: Block diagram of a SMIB system with classical generator model

Fig. 3.2 shows the block diagram model. This diagram is useful to visualize the damping and synchronizing torque and the elements that contribute to this. This model is a simplified version of the more complex block diagram model of the SMIB system with synchronous machine flux linkage variations and field voltage control modelled. Fig. 3.6 shows such a model.

3.2.3 Power oscillation damping – fundamental

With $K_D = 0$ or very small, the system response is purely oscillatory or only slightly damped. An additional component of electrical torque in phase with $\Delta\omega_r$ is required to ensure the oscillations are sufficiently damped. Put differently, a supplementary power is needed to modulate the generated power [4]. If a stabilizer adds an electrical torque [5]

$$\Delta T_e = K_\omega \Delta\omega + K_\delta \Delta\delta\,, \tag{3.10}$$

then Eq. (3.4) is rewritten as

$$p\Delta\omega_r = \frac{1}{2H}\left(\Delta T_m - (K_S + K_\delta)\Delta\delta - (K_D + K_\omega)\Delta\omega_r\right). \tag{3.11}$$

Thus, addition of an oscillation stabilizer modifies the system state-space model of Eq. (3.6) to give

$$\frac{d}{dt}\begin{bmatrix}\Delta\omega_r \\ \Delta\delta\end{bmatrix} = \begin{bmatrix}-\dfrac{K_D + K_\omega}{2H} & -\dfrac{K_S + K_\delta}{2H} \\ \omega_0 & 0\end{bmatrix}\begin{bmatrix}\Delta\omega_r \\ \Delta\delta\end{bmatrix}. \tag{3.12}$$

Eq. (3.12) assumes constant mechanical torque input. In principle, K_ω needs to be such that $K_D + K_\omega$ is positive. This will ensure a positive damping torque and a system that is oscillatory stable. The amount of synchronizing torque $K_\delta \Delta\delta$ the stabilizer introduces depends on the controller phase compensation ([60] pp. 769). K_δ can be either positive or negative.

This section presented the block diagram model of a SMIB system with generator represented by a simplified model. The influence of damping and synchronizing torques on the electromechanical oscillations is presented. The fundamental principle of stability enhancement is described. Section 3.3 presents the state-space and block diagram models of the SMIB system with the generator modelled in more detail. A discussion on the various influences on the damping and synchronizing torques follow later in the chapter.

3.3 System Model

Refs [60] pp. 737-762 and [61] pp. 66-71 derive the small perturbation (linear) model of the SMIB system with synchronous machine represented by the higher order model. This model is an extension of the classical model of section 3.2 to include the effect of field flux linkage variations. This present section presents the main expressions describing the model (the derivation is reproduced from theory and given in Appendix D), as well as the state-space and block diagram models.

Amortisseur (damper winding) effects are neglected for two reasons: (a) to reduce computational effort; (b) inclusion would only act to aid the system damping [22]. Thus a worst-case scenario is created whereby the need of damping is amplified.

In the literature it is often found that armature resistance and saturation effects are neglected to minimize data requirements and calculation times. These simplifications do not affect the fundamental principles and the governing block diagram representation of the system, but only the underlying detailed equations of parameters in the diagram and state-space representation (to be discussed). In this research, for the sake of completeness, armature resistance and saturation effects are included in the system model.

3.3.1 Small perturbation equations

The state variables on which the state-space model is based are $\Delta\omega_r$, δ, which is the sum of the internal machine angle δ_i and the angle by which E_t leads E_B (see Fig. 3.3), and field

flux linkage ψ_{fd}. These and subsequent variables in this section are in per unit. Time is in seconds, and angles in radians.

The expression

$$\Delta\delta = \frac{\omega_0}{s}\Delta\omega_r \tag{3.13}$$

relates the rotor angle to the per unit speed deviation. s is the Laplacian operator and frequency equivalent to p.

The electrical torque in terms of perturbed values,

$$\Delta T_e = K_1\Delta\delta + K_2\Delta\psi_{fd}, \tag{3.14}$$

is used to write the speed deviation from ω_0 as

$$\Delta\omega_r = \frac{1}{2Hs + K_D}\left(\Delta T_m - K_1\Delta\delta - K_2\Delta\psi_{fd}\right). \tag{3.15}$$

The coefficients K_1 and K_2 (Eqs (D.60), (D.61)) are functions of the system characteristic (impedances) and condition (power flow) and define the sensitivity of electrical torque to variations in angle and field flux linkage, respectively. These and other K-parameters are useful as they simplify the analysis of small-signal stability of the system.

The small perturbation field flux linkage is derived as

$$\Delta\psi_{fd} = \frac{K_3}{1 + sT_{3fd}}\left(\Delta E_{fd} - K_4\Delta\delta\right), \tag{3.16}$$

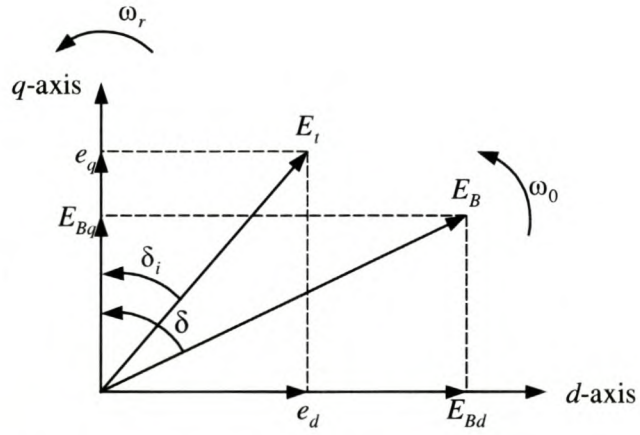

Fig. 3.3: Axis representation of system voltages and angles

and is a function of the exciter output voltage E_{fd} and rotor angle. This expression shows that rotor angle affects the field flux linkage, but only after a delay. As with K_1 and K_2, the parameters K_3, K_4 and T_{3fd} (Eqs (D.62) to (D.64)) are system characteristic and condition dependent and aid in the analysis of system stability. K_3 and T_{3fd} describe the field circuit transfer function, and K_4 the influence of $\Delta\delta$ on field flux linkage variations when $\Delta E_{fd} = 0$.

With the field voltage (exciter output voltage) assumed constant, Eqs (3.13) through (3.16) model the small-signal stability behaviour of the SMIB system without excitation control. These equations form part of the block diagram model of Fig. 3.6. The expressions for the state variables are rearranged in the state-space form:

$$p\Delta\delta = \omega_0 \Delta\omega_r \tag{3.17}$$

$$p\Delta\omega_r = \frac{1}{2H}\left(\Delta T_m - K_1\Delta\delta - K_2\Delta\psi_{fd} - K_D\Delta\omega_r\right) \tag{3.18}$$

$$p\Delta\psi_{fd} = \frac{1}{T_{3fd}}\left(-\Delta\psi_{fd} + K_3\left(\Delta E_{fd} - K_4\Delta\delta\right)\right) \tag{3.19}$$

These expressions form part of the system state-space model of Eq. (3.24).

3.3.2 Excitation system

Constant field voltage (exciter output voltage) implies $\Delta E_{fd} = 0$. Analysis of the system without excitation control gives valuable information regarding inherent machine stability [13]. The influence of excitation control on the damping of system oscillations is mostly negative [2][12]. It is this negative damping of system oscillations that needs to be counterattacked by adding damping support in the system.

Fig. 3.4 shows a typical functional block diagram of the generator excitation control system.

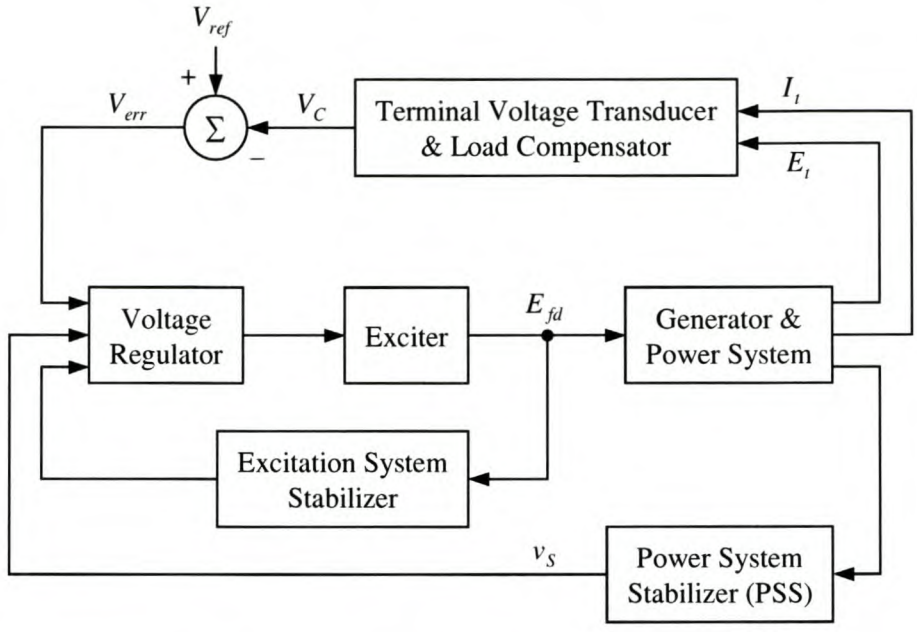

Fig. 3.4: Functional block diagram for generator excitation control system

Voltage regulator and exciter

A thyristor type excitation system is considered. The reason for this is two-fold: (a) it is a mathematically simple excitation system model – a gain K_A models the voltage regulator, and a single time constant T_A the exciter [2][19]; (b) thyristor excitation systems are very popular in the case of hydro units [21].

This report focuses on the need for damping, and the ability to provide such damping support given a particular system circumstance. According to references [2] and [60] pp.765, a higher gain exciter introduces more negative damping torque into the system, thus aggravating system stability more. This creates a worse case scenario for needed damping support. Ref. [60] pp.765 suggests an exciter gain of about 200. Ref. [2] suggests the gain K_A to be equal to or less than $T'_{d0}/2T_A$, with T'_{d0} the machine *d*-axis (transient) open-circuit time constant. Therefore, with $T_A = 0.02$ seconds (suggested in Refs [20], [24] and [71]) and T'_{d0} given in Appendix B, K_A should be 200 or less. The value of 200 is used. The influence of this assumption for K_A on results will be discussed later in this report, in sections 3.8.5, 4.6.5 and 5.8.5.

Excitation system stabilizer

An excitation system stabilizer is generally employed to ensure stable off-line operation, although for high initial response excitation systems such stabilization is normally not required [19][26]. The exciter time constant is quite small (see discussion above); hence no stabilization by feedback or TGR of the excitation system is modelled.

Neglecting TGR also creates a worse case scenario for the following reasons:

- TGR is used to reduce the voltage regulator gain at high frequencies to *minimize* the negative contribution of the regulator to system damping [19].
- TGR on the excitation system without PSS improves local mode damping but decreases inter-area mode damping [25].

This report focuses on the damping of local mode oscillations, and a worse case scenario is desirable from the view of system damping enhancement. Also, when TGR is neglected an increase in oscillation stabilizer gain improves damping as well as transient stability. In contrast, for the scheme with TGR increasing stabilizer gain results in a deterioration of transient stability.

Power system stabilizer

Chapter 4 considers stabilization of the system by a PSS.

Terminal voltage transducer and load compensator

For many systems, the voltage transducer time constant is very small [19]. It is therefore neglected.

Refs [60] pp. 335-337 and [19] identify the following situations to use load compensation:

1. When generators are bussed together at their terminals, sharing a common step-up transformer.
2. When a single unit is connected through significant impedance to the system.

The first scenario is beyond the scope of this research. Only the case of a single machine is considered. The second scenario appears feasible as the influence of external system impedance on system damping performance is investigated (sections 3.8, 4.6 and 5.8), and the effect of considerable impedance (signifying a weak system) is also considered. However, for the purpose of results comparison, all analyses are based on the same assumptions. The excitation system control is assumed such as to regulate the machine

terminal voltage at a constant predefined value (in this research, 1.0 p.u.). Therefore, load compensation is not considered.

Fig. 3.5 shows the resultant generator excitation system, used throughout this report.

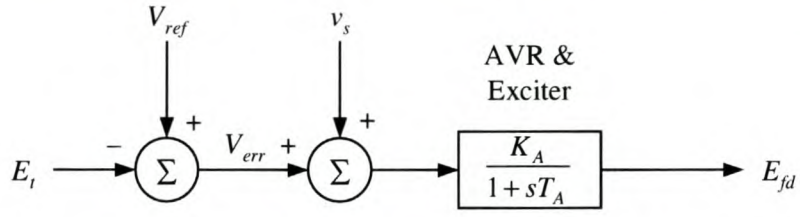

Fig. 3.5: Generator excitation control system

This chapter focuses on the need for damping support, in a system without added power oscillation stabilizers. Therefore, the PSS output voltage v_s is set to zero. Chapter 4 considers the SMIB system with PSS.

The expression

$$E_{fd} = \frac{K_A}{1+sT_A}(V_{ref} - E_t). \tag{3.20}$$

expresses Fig. 3.5 mathematically. Appendix D derives the terminal voltage in linear form as:

$$\Delta E_t = K_5\Delta\delta + K_6\Delta\psi_{fd} \tag{3.21}$$

The direct effect of rotor angle on terminal voltage is described by the coefficient K_5. K_6 defines the sensitivity of E_t to variations in field flux linkage . Eqs (D.65) and (D.67) express K_5 and K_6 as functions of system impedance and loading condition.

The small perturbation form of the exciter output voltage (3.20) is

$$\Delta E_{fd} = \frac{K_A}{1+sT_A}(\Delta V_{ref} - (K_5\Delta\delta + K_6\Delta\psi_{fd})). \tag{3.22}$$

ΔE_t is replaced by Eq. (3.21). Eq. (3.22) forms part of the block diagram model of Fig. 3.6, and can be rearranged to give

$$p\Delta E_{fd} = \frac{1}{T_A}(-K_A(K_5\Delta\delta + K_6\Delta\psi_{fd}) - \Delta E_{fd} + K_A\Delta V_{ref}). \tag{3.23}$$

This expression forms part of the state-space model of Eq. (3.24).

3.3.3 System state-space model and block diagram

Eq. (3.24) gives the state-space model of the SMIB system. The embellishment "˙" on the state variables signify differentiation to time, d/dt. The eigenvalues of the state matrix are a useful indication of the stability of the system (see section 3.2.2). The eigenvalue associated with the rotor angle oscillation mode is used as the complex frequency to evaluate the system damping torques (see section 3.7).

$$\begin{bmatrix} \Delta\dot{\omega}_r \\ \Delta\dot{\delta} \\ \Delta\dot{\psi}_{fd} \\ \Delta\dot{E}_{fd} \end{bmatrix} = \begin{bmatrix} \frac{-K_D}{2H} & \frac{-K_1}{2H} & \frac{-K_2}{2H} & 0 \\ \omega_0 & 0 & 0 & 0 \\ 0 & \frac{-K_3K_4}{T_{3fd}} & \frac{-1}{T_{3fd}} & \frac{K_3}{T_{3fd}} \\ 0 & \frac{-K_AK_5}{T_A} & \frac{-K_AK_6}{T_A} & \frac{-1}{T_A} \end{bmatrix} \begin{bmatrix} \Delta\omega_r \\ \Delta\delta \\ \Delta\psi_{fd} \\ \Delta E_{fd} \end{bmatrix} + \begin{bmatrix} \frac{1}{2H} & 0 \\ 0 & 0 \\ 0 & 0 \\ 0 & \frac{K_A}{T_A} \end{bmatrix} \begin{bmatrix} \Delta T_m \\ \Delta V_{ref} \end{bmatrix} \tag{3.24}$$

Fig. 3.6 shows the block diagram model. This model was first derived by Heffron and Phillips [1], and became known as the Phillips-Heffron model of the SMIB system. *This block diagram is a useful tool in understanding the performance of the system.* Expressions for torque contribution of the individual system elements are easily obtained using this block diagram.

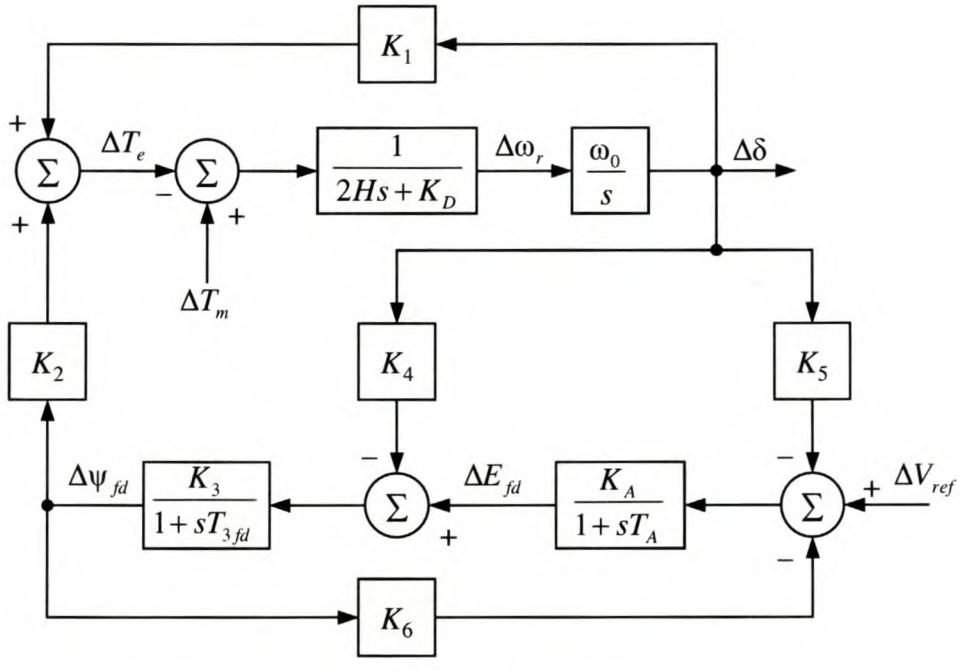

Fig. 3.6: Block diagram model of SMIB system

Sections 3.7 and 3.8 discuss the system synchronizing and damping torques and variation thereof with respect to changes in system characteristic or condition. These torques are functions of the system model K-parameters; hence the stability of the system depends on the signs of the parameters $K_1 \ldots K_6$ [12]. Section 3.6 investigates the effects of system impedance and generator loading – and assumptions made in the modelling process – on the parameters $K_1 \ldots K_6$.

3.4 Line Resistance and Local Load

This present section helps put the results of the analysis sections on the K-parameters and system performance into perspective. The concepts of line resistance, local load and the equivalent SMIB system are considered in more detail. The degree of series capacitive compensation influences the effective resistance to reactance ratio, R_E/X_E. Also, the amount of local load resistance alters both the system effective resistance and reactance, and the infinite bus voltage in the equivalent system model. These issues are considered in more detail.

3.4.1 SMIB system model

This investigation focuses on the presence of sufficient damping torque in the system, and follows the following pattern: (a) with constant E_t and E_B, evaluate the parameter under investigation for a certain system impedance and loading; (b) change the loading or impedance; (c) re-evaluate the parameter. The end-result is a set of plots that illustrate the variation of the parameter under consideration vs. variation in generator loading and external or system impedance.

The response of point load to sinusoidal variations in voltage and frequency [27] is not considered in this report. This investigation also does not consider reactive power load, to allow the block diagram model of section 3.3 to be used [28]. Therefore, a constant resistance models the local load, and load power varies directly with the square of the voltage magnitude [27]. Since oscillations in the local mode are also insensitive to the load model [32], this is appropriate. The local load voltage equals the generator terminal voltage (see Fig. 3.7). With constant E_t, the local load power P_{load},

$$P_{load} = \frac{E_t^2}{R_{load}}, \tag{3.25}$$

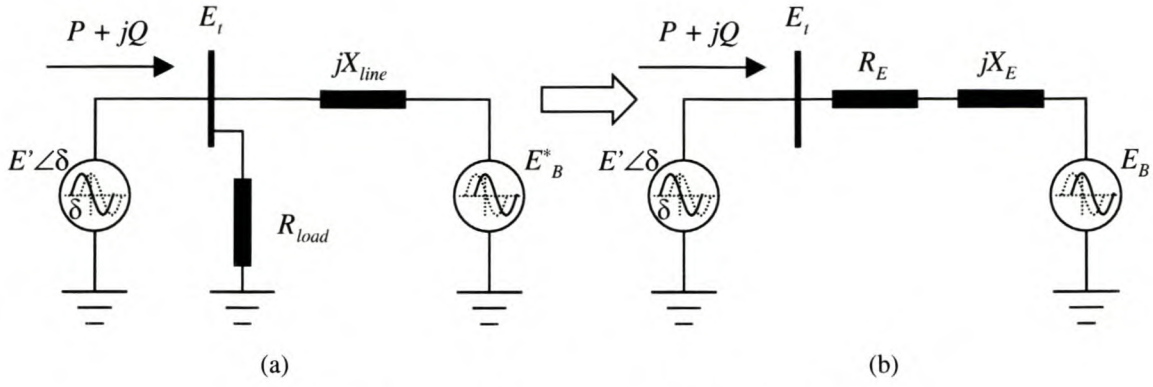

Fig. 3.7: Local load case and Thevenin equivalent

is constant for a constant local load resistance R_{load}.

Fig. 3.7 shows the case of the system with local load, and the equivalent series impedance configuration obtained by Thevenin transformation [2][13]. In Fig. 3.7(a) E_B^* is the infinite bus voltage of the system with local load, and X_{line} denotes line reactance. Fig. 3.7(b) shows the Thevenin equivalent representation, on which the state-space and block diagram models are based. The resistance

$$R_E = \frac{R_{load} X_{line}^2}{R_{load}^2 + X_{line}^2}, \tag{3.26}$$

and reactance

$$X_E = \frac{X_{line} R_{load}^2}{R_{load}^2 + X_{line}^2}, \tag{3.27}$$

define the equivalent impedance. The equivalent infinite bus voltage is

$$E_B = E_B^* \cdot \frac{R_{load}}{R_{load} + jX_{line}}. \tag{3.28}$$

E_B serves as a reference phasor for the line and rotor angles (see Fig. 3.3); hence only its magnitude (absolute value) is used in the calculations.

3.4.2 Line resistance scenario

Typically, the resistance to reactance ratio of a power line increases with power line construction from transmission to sub-transmission and distribution voltage levels. For example, in a 400 kV 50 Hz power line R_E/X_E is around 0.10 – 0.15 ([67] pp. 415, [73]). In

a 66 kV power line R_E/X_E varies between 0.35 and 0.70, depending on conductor type and bundling, and tower configuration.

Consider the case of a series capacitor implemented in the line. This reduces the effective series reactance, with a resultant increase in resistance to reactance ratio. As an example, consider a power line with $R_E/X_E = 0.4$ (characteristic of a 66 kV line). 50% reactance compensation increases R_E/X_E to 0.8:

$$\frac{R_E}{X_{E(new)}} = \frac{R_E}{X_{E(old)} \times 0.5} = \frac{0.4}{0.5} = 0.8$$

Similarly, 80% compensation effectively increases the resistance to reactance ratio to 2.0. This is a five-fold increase in R_E/X_E. For a transmission line with $R_E/X_E = 0.1$, 50% series reactance compensation doubles R_E/X_E to 0.2, and 80% compensation increases the effective R_E/X_E from 0.1 to 0.5. This illustrates the necessity to model external resistance: *an increase in the degree of series capacitive compensation causes an increase in* R_E/X_E. Separate sections throughout this report investigate how this influences system stability and stabilizer (PSS or CSC) performance.

3.4.3 Local load scenario

Consider the case of a SMIB system with negligible line resistance, but with significant local load at the generator end of the line such as Fig. 3.7(a) illustrates. Dividing Eq. (3.26) by (3.27) gives the following relation:

$$\frac{R_E}{X_E} = \frac{X_{line}}{R_{load}} \tag{3.29}$$

Eq. (3.29) indicates R_E/X_E increases by (a) increase of the local load (reduced R_{load}), (b) increase in transmission line length (larger X_{line}), or (c) a combination of the two. In this case adding fixed series compensation reduces X_{line} and hence also R_E/X_E. However, the influence on system stability and stabilizer performance is a complex function of both this and the variation in E_B with changes in R_{load} or X_{line} (Eq. (3.28)). Again, separate sections throughout this report investigate how this influences system stability and stabilizer performance.

3.5 Reactive Power Requirement

Section 3.4 discusses external system resistance and the factors that influence the ratio R_E/X_E. This present section continues on the discussion of section 3.4 by considering the influence thereof on system reactive power flow. The focus is on the reactive power support required of the synchronous generator, given a particular voltage gradient and active power transmission across the external system impedance. Section 3.5.1 discusses the familiar case of a SMIB system without external resistance. The principle of a symmetrical line and the reactive power flow is presented. Section 3.5.2 extends on these concepts by including resistance in the system.

3.5.1 No external resistance

Ref. [60] pp. 250-254 presents a discussion on the scenario of a lossless line. Fig. 3.8 shows a simplified view of a system with no external resistance. The power angle δ is used here for illustrative purposes, and is not to be confused with the rotor angle δ of section 3.3. The shunt capacitances of transmission lines do not explicitly appear in the model; their effects are implicitly represented by the net reactive power transmitted. This simplified analysis gives useful insight into the characteristics of ac transmission systems.

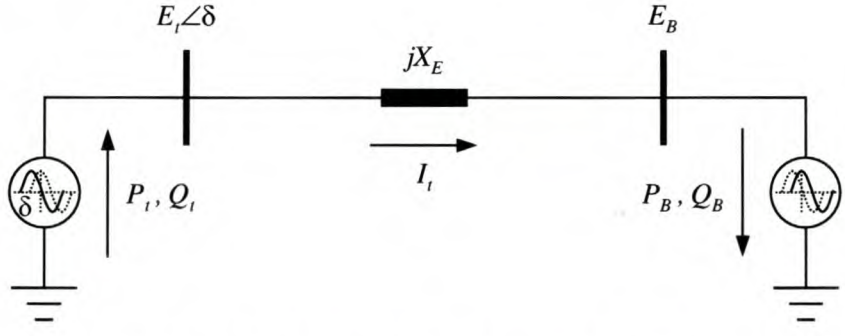

Fig. 3.8: SMIB system with no external resistance

By definition, a symmetrical line has equal sending- and receiving-end voltages ([62] pp. 70). This implies that $E_t = E_B$ in Fig. 3.8. Also, under load, (a) E_t leads E_B in phase, and (b) by symmetry, the power factor angle at one end of the line is the negative of the angle at the other end.

The levels of voltage and power transmission, as well as the line reactance, determine the reactive power required of the sending- and receiving-end sources. Consider first the case of a symmetrical line, with end-point voltages E. The relation

$$Q_t = -Q_B = \frac{E^2}{X_E}(1-\cos\delta) \tag{3.30}$$

relates the sending-end and receiving-end reactive powers (Fig. 3.8). This expression shows that, (a) the synchronous machine delivers positive reactive power regardless of the machine active power load (provided $\delta < 90°$), and (b) each end provides half the reactive power consumed by the line reactance when the system is symmetrical.

Transfer of reactive power from one line end to another requires a voltage gradient across the line. Flow is then from the side with higher voltage magnitude to the lower voltage side.

3.5.2 System with external resistance

This section extends the concepts of section 3.5.1 by including resistance in the equations. Section 3.4 describes resistance in a SMIB system as being either (a) line resistance, or (b) the resistance in a local load. A constant resistance models the local load, for reasons discussed.

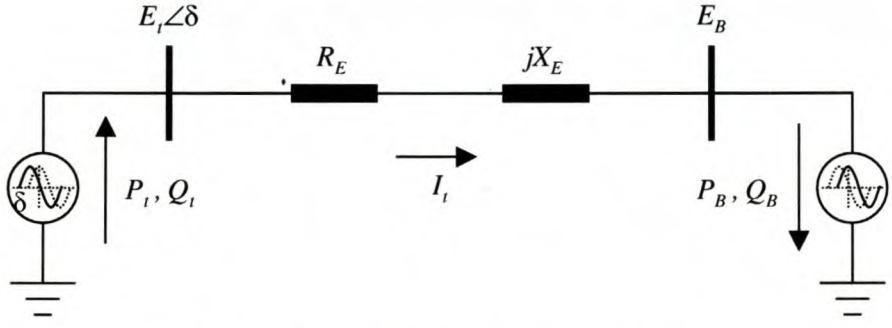

Fig. 3.9: SMIB system with external resistance

Fig. 3.9 shows a simplified view of a SMIB system with external resistance included. In the local load case, Fig. 3.9 represents the Thevenin equivalent circuit of Fig. 3.7(b). As with the case without external resistance (section 3.5.1), the power angle δ is used here for illustrative purposes, and is not to be confused with the δ of section 3.3.

From Fig. 3.9, the apparent power at the receiving (infinite bus) end is

$$S_B = P_B + jQ_B = \tilde{E}_B \tilde{I}_t^* = \tilde{E}_B \left(\frac{\tilde{E}_t - \tilde{E}_B}{R_E + jX_E} \right)^{*}. \tag{3.31}$$

P_B is the active power *towards* the infinite bus, and I_t the line current. The embellishment "~" implies voltages and current in this expression are complex phasors. With E_B the

reference phasor, $\tilde{E}_t = E_t e^{j\delta} = E_t \cos\delta + jE_t \sin\delta$, and the real and reactive powers at the receiving end are

$$P_B = \frac{E_B(E_t X_E \sin\delta + E_t R_E \cos\delta - E_B R_E)}{R_E^2 + X_E^2}, \tag{3.32}$$

$$Q_B = -\frac{E_B(E_t R_E \sin\delta - E_t X_E \cos\delta + E_B X_E)}{R_E^2 + X_E^2}. \tag{3.33}$$

Similarly the sending-end real and reactive powers are

$$P_t = \frac{E_t(E_B X_E \sin\delta - E_B R_E \cos\delta + E_t R_E)}{R_E^2 + X_E^2}, \tag{3.34}$$

$$Q_t = -\frac{E_t(E_B R_E \sin\delta + E_B X_E \cos\delta - E_t X_E)}{R_E^2 + X_E^2}. \tag{3.35}$$

These equations describe the way active and reactive power is transferred between active ends of a network characterized by an impedance $Z_E = R_E + jX_E$. The following discussion focuses on the influence of voltage magnitudes and the angle δ on the sending- and receiving-end active and reactive power flows.

Difference in voltage magnitudes

To consider the effect of voltage gradient on the power flows, assume $\delta = 0$. Eqs (3.32) to (3.35) then reduce to

$$\begin{aligned} P_B &= \frac{E_B R_E(E_t - E_B)}{R_E^2 + X_E^2} & Q_B &= \frac{E_B X_E(E_t - E_B)}{R_E^2 + X_E^2} \\ P_t &= \frac{E_t R_E(E_t - E_B)}{R_E^2 + X_E^2} & Q_t &= \frac{E_t X_E(E_t - E_B)}{R_E^2 + X_E^2} \end{aligned} \tag{3.36}$$

The transmission of active power from the sending end to the receiving end is still possible even with $\delta = 0$, provided a voltage rise or drop (voltage gradient) exists across the line. In the case of a system with local load, a voltage *drop* will always exist across the line, as Eq. (3.28) appears to indicate. Table 3.1 gives the values of E_B evaluated for systems with local load. Notice $E_B < 1.0$ (and hence $< E_t$) for all values of local load. Eq. (3.36) gives the active power contribution by each end of the line to support the local load.

A voltage gradient is also essential for the transfer of reactive power. With $E_t > E_B$, both Q_t and Q_B is positive and $Q_t > Q_B$; in other words, reactive power is transmitted from the sending end to the receiving end and partly absorbed by the line reactance. Fig. 3.10(a) shows the corresponding phasor diagram. The opposite is true when $E_B > E_t$ (a voltage rise): then both Q_t and Q_B is negative, and reactive power is transmitted from the receiving end to the sending end. Fig. 3.10(b) shows the corresponding phasor diagram.

Fig. 3.10 illustrates the following:

1. Transmission of lagging current through an inductive impedance causes a voltage drop in the receiving-end voltage.
2. Transmission of leading current through an inductive impedance causes a voltage rise in the receiving-end voltage.

In each case, the line reactance consumes the reactive power difference between the line end-points:

$$Q_t - Q_B = \frac{(E_t - E_B)^2 X_E}{R_E^2 + X_E^2}. \tag{3.37}$$

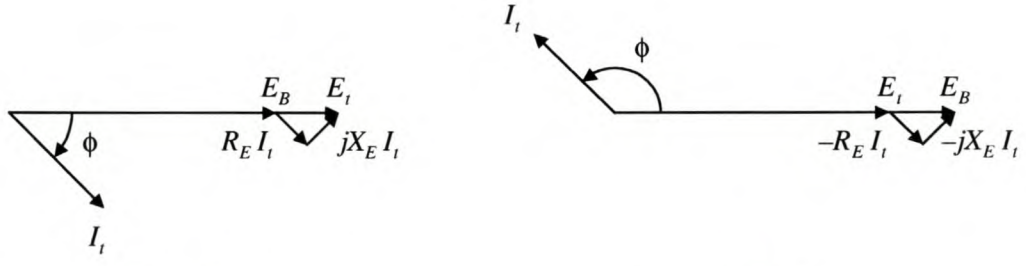

(a) $E_t > E_B$ (b) $E_B > E_t$

Fig. 3.10: Phasor diagrams with $\delta = 0$

Difference in voltage angles

To consider the effect of $\delta \neq 0$ on the power flows, assume $E_t = E_B = E$. In the system with resistance neglected (section 3.5.1), this constitutes a symmetrical line case: no reactive power is transferred from one end to another; instead, each end provides half the reactive power consumption of the line.

For the system of Fig. 3.9 with external resistance, Eqs (3.32) to (3.35) reduce to

$$P_B = \frac{E^2(X_E \sin\delta + R_E \cos\delta - R_E)}{R_E^2 + X_E^2} \qquad Q_B = -\frac{E^2(R_E \sin\delta - X_E \cos\delta + X_E)}{R_E^2 + X_E^2}$$
$$P_t = \frac{E^2(X_E \sin\delta - R_E \cos\delta + R_E)}{R_E^2 + X_E^2} \qquad Q_t = -\frac{E^2(R_E \sin\delta + X_E \cos\delta - X_E)}{R_E^2 + X_E^2} \tag{3.38}$$

With δ positive, active power flows from the sending end to the receiving end. If R_E is high compared to X_E, P_B may be negative. Active power then flows from both the sending and receiving ends.

By definition, this scenario with $E_t = E_B$ is a symmetrical case, though it is clear from Eq. (3.38) that the reactive support from the line ends are no longer equally divided (compare (3.30) for the no resistance scenario). Rewrite Q_B and Q_t in (3.38) as follows:

$$-Q_B = \frac{E^2 X_E(1-\cos\delta)}{R_E^2 + X_E^2} + \frac{E^2 R_E \sin\delta}{R_E^2 + X_E^2}$$
$$Q_t = \frac{E^2 X_E(1-\cos\delta)}{R_E^2 + X_E^2} - \frac{E^2 R_E \sin\delta}{R_E^2 + X_E^2} \tag{3.39}$$

Observation: a larger δ increases the influence of line resistance R_E on the reactive powers Q_t and Q_B. An increase in R_E or decrease in X_E (see section 3.4.2) reduces the reactive power flow from the sending end (Q_t less positive). The reactive power "support" of the synchronous machine can even become negative with significant R_E. The machine then acts as a sink of reactive power, rather than a source of it. For reasons discussed in [62] pp. 65-67, the reactive power absorption capability of synchronous generators are normally limited to 0.45 p.u. of the MVA rating. The use of shunt inductive compensation can help alleviate this problem and allow the synchronous generator to be more effective to provide continuous reactive power support to the system.

An increase in R_E increases the reactive power flow $-Q_B$ from the receiving end of the line. A decrease in X_E (see section 3.4.2) reduces $-Q_B$.

In conclusion:

1. The reactive power output of the synchronous machine can be positive or negative.
2. Line voltages, the amount of real power transmitted, as well as the effective resistance and reactance influence the generator reactive power load. The impedance resistance to

reactance ratio dictates how much each end of the line provides to the line reactive power consumption. An increase in R_E results in increased reactive power support from the external system, while the synchronous generator reactive power support reduces to the point the machine absorbs reactive power.

The external large system is assumed strong and able to provide the necessary reactive power and keep E_B constant.

The analysis in this and the previous section presented an analytical discussion on resistance in the SMIB system. The following and other sections in this report discuss the influence of line reactance, local load, etc. on the block diagram model as well as the stability performance of the system. The discussion on resistance aimed to put the results obtained by simulation in perspective.

3.6 *K*-constants Analysis

Fig. 3.6 portrays the SMIB system as a function of the system *K*-parameters. Sections 3.7 and 3.8 discuss the system synchronizing and damping torques and variation thereof with respect to changes in generator loading or network structure (impedance). These torques are functions of the system model *K*-parameters; the stability of the system depends on the signs of the constants $K_1 \ldots K_6$ [12], hence the significance of investigating the trends of the *K*-parameters. This is the focus of this section: to know the effects of network structure and loading – and assumptions made in the modelling process – on the parameters $K_1 \ldots K_6$. Ref. [12] gives results in this regard, albeit under different assumptions and method of analysis.

Results from section 3.8 indicate the system damping and synchronizing torques are most influenced by the parameters K_1, K_4 and K_5. The discussions focus more on these parameters. The parameters K_2, K_3 and K_6 are mentioned only briefly in this section.

The following section discusses the analysis procedure of Ref. [12], and that used in this research. Sections 3.6.2 to 3.6.4 investigate the influence of machine loading and system reactance and resistance on the *K*-parameters by MATLAB simulation. Machine saturation is modelled. Section 3.6.5 discusses the effect of neglecting saturation on results. In the concluding summary, attention is drawn to where results differ from previous research on this subject.

3.6.1 Analysis procedure

Previous research [12] plotted graphs for K_1, K_2, $K_4 \ldots K_6$ vs. P_t, for various values of machine reactive power load Q_t and a constant external impedance. K_3 was excluded since machine saturation was neglected. There is no definite mention of assumptions, especially pertaining to the machine terminal and infinite bus voltages. The control of Q_t at a fixed value suggests that either E_t and E_B was allowed to vary ([60] pp. 746). Reproduction of the results of [12] shows with E_t constant, E_B may be as low as 0.7 p.u. for some of the conditions considered in that paper.

The research presented in this report assumes both end-point voltages constant at unity. Section 3.5 discusses the implications of this assumption. No control is placed on the machine reactive load, and as a result Q_t can become negative (machine a sink of reactive power – see Eq. (3.39)), particularly as the external effective resistance increases.

With E_t and E_B constant at 1.0 p.u., plots of $K_1 \ldots K_6$ vs. generator load, for various X_E, line R_E/X_E, and R_{load}, are generated by MATLAB simulation. Cases considered are as follows (values in p.u.):

X_E = 0.2, 0.4, 0.8

R_E/X_E = 0.1, 0.4, 0.7, with X_E as above

R_{load} = 5.0, 2.0, 1.0, with X_E as above

X_E represents the total external series reactance, comprising both transformer reactance and line reactance. According to Ref. [1] $X_E = 0.8$ p.u. is an unusually high value for external reactance. It is such high values of external reactance that pose a problem to stability.

The values of R_E/X_E were chosen in accordance with values in Refs [67] pp. 415 and [73]. 0.1 is the ratio typical of transmission level voltages, while 0.4 and 0.7 represent sub-transmission (132-220 kV) and distribution level (66 kV) voltages.

Appendix B describes the test system used to obtain results.

3.6.2 Machine load and line reactance

This section neglects system external resistance. This simplifies analysis and results are typical of the case where a power source is connected to a large system through high voltage transmission line(s), with no or negligible local load.

Fig. 3.11 shows plots of the trends of the K-parameters with respect to changes in machine load and external reactance. The following discussion focuses on each K-parameter plot individually. Where appropriate, the expression for the K-parameter (see Appendix D.6) is investigated to verify or explain results.

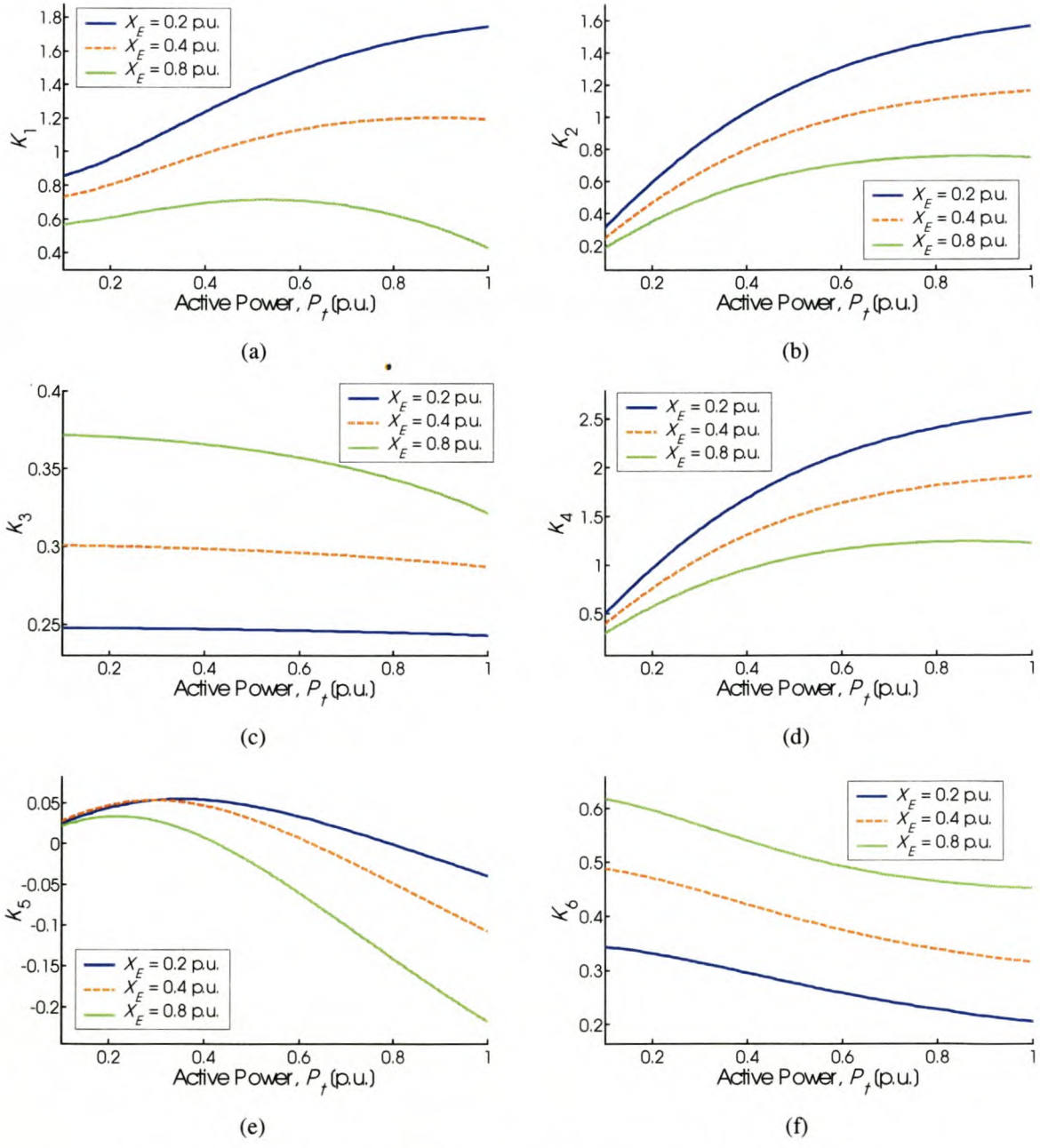

Fig. 3.11: Parameters $K_1 \ldots K_6$ vs. machine load and external reactance

Fig. 3.11(a): K_1 increases as P_t increases, reaches a maximum, and decreases with any further increase in P_t. K_1 is also larger in a stronger system (smaller X_E). K_1 is termed the transient synchronizing torque (section 3.7.2) and has a dominant influence on the system synchronizing torque (sections 3.7.5 and 3.8).

It is possible for K_1 to be negative. Fig. 3.12(a) illustrates the scenario of very high X_E (very weak system) with relative high loading. This situation of negative K_1 is of academic rather than practical importance [2]. It is included here for thoroughness.

With external resistance neglected and noticing that the per unit armature resistance R_a is significantly smaller than machine per unit reactances (Table B.1), the expression for K_1 (Eq. (D.60)) reduces to

$$K_1 = \frac{E_B E_{q0}}{D} X_{Td} \cos\delta_0 + \frac{E_B i_{q0}}{D}\left(X_q - X'_d\right) X_{Tq} \sin\delta_0 . \tag{3.40}$$

The parameters in this expression are defined in Appendix D. When X_E is very large and generator load relatively high, δ_0 approaches and possibly exceeds 90°. Fig. 3.12(b) shows this angle. Now, $\cos\delta_0 \approx 0.0$ at high δ_0, and is negative with $\delta > 90°$. As a result the first term of Eq. (3.40) is more negative than the second term is positive; consequently K_1 is negative.

Fig. 3.11(b): K_2 increases as P_t increases and/or system strength increases.

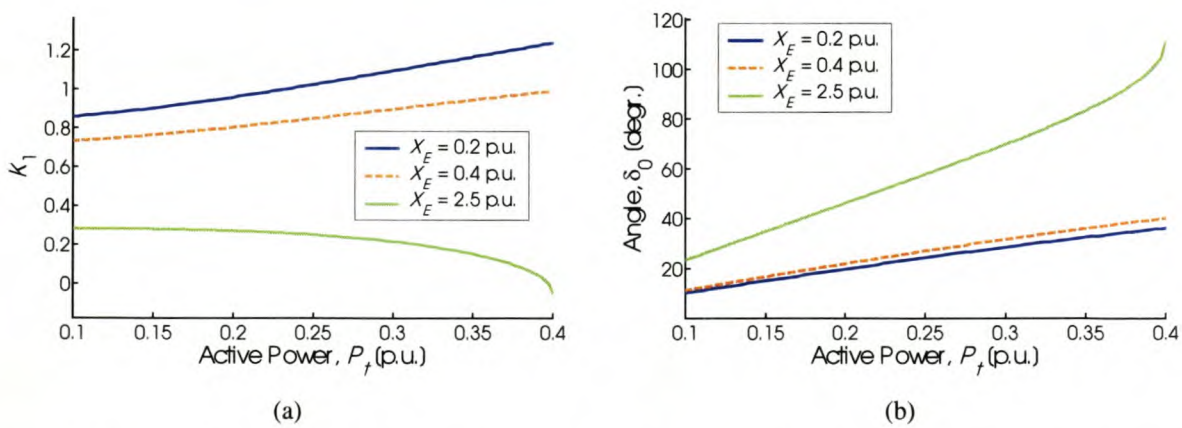

Fig. 3.12: K_1 and rotor angle δ_0 vs. machine load and external reactance – influence of very long ties

Fig. 3.11(c): K_3 decreases with increase in machine load, particularly in a system with higher X_E. This can be attributed to machine saturation. Section 3.6.5 discusses the influence of saturation on K_3 in more depth. K_3 decreases as system strength increases.

Fig. 3.11(d): K_4 increases as P_t increases and/or system strength increases. K_4 has a direct influence on the field circuit damping and synchronizing torques. Sections 3.7.3 and 3.8 discuss this.

Fig. 3.11(e): K_5 is positive and increases as P_t increases from zero, reaches a maximum, and decreases becoming negative with any further increase in P_t. K_5 is also more positive in a stronger system.

With external resistance and R_a neglected (see discussion on K_1), the expression for K_5 (Eq. (D.65)) reduces to

$$K_5 = \frac{e_{d0}}{E_{t0}} X_q \left(\frac{X_{Td} E_B \cos\delta_0}{D} \right) - \frac{e_{q0}}{E_{t0}} X'_d \left(\frac{X_{Tq} E_B \sin\delta_0}{D} \right). \tag{3.41}$$

δ_0 increases as P_t increases. Consequently, $\cos\delta_0$ decreases from 1.0 and $\sin\delta_0$ increases from zero as P_t increases. Initially $\cos\delta_0 > \sin\delta_0$, the first term in Eq. (3.41) dominates and K_5 is positive. With further increase in P_t, $\sin\delta_0$ increases and $\cos\delta_0$ decreases, the second term in (3.41) starts to dominate and K_5 is negative for moderate to high P_t.

K_5 has a direct influence on the damping and synchronizing torques attributed to the excitation system. Sections 3.7.4 and 3.8 discuss this in detail.

Fig. 3.11(f): K_6 decreases as P_t increases and/or system strength increases.

The parameters K_2 and K_6 (rather, $1/K_6$) play a significant role in the ability of PSS to provide damping (this in a system with negligible line resistance or local load). The discussion in section 4.6.2 focuses on this in more detail.

3.6.3 Line resistance

Section 3.6.2 neglected system external resistance to simplify analysis and obtain results typical to the case where a power source is connected to a large system through high voltage transmission line(s), with no or negligible local load. This present section focuses on the influence of line resistance on the system model *K*-parameters.

Fig. 3.13 shows plots of the trends of the parameters K_1, K_4 and K_5 with respect to changes in machine load and line R_E/X_E, when $X_E = 0.8$ p.u. The following discussion focuses on each K-parameter plot individually (plots for other parameters and other X_E in Appendix E.1).

Fig. 3.13(a): K_1 decreases as R_E/X_E increases when the machine is lightly loaded. At moderate to high loading K_1 initially increases then decreases with increase in R_E/X_E.

The parameters K_2, K_3 and K_6 all increases with increase in R_E/X_E.

Fig. 3.13(b): K_4 increases as R_E/X_E increases when the machine operates into a strong system. This tendency reverses with reduction in system strength (larger X_E) and/or machine load.

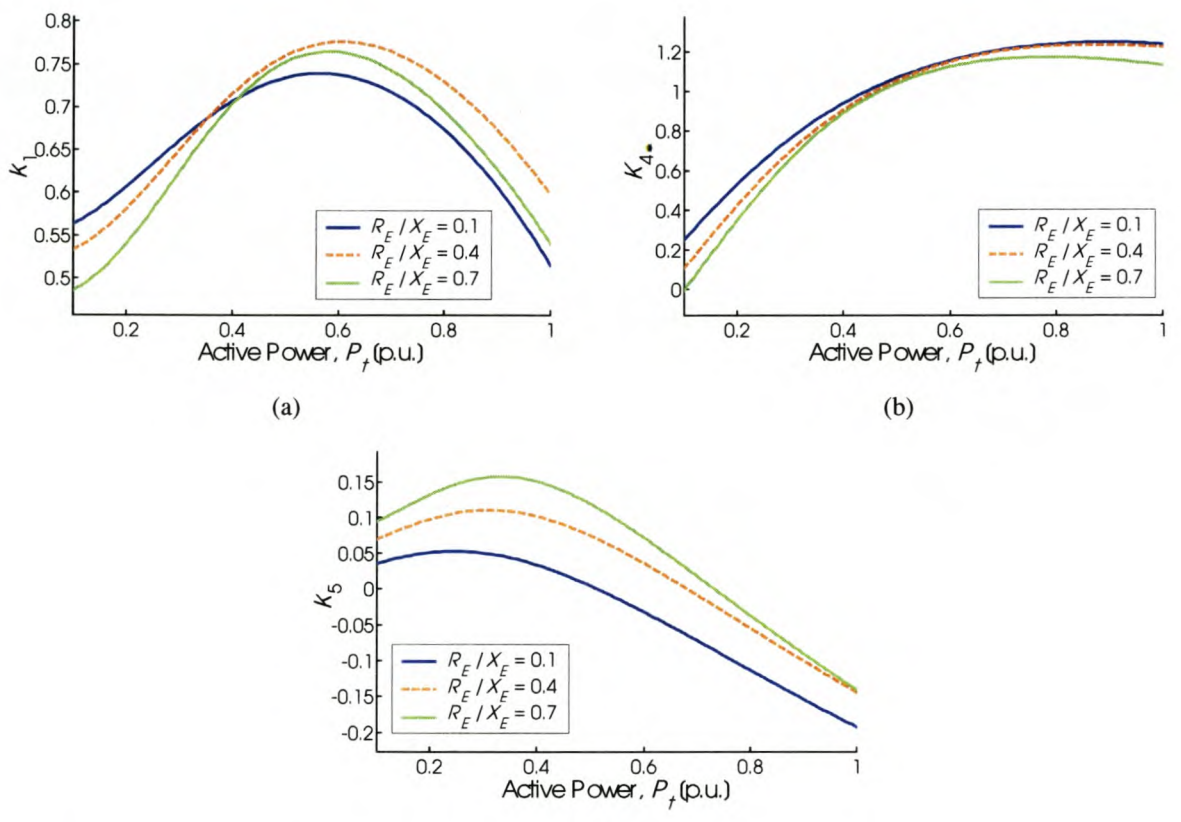

Fig. 3.13: Parameters K_1, K_4 and K_5 vs. machine load and line resistance, with $X_E = 0.8$ p.u.

Fig. 3.14(a) shows the parameter K_4 in the very low P_t region, with $X_E = 0.8$ p.u. Observation: K_4 changes its sign from positive to negative when the generator operates at light load into a weak system with large R_E/X_E. The expression for K_4 (Eq. (D.64)) is reproduced below:

$$K_4 = L_{adu}\frac{L_{ads}}{L_{ads}+L_{fd}}\frac{E_B}{D}X_{Tq}\sin\delta_0 - L_{adu}\frac{L_{ads}}{L_{ads}+L_{fd}}\frac{E_B}{D}R_T\cos\delta_0 \tag{3.42}$$

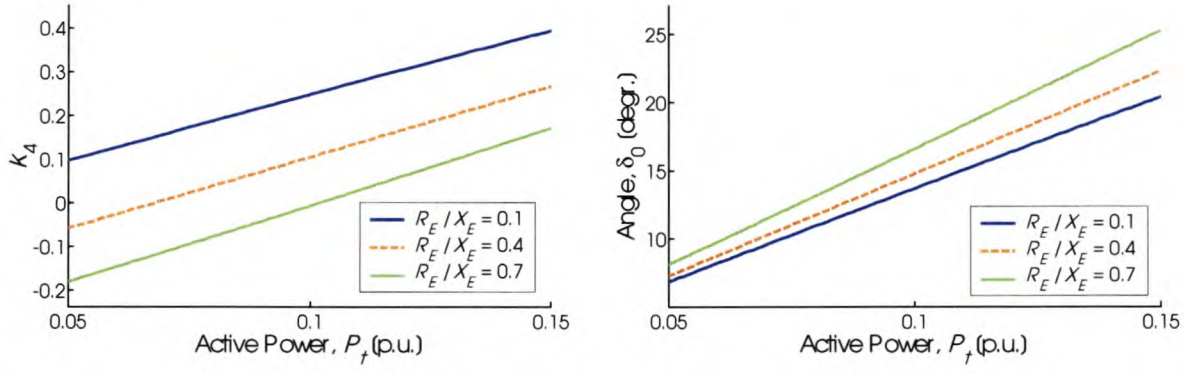

(a) (b)

Fig. 3.14: K_4 and rotor angle δ_0 at low P_t, with $X_E = 0.8$ p.u.

At low P_t, δ_0 is small (Fig. 3.14(b)) and $\cos\delta_0 > \sin\delta_0$. As a result, the second term in Eq. (3.42) dominates over the first term when R_E/X_E is large; hence K_4 is negative. This has significance for the armature reaction damping torque contribution. See discussion on Fig. 3.24(b).

Fig. 3.13(c): K_5 increases as R_E/X_E increases. This has significance for the damping stability of the excitation system and the system as a whole (section 3.8.3).

3.6.4 Local load

This section discusses the influence of local load on the system model *K*-parameters. It is observed that the influence of local load on the *K*-parameters in some cases affect the trends described in section 3.6.2. Where appropriate reference to this fact will be made.

For reasons discussed in section 3.4.1, a resistance R_{load} models the local load. Table 3.1 gives the X_{line} and R_{load} value combinations used in the investigation, and the resulting X_E, R_E and E_B values from which the system parameters are determined (see discussion on Fig. 3.7). A reduction in R_{load} constitutes an increase in the local load active power

consumption P_{load}. The term "local load" is used to describe variations in P_{load}; hence an increase in local load signifies an increase in local load active power consumption.

Fig. 3.15 shows plots of the trends of the parameters K_1, K_4 and K_5 with respect to changes in machine load and local load resistance, when $X_{line} = 0.8$ p.u. The following discussion focuses on each K-parameter plot individually (plots for other parameters and other X_{line} in Appendix E.2).

Table 3.1: Equivalent system resistance, reactance and infinite bus voltage values

X_{line} [p.u.]	R_{load} [p.u.] (P_{load} [p.u.])	X_E [p.u.]	R_E [p.u.]	E_B [p.u.]
0.2	5.0 (0.2)	0.1997	0.0080	0.9992
	2.0 (0.5)	0.1980	0.0198	0.9950
	1.0 (1.0)	0.1923	0.0385	0.9806
0.4	5.0 (0.2)	0.3975	0.0318	0.9968
	2.0 (0.5)	0.3846	0.0769	0.9806
	1.0 (1.0)	0.3448	0.1379	0.9285
0.8	5.0 (0.2)	0.7800	0.1248	0.9874
	2.0 (0.5)	0.6897	0.2759	0.9285
	1.0 (1.0)	0.4878	0.3902	0.7809

Results show that the presence of a local load has little or no influence on the values of $K_1 \ldots K_4$ when the generator operates into a strong system, such as with $X_{line} = 0.2$ p.u. K_5 and K_6 are exceptions.

Fig. 3.15(a): K_1 increases as the local load is increased.

K_2 and K_6 increases with increase in local load, whereas K_3 decreases. Local load affects the trend of K_3 with respect to P_t – a large local load causes K_3 to increase with an increase in P_t, reach a maximum and then decrease with any further increase in machine load.

Fig. 3.15(b): K_4 decreases as local load increases, to such an extent that it changes its positive sign under low P_t conditions – here K_4 is even more negative with increase in line reactance.

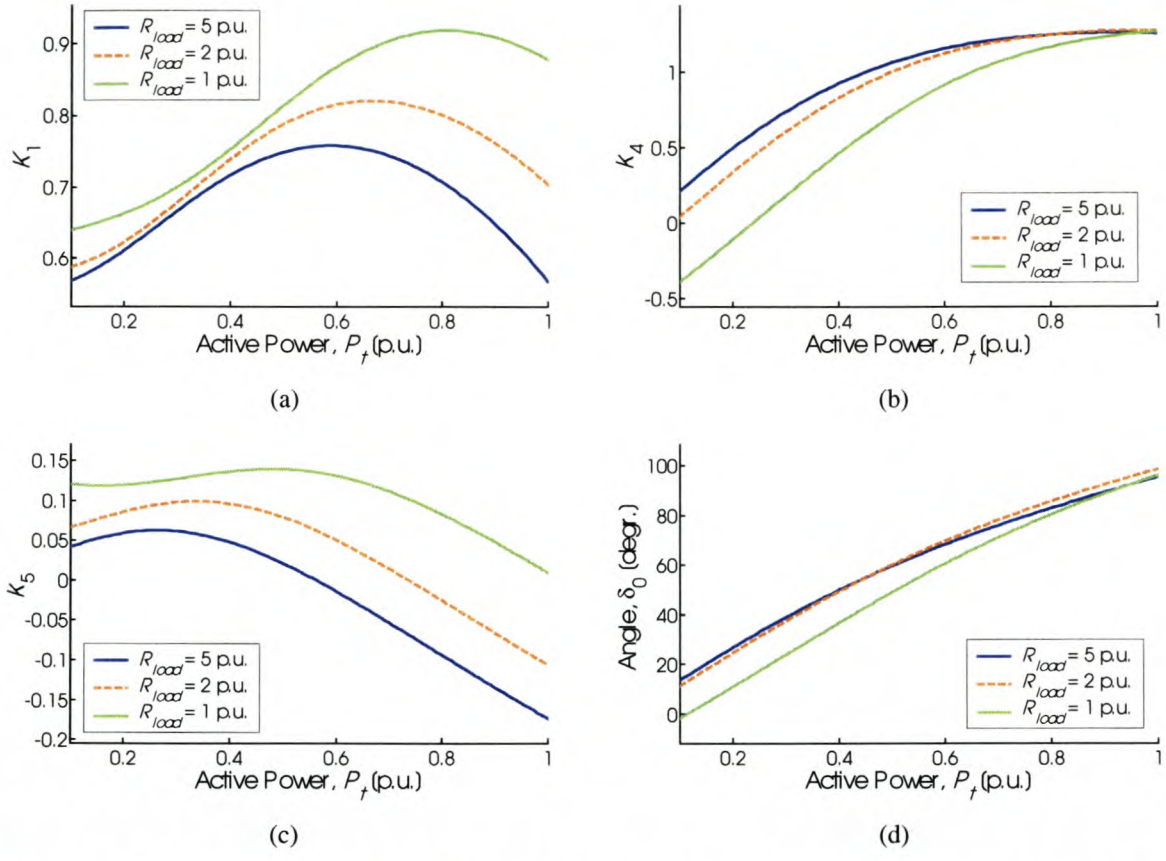

Fig. 3.15: Parameters K_1, K_4 and K_5 vs. machine load and local load resistance, with X_{line} = 0.8 p.u.

The expression for K_4 (Eq. (D.64)) is reproduced below:

$$K_4 = L_{adu}\frac{L_{ads}}{L_{ads}+L_{fd}}\frac{E_B}{D}X_{Tq}\sin\delta_0 - L_{adu}\frac{L_{ads}}{L_{ads}+L_{fd}}\frac{E_B}{D}R_T\cos\delta_0 \tag{3.43}$$

Fig. 3.15(d) shows the rotor angle δ_0 is very small at low P_t, and even negative when feeding a significant local load. As a result, $\cos\delta_0 \approx 1.0$ and $\sin\delta_0 \approx 0.0$ or even negative. The second term in Eq. (3.42) dominates the first term (which can even be negative), and K_4 is negative.

Fig. 3.15(c): K_5 increases as the local load is increased. Increase in local load has an opposite effect to that of increased line reactance. Fig. 3.16 shows K_5 as a function of machine load and line reactance, with $R_{load} = 1.0\,\text{p.u}$. With significant local load K_5 decreases as X_{line} decreases. Compare Fig. 3.11(e). Notice that, regardless of P_t or X_{line}, K_5 remains positive when the machine feeds a large local load.

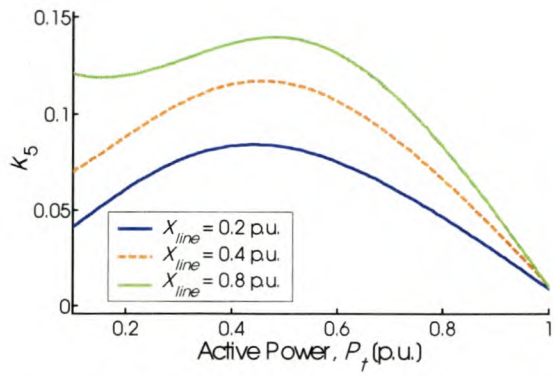

Fig. 3.16: Parameter K_5 vs. machine load and line reactance, when R_{load} = 1.0 p.u.

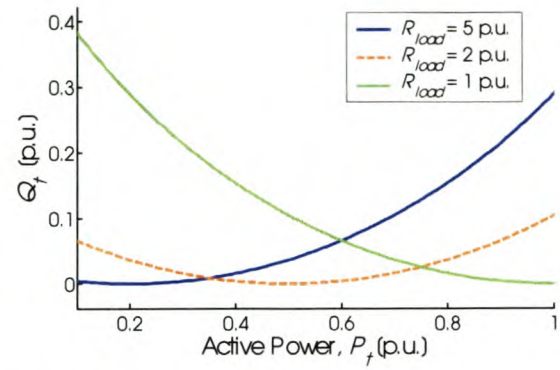

Fig. 3.17: Machine reactive load Q_t vs. machine load and local load resistance, with X_{line} = 0.8 p.u.

Fig. 3.17 shows the generator reactive power loading vs. generator active power load and local load resistance. With increased local load, the reactive loading on the generator increases as the generator active power decreases. The generator approaches synchronous condenser operation. Section 3.8.4 discusses the implication of this on system damping.

3.6.5 Influence of saturation

Synchronous machine saturation was modelled to obtain the results of the previous sections. Appendix C explains the modelling of saturation in the synchronous machine. This section considers the influence of neglecting saturation, often the assumption in literature. Results for the previous sections were regenerated for the system of Appendix B with machine saturation neglected (constant machine inductances/reactances). Appendix E.3 contains the results.

Neglecting machine saturation influences the results of *machine load and external reactance* (section 3.6.2), *line resistance* (section 3.6.3) and *local load* (section 3.6.4) as follows:

1. K_1 values are lower when machine saturation is not modelled.
2. The parameters K_2 through K_6 are all larger in value.

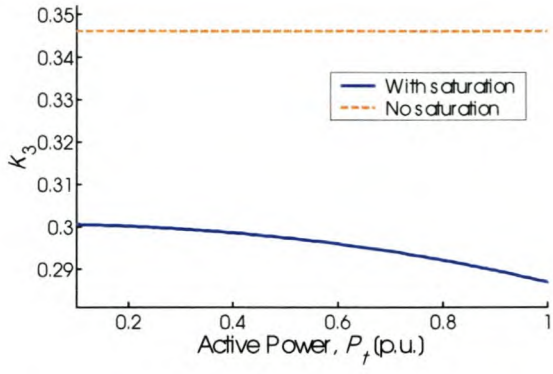

Fig. 3.18: K_3 vs. P_t, with and without saturation; X_E = 0.4 p.u.

Neglecting saturation effect does not influence the trends of K_1, K_2, K_4, K_5 and K_6 with respect to machine load P_t, nor does it influence the trends of all the K-parameters with respect to X_E, R_E/X_E or R_{load}. It is, however, necessary to model machine saturation to obtain the correct values and trends of K_3 with respect to P_t: without machine saturation, K_3 is constant regardless of P_t. Fig. 3.18 illustrates this, with $X_E = 0.4$ p.u. and no external resistance.

Literature often disregards the influence of saturation [2][12][13]. When saturation is modelled, the assumption of constant K_3 regardless of P_t made in Ref. [12] is valid, as the deviation in K_3 with respect to P_t is small. However, K_3 is about 15% smaller in magnitude when saturation is considered, compared to when saturation is not modelled. For this reason it is considered necessary to model saturation.

Machine load influences K_3 indirectly through its influence on the saturation factor and hence the machine reactances/inductances:

$$K_3 = \frac{L_{ads} + L_{fd}}{L_{adu}} \left(1 + \frac{X_{Tq}}{D} \left(X_d - X'_d \right) \right)^{-1} \tag{3.44}$$

3.6.6 Summary of results

The trends of the system model K-parameters, with respect to *machine load and external reactance* (section 3.6.2), *line resistance* (section 3.6.3) and *local load* (section 3.6.4) were examined. The influence of *saturation modelling* on the results was also considered (section 3.6.5).

A summary of the results of section 3.6 follows. The trends are compared to results from previous investigations on the *K*-parameters of the SMIB system model.

K_1 increases as P_t increases, reaches a maximum, and decreases with any further increase in P_t. This result is also obtained in [12], particularly with low Q_t-output. K_1 is also larger in a stronger system (smaller X_E). This is true according to Ref. [2]. Results in [12] indicate K_1 is negative when feeding a local load with high generator Q_t-output. This report does not consider this scenario, as Q_t is not a controlled variable.

The variation of K_1 with respect to line resistance to reactance ratio depends on the machine load P_t. K_1 increases with increase in local load.

The value of K_1 has significant bearing on the system synchronizing stability. Sections 3.7.2 and 3.8 discuss this in more detail.

K_2 increases as P_t increases. This result was also obtained in [12]. The parameter K_2 also increases with increase in system strength [16]. K_2 increases with increase in either R_E/X_E or local load. When part of the local load is supplied by the external system, K_2 decreases as X_{line} decreases. K_2 remains positive for all conditions considered ([2], [12], [60] pp. 750).

The parameter K_2 influences the "plant" transfer function pertaining to the PSS controller of chapter 4, and hence PSS performance in the system with no external resistance Sections 4.4.1 and 4.6.2 discuss this in more depth.

How **K_3** varies when machine load P_t is increased, depends on the line reactance X_E (or X_{line}) and the presence or not of line resistance and local load. When machine saturation effect is neglected, K_3 is independent of P_t as stated also in Ref. [12]. Hence it is necessary to model saturation to get a correct indication of K_3 for a particular machine load P_t. K_3 decreases as system strength increases. K_3 increases with increase in R_E/X_E, but decreases with increase in local load. K_3 remains positive for all conditions considered ([60] pp. 750, [2]).

The coefficient K_3 is a field circuit parameter, and exerts only an indirect influence on the field flux linkage variations due to field voltage or rotor angle changes.

$\boldsymbol{K_4}$ increases as P_t increases. This result was also obtained in [12]. K_4 also increases with increase in system strength. The variation of K_4 with respect to R_E/X_E depends on the P_t and the line reactance. K_4 decreases with increase in local load.

In the case of large R_E/X_E or large local load, K_4 changes its sign from positive to negative when the generator operates at light load. This result was also obtained in Refs [12] and [13]. Under such conditions K_4 is even more negative in a weaker system (larger X_E or X_{line}) [13]. In practice, negative K_4 can be due to (a) a hydraulic generator without damper windings operating at light load through a line with high R_E/X_E to a large system ([60] pp. 752), or (b) in the case of a machine connected to a large local load that is also partly supplied by a remote large system [13]. Results show K_4 is negative when operating under such conditions.

The value of K_4 has significant bearing on the influence of armature reaction effect on the damping of oscillations. Sections 3.7.3 and 3.8 discuss this in more detail.

$\boldsymbol{K_5}$ is positive for low to medium P_t, and increases as machine load P_t increases from zero, reaches a maximum, and decreases becoming negative when P_t is high. K_5 also increases with increase in system strength (smaller X_E). Refs [2], [12] and [60] pp. 765-766 obtained this result. K_5 increases with increase in either R_E/X_E or local load. Significant local load has the ability to reverse the trend of K_5 with respect to increase/decrease in external reactance.

The value of K_5 has significant bearing on the influence of excitation control effect on the damping of oscillations. Sections 3.7.4 and 3.8 discuss this in more detail.

$\boldsymbol{K_6}$ decreases as P_t increases. This result was also obtained in Refs [2] and [12]. K_6 also decreases with increase in system strength (lower X_E) [16], and increases with increase in either R_E/X_E or local load. This is true according to [2]. The presence of line resistance or local load influences the trend of K_6 with respect to machine load P_t – with significant line resistance or large local load, K_6 increases as P_t increases, reaches a maximum, and decreases with any further increase in P_t. K_6 remains positive for all conditions considered ([60] pp. 762, [2], [12]).

The parameter K_6 (or rather $1/K_6$) influences the "plant" transfer function pertaining to the PSS controller of chapter 4. Sections 4.4.1 and 4.6.2 discuss this in more depth.

Sections 3.7 and 3.8 discuss the system synchronizing and damping torques and variation thereof with respect to changes in system characteristic or condition. These torques are functions of the system model K-parameters. Results are interpreted in terms of the results of the K-parameters of this present section.

3.7 SMIB System Stability – Theoretical Background

This section presents theoretical background on the system elements and the respective torque components. Expressions for the damping and synchronizing torque components of the machine elements are given. Section 2.3 discusses these torque concepts. These expressions are derived from the model of Fig. 3.6 and based on the K-parameters discussed in section 3.6.

Section 3.7.1 presents the respective machine elements that influence stability. The remainder of section 3.7 focuses on these machine elements and the respective synchronizing and damping torque coefficients.

3.7.1 Synchronous machine elements and stability

The basic phenomenon in question is the stability of the torque-angle loop, i.e., the behaviour of the rotor angle and speed following a small disturbance. The block diagram approach graphically illustrates the influence of the machine elements on stability. Fig. 3.19 indicates the torque-angle loops of the machine elements that influence system synchronizing and damping stability:

1. "Direct feedback" torque-angle loop
2. Armature reaction (AR) torque-angle loop
3. AVR and exciter torque-angle loop

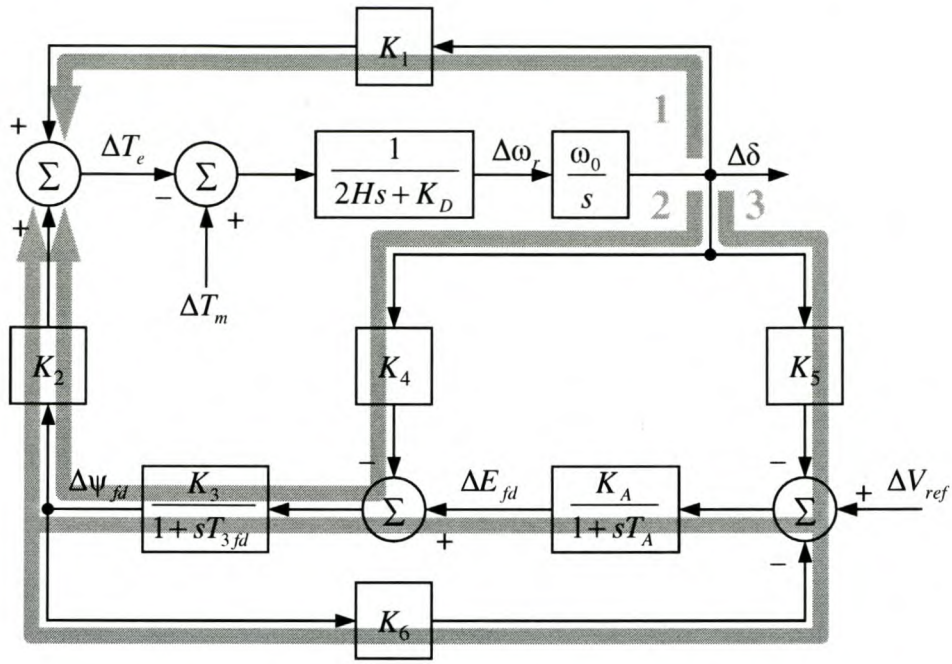

Fig. 3.19: Synchronous machine power-angle loops

These elements combine to give the machine total synchronizing and damping stability. The following sections discuss the contribution of each element. Where appropriate, mention is made of a K-parameter's predominant influence on the torque contributed by a generator element.

3.7.2 Transient synchronizing torque

This is loop 1 in Fig. 3.19. The transient synchronizing torque component (the direct influence of rotor angle on air-gap torque) has no influence on the system damping torques but is the predominant influence on the system synchronizing torque [12]. The change in electrical torque through direct influence of rotor angle variation is

$$\Delta T_e = K_1 \Delta\delta\,. \tag{3.45}$$

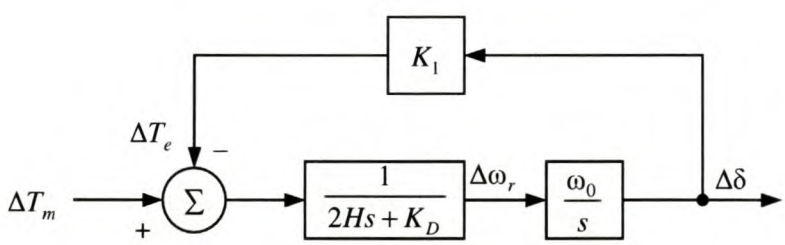

Fig. 3.20: Small perturbation torque-angle relationship – condition of constant *d*-axis flux linkages

Fig. 3.20 shows the torque-angle relationship. This is similar to the classical model scenario, discussed in section 3.2. The coefficient K_1 is also termed the transient synchronizing torque coefficient.

Section 3.6 examines the influence of network structure and loading on K_1. In most practical cases K_1 is positive. The case of very long ties and relative high loading on these ties is identified as one scenario when K_1 can be negative (Fig. 3.12, [2]). In a system with considerable external resistance, K_1 can also be negative as machine Q_t increases and/or power factor decreases [12]. In such instances the system would be unstable by aperiodic drift in rotor angle. However, such cases are very rare and instability is generally a case of insufficient damping of oscillations ([60] pp. 25).

3.7.3 Armature reaction

Fig. 3.21 shows the armature reaction loop of Fig. 3.19. With constant field voltage, field flux linkage variations are caused by feedback of $\Delta\delta$ through K_4. This represents the demagnetising effect of the armature reaction. The expression

$$\frac{\Delta T_e|_{AR}}{\Delta\delta} = -\frac{K_2 K_3 K_4}{1+sT_{3fd}} \tag{3.46}$$

relates the contribution of armature reaction to the machine net torque. The coefficients in this expression are almost always positive. K_4 is negative when the machine under light active power load and/or high reactive load, is connected through considerable external resistance [12][13]. Fig. 3.14(a) and Fig. 3.15(b) illustrate scenarios when K_4 is negative.

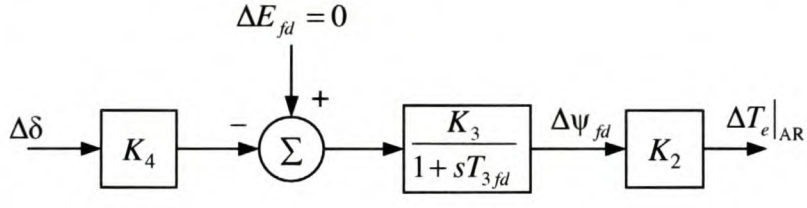

Fig. 3.21: Torque-angle relationship by direct axis field effect

Steady state

At steady state or low oscillating frequencies ($s=0$ in Eq. (3.46)), ΔT_e due to field flux linkage variations is

$$\frac{\Delta T_e\big|_{AR(SS)}}{\Delta\delta} = -K_2K_3K_4 \tag{3.47}$$

This is opposite in sign to the transient synchronizing torque component $K_1\Delta\delta$, and reduces the net steady-state synchronizing torque coefficient $K_{S(SS)}$. The opposite happens whenever $K_4 < 0$ – then ΔT_e due to field flux linkage variations increases $K_{S(SS)}$. The steady-state stability limit (with constant field voltage) is reached when $K_2K_3K_4$ equals K_1.

Ref. [12] discusses the unusual circumstance that $Q_t >> P_t$ in a system with local load such that $R_E > X_E$. It is observed that whenever K_1 is negative then K_4 is also negative. The result is a positive steady-state synchronizing torque coefficient $(K_1 - K_2K_3K_4)$.

High oscillating frequencies

At frequencies $\omega >> 1/T_{3fd}$ the phase angle of the torque component given by Eq. (3.46) is +90° ([60] pp. 751), i.e. ΔT_e is in phase with $\Delta\omega_r$. This results in a positive damping torque whenever K_4 is positive. In the situations discussed above, when K_4 is negative, then also will the damping torque due to armature reaction be negative.

Typical machine oscillating frequencies

At typical machine oscillating frequencies, Eq. (3.46) is written as

$$\frac{\Delta T_e\big|_{AR}}{\Delta\delta} = -\frac{K_2K_3K_4}{1+(\sigma+j\omega)T_{3fd}}, \tag{3.48}$$

where s is replaced by the system eigenvalue associated with the rotor angle oscillation mode obtained from the system state matrix Eq. (3.24). Appendix A.2 discusses finding the synchronizing and damping torque components from a complex ΔT_e in phase with $\Delta\delta$. Eq. (A.6) applied to (3.48) gives

$$\begin{aligned} K_{D(AR)} &= \left(\frac{\omega_0}{\omega}\right)\mathrm{Im}\left(\frac{\Delta T_e\big|_{AR}}{\Delta\delta}\right) \\ &= \frac{\omega_0K_2K_3K_4T_3}{(1+\sigma T_{3fd})^2+\omega^2T_{3fd}^2} \end{aligned}. \tag{3.49}$$

This is the armature reaction damping torque coefficient. The expression shows $K_{D(\mathrm{AR})}$ to be positive when K_4 is positive, and vice versa. Section 3.8 discusses the influence of network structure and loading on $K_{D(\mathrm{AR})}$ in more detail.

Eq. (A.5) gives the synchronizing torque coefficient of a complex ΔT_e in phase with $\Delta\delta$. Applied to (3.48) gives

$$\begin{aligned} K_{S(\mathrm{AR})} &= \mathrm{Re}\left(\frac{\Delta T_e|_{\mathrm{AR}}}{\Delta\delta}\right) - \left(\frac{\sigma}{\omega}\right)\mathrm{Im}\left(\frac{\Delta T_e|_{\mathrm{AR}}}{\Delta\delta}\right) \\ &= -\frac{K_2K_3K_4\left(1+2\sigma T_{3fd}\right)}{1+2\sigma T_{3fd}+T_{3fd}^2\left(\sigma^2+\omega^2\right)} \end{aligned} \quad . \tag{3.50}$$

This is the armature reaction synchronizing torque coefficient. $K_{S(\mathrm{AR})}$ does not constitute a significant influence on the system synchronizing stability ([60] pp. 751).

Armature reaction with excitation control

Eqs (3.46) through (3.50) describe the torque components due to armature reaction in a system without field voltage control ($\Delta E_{fd}=0$ in Fig. 3.19). When excitation control is included (see section 3.7.4), the expressions for armature reaction torque influence must include the feedback of $\Delta\psi_{fd}$ through K_6 also. Eq. (3.46) then changes to

$$\frac{\Delta T_e|_{\mathrm{AR}}}{\Delta\delta} = -\frac{K_2K_3K_4\left(1+sT_A\right)}{\left(1+sT_{3fd}\right)\left(1+sT_A\right)+K_3K_6K_A} . \tag{3.51}$$

It is important to distinguish between the armature reaction torques that contribute to the stability of a machine without field voltage control (3.46), and those in a machine with field voltage control (3.51). An excitation system for voltage control is included in the system model (section 3.3.2); hence Eq. (3.51) is used in the investigation of section 3.8.

At steady-state or low oscillating frequencies, the synchronizing torque due to armature reaction in a system with excitation control is

$$\frac{\Delta T_e|_{\mathrm{AR(SS)}}}{\Delta\delta} = -\frac{K_2K_3K_4}{1+K_3K_6K_A} , \tag{3.52}$$

obtained by setting $s=0$ in Eq. (3.51). This synchronizing torque is still negatively proportional to K_4 and the discussion on (3.47) applies.

At typical machine oscillating frequencies, Eq. (3.51) is written as

$$\frac{\Delta T_e|_{AR}}{\Delta\delta} = -\frac{K_2K_3K_4(1+(\sigma+j\omega)T_A)}{(1+(\sigma+j\omega)T_{3fd})(1+(\sigma+j\omega)T_A)+K_3K_6K_A}, \tag{3.53}$$

where $\sigma+j\omega$ replaced s. The same expressions in Appendix A.2 used to obtain Eqs (3.49) and (3.50) apply. The armature reaction damping torque coefficient is

$$\begin{aligned} K_{D(AR)} &= \left(\frac{\omega_0}{\omega}\right)\mathrm{Im}\left(\frac{\Delta T_e|_{AR}}{\Delta\delta}\right) \\ &= \frac{\omega_0}{\omega}\frac{K_2K_3K_4}{B_1^2+B_2^2}(-\omega T_A\cdot B_1+(1+\sigma T_A)\cdot B_2) \end{aligned}, \tag{3.54}$$

where

$$\begin{aligned} B_1 &= 1+\sigma(T_{3fd}+T_A)+T_{3fd}T_A(\sigma^2-\omega^2)+K_AK_3K_6 \\ B_2 &= \omega(T_{3fd}+2\sigma T_{3fd}T_A+T_A) \end{aligned}.$$

With no field voltage control (K_A and T_A set to zero), Eq. (3.54) reduces to (3.49). The expression shows $K_{D(AR)}$ is proportional to K_4, which has the predominant influence on $K_{D(AR)}$. Section 3.8 discusses the influence of system loading and network structure on $K_{D(AR)}$ in more detail.

Similarly, the armature reaction synchronizing torque coefficient is

$$\begin{aligned} K_{S(AR)} &= \mathrm{Re}\left(\frac{\Delta T_e|_{AR}}{\Delta\delta}\right)-\left(\frac{\sigma}{\omega}\right)\mathrm{Im}\left(\frac{\Delta T_e|_{AR}}{\Delta\delta}\right) \\ &= -\frac{K_2K_3K_4}{B_1^2+B_2^2}\left((1+\sigma T_A)\left(B_1+\frac{\sigma}{\omega}\cdot B_2\right)+\omega T_A\left(B_2-\frac{\sigma}{\omega}\cdot B_1\right)\right) \end{aligned}, \tag{3.55}$$

with B_1 and B_2 as above. Research results show $K_{S(AR)}$ to be much smaller in value than K_1, and hence does not constitute a significant influence on the system synchronizing stability. This is in agreement with Ref. [60] pp. 751.

3.7.4 Excitation control

Fig. 3.22 shows the AVR and exciter torque-angle loop of Fig. 3.19. With excitation control action, variations in field flux linkage are caused by field voltage variations, in addition to the armature reaction effect. The change in air-gap torque solely due to AVR action only is

$$\begin{aligned}\frac{\Delta T_e\big|_{\text{AVR}}}{\Delta\delta} &= K_2 \cdot \frac{\Delta\psi_{fd}\big|_{\text{AVR}}}{\Delta\delta} \\ &= \frac{-K_2K_3K_5K_A}{(1+sT_{3fd})(1+sT_A)+K_3K_6K_A}\end{aligned} \tag{3.56}$$

The constants K_2, K_3 and K_6 are always positive [2][12]. The expressions for these parameters in Appendix D and research results in section 3.6 indicate this to be true. K_5 can be either positive or negative, and attain values in a considerable range, depending on the external impedances and operating condition (generator loading), as discussed in section 3.6 and by refs [2], [12] and [60] pp. 765-766. The effect of the AVR on system stability is therefore primarily determined by K_5 and the exciter characteristic ([2], [60] pp.762).

Steady state

At steady state or low-oscillating frequencies ($s=0$ in Eq. (3.56)), ΔT_e due to excitation control is

$$\frac{\Delta T_e\big|_{\text{AVR(SS)}}}{\Delta\delta} = \frac{-K_2K_3K_5K_A}{1+K_3K_6K_A}. \tag{3.57}$$

In a SMIB system that utilizes a high gain AVR, this expression reduces to

$$\frac{\Delta T_e\big|_{\text{AVR(SS)}}}{\Delta\delta} \approx \frac{-K_2K_5}{K_6}. \tag{3.58}$$

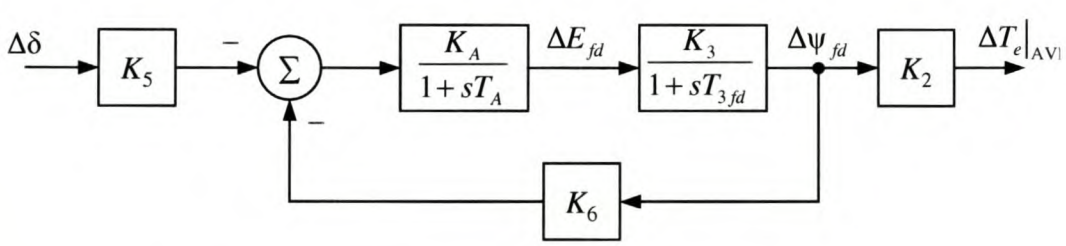

Fig. 3.22: Component of torque produced by AVR action

The excitation control steady-state synchronizing torque component is proportional to K_5, and is positive when K_5 is negative – the more commonly encountered situation ([60] pp. 766). This is beneficial in those cases where the transient synchronizing torque coefficient K_1 is low or negative, or when the steady-state synchronizing coefficient without regulator $(K_1 - K_2K_3K_4)$ is negative [2]. When K_5 is positive, excitation control reduces the steady-state synchronizing torque component.

Typical machine oscillating frequencies

At typical machine oscillating frequencies, Eq. (3.56) is rewritten as

$$\frac{\Delta T_e|_{\text{AVR}}}{\Delta\delta} = \frac{-K_2K_3K_5K_A}{(1+(\sigma+j\omega)T_{3fd})(1+(\sigma+j\omega)T_A)+K_3K_6K_A}, \tag{3.59}$$

where $\sigma + j\omega$ replaced s in (3.56). Eq. (A.6) gives the damping torque coefficient of a complex ΔT_e in phase with $\Delta\delta$. Applied to (3.59) gives

$$\begin{aligned} K_{D(\text{AVR})} &= \left(\frac{\omega_0}{\omega}\right)\text{Im}\left(\frac{\Delta T_e|_{\text{AVR}}}{\Delta\delta}\right), \\ &= \frac{\omega_0}{\omega}\frac{K_2K_3K_5K_A \cdot B_2}{B_1^2+B_2^2} \end{aligned} \tag{3.60}$$

with B_1 and B_2 as before. Eq. (3.60) is the excitation control damping torque coefficient. The expression shows $K_{D(\text{AVR})}$ to be positive when K_5 is positive, and vice versa. Eq. (A.5) applied to (3.59) gives

$$\begin{aligned} K_{S(\text{AVR})} &= \text{Re}\left(\frac{\Delta T_e|_{\text{AVR}}}{\Delta\delta}\right) - \left(\frac{\sigma}{\omega}\right)\text{Im}\left(\frac{\Delta T_e|_{\text{AVR}}}{\Delta\delta}\right), \\ &= -\frac{K_2K_3K_5K_A}{B_1^2+B_2^2}\left(B_1 + \frac{\sigma}{\omega}\cdot B_2\right) \end{aligned} \tag{3.61}$$

This is the excitation control synchronizing torque coefficient. The expression shows excitation control introduces positive synchronizing torque when K_5 is negative. Section 3.8 discusses the influence of network loading and structure on $K_{D(\text{AVR})}$ and $K_{S(\text{AVR})}$ in more detail.

With armature reaction included, Eqs (3.51) and (3.56) combine to give the total change in air-gap torque due to field flux linkage variations:

$$\frac{\Delta T_e|_{\text{AVR+AR}}}{\Delta\delta} = \frac{-K_2K_3(K_4(1+sT_A)+K_5K_A)}{(1+sT_{3fd})(1+sT_A)+K_3K_6K_A} \tag{3.62}$$

3.7.5 Total system torques

The discussion above considered the damping and synchronizing torque coefficients of the various machine elements individually. This section presents expressions for the combined (total) system torques.

The steady-state synchronizing torque of the SMIB system, consists of (a) the transient synchronizing torque (3.45), (b) the contribution by armature reaction effect (3.52), and (c) the excitation control steady-state synchronizing torque (3.57). Then

$$K_{S(\text{SS})} = K_1 - \frac{K_2K_3(K_4+K_5K_A)}{1+K_3K_6K_A} \tag{3.63}$$

is the total (net) steady-state synchronizing torque coefficient. The discussion on Eq. (3.57) focuses on the influences of the different components on $K_{S(\text{SS})}$.

The damping torque of the SMIB system with field voltage control, consists of (a) the damping contribution of the armature reaction effect (3.54), and (b) the damping contribution of excitation control (3.60). This investigation does not consider the influence of damper windings (amortisseur) on system damping (section 3.3). The total (net) damping torque coefficient is then

$$\begin{aligned} K_D &= K_{D(\text{AR})} + K_{D(\text{AVR})} \\ &= \frac{\omega_0}{\omega}\frac{K_2K_3}{B_1^2+B_2^2}\left[K_4(-\omega T_A\cdot B_1+(1+\sigma T_A)\cdot B_2)+K_5K_A\cdot B_2\right] \end{aligned} \tag{3.64}$$

with B_1 and B_2 as before.

K_D of Eq. (3.64) represents the total electrical damping torque on the generator air-gap. This is not to be confused with K_D of section 3.2. This latter coefficient represents damping provided by amortisseurs, and is set to zero for reasons discussed in section 3.3.

The synchronizing torque of the SMIB system with field voltage control, consists of (a) the transient synchronizing torque (3.45), (b) the armature reaction synchronizing torque (3.55), and (c) the excitation control synchronizing torque (3.61). Then

$$\begin{aligned} K_S &= K_1 + K_{S(\mathrm{AR})} + K_{S(\mathrm{AVR})} \\ &= K_1 - \frac{K_2 K_3}{B_1^2 + B_2^2}\left((K_4(1+\sigma T_A) + K_5 K_A)\left(B_1 + \frac{\sigma}{\omega}\cdot B_2\right) + K_4 \omega T_A \left(B_2 - \frac{\sigma}{\omega}\cdot B_1\right)\right) \end{aligned} \tag{3.65}$$

is the total (net) synchronizing torque coefficient.

Section 3.7 discussed the respective machine elements that contribute to the SMIB system overall stability. Expressions for the damping and synchronizing torques of the various machine elements, as well as the combined (total) torque coefficients, are presented. Discussion of the torque coefficients focused on the predominant influence of specific *K*-parameters. Section 3.8 investigates the variations of the damping and synchronizing torque coefficients with changes in generator loading or network structure (impedance).

3.8 SMIB System Stability Analysis

This section follows up on the discussion of section 3.7 with investigation similar to that in section 3.6. The focus is on the contribution of each machine element to the stability of the system and variation of such contribution with system characteristic and operating condition. Synchronizing and damping torque coefficients are investigated.

The transient synchronizing torque component is not considered. This synchronizing torque components equals K_1, and the results and discussion on K_1 in section 3.6 apply.

The steady-state synchronizing torque coefficient $K_{S(\mathrm{SS})}$ is also not considered in this report. Results obtained shows $K_{S(\mathrm{SS})}$ is positive for all conditions considered, and follows trends similar to the system net synchronizing torque at typical oscillating frequencies, K_S. The discussions on K_S therefore apply. Also, analysis of the steady-state torque coefficient has no significance to identifying possible scenarios of system dynamic instability, the emphasis of this chapter. PSS or CSC control action does not influence $K_{S(\mathrm{SS})}$, as these control actions respond to variations related to machine speed only and the expressions for PSS and CSC torque will show in chapters 4 and 5.

Since the system as a whole is considered, the armature reaction results reflect that in a system with excitation system in service. For further reference, see the discussion on Eq. (3.51). Investigation results show $K_{S(AR)}$ to be mostly negative and thus reduce the total synchronizing torque coefficient. However, values for $K_{S(AR)}$ are very small compared to K_1 and armature reaction has little influence on the system synchronizing torque. Therefore, results for $K_{S(AR)}$ are not presented in this report and can be found in Appendix E.

The following section discusses the analysis procedures and parameter values used. Sections 3.8.2 to 3.8.4 investigate the influence of machine loading and system reactance and resistance on the system torques by MATLAB simulation. Machine saturation is modelled and the AVR gain $K_A = 200$. Section 3.8.5 discusses the influence of K_A on the machine torques; section 3.8.6 the effect of neglecting saturation. In the concluding summary, attention is drawn to where results differ from previous research on this subject.

3.8.1 Analysis procedure

Section 3.6.1 describes the procedure to obtain plots for the machine K-parameters. This same procedure is used here to obtain results of the synchronous machine synchronizing and damping torque coefficients. As in section 3.6, the end-point voltages E_t and E_B are assumed constant at unity; no control is placed on the machine reactive power load. Plots of the synchronizing and damping torque coefficients of armature reaction, excitation system and the system as a whole, vs. P_t are generated by MATLAB simulation. Section 3.6.1 gives the values of X_E, R_E/X_E, and R_{load} considered.

3.8.2 Machine load and line reactance

This section neglects system external resistance. This simplifies analysis and results are typical of the case where a power source is connected to a large system through high voltage transmission line(s), with no or negligible local load.

Fig. 3.23 shows plots of the trends of the torque coefficients with respect to changes in machine load and external reactance. The following discussion focuses on each torque coefficient plot individually.

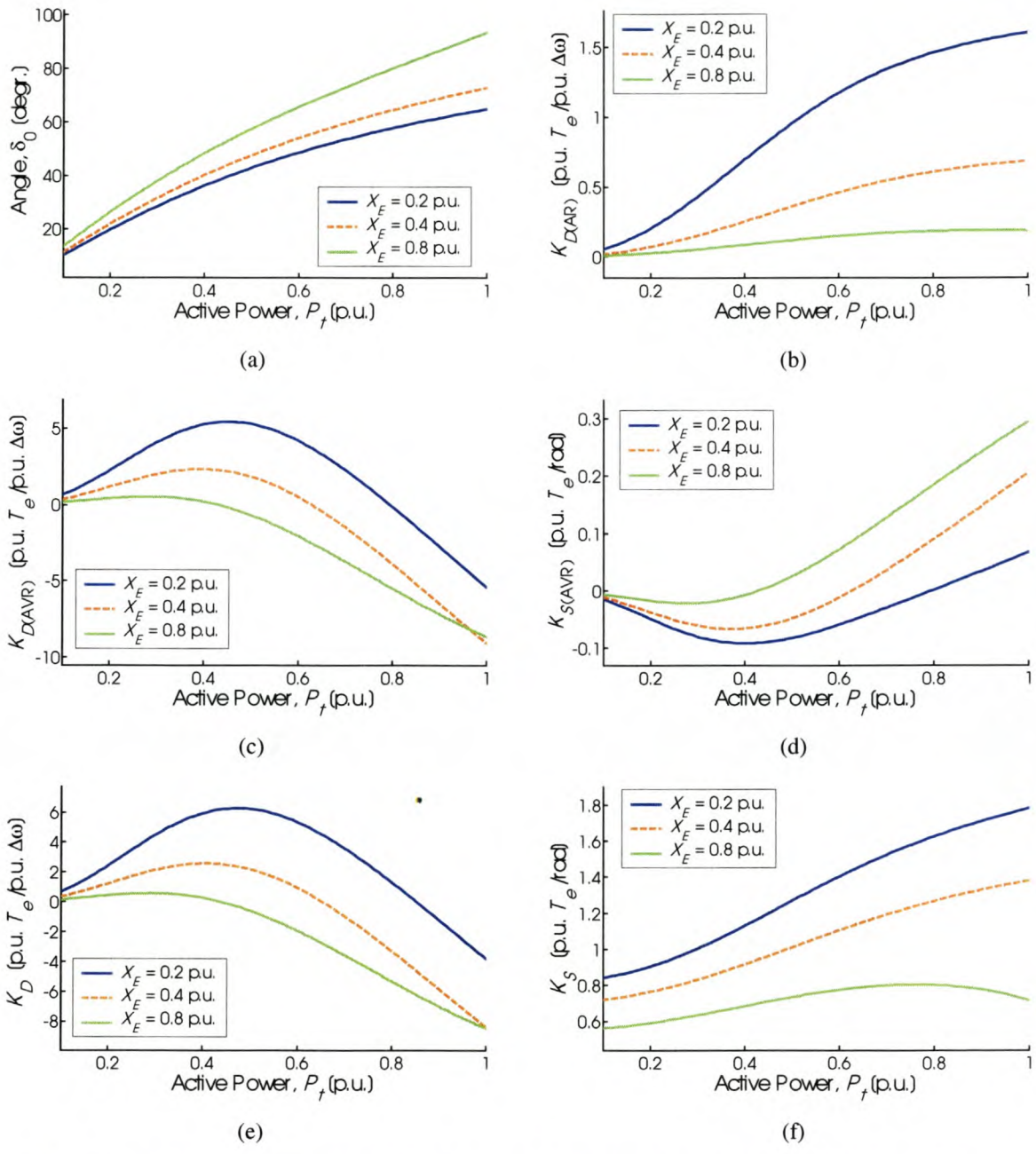

Fig. 3.23: Rotor angle and damping and synchronizing torque coefficients vs. machine load and external reactance

Fig. 3.23(b): The armature reaction damping torque coefficient increases as P_t increases and/or system strength increases.

Eqs (3.49) and (3.54) show $K_{D(\mathrm{AR})}$ to be proportional to the parameters K_2 and K_4. Fig. 3.11(b),(d) shows both K_2 and K_4 increase with increase in P_t and/or system strength; hence $K_{D(\mathrm{AR})}$ also.

Fig. 3.23(c): The excitation control damping torque coefficient is positive and increases as P_t increases from zero, reaches a maximum, and decreases becoming negative with any further increase in P_t. $K_{D(\mathrm{AVR})}$ also increases with increase in system strength.

Eq. (3.60) shows that $K_{D(\mathrm{AVR})}$ is proportional to the parameters K_2, K_3 and K_5. K_5 has the predominant influence on $K_{D(\mathrm{AVR})}$ as it is the only parameter that changes sign; when K_5 is negative, then $K_{D(\mathrm{AVR})}$ is also negative, and vice versa. Compare Fig. 3.23(c) to Fig. 3.11(e).

Fig. 3.23(d): The excitation control synchronizing torque coefficient is negative and decreases as P_t increases from zero, reaches a minimum, and increases becoming positive with any further increase in P_t. $K_{S(\mathrm{AVR})}$ also decreases with increase in system strength.

Eq. (3.61) shows $K_{S(\mathrm{AVR})}$ is negatively proportional to K_5 (and hence $K_{D(\mathrm{AVR})}$); whenever K_5 is negative, $K_{S(\mathrm{AVR})}$ is positive and vice versa. Compare Fig. 3.23(d) to Fig. 3.11(e).

Fig. 3.23(e): This plot shows the total damping torque coefficient. K_D is positive and increases as generator loading increases from zero, reaches a maximum, and decreases becoming negative with any further increase in P_t. K_D also increases with increase in system strength.

$K_{D(\mathrm{AVR})}$ is mostly larger in magnitude than $K_{D(\mathrm{AR})}$; hence K_D is influenced most by $K_{D(\mathrm{AVR})}$ and follows the trends thereof. However, armature reaction damping torque is positive for all system conditions considered and therefore negative $K_{D(\mathrm{AVR})}$ does not necessarily imply negative K_D.

Fig. 3.23(f): The total synchronizing torque coefficient increases with increase in P_t, K_S is also larger in a stronger system (smaller X_E), and remains positive over the range of conditions considered.

Eq. (3.65) shows K_1 has the predominant influence on K_S. One or more filters attenuate the torque components due to armature reaction effect and excitation control; hence the influence of these components is reduced compared to K_1. Fig. 3.11(a) shows the trends of K_1 with respect to P_t and X_E. Results show the influence of $K_{S(\mathrm{AR})}$ is negligible. $K_{S(\mathrm{AVR})}$ is more

positive in a system with larger X_E with high machine load; hence in a weaker system K_S does not reduce with further increase in P_t as much as does K_1.

3.8.3 Line resistance

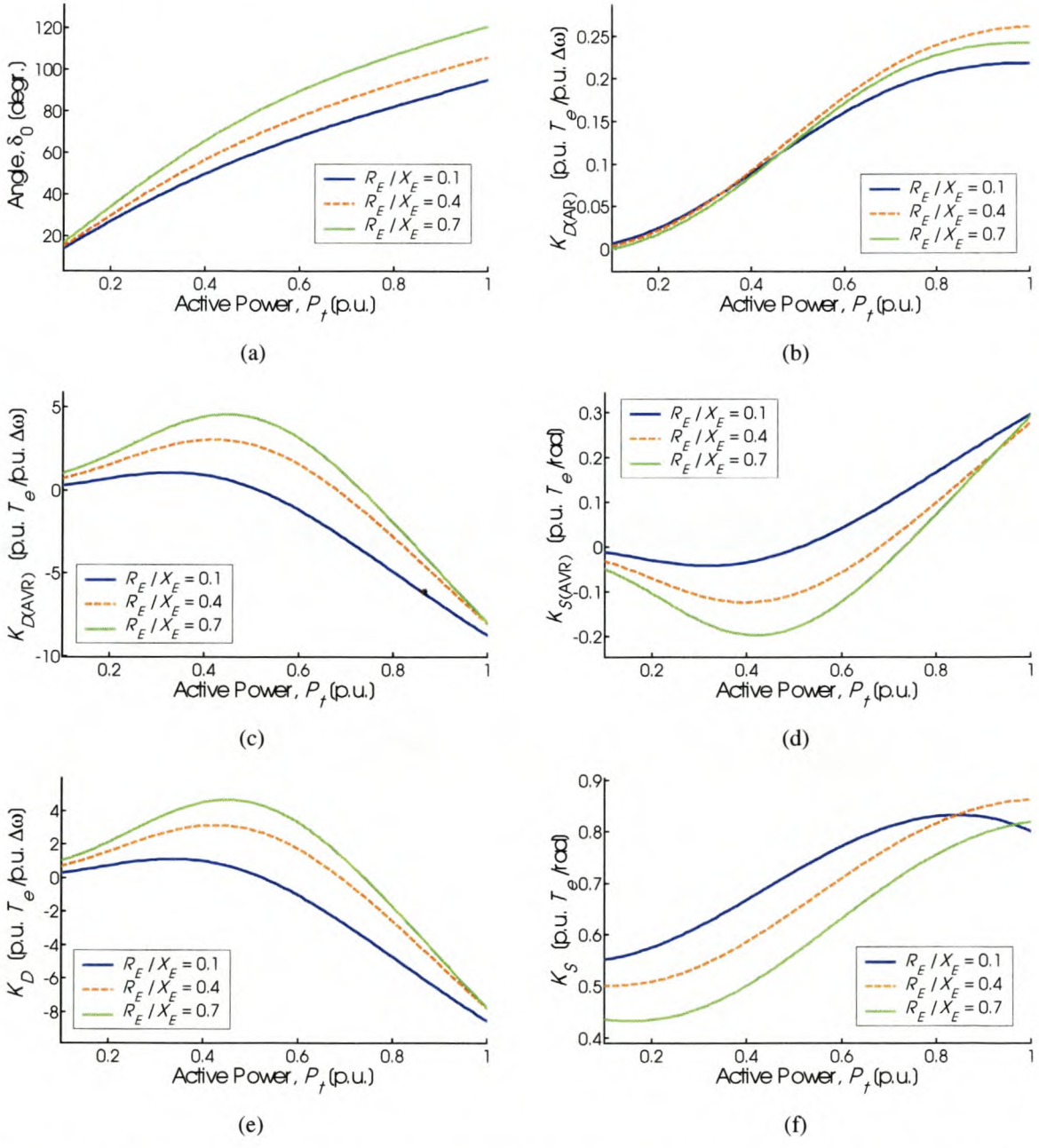

Fig. 3.24: Rotor angle and damping and synchronizing torque coefficients vs. machine load and line resistance, with X_E = 0.8 p.u.

Section 3.8.2 neglected system external resistance to simplify analysis and obtain results typical to the case where a power source is connected to a large system through high voltage

transmission line(s), with no or negligible local load. This section focuses on the influence of line resistance on the system model torque coefficients. Appendix E.4 contains the results.

Fig. 3.24 shows plots of the trends of the torque coefficients with respect to changes in machine load and local load resistance, when $X_E = 0.8\text{p.u}$. The following discussion focuses on each torque coefficient plot individually.

Fig. 3.24(b): The armature reaction damping torque coefficient increases with increase in R_E/X_E when the machine operates into a strong system. A slight decrease with increase in R_E/X_E occurs when the system is weaker and/or P_t is very low.

$K_{D(\text{AR})}$ is proportional to the parameter K_4 (Eqs (3.49), (3.54)). K_4 decreases with increase in R_E/X_E when the generator operates at low P_t, and can even turn negative as illustrated in Fig. 3.25(a). Under such conditions $K_{D(\text{AR})}$ is also negative (Fig. 3.25(b)). Observation: even though $K_{D(\text{AR})}$ is negative when P_t is low, this is very small compared to the positive excitation control damping torque coefficient in Fig. 3.24(c); hence the net damping torque coefficient in Fig. 3.24(e) remains positive.

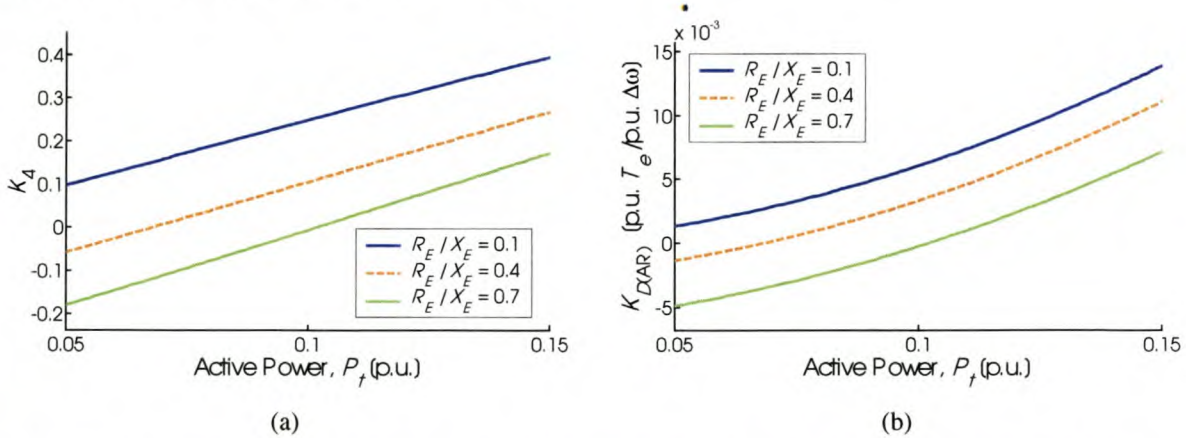

Fig. 3.25: Parameter K_4 and armature reaction damping torque coefficient vs. machine load and line resistance, with X_E = 0.8 p.u.

Fig. 3.24(c): The excitation control damping torque coefficient increases as R_E/X_E increases.

Eq. (3.60) shows that $K_{D(\text{AVR})}$ is proportional to the parameter K_5. K_5 has the predominant influence on $K_{D(\text{AVR})}$ – compare Fig. 3.24(c) to Fig. 3.13(c).

Fig. 3.24(d): The excitation control synchronizing torque coefficient decreases with increase in R_E/X_E.

Eq. (3.61) shows $K_{S(\mathrm{AVR})}$ is negatively proportional to the parameter K_5. Whenever K_5 is positive, $K_{S(\mathrm{AVR})}$ is negative and vice versa. Compare Fig. 3.24(d) to Fig. 3.13(c).

Fig. 3.24(e): The total (net) damping torque coefficient is shown. Both $K_{D(\mathrm{AR})}$ and $K_{D(\mathrm{AVR})}$ increase as R_E/X_E increases; hence K_D also.

Fig. 3.24(f): The total synchronizing torque coefficient decreases with increase in R_E/X_E.

The behaviour of K_S deviates somewhat from that of the mostly dominant K_1 shown in Fig. 3.13(a). The reason for this is the additional reduction increased R_E/X_E causes to $K_{S(\mathrm{AVR})}$ (Fig. 3.24(d)). The influence of synchronizing torque from excitation control on the total synchronizing torque becomes more significant when external resistance is included in the model.

3.8.4 Local load

This section focuses on the influence of local load on the system model torque coefficients. Appendix E.5 contains the results.

For reasons discussed in section 3.4.1, a resistance R_{load} models the local load. Table 3.1 gives the X_{line} and R_{load} value combinations used in the investigation, and the resulting X_E, R_E and E_B values from which the system parameters are determined (see discussion on Fig. 3.7).

Fig. 3.26 shows plots of the trends of the torque coefficients with respect to changes in machine load and local load resistance, when $X_{line} = 0.8$ p.u. The following discussion individually considers each torque coefficient plot.

Fig. 3.26(b): The armature reaction damping torque coefficient decreases as the local load increases over most of the machine load range. The exception is when the generator operates at high load values; then $K_{D(\mathrm{AR})}$ increases with increase in local load.

$K_{D(\mathrm{AR})}$ is proportional to the parameter K_4 (Eqs (3.49), (3.54)). K_4 decreases with increase in local load (Fig. 3.15(b)), and when P_t is low can even turn negative. So does $K_{D(\mathrm{AR})}$.

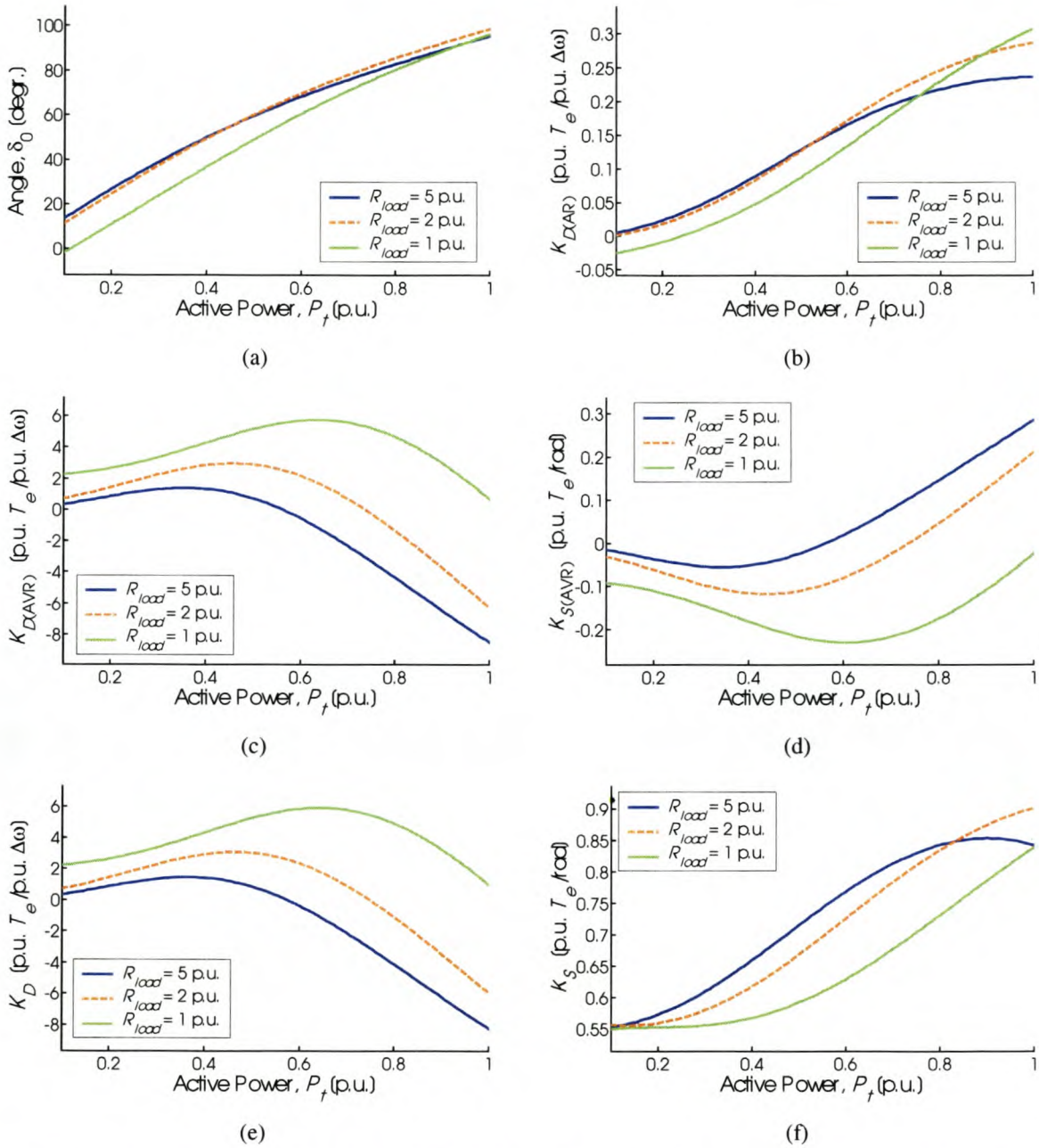

Fig. 3.26: Rotor angle and damping and synchronizing torque coefficients vs. machine load and local load resistance, with X_{line} = 0.8 p.u.

Observation: $K_{D(\mathrm{AR})}$ is more negative when the excitation control damping torque coefficient $K_{D(\mathrm{AVR})}$ is more positive (Fig. 3.26(c)); this negative influence is very small compared to the positive $K_{D(\mathrm{AVR})}$, and thus the net damping torque coefficient in Fig. 3.26(e) remains positive.

Fig. 3.26(c): The excitation control damping torque coefficient increases with increase in local load. The modelling of local load affects the trend of $K_{D(\mathrm{AVR})}$ with respect to changes

in line reactance illustrated in Fig. 3.23(c), especially when the generator operates at a high loading. As with the case of R_E/X_E (section 3.8.3), the behaviour of $K_{D(\mathrm{AVR})}$ with respect to local load can be explained in terms of the dominant influence of the parameter K_5.

Fig. 3.26(d): The excitation control synchronizing torque coefficient decreases with increase in local load. The presence of local load does affect the trend of $K_{S(\mathrm{AVR})}$ with respect to changes in line reactance illustrated in Fig. 3.23(d). As with the case of R_E/X_E, the behaviour of $K_{S(\mathrm{AVR})}$ with respect to local load can be explained in terms of the dominant influence of the parameter K_5. Compare Fig. 3.26(d) to Fig. 3.15(c).

Fig. 3.26(e): The total (net) damping torque coefficient increases as the local load increases. Armature reaction damping torque decreases with increase in local load (Fig. 3.26(b)). However, Fig. 3.26(c) shows $K_{D(\mathrm{AVR})}$ is an order magnitude larger than $K_{D(\mathrm{AR})}$. So also the variation with increased local load, and K_D follows $K_{D(\mathrm{AVR})}$ closely.

Fig. 3.26(f): The total synchronizing torque coefficient decreases with increase in local load, except with the machine lightly loaded – then K_S increases as the local load is increased.

The behaviour of K_S deviates somewhat from that of the mostly dominant K_1 shown in Fig. 3.13(a). The reason for this is the additional reduction an increase in local load causes $K_{S(\mathrm{AVR})}$ (Fig. 3.26(d)). Then, even though K_1 increases, K_S decreases with increase in local load. The influence of synchronizing torque from excitation control on the total system synchronizing torque becomes more significant when the local load is included in the model.

3.8.5 AVR gain

Results for sections 3.8.2 to 3.8.4 are obtained for a system with high initial-response excitation system; in other words, with an AVR gain of 200. Section 3.3.2 discusses the motivation behind assuming such a high gain.

This section considers the influence of assuming a lower K_A on the system model torque coefficients. Results for the previous sections were regenerated for the system of Appendix B but with $K_A = 20$. Appendix E.6 contains the results. The following discussion focuses on the main effects of assuming a smaller K_A on the system synchronizing and damping torques. Each torque coefficient is considered individually.

A reduction in K_A causes the **armature reaction damping torque coefficient** to increase (more positive or more negative), especially in a weaker system (larger external reactance). Eq. (3.54) gives the expression for $K_{D(\mathrm{AR})}$ in a system with field voltage control. This expression is directly influenced by changes in K_A, and also indirectly through a change in the rotor angle oscillation mode eigenvalue obtained from Eq. (3.24). Both the smaller K_A and change in λ interact to bring about the increase in $K_{D(\mathrm{AR})}$ observed.

The **excitation control damping torque coefficient** is smaller (less positive or less negative) when utilizing a lower gain K_A. This reduction is more prominent in a stronger system. Eq. (3.60) gives the expression for $K_{D(\mathrm{AVR})}$. K_A affects $K_{D(\mathrm{AVR})}$ directly, and also indirectly through a change in λ obtained from Eq. (3.24). Both the smaller K_A and change in λ interact to bring about the decrease in $K_{D(\mathrm{AVR})}$ observed.

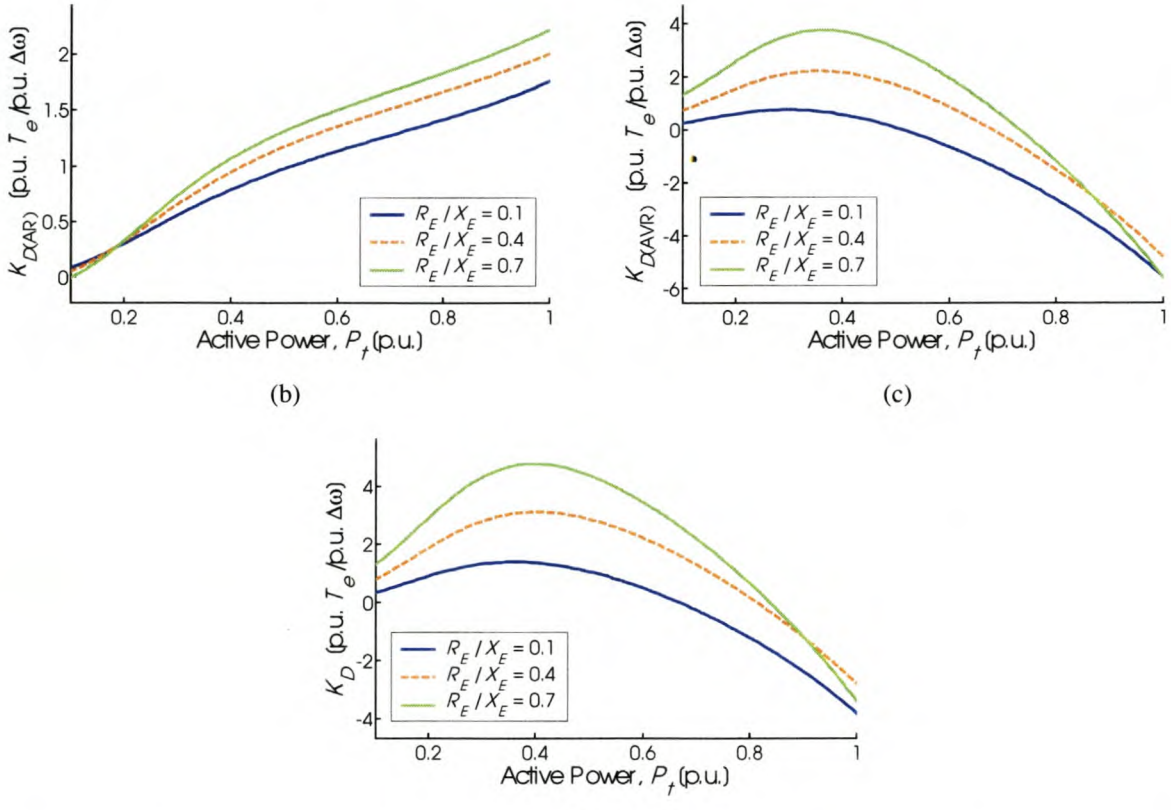

Fig. 3.27: Damping torque coefficients vs. machine load and line resistance, with X_E = 0.8 p.u. and K_A = 20

The influence of reduced K_A is most prominent when line resistance or local load is included in the model, especially in a strong system that operates at a high load. Then the more positive influence of armature reaction exceeds the less negative influence of excitation control on the overall system stability; the overall system stability is positive where it would otherwise be negative when $K_A = 200$. Fig. 3.27 shows the damping torque coefficients of the system with external resistance, when $X_E = 0.8$ p.u. and the AVR gain 20. Compare to the results of Fig. 3.24, obtained under the assumption $K_A = 200$. Notice that when $K_A = 200$, when R_E/X_E is low K_D can be negative (Fig. 3.24(e)), but over the range of values considered this is not the case when the AVR gain is 20 (Fig. 3.27(e)).

The **total (net) damping torque coefficient** decreases (less positive or less negative) with decrease in K_A. The separate influences of armature reaction and excitation control damping torques are discussed above. K_D is less susceptible to be negative when $K_A = 20$, than when a high response excitation system is employed.

Results show a reduction of the AVR gain from 200 to 20 does not affect the trends of the damping torque coefficients $K_{D(\mathrm{AR})}$, $K_{D(\mathrm{AVR})}$ and K_D with respect to changes in machine load or external impedance, discussed in sections 3.8.2 to 3.8.4.

Values for the armature reaction and excitation control synchronizing torque coefficients, $K_{S(\mathrm{AR})}$ and $K_{S(\mathrm{AVR})}$, are much smaller than K_1 when $K_A = 20$. As a result, the **total (net) synchronizing torque coefficient** follows the trends of K_1 when $K_A = 20$. Section 3.6 discusses the trends of K_1 with respect to changes in system characteristic and condition.

3.8.6 Influence of saturation

Synchronous machine saturation was modelled to obtain the results of the previous sections. Appendix C describes the modelling of saturation in the synchronous machine. This section considers the influence of neglecting saturation, often the assumption in literature.

Results for the previous sections were regenerated for the system of Appendix B with machine saturation neglected (constant machine inductances/reactances). Appendix E.7 contains the results.

Neglecting machine saturation influences the results of *machine load and line reactance* (section 3.8.2), *line resistance* (section 3.8.3) and *local load* (section 3.8.4) as follows:

1. Neglecting saturation increases both the armature reaction and excitation control damping torque coefficient values
2. Both the armature reaction and excitation control synchronizing torque coefficients decrease as a result of neglecting saturation

Since both $K_{D(\mathrm{AR})}$ and $K_{D(\mathrm{AVR})}$ are more positive when saturation is neglected, so also K_D.

Section 3.6.5 states that K_1 values are lower when machine saturation is not modelled. Both $K_{S(\mathrm{AR})}$ and $K_{S(\mathrm{AVR})}$ decrease as a result of neglecting saturation; hence also K_S.

Neglecting saturation effect does not influence the trends of the system damping or synchronizing torque coefficients discussed in sections 3.8.2 to 3.8.4.

3.8.7 Summary of results

The trends of the system damping and synchronizing torques, with respect to *machine load and line reactance* (section 3.8.2), *line resistance* (section 3.8.3) and *local load* (section 3.8.4) were examined. The influences of the *AVR gain* (section 3.8.5) and *saturation modelling* (section 3.8.6) on results were also considered.

A summary of the results of section 3.8 follows. The trends are compared to results from previous investigations on the damping and synchronizing torques of the SMIB system.

The **armature reaction damping torque coefficient** measures the amount of damping torque the field circuit introduces into the system. $K_{D(\mathrm{AR})}$ increases as machine load P_t increases and/or system strength increases. This result was also obtained in Refs [12] and [13]. The variation of $K_{D(\mathrm{AR})}$ with respect to changes in R_E/X_E or local load, depends on the generator loading. Reducing the AVR gain, or neglecting to model saturation, gives larger $K_{D(\mathrm{AR})}$ values than is otherwise the case.

It is possible for armature reaction to introduce negative damping into the system. This may happen when P_t is very low and R_E/X_E or the local load is high. Results in Refs [12] and [13] also show this to be true, although obtained under different modelling assumptions. Under such conditions the generator reactive power output is high (Fig. 3.17, [13]). In practice, the negative damping introduced by armature reaction can be due to (a) a hydraulic generator without damper windings operating at light load through a line with high R_E/X_E to a large system ([60] pp. 752), or (b) in the case of a machine connected to a large local

load that is also partly supplied by a remote large system [13]. However, under such conditions of negative $K_{D(\mathrm{AR})}$ the total damping torque remains positive; i.e. the system as a whole remains oscillatory stable.

Ref. [13] discusses this negative inherent damping produced by losses in the field, and explains why such instances are rare while there are numerous cases of local and remote generation in existence. The answer lies in the relative inertia of the sources. In the SMIB configuration, the infinite bus has infinite inertia and damping on this source is of no importance. In practice, the larger external system has a finite inertia. The system damping is primarily determined by the damping on the lighter source.

The **armature reaction synchronizing torque coefficient** measures the amount of synchronizing torque the field circuit introduces into the system. This synchronizing torque is very small compared to the contribution of both K_1 and excitation control to the total synchronizing torque ([60] pp. 751); hence the influence of $K_{S(\mathrm{AR})}$ is negligible.

The **excitation control damping torque coefficient** measures the amount of damping torque the excitation controller introduces into the system. $K_{D(\mathrm{AVR})}$ is positive when the generator operates at low to medium P_t, and negative when P_t is high and the generator operates into a system with high transfer impedances. Excitation control introduces more positive damping in a stronger system than a weaker one of similar loading. This result was also obtained in Refs [2], [12] and [60] pp. 765-766.

Increase in the effective external resistance of the system, whether due to line resistance or an increase in local load, increases the damping torque excitation control inputs into the system (more positive $K_{D(\mathrm{AVR})}$). When saturation effect is neglected, values of $K_{D(\mathrm{AVR})}$ are larger compared to when saturation is modelled. An excitation system with lower K_A introduces less negative torque into the system (when $K_{D(\mathrm{AVR})} < 0$), but also less positive torque [2].

The damping torque excitation control introduces into the system plays a significant role in the overall stability of the system. Although armature reaction introduces positive damping torque when $K_{D(\mathrm{AVR})}$ is negative, under most circumstances this is not enough to prevent the overall system from being negatively damped (oscillatory unstable).

The **excitation control synchronizing torque coefficient** measures the amount of synchronizing torque the excitation controller introduces into the system. The trends of

$K_{S(AVR)}$ with respect to changes of generator load or external system impedance is the negative inverse to that of the excitation control damping torque coefficient.

When the excitation controller gain is low (e.g. $K_A = 20$), the synchronizing torque introduced into the system is negligible. When saturation effect is neglected, values of $K_{S(AVR)}$ are smaller compared to when saturation is modelled.

Typically the voltage regulator gain is assumed high to increase the synchronizing torque and transient stability performance of the system when such performance is required in the system ([60] pp. 766, [2]). However, in doing so excitation control introduces a negative damping into the system that may well exceed the net inherent damping of the machine (armature reaction and damper windings). To offset the negative damping introduced by the excitation system, a special stabilizing component is required. Examples are a power system stabilizer, or the dynamic control of a series capacitor. Chapters 4 and 5 discuss these options in more depth.

The **total (net) damping torque coefficient** is the sum of the damping torque contributions by armature reaction effect and excitation control action and measures the total damping stability of the system (damper windings effect neglected). K_D is influenced most by the excitation control, and follows the trends of $K_{D(AVR)}$. When armature reaction introduces negative damping at low P_t, the total system damping torque remains positive due to the positive damping by the excitation control at such values of generator load.

The net system damping torque is positive when the generator operates at low to medium P_t, and can be negative when P_t is moderate to high depending on the external system impedance. K_D is more positive in a stronger system than a weaker system with similar loading. The system damping torque also increases with increase in R_E/X_E, although this is not sufficient to ensure positive system damping at high values of generator loading. K_D also increases with increase in local load; sufficient local load may cause K_D to be positive when otherwise the system would have been unstable (at the expense of synchronizing torque). K_D is reduced (less positive or less negative) when a lower AVR gain is employed. When saturation is neglected, values for K_D are larger (more positive) compared to when saturation is modelled.

The **total (net) synchronizing torque coefficient** measures the total synchronizing stability of the system. K_S is influenced most by the transient synchronizing torque coefficient K_1 discussed in section 3.6. The synchronizing torque due to armature reaction effect is much smaller than K_1 and its effect negligible. The influence of excitation control on K_S varies, depending on the machine load, system impedance and gain of the excitation system.

For all conditions the system net synchronizing torque is positive. There is thus no need for synchronizing torque support. However, as mentioned above, situations of high P_t and moderate to high external reactance requires additional damping torque to operate stably. Local load may alleviate the problem, but not always. Sources of such additional damping torque may be a power system stabilizer (investigated in chapter 4) or a controlled series capacitor (chapter 5). Section 2.5 discusses these and other methods of enhancing stability briefly.

3.9 Summary

This chapter presented the state-space and block diagram models of the SMIB system without oscillation stabilizer, and determined scenarios of possible system instability. Both the small-signal synchronizing and damping stability of the system was considered.

The system models used are presented in section 3.3, and are based on the parameters $K_1 \ldots K_6$ defined in Appendix D. Expressions for the damping and synchronizing torque coefficients for the different machine elements show the stability of the system can be related to the signs of the K-parameters. The parameters K_1, K_4 and K_5 can change sign from positive to negative under certain conditions. The parameter K_1 has direct influence on the transient synchronizing torque, K_4 on the armature reaction damping torque, and K_5 on the excitation control damping and synchronizing torques.

The system total synchronizing torque is positive for all conditions considered. Hence the system is transiently stable. The system total damping torque can be negative under the following conditions: in a system with generator highly loaded and operating into a moderate to high external reactance, with no or little local load. Line resistance does not add positively to system damping much. Excitation control has the biggest influence on the system damping stability. The gain of the AVR plays a significant role. When oscillations are negatively damped, an increase in AVR gain aggravates the situation.

Under conditions of negative oscillation damping additional damping torque is needed to ensure operation is oscillatory stable. Chapter 4 discusses the use of a power system stabilizer to provide the necessary damping torque. Chapter 5 discusses the use of a controlled series capacitor. Emphasis is placed on the variation of the controller performance under conditions of required additional damping torque.

4 POWER SYSTEM STABILIZER

4.1 Introduction

This chapter introduces the state-space and block diagram models of the SMIB system with power system stabilizer, and investigates the ability of a PSS to enhance system stability in situations when such stability support is required. Results in chapter 3 indicate that a system with generator highly loaded that operates into a moderate to high external impedance, with no or little local load, experiences negative damping.

Section 2.5.1 discusses the power system stabilizer. The basic function of a PSS is to extend the stability limits of the system. It accomplishes this by modulating generator excitation to produce a component of electrical torque on the rotor that is in phase with rotor speed variations. By inducing such a torque, the PSS provides damping to the oscillations of synchronous machine rotors relative to one another.

Section 3.3.2 discusses the generator excitation control system, and the elements that collectively define such a system. Fig. 4.1 shows the generator excitation control system of Fig. 3.5, but with PSS implemented. The stabilizer consists of a gain K_C and transfer function $G_{PSS}(s)$. Section 4.2 discusses the conventional PSS control scheme.

This chapter is sectioned as follows: Section 4.3 presents the system model of the SMIB system with PSS. This model comprises the state-space model, from which the eigenvalues are obtained, and the block diagram model, useful to evaluate torque expressions for use in the investigation. Section 4.4 develops expressions for the PSS damping and synchronizing torque coefficients. These are indicators of the variation of PSS performance with respect to changes in system load and network structure. For every condition considered, the PSS parameters are optimised for that particular condition by the method of section 4.5, an integral of the square error based technique.

Section 4.6 investigates the ability of a PSS to enhance system stability. The characteristics and conditions under investigation are: (a) generator load; (b) system reactance as seen by the generator; (c) the amount of external (line) resistance relative to reactance; (d) load local to the generator (sending-end) side of the SMIB system. Also examined are the influences of AVR gain and machine saturation on results.

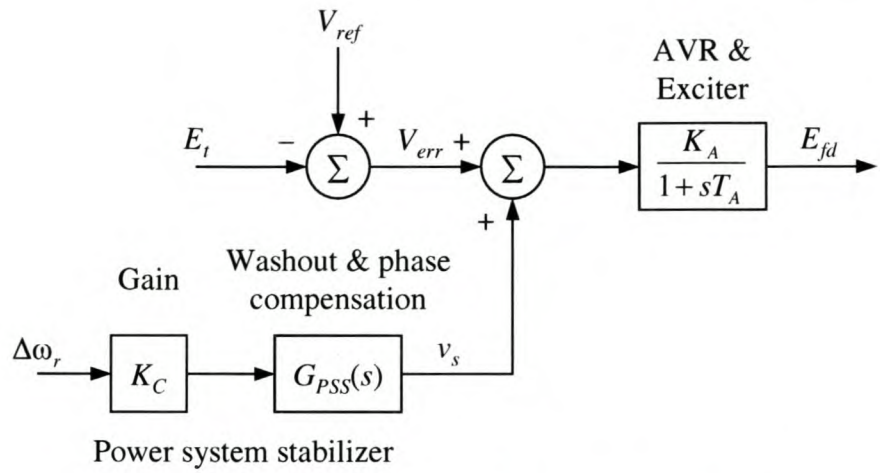

Fig. 4.1: Thyristor excitation system with AVR and PSS

4.2 The Conventional Power System Stabilizer Control Scheme

Fig. 4.2 shows the conventional PSS controller scheme. $\Delta\omega_r$ is used as the input signal. Eq. (4.1) gives the transfer function. The PSS controller consists of three blocks: a gain block, a signal washout block, and a phase compensation block. The following discussion focuses on each of these blocks and some other considerations in more detail. This is based on discussions in Refs [60] pp. 1128-1134, [16]-[18] and [25].

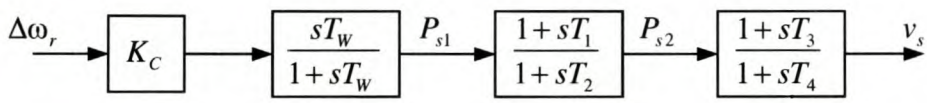

Fig. 4.2: Conventional PSS controller

$$\frac{v_s}{\Delta\omega_r} = K_C\left(\frac{sT_W}{1+sT_W}\right)\left(\frac{1+sT_1}{1+sT_2}\right)\left(\frac{1+sT_3}{1+sT_4}\right). \tag{4.1}$$

4.2.1 Input signal

The purpose of a PSS is to introduce a damping torque component. Hence a logical signal to use for controlling generator excitation is the speed deviation $\Delta\omega_r$. $\Delta\omega_r$ is a state variable (section 3.3); hence it is simpler to integrate the controller of Fig. 4.2 with the block diagram model of Fig. 3.6 and develop expressions in state-space form. The possibility of torsional modes instability has caused utilities to use other signals as input to the PSS controller, such as accelerating power or ac bus frequency. Such instabilities are deemed beyond the scope of this research, as the main focus is the stability of the local-mode oscillations.

4.2.2 Stabilizer gain

Ideally, the stabilizer gain should be set at a value that corresponds to maximum damping. K_C is however often limited by other considerations, such as the influence of the controller on the stability of other modes, and the amplification of the stabilizer input signal noise. Such effects are considered beyond the scope of this research, and the gain used is one that gives optimal controller performance for a given system condition of load and external impedance (section 4.5).

4.2.3 Stabilizing signal washout

A washout stage is included to prevent steady-state voltage offsets as system frequency changes. The value of T_W is not critical and may be anywhere in the range 1 to 20 seconds. The main consideration is that it should be long enough to pass stabilizing signals at the frequencies of interest relatively unchanged, but not so long that it leads to undesirable generator voltage excursions as a result of stabilizer action in the event of system islanding.

Results from [25] indicate that local mode oscillations are largely unaffected by changes in T_W. However, a higher value of T_W is desirable from the viewpoint of small signal and transient stability, particularly without TGR in the excitation system.

4.2.4 Phase-lead compensation

To damp rotor-angle mode oscillations, the PSS must produce a component of electrical torque in phase with $\Delta\omega_r$. Therefore, the PSS transfer function should have an appropriate phase-lead characteristic to compensate for the phase lag between the exciter input and the electrical torque. Slight undercompensation is preferable to overcompensation so that both damping and synchronizing torque components are increased. Ref. [22] shows improved PSS performance when slight undercompensation is employed, compared to full compensation.

Section 4.5.4 discusses the phase compensation, as well as the values for the controller parameters used in the investigation, in more detail.

4.2.5 Stabilizer output limits

This research focuses on small-signal behaviour of a SMIB system. Stabilizer output limits does not influence results, and hence are not considered in the investigation.

4.3 System Model

Section 3.3 gives the state-space and block diagram models of the synchronous machine in a SMIB configuration without oscillation stabilizers. Not included in the models are the transformer voltage terms and the effect of speed variations on the stator voltages. Amortisseur (damper winding) effects are also neglected for reasons discussed in section 3.3. Synchronous machine saturation effects are included in the model. The transfer function

$$G_{ex}(s) = \frac{K_A}{1 + sT_A} \tag{4.2}$$

defines the excitation system.

This section derives the state-space and block diagram models of the SMIB system with power system stabilizer. These models are extensions of those defined by Eq. (3.24) and Fig. 3.6, to include a PSS.

4.3.1 Small perturbation form of machine and network equations

Section 3.3.1 discusses the small perturbation (linear) form of the machine and network equations. The expressions presented describe the system without excitation system. A PSS introduces damping torque into the system by adjusting the excitation system input voltage; hence addition of a PSS to the system model does not modify any of the expressions of section 3.3.1.

4.3.2 Excitation system

A PSS adjusts the excitation system input voltage. Fig. 4.1 shows that addition of a PSS to the system model modifies the expression for E_{fd} (Eq. (3.20)) to give

$$E_{fd} = \frac{K_A}{1 + sT_A}\left(V_{ref} + v_s - E_t\right). \tag{4.3}$$

The small perturbation form of this equation is

$$\Delta E_{fd} = \frac{K_A}{1 + sT_A}\left(\Delta V_{ref} + \Delta v_s - \left(K_5 \Delta\delta + K_6 \Delta\psi_{fd}\right)\right). \tag{4.4}$$

Eq. (3.21) replaces ΔE_t, the generator terminal voltage in linear form. Eq. (4.4) forms part of the block diagram model of Fig. 4.3, and can be rearranged to give

$$p\Delta E_{fd} = \frac{1}{T_A}\left(-K_A\left(K_5\Delta\delta + K_6\Delta\psi_{fd}\right) - \Delta E_{fd} + K_A\Delta v_s + K_A\Delta V_{ref}\right). \tag{4.5}$$

This expression forms part of the state-space model of Eq. (4.13). Expressions for the other state variables ($p\Delta\delta$ (3.17), $p\Delta\omega_r$ (3.18), and $p\Delta\psi_{fd}$ (3.19)) are unaffected by the addition of a PSS to the system.

4.3.3 Power system stabilizer

Fig. 4.2 shows the generic PSS controller employed. It is desired to express the PSS controller transfer function (Eq. (4.1)) in state-space form.

Using perturbed values, ΔP_{s1} is

$$\Delta P_{s1} = K_C\left(\frac{pT_W}{1+pT_W}\right)\Delta\omega_r, \tag{4.6}$$

which is rearranged to give

$$p\Delta P_{s1} = K_C\, p\Delta\omega_r - \frac{1}{T_W}\Delta P_{s1}. \tag{4.7}$$

With $p\Delta\omega_r$ from Eq. (3.18) substituted in (4.7), the expression for $p\Delta P_{s1}$ in terms of the state variables are

$$p\Delta P_{s1} = -\frac{K_C K_D}{2H}\Delta\omega_r - \frac{K_C K_1}{2H}\Delta\delta - \frac{K_C K_2}{2H}\Delta\psi_{fd} - \frac{1}{T_W}\Delta P_{s1} + \frac{K_C}{2H}\Delta T_m. \tag{4.8}$$

Similarly, ΔP_{s2} is

$$\Delta P_{s2} = \left(\frac{1+pT_1}{1+pT_2}\right)\Delta P_{s1}, \tag{4.9}$$

which is rearranged to give

$$p\Delta P_{s2} = \frac{1}{T_2}\Delta P_{s1} + \frac{T_1}{T_2}\,p\Delta P_{s1} - \frac{1}{T_2}\Delta P_{s2}. \tag{4.10}$$

Substituting for $p\Delta P_{s1}$ from Eq. (4.8), $p\Delta P_{s2}$ in terms of the state variables is

$$p\Delta P_{s2} = -\frac{K_C K_D T_1}{2HT_2}\Delta\omega_r - \frac{K_C K_1 T_1}{2HT_2}\Delta\delta - \frac{K_C K_2 T_1}{2HT_2}\Delta\psi_{fd} + \frac{T_W - T_1}{T_W T_2}\Delta P_{s1} - \frac{1}{T_2}\Delta P_{s2} + \frac{K_C T_1}{2HT_2}\Delta T_m.$$

(4.11)

Following the same procedure to obtain $p\Delta P_{s2}$, $p\Delta v_s$ in terms of the state variables is

$$p\Delta v_s = -\frac{K_C K_D T_1 T_3}{2HT_2T_4}\Delta\omega_r - \frac{K_C K_1 T_1 T_3}{2HT_2T_4}\Delta\delta - \frac{K_C K_2 T_1 T_3}{2HT_2T_4}\Delta\psi_{fd} + \frac{(T_W - T_1)T_3}{T_W T_2 T_4}\Delta P_{s1} + \frac{T_2 - T_3}{T_2 T_4}\Delta P_{s2} - \frac{1}{T_4}\Delta v_s + \frac{K_C T_1 T_3}{2HT_2 T_4}\Delta T_m \quad (4.12)$$

Eqs (4.8), (4.11) and (4.12) form part of the state-space model of the system with PSS, Eq. (4.13).

4.3.4 System state-space model and block diagram

The system state-space model is of the form

$$\dot{\mathbf{x}} = \mathbf{A}\mathbf{x} + \mathbf{\Gamma}\mathbf{p}, \quad (4.13)$$

where $\mathbf{x}$ and $\mathbf{p}$ are the state and perturbation vectors respectively, defined as

$$\mathbf{x} = \begin{bmatrix} \Delta\omega_r & \Delta\delta & \Delta\psi_{fd} & \Delta E_{fd} & \Delta P_{s1} & \Delta P_{s2} & \Delta v_s \end{bmatrix}^T$$

$$\mathbf{p} = \begin{bmatrix} \Delta T_m & \Delta V_{ref} \end{bmatrix}^T$$

The system state matrix $\mathbf{A}$ is

$$\mathbf{A} = \begin{bmatrix} \frac{-K_D}{2H} & \frac{-K_1}{2H} & \frac{-K_2}{2H} & 0 & 0 & 0 & 0 \\ \omega_0 & 0 & 0 & 0 & 0 & 0 & 0 \\ 0 & \frac{-K_3K_4}{T_{3fd}} & \frac{-1}{T_{3fd}} & \frac{K_3}{T_{3fd}} & 0 & 0 & 0 \\ 0 & \frac{-K_AK_5}{T_A} & \frac{-K_AK_6}{T_A} & \frac{-1}{T_A} & 0 & 0 & \frac{K_A}{T_A} \\ \frac{-K_CK_D}{2H} & \frac{-K_CK_1}{2H} & \frac{-K_CK_2}{2H} & 0 & \frac{-1}{T_W} & 0 & 0 \\ \frac{-K_CK_DT_1}{2HT_2} & \frac{-K_CK_1T_1}{2HT_2} & \frac{-K_CK_2T_1}{2HT_2} & 0 & \frac{T_W-T_1}{T_2T_W} & \frac{-1}{T_2} & 0 \\ \frac{-K_CK_DT_1T_3}{2HT_2T_4} & \frac{-K_CK_1T_1T_3}{2HT_2T_4} & \frac{-K_CK_2T_1T_3}{2HT_2T_4} & 0 & \frac{(T_W-T_1)T_3}{T_2T_WT_4} & \frac{T_2-T_3}{T_2T_4} & \frac{-1}{T_4} \end{bmatrix}.$$

$\mathbf{A}$ is a function of the system parameters as well as the operating condition. The eigenvalues of the state matrix are a useful indication of the stability of the system, as discussed in

section 3.2.2. The eigenvalue associated with the rotor angle oscillation mode is used as the complex frequency to evaluate the PSS damping torque contribution. Section 4.4 derives an expression for the PSS damping torque coefficient.

The perturbation matrix $\mathbf{\Gamma}$,

$$\mathbf{\Gamma} = \begin{bmatrix} \frac{1}{2H} & 0 & 0 & 0 & \frac{K_C}{2H} & \frac{K_C T_1}{2HT_2} & \frac{K_C T_1 T_3}{2HT_2 T_4} \\ 0 & 0 & 0 & \frac{K_A}{T_A} & 0 & 0 & 0 \end{bmatrix},$$

is a function of the system parameters only, and used to obtain the PSS controller parameters for optimum PSS performance given a certain condition of system load and external impedance. Section 4.5 discusses the performance index and optimisation process.

Fig. 3.6, Fig. 4.1 and Fig. 4.2 combine to give the block diagram model of the SMIB system with PSS, Fig. 4.3. The block diagram model is a useful tool in understanding the performance of a PSS in the system. An expression for the torque contribution by a PSS is easily obtained using this block diagram.

4.4 PSS Torque Coefficients

Section 2.3 discusses the concepts of synchronizing and damping torques. Based on these concepts, the air-gap torque as a result of PSS action can be decomposed into the following components:

$$\Delta T_e\big|_{\text{PSS}} = K_{S(\text{PSS})}\Delta\delta + K_{D(\text{PSS})}\Delta\omega_r \tag{4.14}$$

$K_{D(\text{PSS})}\Delta\omega_r$ is the damping torque component of the air-gap torque due to PSS action, with $K_{D(\text{PSS})}$ the *PSS damping torque coefficient*. $K_{S(\text{PSS})}\Delta\delta$ is the synchronizing torque the PSS controller introduces into the system, with *PSS synchronizing torque coefficient* $K_{S(\text{PSS})}$. This section derives expressions for $K_{D(\text{PSS})}$ and $K_{S(\text{PSS})}$ for use in the investigation.

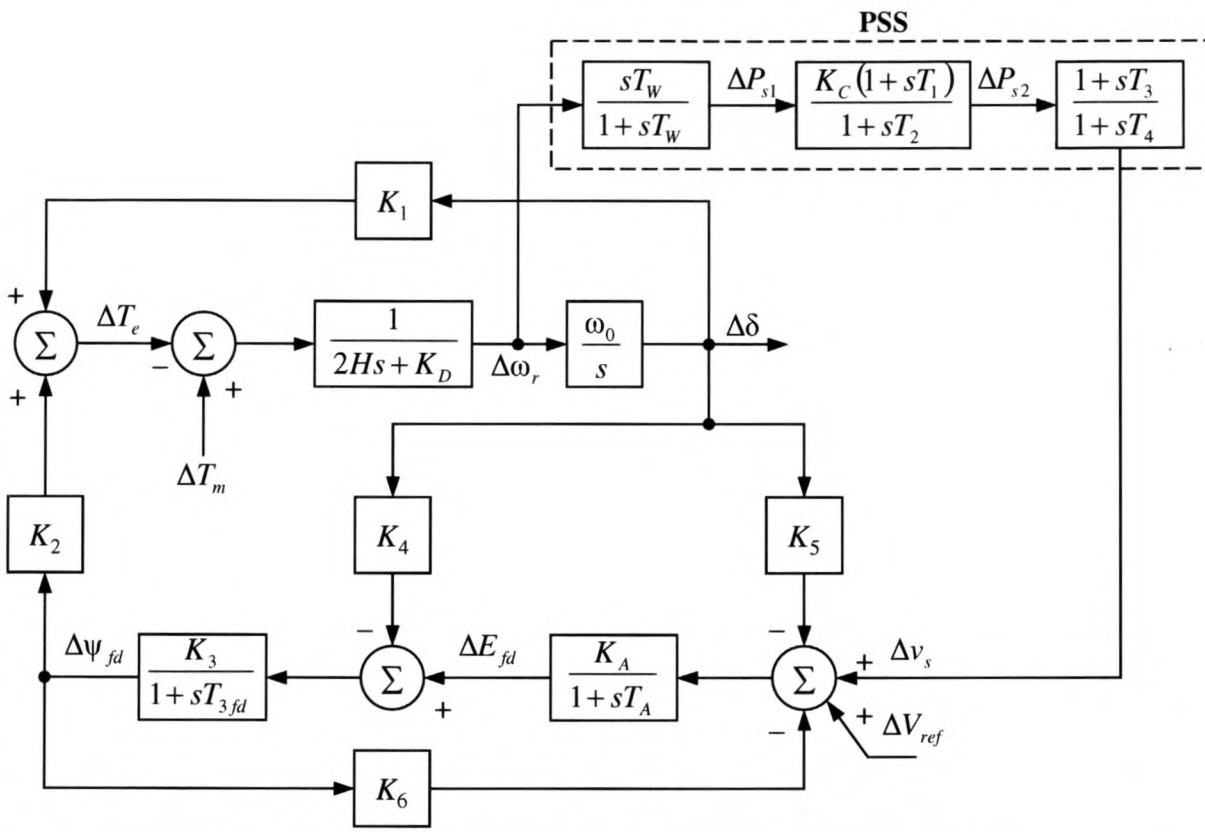

Fig. 4.3: Block diagram model of SMIB system with conventional PSS

4.4.1 *"Plant" transfer function*

Let $GEP(s)\big|_{\text{PSS}}$ denote the transfer function from the stabilizer output Δv_s to the component of electrical air-gap torque ΔT_e that can be modulated via excitation control [16]. Fig. 4.4 illustrates the transfer function when the stabilizer is a PSS controller. Variation of $GEP(s)\big|_{\text{PSS}}$ with voltage regulator gain, generator power level and ac system strength plays a dominant role in PSS performance [16].

According to Fig. 4.4, the variation in field flux linkage due to variation in Δv_s is

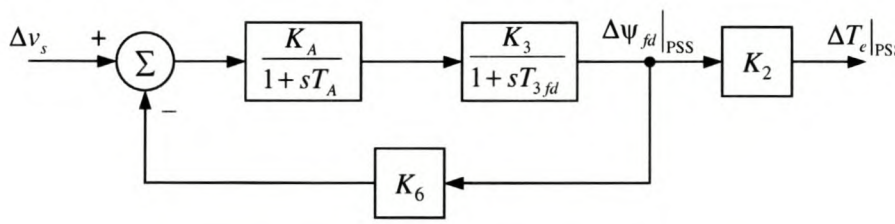

Fig. 4.4: PSS forward path

$$\Delta\psi_{fd}\big|_{\text{PSS}} = \frac{K_3}{1+sT_{3fd}}\frac{K_A}{1+sT_A}\left(\Delta v_s - K_6\Delta\psi_{fd}\big|_{\text{PSS}}\right). \tag{4.15}$$

The field flux linkage variation is fed back through the parameter K_6 to the exciter block input; hence $\Delta\psi_{fd}\big|_{\text{PSS}}$ appears also on the right hand side of Eq. (4.15). This expression is rearranged to give

$$\frac{\Delta\psi_{fd}\big|_{\text{PSS}}}{\Delta v_s} = \frac{K_3K_A}{(1+sT_{3fd})(1+sT_A)+K_3K_6K_A}, \tag{4.16}$$

which is used to express the transfer function $GEP(s)\big|_{\text{PSS}}$ as

$$\begin{aligned} GEP(s)\big|_{\text{PSS}} &= \frac{\Delta T_e\big|_{\text{PSS}}}{\Delta v_s} \\ &= K_2\frac{\Delta\psi_{fd}\big|_{\text{PSS}}}{\Delta v_s} = \frac{K_2K_3K_A}{(1+sT_{3fd})(1+sT_A)+K_3K_6K_A} \end{aligned} \tag{4.17}$$

$GEP(s)\big|_{\text{PSS}}$ exhibits a phase lag at the oscillation frequencies under concern. As a result the PSS controller contains a phase lead block (section 4.2.4) to partially compensate this phase lag. Slight undercompensation ensures the PSS improves the system damping stability without adversely affecting the synchronizing (transient) stability of the system.

4.4.2 Torque expressions

Fig. 4.2 and Eq. (4.1) describe the conventional PSS controller configuration used in the investigation. Combining (4.1) with the expression for $GEP(s)\big|_{\text{PSS}}$ gives the torque contribution due to the PSS controller:

$$\begin{aligned} \Delta T_e\big|_{\text{PSS}} &= \frac{\Delta T_e\big|_{\text{PSS}}}{\Delta v_s}\frac{\Delta v_s}{\Delta\omega_r}\Delta\omega_r \\ &= \frac{K_2K_3K_AK_C(sT_W)(1+sT_1)(1+sT_3)}{\left[(1+sT_{3fd})(1+sT_A)+K_3K_6K_A\right](1+sT_W)(1+sT_2)(1+sT_4)}\Delta\omega_r \end{aligned} \tag{4.18}$$

This is the air-gap torque exerted by PSS action. To evaluate $\Delta T_e\big|_{\text{PSS}}$, the eigenvalue $\lambda = \sigma + j\omega$ corresponding to the rotor angle mode is substituted for s. λ is obtained from the state matrix $\mathbf{A}$ of Eq. (4.13).

Since $\Delta T_e|_{PSS}$ is proportional to $\Delta\omega_r$, the expressions for K_D and K_S derived in Appendix A.3 are used to evaluate the PSS damping and synchronizing torque coefficients:

$$K_{D(PSS)} = \mathrm{Re}\left(\frac{\Delta T_e|_{PSS}}{\Delta\omega_r}\right) + \left(\frac{\sigma}{\omega}\right)\mathrm{Im}\left(\frac{\Delta T_e|_{PSS}}{\Delta\omega_r}\right) \tag{4.19}$$

$$K_{S(PSS)} = -\left(\frac{\sigma^2}{\omega_0\omega} + \frac{\omega}{\omega_0}\right)\mathrm{Im}\left(\frac{\Delta T_e|_{PSS}}{\Delta\omega_r}\right) \tag{4.20}$$

These expressions for $K_{D(PSS)}$ and $K_{S(PSS)}$ are used in the investigation of section 4.6 to evaluate the variation of PSS performance for various system conditions. To evaluate the PSS controller parameters used to determine $\Delta T_e|_{PSS}$, an integral of the square error performance index is employed. The following section deals with this as well as other aspects of controller design.

4.5 Controller Optimisation Using ISE Technique

References [22] and [29] suggest the Integral of Square Error (ISE) performance index for obtaining optimum PSS settings. Ref. [68] pp. 437-448 elaborates on the implementation of the ISE performance index for matrix functions. This section discusses the ISE technique, its mathematical implementation, and assumptions made regarding its implementation.

4.5.1 Preliminary model simplification

Eq. (4.13) gives the state-space model of the system, $\dot{\mathbf{x}} = \mathbf{A}\mathbf{x} + \mathbf{\Gamma}\mathbf{p}$. It is desired to eliminate the perturbation term $\mathbf{\Gamma}\mathbf{p}$.

Define

$$\hat{\mathbf{x}}(t) = \mathbf{x}(t) - \mathbf{x}(\infty), \tag{4.21}$$

where $\mathbf{x}(\infty)$ is the steady-state value of the state vector $\mathbf{x}(t)$, implying $\dot{\mathbf{x}}(\infty) = 0$. $\hat{\mathbf{x}}(t)$ represents the difference (error) between $\mathbf{x}$ at time t, and the steady-state value at time $t = \infty$. Substituting the expression for $\hat{\mathbf{x}}(t)$ into Eq. (4.13) reduces the state-space model to the form

$$\frac{d}{dt}\hat{\mathbf{x}}(t) = \mathbf{A}\hat{\mathbf{x}}(t)\,;\ \hat{\mathbf{x}}(0) = -\mathbf{x}(\infty) \tag{4.22}$$

To evaluate $\hat{\mathbf{x}}(0)$ is to evaluate $\mathbf{x}(\infty)$:

$$\frac{d}{dt}\mathbf{x}(\infty) = 0 = \mathbf{A}\mathbf{x}(\infty) + \mathbf{\Gamma}\mathbf{p} \Rightarrow \therefore \mathbf{x}(\infty) = -\mathbf{A}^{-1}\mathbf{\Gamma}\mathbf{p} \tag{4.23}$$

Hence $\hat{\mathbf{x}}(0) = \mathbf{A}^{-1}\mathbf{\Gamma}\mathbf{p}$. These expressions are used in the controller optimisation calculations discussed below.

4.5.2 Performance index

A system is considered an optimum control system when the system parameters are adjusted so that an index specified, known as the performance index, reaches an extremum value, commonly a minimum value ([68] pp. 139). Then the best system is defined as that system for which the performance index is a minimum.

The integral of the square of the error performance index is defined as

$$\text{ISE} = \int_0^T e^2(t)dt\,. \tag{4.24}$$

The upper limit T is usually chosen as the settling time T_S of the error function $e(t)$; $e(t)$ is the difference between the control output at time t, and the steady-state value at time T_S. The ISE technique discriminates between excessively overdamped systems and excessively underdamped systems ([68] pp. 139). The minimum value of the integral occurs for a compromise value of the damping.

It is desired to obtain parameters for the PSS controller for optimum damping of the rotor angle (electromechanical) oscillation mode. The variables $\Delta\delta$ and $\Delta\omega_r$ pertain to this oscillation mode. Refs [22] and [29] suggest the following quadratic performance index:

$$J = \int_0^\infty \left[\alpha\Delta\hat{\omega}_r^2 + \Delta\hat{\delta}^2\right]dt \tag{4.25}$$

Since $\Delta\hat{\omega}_r$ and $\Delta\hat{\delta}$ are error functions of the respective state variables (Eq. (4.21)), this index J is an ISE index. α is a relative weighting factor. Define $\mathbf{Q}$ as the diagonal matrix with main diagonal $[\alpha \quad 1 \quad 0 \quad 0 \quad 0 \quad 0 \quad 0]$; then Eq. (4.25) can be written as

$$J = \int_0^\infty \left[\hat{\mathbf{x}}^T\mathbf{Q}\hat{\mathbf{x}}\right]dt\,. \tag{4.26}$$

In order to obtain a minimum value for J, the existence of an exact differential, so that

$$\frac{d}{dt}\left(\hat{\mathbf{x}}^T\mathbf{P}\hat{\mathbf{x}}\right)=-\hat{\mathbf{x}}^T\mathbf{Q}\hat{\mathbf{x}}, \tag{4.27}$$

is postulated ([68] pp. 440). $\mathbf{P}$ remains yet to be determined. To simplify the algebra without any loss of generality, a symmetric $\mathbf{P}$ matrix is used; then $p_{ij}=p_{ji}$. From Eq. (4.27),

$$\frac{d}{dt}\left(\hat{\mathbf{x}}^T\mathbf{P}\hat{\mathbf{x}}\right)=\dot{\hat{\mathbf{x}}}^T\mathbf{P}\hat{\mathbf{x}}+\hat{\mathbf{x}}^T\mathbf{P}\dot{\hat{\mathbf{x}}}. \tag{4.28}$$

With $\dot{\hat{\mathbf{x}}}$ from Eq. (4.22),

$$\begin{aligned}\frac{d}{dt}\left(\hat{\mathbf{x}}^T\mathbf{P}\hat{\mathbf{x}}\right)&=\left(\mathbf{A}\hat{\mathbf{x}}\right)^T\mathbf{P}\hat{\mathbf{x}}+\hat{\mathbf{x}}^T\mathbf{P}\left(\mathbf{A}\hat{\mathbf{x}}\right)\\&=\hat{\mathbf{x}}^T\mathbf{A}^T\mathbf{P}\hat{\mathbf{x}}+\hat{\mathbf{x}}^T\mathbf{P}\mathbf{A}\hat{\mathbf{x}}\\&=\hat{\mathbf{x}}^T\left(\mathbf{A}^T\mathbf{P}+\mathbf{P}\mathbf{A}\right)\hat{\mathbf{x}}\end{aligned}. \tag{4.29}$$

Let $\mathbf{A}^T\mathbf{P}+\mathbf{P}\mathbf{A}=-\mathbf{Q}$. Then Eq. (4.29) becomes (4.27), the exact differential sought. Substitution of Eq. (4.27) in (4.26) gives

$$\begin{aligned}J&=\int_0^\infty\left[\hat{\mathbf{x}}^T\mathbf{Q}\hat{\mathbf{x}}\right]dt\\&=\int_0^\infty-\frac{d}{dt}\left(\hat{\mathbf{x}}^T\mathbf{P}\hat{\mathbf{x}}\right)dt\\&=-\hat{\mathbf{x}}^T\mathbf{P}\hat{\mathbf{x}}\Big|_0^\infty=\hat{\mathbf{x}}(0)^T\mathbf{P}\hat{\mathbf{x}}(0)\end{aligned} \tag{4.30}$$

where it is assumed that the system is stable and hence $\hat{\mathbf{x}}(\infty)=0$. $\hat{\mathbf{x}}(0)$ is evaluated using the relation $\hat{\mathbf{x}}(0)=\mathbf{A}^{-1}\mathbf{\Gamma p}$ obtained from Eqs (4.22) and (4.23). Solving the Lyapunov equation $\mathbf{A}^T\mathbf{P}+\mathbf{P}\mathbf{A}=-\mathbf{Q}$ gives the symmetric matrix $\mathbf{P}$ used in (4.30) to give the performance index J.

According to Ref. [29], system dynamic performance with PSS is best when $\alpha=0$ is assumed. The result is a simple ISE-type performance index,

$$J=\int_0^\infty\Delta\hat{\delta}^2dt. \tag{4.31}$$

The state variable $\Delta\hat{\delta}$ is penalized in order to obtain optimum performance.

4.5.3 Optimisation process

From the discussion above, the steps to design an optimum controller are as follows:

1. Given a set of particular controller parameters, solve for $\mathbf{P}$ from the Lyapunov equation $\mathbf{A}^T\mathbf{P}+\mathbf{P}\mathbf{A}=-\mathbf{Q}$. $\mathbf{A}$ is the system state matrix, and $\mathbf{Q}$ the diagonal matrix with main diagonal $[0 \quad 1 \quad 0 \quad 0 \quad 0 \quad 0 \quad 0]$ (note that $\alpha = 0$).
2. Evaluate $\hat{\mathbf{x}}(0)$ using the relation $\hat{\mathbf{x}}(0) = \mathbf{A}^{-1}\boldsymbol{\Gamma}\mathbf{p}$, where both $\mathbf{A}$ and $\boldsymbol{\Gamma}$ are known. $\mathbf{p}$ is the perturbation vector $\mathbf{p} = [\Delta T_m \quad \Delta V_{ref}]^T$, assumed to be a step perturbation vector remaining constant during the dynamics of the process. Since the investigation focuses on rotor angle mode oscillations, $\Delta T_m = 1$ and $\Delta V_{ref} = 0$ is assumed [29]. The value of ΔT_m used does not influence the results.
3. Evaluate the performance index J using the relation $J = \hat{\mathbf{x}}(0)^T \mathbf{P}\hat{\mathbf{x}}(0)$.
4. Repeat the process until a minimum J is obtained.

The procedure above is implemented as follows: plot J versus K_C for several values of T_1 ($T_1 = T_3$ and $T_2 = T_4$; T_2 is constant – see section 4.5.4). For any T_1, J decreases with increase in K_C, reaches a minimum $J_{\min}$, and increases with further increase in K_C. The values for K_C and T_1 that correspond to the minimum of $J_{\min}$ are the optimum PSS parameters.

4.5.4 PSS Controller Design

Section 4.5.3 describes a procedure for obtaining the parameters of any oscillation stabilizer controller to give optimum performance. In the case of a PSS, the parameters to be optimised are the time constants T_W, T_1 . . . T_4 and the gain K_C.

The washout time constant ought to be high enough to pass stabilizing signals at the frequencies of interest (normally 0.7 – 3.0 Hz) relatively unchanged. A value of $T_W = 10$ s is chosen [17][25][29][11]. At this value the washout block has virtually no impact upon the local mode oscillations, the focus of this investigation.

With reference to the universally applicable stabilizing function of [2], and to simplify the problem ([22], [29]), two identical cascade lead-lag networks are considered for the PSS. This may not be necessary for all system scenarios considered, but is done so to generalise the investigation and enable comparison of results on the same basis. Hence $T_1 = T_3$ and

$T_2 = T_4$ in Fig. 4.2. In all ensuing discussions, reference to T_1 implies both the time constants T_1 and T_3; similarly T_2 implies both T_2 and T_4. This is done to facilitate ease of reading.

Ref. [2] suggests a minimum of 0.05 s for the lag time constants, reasons it being physically realizable and a more conservative approach. Such a minimum ensures the PSS has only minimal influence on oscillations at frequencies beyond the rotor angle mode range (0.1 – 3.0 Hz or 0.628 – 18.85 rad/s ([60] pp. 1133); $T_2 = 0.05$ s corresponds to 20 rad/s), such as torsional oscillating frequencies. Refs [22], [30] and [11] assume $T_2 = 0.05$ s in the investigations.

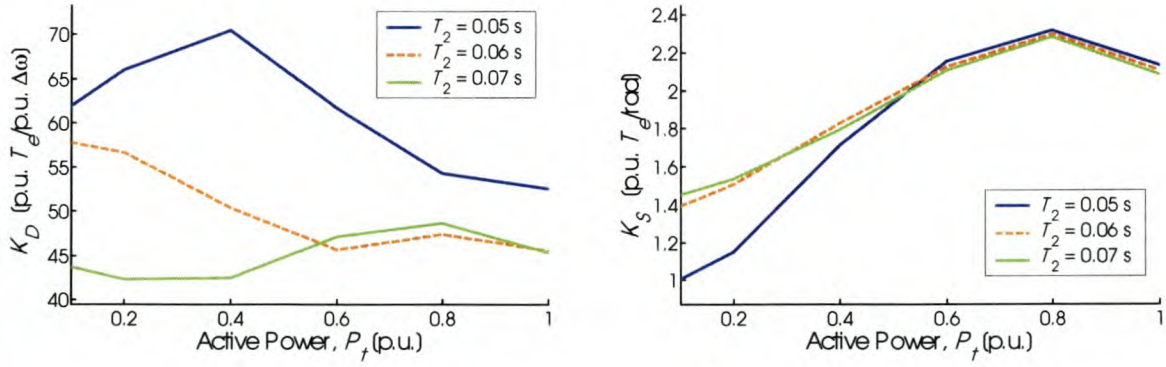

Fig. 4.5: System torques vs. machine load and PSS controller time constant T_2, with X_E = 0.8 p.u.

A comparison of PSS controller optimum damping and corresponding system total damping results for various T_2, for the system without external resistance, suggest 0.05 s to be an appropriate value. Fig. 4.5(a) illustrates K_D for various T_2, when $X_E = 0.08$ p.u. Appendix F.1 contains results for K_D and K_S for other X_E. In obtaining these results, a lower limit of 0.05 s was imposed on T_1 (see discussion on Fig 4.6(b)). Added damping torque is required more in a weaker system and/or a system that is more highly loaded (chapter 3). Results show a PSS controller with $T_2 = 0.05$ s gives more effective damping performance when such damping performance is required, compared to damping controllers with higher T_2 values. Fig. 4.5(b) shows the choice of T_2 does sacrifice the system synchronizing torque for some system conditions. There is no need for added synchronizing torque in the system (chapter 3); hence this is of no particular concern.

With $T_2 = 0.05$ s, the PSS parameters K_C and T_1 are optimised according to the method described in section 4.5.3. Fig 4.6 shows the PSS optimised parameters K_C and T_1 for the

system without resistance. The following observations also hold for the system with external line or local load resistance (results in Appendix F).

Values for K_C are high at low P_t and reduces with increase in machine load (Fig 4.6(a)). T_1 values are generally higher when K_C values are lower (Fig 4.6(b)). The very high K_C values at low P_t may prove problematic in transient stability studies of practical systems. PSS output hard limits are ±0.05 p.u. in practical implementations [31] – PSS performance is impeded if these are reached during a transient. However, limiting the values of K_C only serves to reduce the PSS small-signal performance at low P_t. This investigation focuses on small-signal behaviour; transient stability is beyond the scope of this research. Consequently, K_C values are not limited to a maximum in the modelling process.

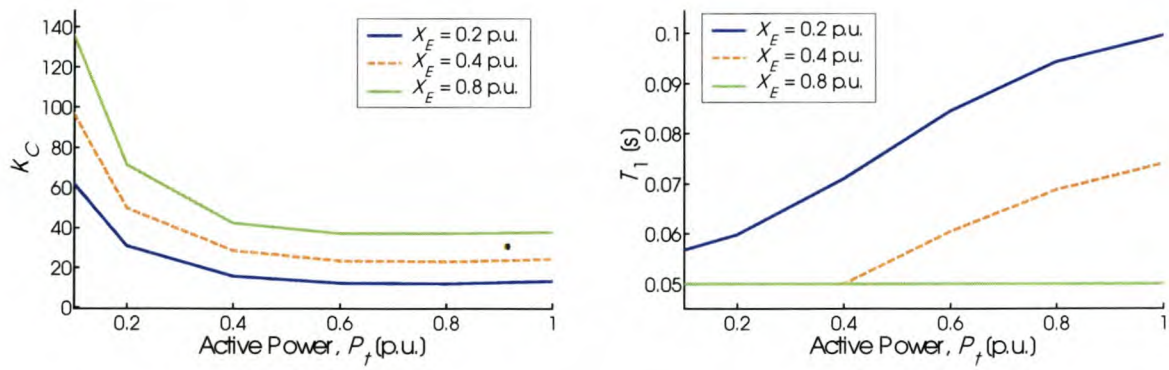

Fig 4.6: Optimised PSS parameters K_C and T_1 vs. machine load and external reactance

It is possible to obtain T_1 values smaller than 0.05 s that give optimum PSS performance by the ISE technique discussed. In such instances the PSS controller would introduce a phase lag that, combined with the phase lag of the "plant" transfer function (section 4.4.1), results in a still greater net phase lag. However, to ensure the controller does not influence oscillations beyond the rotor angle mode scope (see discussion on T_2 above), values of T_1 are limited to a minimum of 0.05 s. Whenever T_1 equals 0.05 s (such as $X_E = 0.8$ p.u. in Fig 4.6(b)), the PSS controller exhibits no phase compensation and consists only of a gain and signal washout function (Fig. 4.2).

Relatively low values are obtained for the time constant T_1. This can be attributed to the reduced phase lag contributed to $GEP(s)\big|_{\text{PSS}}$ by the static excitation system, compared to a

dc-type excitation system. A PSS controller in a system with dc-type excitation system optimised by the ISE technique has higher T_1-values [22].

Ref. [18] suggests the net phase lag of the PSS controller torque function (Eq. (4.18)) at the undamped natural frequencies ω_n to be between 0° and 45° to minimize the effect of system changes on stabilizer performance. Investigation of the system with PSS optimised by the ISE technique shows the net phase lags at ω_n to be between 23° and 52°, depending on generator load an system impedance. The net phase lag has a greater influence on the PSS synchronizing torque; hence this is considered suitable for comparative investigation.

4.6 PSS Performance Analysis

This section investigates the ability of a PSS controller to provide damping torque to the system when such damping torque is needed, as determined in chapter 3. Eq. (4.19) gives the expression for the PSS damping torque coefficient used in the investigation. The procedure used is similar to the procedure of sections 3.6 and 3.8.

The investigation wishes to compare PSS and CSC capability given a certain condition of system impedance and load. For each condition, the controller is optimised for that particular condition and the torque coefficients reflect such optimum control. This method differs from that normally found in literature, where the controller is optimised for a particular system condition (usually the strong system condition [16]) and the robustness of this controller evaluated for a range of system conditions.

The optimisation process described in section 4.5.3 requires a significant amount of computations and iterations. To minimize simulation time, solutions are evaluated and plotted for only selected values of system load.

The PSS synchronizing torque coefficient, Eq. (4.20), is also analysed to assess the influence of the PSS controller on the system synchronizing stability whilst improving the damping stability.

The following section discusses the analysis procedure used in this research. Sections 4.6.2 to 4.6.4 investigate the influence of machine loading and system reactance and resistance on the PSS torque coefficients by MATLAB simulation. Machine saturation is modelled and $K_A = 200$. Section 4.6.5 discusses the influence of assuming a lower K_A on PSS

performance; section 4.6.6 the effect of neglecting saturation. Section 4.6 ends with a concluding summary.

4.6.1 Analysis procedure

Section 3.8.1 discusses the procedure and parameter values used to obtain plots for the system damping and synchronizing torque coefficients. This same procedure and assumptions are used in the investigation of PSS controller performance. This research assumes both end-point voltages in Fig. 3.1 constant at unity. Section 3.5 discusses the implications of this. No control is placed on the machine reactive load Q_t; hence Q_t can become negative (machine a sink of reactive power – see Eq. (3.39)), particularly as the external resistance increases.

With E_t and E_B constant at 1.0 p.u., plots of the PSS damping and synchronizing torques, and other parameters, vs. machine load, for various external reactance, external resistance to reactance ratio, and local load resistance, are generated by MATLAB simulation. Section 3.6.1 gives the values of X_E, R_E/X_E, and R_{load} considered in the investigation. Appendix B describes the test system used.

4.6.2 Machine load and line reactance

This section neglects system external resistance. This simplifies analysis and results are typical of the case where a power source is connected to a large system through high voltage transmission line(s), with no or negligible local load.

Fig. 4.7 shows plots of the PSS and system total torque coefficients. The damping and synchronizing torques are evaluated by use of the system eigenvalue corresponding to the local mode oscillation substituted for s in Eq. (4.18). Whenever T_1 is forced to the minimum value of 0.05 s, Fig. 4.8(b) shows the damping ratio increases significantly. This results in a deviation of $K_{D(\mathrm{PSS})}$ from the characteristic it attains when T_1 exceeds the threshold of 0.05 s.

Whenever T_1 equals the lower limit of 0.05 s (section 4.5.4), the PSS damping torque is higher and the synchronizing torque lower than would have been if no lower limit were assumed. This explains why in a weaker more lightly loaded system the optimum PSS controller provides more damping torque than one in a stronger system with similar loading. At higher loading, when T_1 exceeds the lower limit of 0.05 s, the PSS optimum damping capability increases with increase in system strength and load.

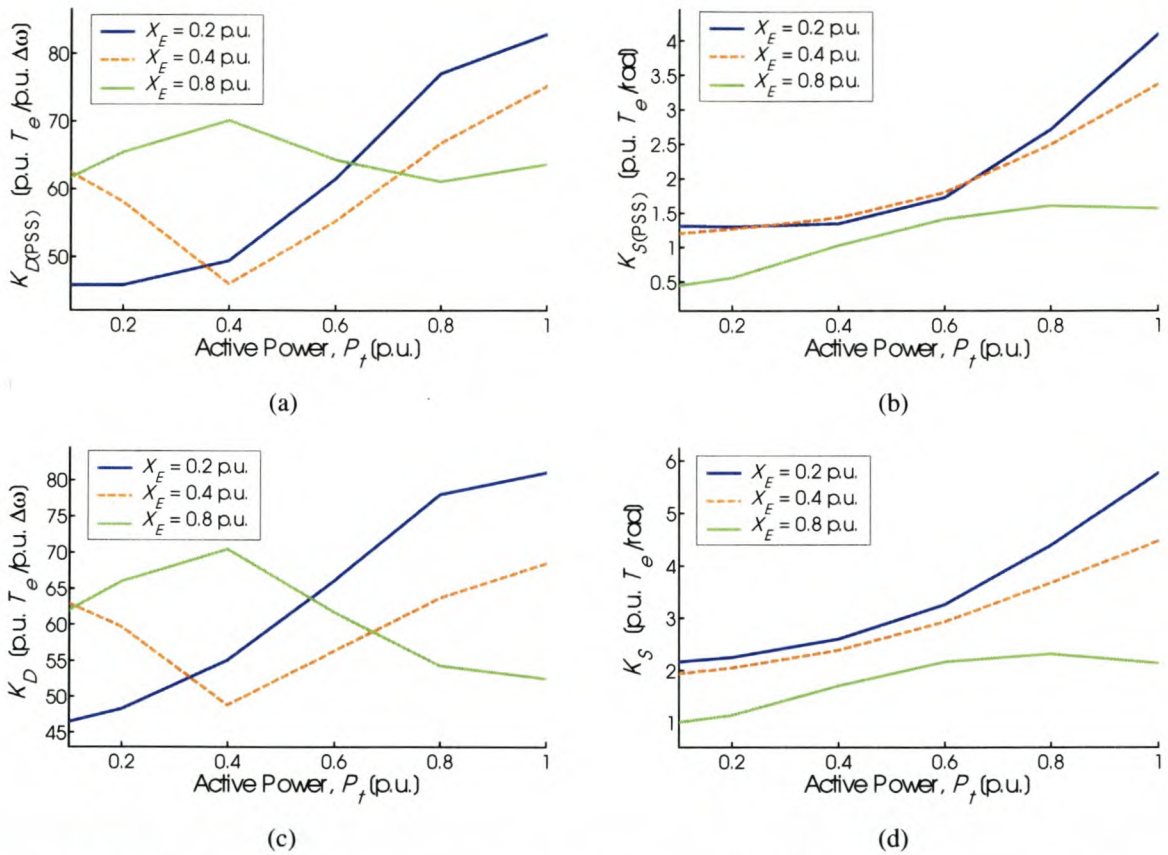

Fig. 4.7: PSS and system torque coefficients vs. machine load and external reactance

To gain insight into the behaviour of optimal PSS stabilization versus system load and strength (when T_1 exceeds 0.05 s), $GEP(s)\big|_{\text{PSS}}$ and the stabilizer transfer function gains were analysed at the oscillating frequency ω_n. Fig. 4.8(a) shows ω_n for the system conditions considered. Fig. 4.8(b) shows there is little variation in the damping ratio of the stabilized system when T_1 does not equal 0.05 s (compare Fig 4.6(b)); hence considering the transfer function gains at ω_n can give valuable information on the influence certain factors have on PSS performance.

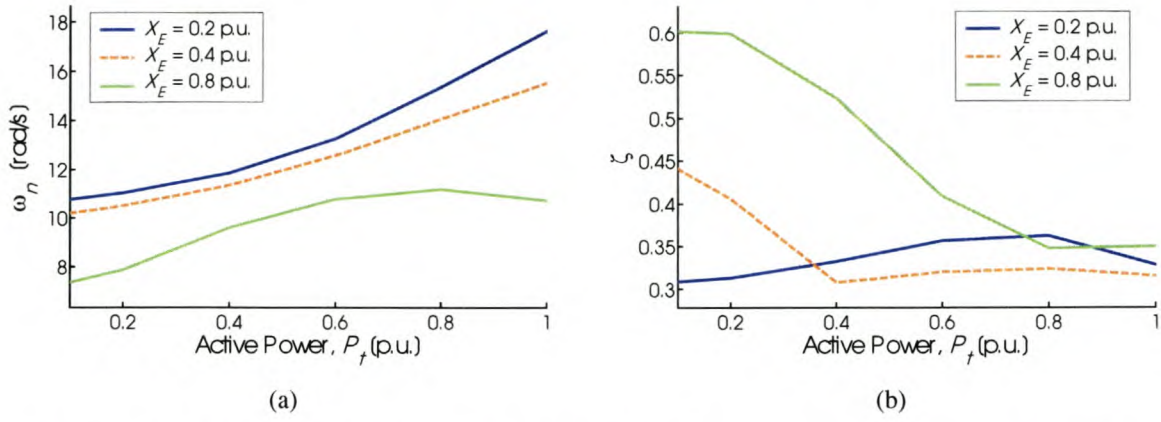

(a) (b)

Fig. 4.8: Undamped natural frequency and damping ratio vs. machine load and external reactance

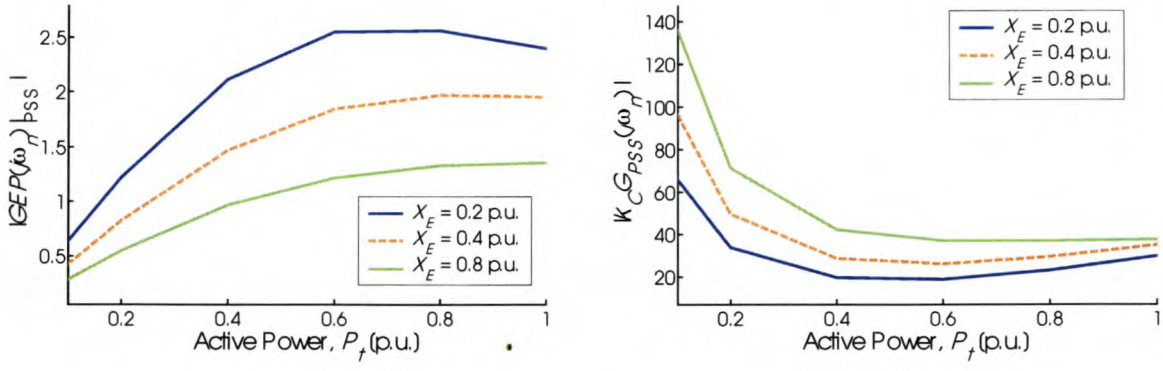

(a) (b)

Fig. 4.9: "Plant" and PSS controller transfer function gains vs. machine load and external reactance

Fig. 4.9 shows the "plant" and controller transfer function gains for the system. Consider the case of $X_E = 0.2$ p.u., where T_1 is larger than 0.05 s (Fig 4.6(b)). As the system load increases, $\left|GEP(s)\right|_{\text{PSS}}\left|\right.$ increases and the controller gain at ω_n decreases in value. Although the controller gains are significantly larger in value than $\left|GEP(s)\right|_{\text{PSS}}\left|\right.$, the increase in $\left|GEP(s)\right|_{\text{PSS}}\left|\right.$ exceeds the decrease in the controller gain. The result is a net increase in PSS torque transfer function gain.

This discussion illustrates that, although K_C reduces with increased P_t and system strength (Fig 4.6(a)), the characteristics of $GEP(s)\big|_{\text{PSS}}$ play a significant role in the behaviour of $\Delta T_e\big|_{\text{PSS}}$. According to Ref. [16], this behaviour can be described in terms of the parameters K_2 and K_6 of Fig. 3.11, and the exciter gain. With constant K_A, $\Delta T_e\big|_{\text{PSS}}$ (and hence $K_{D(\text{PSS})}$

also – Eq. (4.19)) is proportional to K_2 and $1/K_6$ (Eq. (4.18)). Since both K_2 and $1/K_6$ increase with increase in system load and strength, so does the PSS performance.

Fig. 4.7(b) shows the PSS synchronizing torque. The PSS controller optimised by the ISE technique is such that the PSS torque transfer function of Eq. (4.18) exhibits a slight phase lag [22]. As a result, the PSS controller introduces positive synchronizing torque into the system that increases with increase in P_t and system strength. The PSS controller adds to the net synchronizing torque shown in Fig. 4.7(d) and enhances the synchronous machine transient stability. Whenever T_1 is forced to the minimum value of 0.05 s the PSS controller introduces less synchronizing torque, and values for ω_n and K_S are lower than would have been the case if no lower limit were imposed on T_1.

Fig. 4.7(c) shows the total system damping torque. $K_{D(\mathrm{PSS})}$ of Fig. 4.7(a), as well as the AVR and AR damping torques of Fig. 3.23, increase with increase in system strength; hence K_D also. Values for $K_{D(\mathrm{PSS})}$ are much higher than the damping torque coefficient of the system without oscillation stabilizer (Fig. 3.23(e)). Consequently, K_D follows the trends of $K_{D(\mathrm{PSS})}$ with respect to changes in external reactance and system load. The slight reduction of K_D with increase in P_t at high generator load conditions is caused by the AVR damping torque – see Fig. 3.23(c).

4.6.3 Line resistance

Section 4.6.2 neglected system external resistance. This section focuses on the influence of line resistance on the PSS torque coefficients. Appendix F.2 contains results for this section.

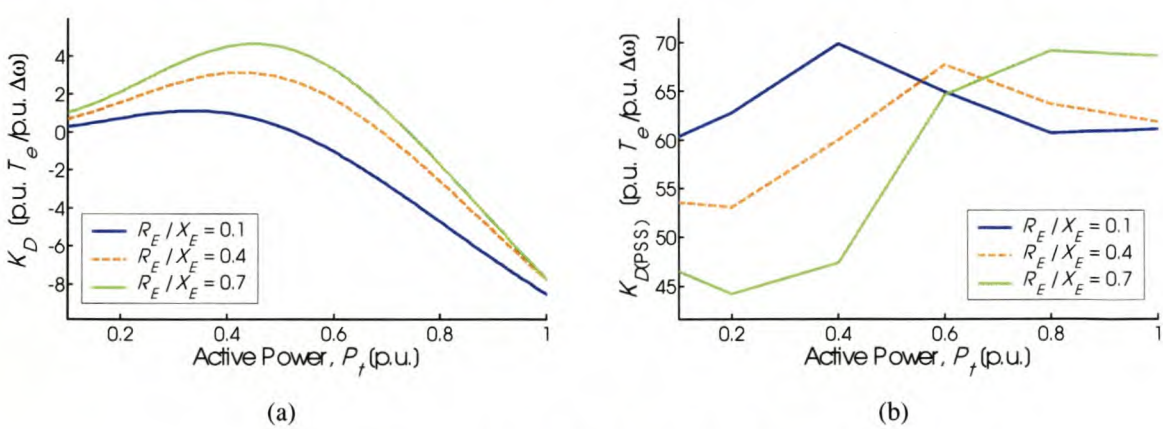

Fig. 4.10: Damping torques for system with X_E = 0.8 p.u.

Damping torque is particularly needed in a system with high external reactance, regardless of R_E/X_E. Fig. 4.10(a) shows K_D for the system with no stabilizer when $X_E = 0.8$ p.u. At high P_t line resistance does not sufficiently improve the system stability. However, the PSS controller optimised by the ISE technique (which incidentally has $T_1 = 0.05$ s for all conditions when $X_E = 0.8$ p.u.) is able to provide the needed damping (Fig. 4.10(b)). Since T_1 is constant, there is no definite trend in $K_{D(\text{PSS})}$ with respect to R_E/X_E. Results obtained for lower values of X_E show $K_{D(\text{PSS})}$ decreases with increase in R_E/X_E whenever $T_1 > 0.05$ s. This is desirable, since the stability problems for which the stabilizer is needed increases with decrease in R_E/X_E (section 3.8.3, Fig. 4.10(a)).

The synchronizing torque of the system without an oscillation stabilizer decreases with increase in R_E/X_E (section 3.8.3), particularly in a weaker system. To ensure greater transient stability if the need be, more K_S is needed. However, results show $K_{S(\text{PSS})}$ decreases with increase in R_E/X_E; hence the PSS controller optimised by the ISE technique is not able to introduce more synchronizing torque when more is needed. $K_{S(\text{PSS})}$ may be increased by changing the controller time constants, but this increase will most probably be at the expense of damping torque.

4.6.4 Local load

This section focuses on the influence of local load on $K_{D(\text{PSS})}$. Appendix F.3 contains the results for this section.

For reasons discussed in section 3.4.1, a resistance R_{load} models the local load. Table 3.1 gives the X_{line} and R_{load} value combinations used in the investigation, and the resulting X_E, R_E and E_B values from which the system parameters are determined (see discussion on Fig. 3.7).

The system damping, as well as the damping by the optimal PSS controller for a given system condition, behaves in a manner similar to the scenario with external line resistance (section 4.6.3). Local load inherently provides damping torque to the system (section 3.8.4), and if sufficient ensures damping stability when otherwise would not be the case (at the expense of synchronizing torque). On the other hand, if the local load is not sufficient to

provide the needed damping (particularly when X_{line} is large), an oscillation stabilizer is required for stability support.

Fig. 4.11(a) shows K_D for the system with no stabilizer when $X_{line} = 0.8$ p.u . At high P_t, if significant local load is not available the system is oscillatory unstable. However, the PSS controller optimised by the ISE technique (which incidentally has $T_1 = 0.05$ s for all conditions when $X_{line} = 0.8$ p.u.) is able to provide the needed damping (Fig. 4.11(b)). Since T_1 is constant, there is no definite trend in $K_{D(\mathrm{PSS})}$ with respect to local load. Results obtained for lower values of X_{line} show $K_{D(\mathrm{PSS})}$ increases with decrease in local load whenever $T_1 > 0.05$ s . This is desirable, since the stability problems for which the stabilizer is needed increases with decrease in local load (section 3.8.4, Fig. 4.11(a)).

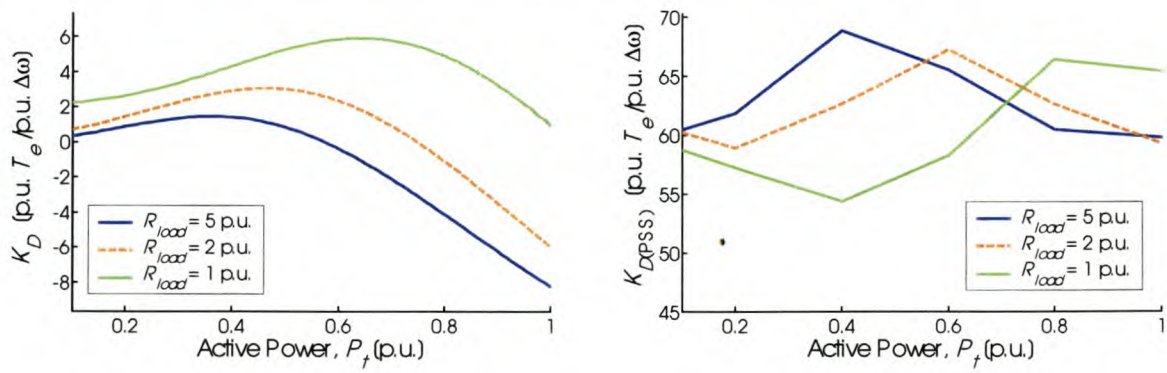

(a) (b)

Fig. 4.11: Damping torques for system with X_{line} = 0.8 p.u.

The synchronizing torque of the system without an oscillation stabilizer decreases with increase in local load (section 3.8.4), particularly in a weaker system. Although K_S of Fig. 3.26(f) is positive for the range of conditions, should there be a desire to ensure greater transient stability more K_S is needed. However, results show $K_{S(\mathrm{PSS})}$ decreases with increase in local load; hence the PSS controller optimised by the ISE technique is not able to introduce more synchronizing torque when more is needed. $K_{S(\mathrm{PSS})}$ may be increased by changing the controller time constants, possibly at the expense of damping torque.

4.6.5 Excitation system gain

Results for sections 4.6.2 to 4.6.4 reflect a system with high initial-response excitation system; i.e. with an AVR gain of 200. Section 3.3.2 discusses the motivation behind

assuming such a high gain. This section considers the influence of assuming a lower K_A on the PSS performance. Results for the previous sections were regenerated for the system of Appendix B, but with $K_A = 20$. Appendix F.4 contains the results.

Less damping support is needed in a system with lower K_A (section 3.8.5). Yet, under conditions of large external reactance and generator loading K_D is still negative, and there is a need for stability support.

In a system with lower AVR gain, values for K_C and T_1 are higher compared to a system with higher K_A. As a result, T_1 for the controller optimised by the ISE technique exceeds the minimum threshold of 0.05 s for all conditions considered, and the trends of $K_{D(\mathrm{PSS})}$ and $K_{S(\mathrm{PSS})}$ reflect that.

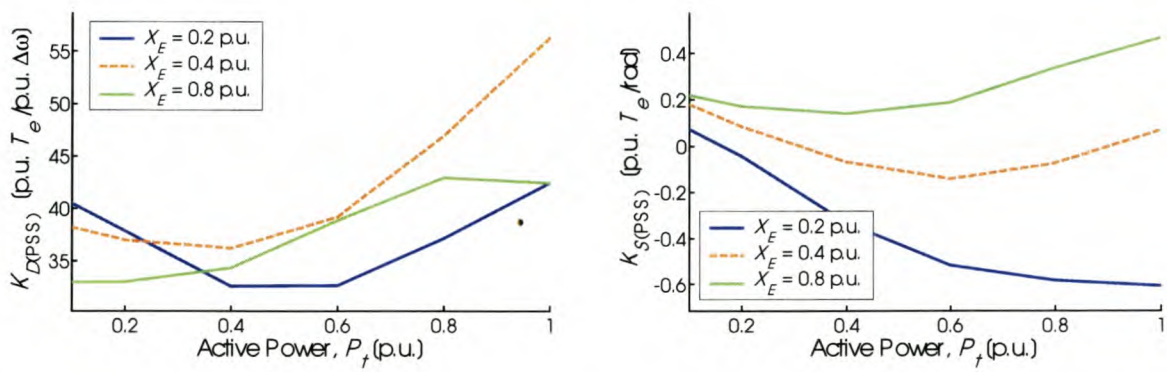

Fig. 4.12: PSS damping and synchronizing torque coefficients vs. machine load and external reactance, when $K_A = 20$

Fig. 4.12(a) shows the PSS damping torque coefficient for the system with $K_A = 20$. Comparison to Fig. 4.7(a) shows values for $K_{D(\mathrm{PSS})}$ are lower in a system with lower K_A, despite the increase in K_C. $K_{D(\mathrm{PSS})}$ for moderate to high X_E increase with P_t, which is desirable (section 3.8.5). However, the PSS controller performance is lower in a weaker system of similar loading (for systems of moderate to high X_E), so that the influence of the stabilizer decreases when the power system requires it most.

Fig. 4.12(b) shows the synchronizing torque of the PSS controller optimised by the ISE technique, for the system with $K_A = 20$. Comparison to Fig. 4.7(b) shows $K_{S(\mathrm{PSS})}$ to be much lower in value and reduces with increase in system strength, even so that $K_{S(\mathrm{PSS})}$ is

negative in a strong system when $K_A = 20$. Negative $K_{S(\text{PSS})}$ is a result of overcompensation of the "plant" phase lag – the transfer function of Eq. (4.18) has a phase lead at the oscillation frequencies of concern, causing a reduction in the net system synchronizing torque and ω_n ([60] pp. 769, [16]). Regardless of this negative $K_{S(\text{PSS})}$, K_S for the system with PSS remains positive and the system transiently stable.

This is not of particular concern; a PSS would seldom be installed in a strong system (such as $X_E = 0.2$ p.u. for the system considered) where there is no need of additional damping torque.

If it is required that the PSS controller enhance the system transient stability as well as the damping stability, T_1 can be altered to achieve the desired effect. An increase of $K_{S(\text{PSS})}$ would however be at the expense of damping torque.

For the systems with line resistance or local load accounted for, values for $K_{D(\text{PSS})}$ are lower when the AVR gain is lower, whereas K_C and T_1 values are higher (see results in Appendix F.4). This is similar to results for the system without external resistance. Results show the PSS controller damping torque increases with reduction in R_E/X_E or local load. This is desirable, since the stability problems for which the stabilizer is applied also increase with reduced external line resistance or local load (section 3.8.5).

The trends of $K_{S(\text{PSS})}$ with respect to changes in R_E/X_E or local load does not change when a lower K_A is assumed, and reduces with increase in R_E/X_E or local load. As a result $K_{S(\text{PSS})}$ can be negative, particularly in a strong system but also in weaker systems with high R_E/X_E or local load – conditions when damping support by a PSS may be needed. The system net synchronizing torque (and ω_n) is then reduced, although the higher transient synchronizing torque (K_1 – section 3.6) ensures K_S remains positive for all system conditions considered.

4.6.6 Influence of saturation

Synchronous machine saturation was modelled to obtain the results of the previous sections. Appendix C explains the modelling of saturation in the synchronous machine. This section considers the influence of neglecting saturation, often the assumption in literature.

The results of section 4.6.2 (system without external resistance, and $K_A = 200$) were regenerated for the system of Appendix B with machine saturation neglected (constant machine inductances/reactances). Appendix F.5 contains the results.

Results show values of K_C and T_1 of the ISE-optimised PSS controller are lower when saturation effect is neglected compared to when saturation is modelled. With some exceptions, values of the PSS damping and synchronizing torques are also lower in magnitude, sometimes significant – this depends on whether T_1 attains the minimum threshold value; since values of T_1 are lower when saturation is neglected this is more often the case when otherwise it would not have been.

These results indicate the need to model saturation: (a) to ensure more reliable PSS controller design by the ISE technique, and (b) to more correctly assess the influence of such controller on system stability, whether damping or synchronizing.

4.6.7 Summary of results

The trends of the PSS damping torque coefficient, with respect to *machine load and external reactance* (section 4.6.2), *line resistance* (section 4.6.3) and *local load* (section 4.6.4) were examined. The influences of the *AVR gain* (section 4.6.5) and *saturation modelling* (section 4.6.6) on results were also considered.

A summary of the results of section 4.6 follows.

The PSS controller gain, as obtained by the ISE optimisation method, is high at low P_t and decreases with increase in machine load. K_C values are also lower in a stronger system. In a system with lower AVR gain but similar in all other respects, the optimisation process obtains a higher K_C value necessary for optimum performance. When saturation is neglected, values for K_C are lower compared to when saturation is modelled.

Values for T_1 by the ISE optimisation method increase with increase in system load or strength. However, to ensure the controller does not influence oscillations beyond the rotor angle mode scope, values of T_1 are limited to a minimum of 0.05 s. In a system with lower AVR gain but similar in all other respects, the optimisation process obtains a higher T_1 value necessary for optimum performance. When saturation is neglected, values for T_1 are lower compared to when saturation is modelled.

Whenever the value of T_1 is at the minimum of 0.05 s, the PSS damping torque is higher than would have been if no lower limit were assumed. Under such conditions there is no definite trend in the variation of $K_{D(\mathrm{PSS})}$ with P_t, X_E, R_E/X_E or local load. For system conditions such that T_1 corresponding to optimum performance exceeds the lower limit of 0.05 s, the PSS optimum damping capability increases with increase in system strength and load and decreases with increase in R_E/X_E or local load. The latter characteristic is desirable, since the stability problems for which the stabilizer is needed increases with decrease in R_E/X_E or local load. Values for $K_{D(\mathrm{PSS})}$ are lower in a system with lower K_A. This is also favourable – less damping torque is needed in a system with lower K_A. When saturation is neglected, with some exceptions values of the PSS damping torque are lower compared to when saturation is modelled.

The PSS synchronizing torque is lower when the T_1 is at the minimum of 0.05 s, than would have been if no lower limit were assumed. The PSS controller optimised by the ISE technique introduces positive synchronizing torque into the system that increases with increase in P_t, but decreases with increase in R_E/X_E or local load. The variation of $K_{S(\mathrm{PSS})}$ with respect to external reactance depends on the gain of the generator AVR. Values for $K_{S(\mathrm{PSS})}$ are lower in a system with lower K_A – then $K_{S(\mathrm{PSS})}$ is even negative under certain conditions of system reactance, R_E/X_E and local load. The total system synchronizing torque however remains positive for all system conditions investigated. When saturation is neglected, with some exceptions values of the PSS synchronizing torque are lower compared to when saturation is modelled.

4.7 Summary

This chapter presented the state-space and block diagram models of the SMIB system with PSS, and determined the ability of a PSS to enhance system stability in situations when such stability support is required, according to results from chapter 3. For purpose of investigation the conventional (classic) PSS controller configuration was assumed.

Expressions for the PSS damping and synchronizing torque coefficients show the performance of the stabilizer for a certain system condition can be related to the constants K_2 and K_6 discussed in chapter 3, the gain of the generator AVR as well as the PSS controller

parameters. The parameters of the PSS are evaluated for every system condition to give optimum performance at the particular system condition. An optimisation technique based on the integral of the square error performance index is presented and used for that purpose. Some assumptions are made to simplify the optimisation process.

The investigation shows the PSS controller is able to provide both damping and synchronizing torque to the system. For conditions such that T_1 of the optimised PSS controller exceeds a minimum threshold value, the damping support behaves favourably with respect to variation in generator load, R_E/X_E or local load, or gain of the generator AVR. This is not the case with respect to changes in external system reactance.

The influence of the optimised PSS controller on the system synchronizing stability is also investigated. When a low gain AVR is employed the controller introduces negative synchronizing torque into the system for some conditions of external impedance. The system synchronizing torque however remains positive and the system transiently stable for all conditions.

5 CONTROLLED SERIES CAPACITOR

5.1 Introduction

This chapter introduces the state-space and block diagram models of the SMIB system with controlled series capacitor, and investigates the ability of a CSC to enhance system stability in situations when such stability support is required. Results in chapter 3 indicate that a system with generator highly loaded that operates into a moderate to high external impedance, with no or little local load, experiences negative damping.

Section 2.5.2 discusses the controlled series capacitor. The CSC has several functions, such as power flow control and extending stability limits. The latter is the focus of this research. It accomplishes this by modulating transmission line reactance to produce a component of electrical torque on the rotor that is in phase with rotor speed variations. By inducing such a torque, the CSC provides damping to the oscillations of synchronous machine rotors relative to one another.

Section 5.2 discusses the classic model SMIB system with CSC to illustrate the basic stability concepts by which the CSC operates. The model of section 5.4 builds on the concepts of section 5.2 by incorporating a higher-order generator definition and a conventional control scheme for the CSC controller.

The concepts of damping and synchronizing torques are used to evaluate the performance of the CSC controller. These torque expressions are functions of the system model K-parameters and the CSC controller parameters. Chapter 3 discusses the parameters $K_1 \ldots K_6$. Section 5.5 considers the parameters K_p, K_q and K_v. For every condition considered, the CSC parameters are optimised for that particular condition by the method of section 5.7, an integral of the square error based technique.

The characteristics and conditions under investigation are: (a) generator load; (b) system reactance as seen by the generator; (c) the amount of external (line) resistance relative to reactance, and (d) load local to the generator (sending-end) side of the SMIB system. The influences of AVR gain and machine saturation on results are also examined. The investigation places emphasis on the ability to provide stability support when such support is needed.

5.2 Classic Generator Model

Section 3.2 describes the SMIB system model with generator represented by a voltage source behind an effective transient reactance. A constant infinite bus voltage and reactance represents the external system.

This section builds on the concepts of section 3.2 by inclusion of a variable reactance as representative of a controlled series capacitor in the transmission line connecting the generator to the external system. The effect of synchronizing and damping torques on the system oscillations is already discussed (section 3.2.2). Here, rather, the focus is on the influence of a controlled series capacitor on the system synchronizing and damping torques that affect the system oscillations. To help understand the influence of a CSC on system behaviour, the state-space and block diagram models of the SMIB system with CSC is derived.

5.2.1 Small perturbation equations

Fig. 5.1 shows the SMIB system with CSC of reactance X_C. The capacitor reactance is a controlled element and needs to be treated as such in developing the system equations.

In section 3.2.1 the swing equation, Eq. (2.1), is expressed as a set of two first-order differential equations:

$$p\Delta\omega_r = \frac{1}{2H}(T_m - T_e - K_D\Delta\omega_r), \tag{5.1}$$

$$p\delta = \omega_0\Delta\omega_r. \tag{5.2}$$

These equations form the basis of developing state-space and block diagram models used to investigate the system steady-state stability performance. Eq. (3.3) describes the air-gap electrical torque (in per unit), reproduced below:

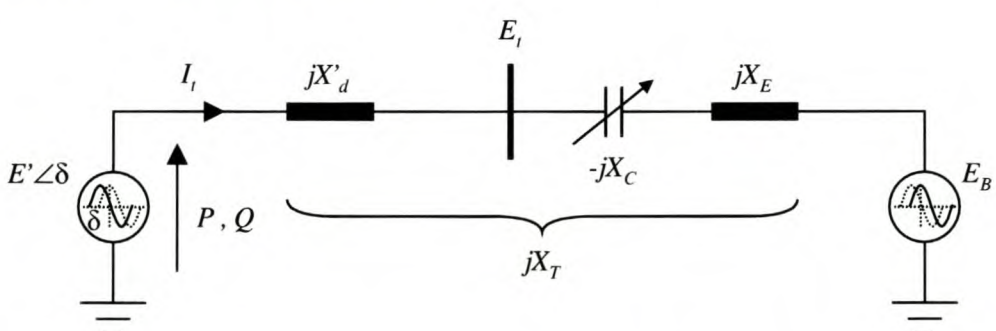

Fig. 5.1: SMIB system with CSC, classical generator model

$$T_e = P_e = \frac{E'E_B}{X_T}\sin\delta\,. \tag{5.3}$$

In this expression, Fig. 5.1 shows the total external reactance is

$$X_T = X'_d + X_E - X_C\,. \tag{5.4}$$

To obtain the state-space and block diagram models, substitute the expression for T_e into Eq. (5.1) and linearise about the initial condition represented by $\delta = \delta_0$ and $X_C = X_{C0}$. The following expression results:

$$p\Delta\omega_r = \frac{1}{2H}\left(\Delta T_m - K_S\Delta\delta - K_X\Delta X_C - K_D\Delta\omega_r\right) \tag{5.5}$$

K_S is the synchronizing torque coefficient defined in section 3.2.1. In a SMIB system with CSC, the coefficients K_S and K_X are

$$\begin{aligned} K_S &= \frac{E'E_B}{X'_d + X_E - X_{C0}}\cos\delta_0 \\ K_X &= \frac{E'E_B}{\left(X'_d + X_E - X_{C0}\right)^2}\sin\delta_0\,. \end{aligned} \tag{5.6}$$

Eqs (5.5) and (5.2) describe the system in small perturbation form. These expressions combined give the system state-space and block diagram models.

Eq. (5.6) indicates that the insertion of a fixed series capacitor increases the synchronizing torque coefficient (by decreasing the line reactance). This is a bonus, as small-signal stability is largely a problem of insufficient damping of oscillations [60].

5.2.2 System state-space model and block diagram

Eqs (5.2) and (5.5) can be combined in matrix format to give

$$\frac{d}{dt}\begin{bmatrix}\Delta\omega_r \\ \Delta\delta\end{bmatrix} = \begin{bmatrix}-\frac{K_D}{2H} & -\frac{K_S}{2H} \\ \omega_0 & 0\end{bmatrix}\begin{bmatrix}\Delta\omega_r \\ \Delta\delta\end{bmatrix} + \begin{bmatrix}\frac{1}{2H} & -\frac{K_X}{2H} \\ 0 & 0\end{bmatrix}\begin{bmatrix}\Delta T_m \\ \Delta X_C\end{bmatrix}. \tag{5.7}$$

This is the state-space model of the SMIB system with CSC, and is of the form $\dot{\mathbf{x}} = \mathbf{A}\mathbf{x} + \mathbf{b}u$. $\mathbf{A}$ is the state matrix of the system.

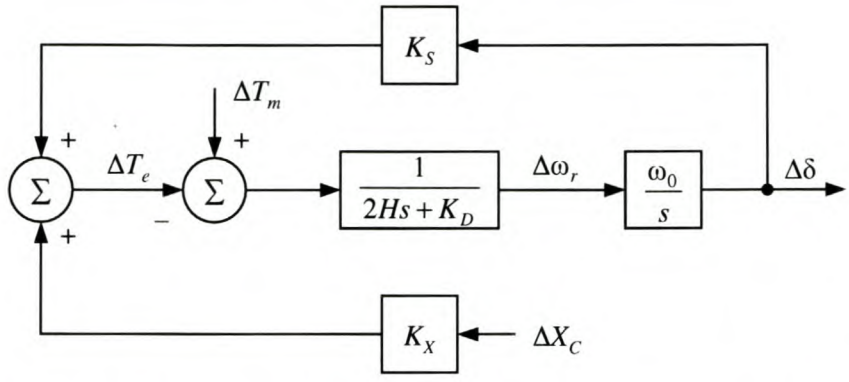

Fig. 5.2: Block diagram of SMIB system with controlled series reactance

In order to correctly evaluate the system eigenvalues, a specific control structure for the CSC ought to be implemented. Section 3.2.2 discusses the eigenvalues and their relation to system synchronizing and damping stability.

Fig. 5.2 shows the block diagram model. Observe that this is an extension of Fig. 3.2 with the CSC influence through K_X included. This diagram is useful to visualize the damping and synchronizing torque contributions, and how CSC action affects these torque components.

5.2.3 CSC and oscillation damping

Assume no damper windings are modelled, and $K_D = 0$. The system will oscillate by itself without damping, and only the CSC can contribute to the damping torque required for stable operation. To provide positive damping to the oscillations, a component of torque in phase with the rotor speed deviation is required (section 2.3). For purpose of illustration, consider the following control scenario [4]:

$$\Delta X_C = K_C \Delta\omega_r \tag{5.8}$$

K_C is a positive gain. Fig. 5.2 shows the CSC control operates through the coefficient K_X and introduces only damping torque into the system:

$$\begin{aligned} \Delta T_e\big|_{\text{CSC}} &= K_X \Delta X_C \\ &= K_X K_C \Delta\omega_r \end{aligned} \tag{5.9}$$

With control as per Eq. (5.8) and $K_D = 0$, the state-space model, Eq. (5.7), is modified to give

$$\frac{d}{dt}\begin{bmatrix}\Delta\omega_r \\ \Delta\delta\end{bmatrix}=\begin{bmatrix}-\frac{K_{DX}}{2H} & -\frac{K_S}{2H} \\ \omega_0 & 0\end{bmatrix}\begin{bmatrix}\Delta\omega_r \\ \Delta\delta\end{bmatrix}, \tag{5.10}$$

where

$$K_{DX}=K_X K_C=\frac{E'E_B K_C}{(X'_d+X_E-X_{C0})^2}\sin\delta_0 . \tag{5.11}$$

Eq. (5.10) assumes constant mechanical torque input. In this expression, K_{DX} is K_ω in section 3.2.3. K_δ is zero as a result of the control strategy of Eq. (5.8).

To ensure positively damped oscillations in the system, K_{DX} must be positive. Examination of the expression for K_{DX} (5.11) reveals important aspects regarding the damping capabilities of a CSC [4]:

- A CSC can enhance the damping of electromechanical oscillations.
- The CSC damping effect increases with increase in controller gain and/or fixed capacitor reactance – larger K_C and/or X_{C0} implies larger K_{DX}.
- The damping effect increases with transmission line loading (increased δ_0). This is very important, since the damping of the system is generally lower at heavily loaded lines.

The scenario depicted above is quite simple, yet gives useful insight into the advantages of controlled series compensation. More advanced control strategies would introduce damping as well as synchronizing torque components into the system. It is important that the regulator design take into account not only that which is desired (the damping of oscillations), but other effects/influences as well.

5.3 The Conventional Controlled Series Capacitor Control Scheme

Fig. 5.3 shows the conventional CSC controller scheme ([34], [35]) used in the investigation. $\Delta\omega_r$ is used as the input signal. Eq. (5.12) gives the transfer function. The CSC controller consists of three blocks: a gain block, a signal washout block, and a phase compensation block. Some researchers ([4], [39], [40]) prefer to assume a double lead-lag stage such that $T_1=T_3$ and $T_2=T_4$. This is the view taken in this investigation (section 5.7.2). The

following discussion focuses on each of these blocks and some other considerations in more detail.

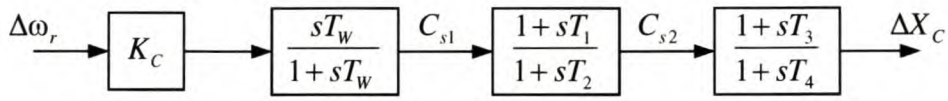

Fig. 5.3: Conventional CSC controller

$$\frac{\Delta X_C}{\Delta\omega_r} = K_C\left(\frac{sT_W}{1+sT_W}\right)\left(\frac{1+sT_1}{1+sT_2}\right)\left(\frac{1+sT_3}{1+sT_4}\right) \tag{5.12}$$

5.3.1 Input signal

The purpose of a CSC damping controller is to introduce a damping torque component. Hence a logical signal to use for controlling the transmission line impedance is the speed deviation $\Delta\omega_r$ ([37], [9]). For the SMIB system, $\Delta\omega_r$ would be the speed difference between the speeds of the synchronous generator and infinite bus.

In practice such a signal (dubbed a global signal) is not always realisable, and other signals (local signals) may be employed. These include the line active power ([4], [35], [36], [37]), local bus / capacitor node voltage ([4], [35], [37]), generator frequency deviation [37] or magnitude of current in the transmission line [38]. Which signal is more appropriate and gives the best performance depends on the system under consideration.

$\Delta\omega_r$ is chosen as the input to the CSC damping controller. Although this signal is a global signal and additional expense associated with communication is involved [37], to simplify the analysis and integration of the controller with the block diagram model of Fig. 5.5, this signal is appropriate. Also, all kinds of delay and the influence of any filter is excluded to have a basis for analytical comparison with the PSS results of chapter 4 [9].

5.3.2 Stabilizer gain

In practice the stabilizer gain would be limited by physical considerations such as the controllable reactance range and saturation of the CSC, which can significantly deteriorate the expected performance during transient oscillations [33]. This research, however, focuses on small-signal behaviour and the damping of local modes of oscillation in a SMIB system configuration. For this reason no maximum limit is placed on the controller gain, as obtained

for optimum performance by the integral of the square of the error technique employed (section 5.7).

5.3.3 Stabilizing signal washout

The value of T_W is not critical and may be anywhere in the range 1 to 20 seconds. The main consideration is that it be long enough to pass stabilizing signals relatively unaffected at the frequencies of interest [39].

5.3.4 Phase-lead compensation

To damp rotor-angle mode oscillations, the CSC damping controller must produce a component of electrical torque in phase with $\Delta\omega_r$. Therefore, the CSC transfer function should have an appropriate phase-lead characteristic to compensate for the phase lag/lead between the controller output and the electrical torque (phase of the "plant" transfer function described in section 5.6.1). Results under various conditions of generator loading and system impedance show the "plant" transfer function to exhibit a phase lead at the frequencies of oscillation, so that the controller transfer function is a phase lag function.

Section 5.7.2 discusses the phase compensation, as well as the values for the controller parameters used in the investigation, in more detail.

5.3.5 Stabilizer output limits

This research focuses on small-signal behaviour of a SMIB system. Stabilizer output limits does not influence results, and hence are not considered in the investigation.

5.4 System Model

This section derives the state-space and block diagram models of the SMIB system with CSC. Fig. 5.1 illustrates this configuration for the system with generator defined by the classical model. This section extends on the concepts of section 5.2, by representing the generator by a higher order synchronous machine model ([60] chapter 3, [61] pp. 41-44) and the CSC controller by the configuration of section 5.3.

Section 3.3 describes the state-space model of the SMIB configuration without CSC (derived in Appendix D). The following are neglected (also assumed for the system with CSC):

1. Amortisseur (damper windings) effects
2. The transformer voltage terms (armature $p\psi$ terms) from the stator voltage equations

3. The effect of speed variations on stator voltages

The methodology followed to derive the state-space model of the SMIB system with CSC is similar to that in Appendix D. The details differ in that the added series capacitor in the external reactance is a controlled variable and needs to be treated as such. With X_C the series capacitor reactance, the total reactance in the d- and q-axis are

$$\begin{aligned} X_{Td} &= X'_{ds} + X_E - X_C \,, \\ X_{Tq} &= X_{qs} + X_E - X_C \end{aligned} \tag{5.13}$$

where X'_{ds} and X_{qs} are saturated d- and q-axis machine reactances, and X_E is the line inductive reactance.

5.4.1 Synchronous machine equations

Appendix D.1 (Eqs (D.1) to (D.18)) describes the synchronous machine d-and q-axis stator voltages and flux linkages, field flux linkage, air-gap torque and swing equation. Inclusion of CSC in the system model does not alter any of these expressions, since these represent the machine only and are not altered by changes in the external system.

5.4.2 Network equations

Fig. 5.4 shows the d- and q-axis components of the machine terminal and system infinite bus voltages, E_t and E_B, defined in Fig. 5.1. It is desired to relate these voltages and evaluate the currents flowing in the stator windings of the machine.

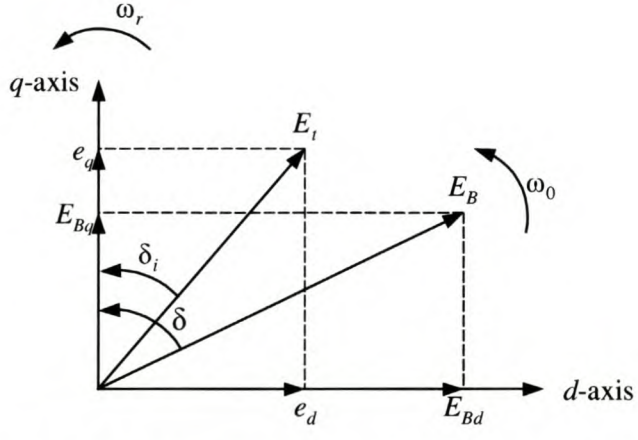

Fig. 5.4: Axis representation of system voltages and angles

A series capacitor of reactance X_C modifies the network by altering the external impedance to $R_E + j(X_E - X_C)$. The expression

$$\tilde{E}_t = \tilde{E}_B + (R_E + j(X_E - X_C))\tilde{I}_t \tag{5.14}$$

relates the machine terminal and infinite bus voltages. In terms of *d*-and *q*-axis components, Eq. (5.14) is written as

$$(e_d + je_q) = (E_B \sin\delta + E_B \cos\delta) + (R_E + j(X_E - X_C))(i_d + ji_q). \tag{5.15}$$

By equating the real and imaginary terms, e_d and e_q is

$$\begin{aligned} e_d &= R_E i_d - (X_E - X_C) i_q + E_B \sin\delta \\ e_q &= R_E i_q + (X_E - X_C) i_d + E_B \cos\delta \end{aligned} \tag{5.16}$$

These expressions are similar to (D.22), with X_E replaced by $(X_E - X_C)$ to account for the CSC reactance.

It is desired to express the stator currents i_d and i_q in terms of the machine and system reactances and resistances, infinite bus voltage E_B, and the rotor angle δ. The rotor angle is the sum of the internal machine angle δ_i and the angle by which E_t leads E_B (Fig. 5.4). Appendix D.2 explains the procedure followed to derive i_d and i_q:

$$i_d = \frac{X_{Tq}}{D}\left[\psi_{fd}\left(\frac{L_{ads}}{L_{ads} + L_{fd}}\right) - E_B \cos\delta\right] - \frac{R_T E_B}{D}\sin\delta \tag{5.17}$$

$$i_q = \frac{R_T}{D}\left[\psi_{fd}\left(\frac{L_{ads}}{L_{ads} + L_{fd}}\right) - E_B \cos\delta\right] + \frac{X_{Td} E_B}{D}\sin\delta \tag{5.18}$$

These equations are exactly (D.23) and (D.24). However, Eq. (5.13) shows X_{Td} and X_{Tq} now also contain the series capacitor reactance X_C. Eqs (5.17) and (5.18) are nonlinear. The motivation behind obtaining these expressions will become apparent in the following section.

5.4.3 Small perturbation form of machine and network equations

The state-space model of the SMIB system with CSC is desired. This is a small perturbation (linear) model, and hence the small perturbation form of i_d and i_q are required. Eqs (5.17)

and (5.18) in small perturbation form, linearized about the initial condition defined by $\delta = \delta_0$, $\psi_{fd} = \psi_{fd0}$ and $X_C = X_{C0}$, are

$$\Delta i_d = m_1 \Delta\delta + m_2 \Delta\psi_{fd} + m_3 \Delta X_C , \tag{5.19}$$

$$\Delta i_q = n_1 \Delta\delta + n_2 \Delta\psi_{fd} + n_3 \Delta X_C , \tag{5.20}$$

where

$$\begin{aligned} m_3 &= \frac{\partial i_d}{\partial X_C} = \frac{-M}{D} + \frac{1}{D^2}\left(X_{Td} + X_{Tq}\right)\left(X_{Tq} M - R_T E_B \sin\delta_0\right) \\ n_3 &= \frac{\partial i_q}{\partial X_C} = \frac{-E_B \sin\delta_0}{D} + \frac{1}{D^2}\left(X_{Td} + X_{Tq}\right)\left(R_T M + X_{Td} E_B \sin\delta_0\right) \end{aligned} , \tag{5.21}$$

with

$$M = \frac{L_{ads}}{L_{ads} + L_{fd}} \psi_{fd0} - E_B \cos\delta_0 .$$

Eqs (D.28) and (D.29) define the coefficients m_1, n_1, m_2 and n_2. m_3 and n_3 define the sensitivity of the respective stator winding currents to variation in CSC reactance.

Eqs (D.30) and (D.31) give the flux linkages ψ_{ad} and ψ_{aq} in small perturbation form for the system of section 3.3 and Appendix D. By the same procedure used to obtain (D.30) and (D.31), $\Delta\psi_{ad}$ and $\Delta\psi_{aq}$ for the SMIB system with CSC are

$$\Delta\psi_{ad} = -m_1 L'_{ads} \Delta\delta + \left(\frac{1}{L_{fd}} - m_2\right) \Delta\psi_{fd} - m_3 L'_{ads} \Delta X_C , \tag{5.22}$$

$$\Delta\psi_{aq} = -n_1 L_{aqs} \Delta\delta - n_2 L_{aqs} \Delta\psi_{fd} - n_3 L_{aqs} \Delta X_C . \tag{5.23}$$

Eq (D.32) gives the linear form of air-gap torque T_e:

$$\Delta T_e = \psi_{ad0} \Delta i_q + \Delta\psi_{ad} i_{q0} - \psi_{aq0} \Delta i_d - \Delta\psi_{aq} i_{d0} . \tag{5.24}$$

By substitution of the linear forms of i_d, i_q, ψ_{ad} and ψ_{aq} derived above,

$$\Delta T_e = K_1 \Delta\delta + K_2 \Delta\psi_{fd} + K_p \Delta X_C , \tag{5.25}$$

with

$$K_P = n_3\left(\psi_{ad0} + L_{aqs} i_{d0}\right) - m_3\left(\psi_{aq0} + L'_{ads} i_{q0}\right). \tag{5.26}$$

K_P measures the degree of direct influence CSC damping control has on the deviation of air-gap torque from the nominal (steady-state) value. In per unit, air-gap torque equals machine loading P_t, hence the subscript P. The notation is chosen to coincide with that used in Refs [14] and [15].

Eqs (D.34) and (D.35) define the parameters K_1 and K_2. Section 3.6 discusses the influence of system load and network structure on the values of K_1 and K_2. Section 5.5 considers the effect on K_P.

Eq. (D.9) gives the swing equation for the system:

$$p\Delta\omega_r = \frac{1}{2H}\left(T_m - T_e - K_D\Delta\omega_r\right), \tag{5.27}$$

$$p\delta = \omega_0\Delta\omega_r. \tag{5.28}$$

The small perturbation form of $p\Delta\omega_r$ is

$$p\Delta\omega_r = \frac{1}{2H}\left(\Delta T_m - K_1\Delta\delta - K_2\Delta\psi_{fd} - K_P\Delta X_C - K_D\Delta\omega_r\right), \tag{5.29}$$

where Eq. (5.25) was substituted for ΔT_e.

This equation solves for $\Delta\omega_r$ to give

$$\Delta\omega_r = \frac{1}{2Hs + K_D}\left(\Delta T_m - K_1\Delta\delta - K_2\Delta\psi_{fd} - K_P\Delta X_C\right). \tag{5.30}$$

Eq. (5.28) in small perturbation form is

$$p\Delta\delta = \omega_0\Delta\omega_r, \tag{5.31}$$

or

$$\Delta\delta = \frac{\omega_0}{s}\Delta\omega_r. \tag{5.32}$$

The expressions for $p\Delta\omega_r$ and $p\Delta\delta$ form part of the state-space model of Eq (5.50), while the expressions for $\Delta\omega_r$ and $\Delta\delta$ are used to obtain the block diagram model of Fig. 5.5 for the SMIB system with CSC.

5.4.4 Field circuit equations

Eq. (D.39) gives the field current. Substituting for $\Delta\psi_{ad}$ from Eq. (5.22) into the small perturbation form of i_{fd} gives

$$\Delta i_{fd} = m_1 \frac{L'_{ads}}{L_{fd}} \Delta\delta + \frac{1}{L_{fd}} \left(1 - \frac{L'_{ads}}{L_{fd}} + m_2 L'_{ads} \right) \Delta\psi_{fd} + m_3 \frac{L'_{ads}}{L_{fd}} \Delta X_C \,. \tag{5.33}$$

Δi_{fd} is substituted in the expression for $p\Delta\psi_{fd}$ (Eq. (D.41)) to give

$$p\Delta\psi_{fd} = \frac{1}{T_{3fd}} \left(-\Delta\psi_{fd} + K_3 \left(\Delta E_{fd} - K_4 \Delta\delta - K_q \Delta X_C \right) \right). \tag{5.34}$$

This expression forms part of the system state-space model of Eq (5.50). The coefficient K_q,

$$K_q = \frac{L_{adu}}{L_{fd}} m_3 L'_{ads} \,, \tag{5.35}$$

defines the influence of the CSC damping control on the field circuit input voltage. The notation is chosen to coincide with that used in Refs [14] and [15]. Eqs (D.44) through (D.46) define the parameters K_3, K_4 and T_{3fd}. Section 3.6 discusses the influence of system load and network structure on the values of K_3 and K_4. Section 5.5 considers the effects on K_q.

The expression for $p\Delta\psi_{fd}$ is often written in the following form used to obtain the block diagram model of Fig. 5.5:

$$\Delta\psi_{fd} = \frac{K_3}{1 + sT_{3fd}} \left(\Delta E_{fd} - K_4 \Delta\delta - K_q \Delta X_C \right) \tag{5.36}$$

$\frac{K_3}{1 + sT_{3fd}}$ is the field circuit transfer function.

5.4.5 Excitation system

Section 3.3.2 describes the excitation system model, and explains the assumptions and simplifications made. Fig. 3.5 shows the excitation control system considered. The exciter is modelled by a single time constant and gain:

$$G_{ex}(s) = \frac{K_A}{1+sT_A}$$
$$\therefore E_{fd} = \frac{K_A}{1+sT_A}\left(V_{ref} - E_t\right) \tag{5.37}$$

The small perturbation form of the exciter output voltage is

$$\Delta E_{fd} = \frac{K_A}{1+sT_A}\left(\Delta V_{ref} - \Delta E_t\right), \tag{5.38}$$

In Appendix D.5, the expression for ΔE_t (Eq. (D.50)) is derived from (D.19). Following this same procedure, but with Eqs (5.19), (5.20), (5.22) and (5.23), gives

$$\Delta E_t = K_5\Delta\delta + K_6\Delta\psi_{fd} + K_V\Delta X_C\,. \tag{5.39}$$

The coefficient K_V,

$$K_V = \frac{e_{d0}}{E_{t0}}\left(-R_a m_3 + L_l n_3 + L_{aqs} n_3\right) + \frac{e_{q0}}{E_{t0}}\left(-R_a n_3 - L_l m_3 - L'_{ads} m_3\right), \tag{5.40}$$

defines the influence of the CSC damping control on the machine terminal voltage E_t. This notation is used in Refs [14] and [15]. Eqs (D.51) and (D.52) define the parameters K_5 and K_6. Section 3.6 discusses the influence of system load and network structure on the values of K_5 and K_6. Section 5.5 investigates K_V.

Substituting ΔE_t in Eq. (5.38) gives

$$\Delta E_{fd} = \frac{K_A}{1+sT_A}\left(-\left(K_5\Delta\delta + K_6\Delta\psi_{fd} + K_V\Delta X_C\right) + \Delta V_{ref}\right). \tag{5.41}$$

This expression forms part of the block diagram model of Fig. 5.5, and can rearranged to give

$$p\Delta E_{fd} = \frac{1}{T_A}\left(-K_A\left(K_5\Delta\delta + K_6\Delta\psi_{fd} + K_V\Delta X_C\right) - \Delta E_{fd} + K_A\Delta V_{ref}\right). \tag{5.42}$$

The expression for $p\Delta E_{fd}$ forms part of the state-space model of Eq. (5.50).

5.4.6 Controlled series capacitor

Fig. 5.3 shows the generic CSC controller employed. It is desired to express the CSC controller transfer function (Eq. (5.12)) in state-space form.

Using perturbed values, ΔC_{s1} is

$$\Delta C_{s1} = K_C \left(\frac{pT_W}{1+pT_W} \right) \Delta\omega_r , \tag{5.43}$$

which is rearranged to give

$$p\Delta C_{s1} = K_C\, p\Delta\omega_r - \frac{1}{T_W}\Delta C_{s1} . \tag{5.44}$$

With $p\Delta\omega_r$ from Eq. (5.29) substituted in (5.44), the expression for $p\Delta C_{s1}$ in terms of the state variables are

$$p\Delta C_{s1} = -\frac{K_C K_D}{2H}\Delta\omega_r - \frac{K_C K_1}{2H}\Delta\delta - \frac{K_C K_2}{2H}\Delta\psi_{fd} - \frac{1}{T_W}\Delta C_{s1} - \frac{K_C K_P}{2H}\Delta X_C + \frac{K_C}{2H}\Delta T_m . \tag{5.45}$$

Similarly, ΔC_{s2} is

$$\Delta C_{s2} = \left(\frac{1+pT_1}{1+pT_2} \right) \Delta C_{s1} , \tag{5.46}$$

which is rearranged to give

$$p\Delta C_{s2} = \frac{1}{T_2}\Delta C_{s1} + \frac{T_1}{T_2}\, p\Delta C_{s1} - \frac{1}{T_2}\Delta C_{s2} . \tag{5.47}$$

Substituting for $p\Delta C_{s1}$ from Eq. (5.45), $p\Delta C_{s2}$ in terms of the state variables are

$$\begin{aligned} p\Delta C_{s2} = &-\frac{K_C K_D T_1}{2HT_2}\Delta\omega_r - \frac{K_C K_1 T_1}{2HT_2}\Delta\delta - \frac{K_C K_2 T_1}{2HT_2}\Delta\psi_{fd} + \frac{T_W - T_1}{T_W T_2}\Delta C_{s1} - \frac{1}{T_2}\Delta C_{s2} \\ &- \frac{K_C K_P T_1}{2HT_2}\Delta X_C + \frac{K_C T_1}{2HT_2}\Delta T_m . \end{aligned} \tag{5.48}$$

Following the same procedure to obtain (5.48), $p\Delta X_C$ is

$$\begin{aligned} p\Delta X_C = &-\frac{K_C K_D T_1 T_3}{2HT_2 T_4}\Delta\omega_r - \frac{K_C K_1 T_1 T_3}{2HT_2 T_4}\Delta\delta - \frac{K_C K_2 T_1 T_3}{2HT_2 T_4}\Delta\psi_{fd} + \frac{(T_W - T_1)T_3}{T_W T_2 T_4}\Delta C_{s1} \\ &+ \frac{T_2 - T_3}{T_2 T_4}\Delta C_{s2} - \left(1 + \frac{K_C K_P T_1 T_3}{2HT_2} \right) \frac{1}{T_4}\Delta X_C + \frac{K_C T_1 T_3}{2HT_2 T_4}\Delta T_m . \end{aligned} \tag{5.49}$$

Eqs (5.45), (5.48) and (5.49) form part of the state-space model of the system with CSC.

5.4.7 System state-space model and block diagram

The system state-space model is given by

$$\dot{\mathbf{x}} = \mathbf{A}\mathbf{x} + \mathbf{\Gamma}\mathbf{p} \tag{5.50}$$

where $\mathbf{x}$ and $\mathbf{p}$ are the state and perturbation vectors respectively, defined as

$$\mathbf{x} = \begin{bmatrix} \Delta\omega_r & \Delta\delta & \Delta\psi_{fd} & \Delta E_{fd} & \Delta C_{s1} & \Delta C_{s2} & \Delta X_C \end{bmatrix}^T$$

$$\mathbf{p} = \begin{bmatrix} \Delta T_m & \Delta V_{ref} \end{bmatrix}^T$$

The system state matrix $\mathbf{A}$ is

$$\mathbf{A} = \begin{bmatrix} \frac{-K_D}{2H} & \frac{-K_1}{2H} & \frac{-K_2}{2H} & 0 & 0 & 0 & \frac{-K_p}{2H} \\ \omega_0 & 0 & 0 & 0 & 0 & 0 & 0 \\ 0 & \frac{-K_3K_4}{T_{3fd}} & \frac{-1}{T_{3fd}} & \frac{K_3}{T_{3fd}} & 0 & 0 & \frac{-K_3K_q}{T_{3fd}} \\ 0 & \frac{-K_AK_5}{T_A} & \frac{-K_AK_6}{T_A} & \frac{-1}{T_A} & 0 & 0 & \frac{-K_AK_V}{T_A} \\ \frac{-K_CK_D}{2H} & \frac{-K_CK_1}{2H} & \frac{-K_CK_2}{2H} & 0 & \frac{-1}{T_W} & 0 & \frac{-K_CK_P}{2H} \\ \frac{-K_CK_DT_1}{2HT_2} & \frac{-K_CK_1T_1}{2HT_2} & \frac{-K_CK_2T_1}{2HT_2} & 0 & \frac{T_W-T_1}{T_2T_W} & \frac{-1}{T_2} & \frac{-K_CK_PT_1}{2HT_2} \\ \frac{-K_CK_DT_1T_3}{2HT_2T_4} & \frac{-K_CK_1T_1T_3}{2HT_2T_4} & \frac{-K_CK_2T_1T_3}{2HT_2T_4} & 0 & \frac{(T_W-T_1)T_3}{T_2T_WT_4} & \frac{T_2-T_3}{T_2T_4} & -\left(1+\frac{K_CK_PT_1T_3}{2HT_2}\right)\frac{1}{T_4} \end{bmatrix}$$

$\mathbf{A}$ is a function of the system parameters as well as the operating condition. The eigenvalues of the state matrix are a useful indication of the stability of the system, as discussed in section 3.2.2. The eigenvalue associated with the rotor angle oscillation mode is used as the complex frequency to evaluate the CSC torque contribution. Section 5.6 derives expressions for the CSC damping and synchronizing torque coefficient.

The perturbation matrix $\mathbf{\Gamma}$,

$$\mathbf{\Gamma} = \begin{bmatrix} \frac{1}{2H} & 0 & 0 & 0 & \frac{K_C}{2H} & \frac{K_CT_1}{2HT_2} & \frac{K_CT_1T_3}{2HT_2T_4} \\ 0 & 0 & 0 & \frac{K_A}{T_A} & 0 & 0 & 0 \end{bmatrix},$$

is a function of the system parameters only, and used to obtain the CSC controller parameters K_C and T_2 for optimum control. Section 5.7 discusses the optimisation process.

Fig. 5.5 shows the block diagram model of the SMIB system with CSC. The block diagram model is a useful tool in understanding the performance of a CSC in the system. An expression for the torque contribution by a CSC is easily obtained using this block diagram.

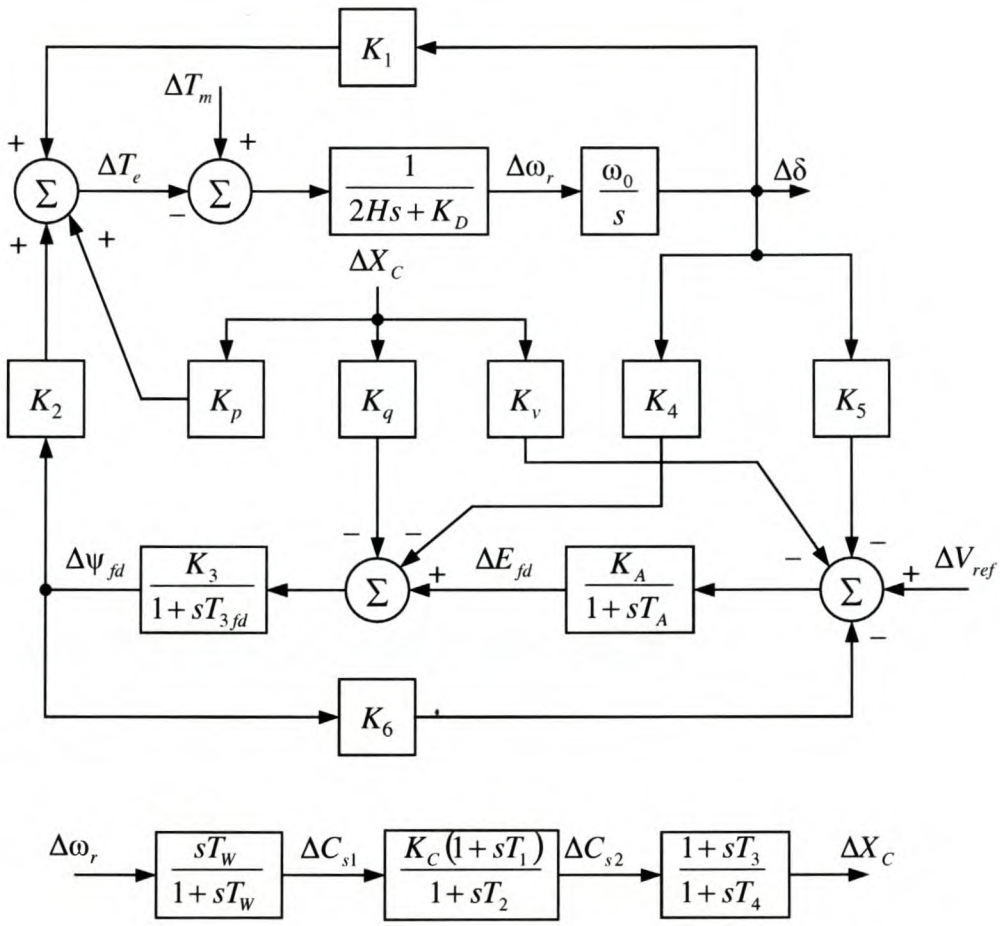

Fig. 5.5: Block diagram model of SMIB system with conventional CSC

5.4.8 System model summary

The state-space and block diagram models for the SMIB system with CSC is derived (Eq. (5.50) and Fig. 5.5). The eigenvalues of the state matrix are a useful indication of the stability of the system, and used as the complex frequency to determine the system damping torques. The block diagram is useful to analyse the performance of the CSC for various system conditions and modelling assumptions. This is considered in section 5.8.

Section 3.6 discusses the influence of system conditions and modelling assumptions on the parameters $K_1 \ldots K_6$. An understanding of the behaviour of these parameters is essential in evaluating the need for damping in a SMIB system. Similarly, an understanding of the effects of system conditions and modelling assumptions on K_P, K_q and K_V defined in this

section is necessary to comprehend the damping behaviour of a CSC. Section 5.5 analyses the behaviours of K_P, K_q and K_V for various system conditions and modelling assumptions.

5.5 *K*-constants Analysis

Fig. 5.5 describes the SMIB system with CSC as a function of the system *K*-parameters. Sections 5.6 and 5.8 discuss the CSC synchronizing and damping torques and variation thereof with respect to changes in system characteristic and condition. These torques are functions of the system model *K*-parameters and will be interpreted as such in section 5.8. As a result the trends of the *K*-parameters are investigated. Section 3.6 considered the parameters $K_1 \ldots K_6$. The focus of section 5.5 is to understand the effects of system load and network structure – and assumptions made in the modelling process – on the parameters K_P, K_q and K_V. K_P has the more dominant influence (see section 5.6.1), therefore the discussions focus more on K_P.

The following section discusses the analysis procedure used in this research. Sections 5.5.2 to 5.5.4 investigate the influence of machine loading and system reactance and resistance on the *K*-parameters by MATLAB simulation. Machine saturation is modelled. Section 5.5.5 discusses the influence of neglecting saturation on results. In the concluding summary, attention is drawn to where results differ from previous research on this subject.

5.5.1 Analysis procedure

Previous research [5] generated plots for K_P vs. P_t, for various values of system external reactance (quantified as number of connecting transmission lines). The influence of line resistance and local load was not considered and no definite mention of assumptions was made. Also, plots for the parameters K_q and K_V were not presented as it was assumed the influence of the indirect component of the "plant" transfer function is negligible. Section 5.6.1 discusses the "plant" transfer function and its direct and indirect components.

The investigation of the trends of the parameters K_P, K_q and K_V follows the same procedure and assumptions used to obtain plots for the parameters $K_1 \ldots K_6$ in section 3.6. The end-point voltages E_t and E_B in Fig. 5.1 are assumed constant at unity, and no control is placed on the machine reactive load Q_t. Plots of K_P, K_q and K_V vs. machine load P_t, for

various X_E, external impedance R_E/X_E, and R_{load}, are generated by MATLAB simulation. Cases considered are as follows (values in p.u.):

X_E = 0.2, 0.4, 0.8

R_E/X_E = 0.1, 0.4, 0.7, with X_E as above

R_{load} = 5.0, 2.0, 1.0, with X_E as above

For the remainder of this chapter X_E represents the total of transformer, transmission line and fixed series capacitor reactances; i.e. X_E is X_T in Fig. 5.1. Appendix B describes the test system used in the investigation.

5.5.2 Machine load and line reactance

This section neglects system external resistance. This simplifies analysis and results are typical of the case where a power source is connected to a large system through high voltage transmission line(s), with no or negligible local load.

Fig. 5.6 shows plots of the trends of the *K*-parameters with respect to changes in machine load and external reactance. The following discussion focuses on each *K*-parameter plot individually. Where appropriate, the expression for the *K*-parameter (derived in section 5.4) is investigated to verify or explain results.

Fig. 5.6(a): K_P increases as machine load increases and/or system strength increases (smaller X_E). K_P also remains positive over the range of conditions considered.

K_P has significant influence on the effectiveness of the CSC controller. Section 5.8.2 discusses this in more detail.

Fig. 5.6(b): K_q is negative for low P_t, and increases as P_t increases form zero becoming positive. When the generator operates at low load K_q decreases with increase in system strength; the opposite is true at moderate to high P_t.

With external resistance neglected, the expression for K_q (Eq. (5.35)) can be written as

$$K_q = E_B \cos\delta_0 \cdot A + \frac{L_{ads}}{L_{ads} + L_{fd}} \psi_{fd0} \cdot (-A), \tag{5.51}$$

where

$$A = \frac{L_{adu}}{D}\frac{L_{ads}}{L_{ads}+L_{fd}} - \left(X_{Td}+X_{Tq}\right)\frac{X_{Tq}}{D^2}.$$

A is always negative, which is the result of the total d- and q-axis reactance being larger than the machine internal reactances. Investigative plots confirm this. When P_t is low, Fig. 5.6(d) shows δ_0 is smaller, and hence $\cos\delta_0$ larger. The first term in Eq. (5.51) dominates over the second term when P_t is low, and K_q is negative. For larger δ_0 $\cos\delta_0$ is smaller and K_q more positive.

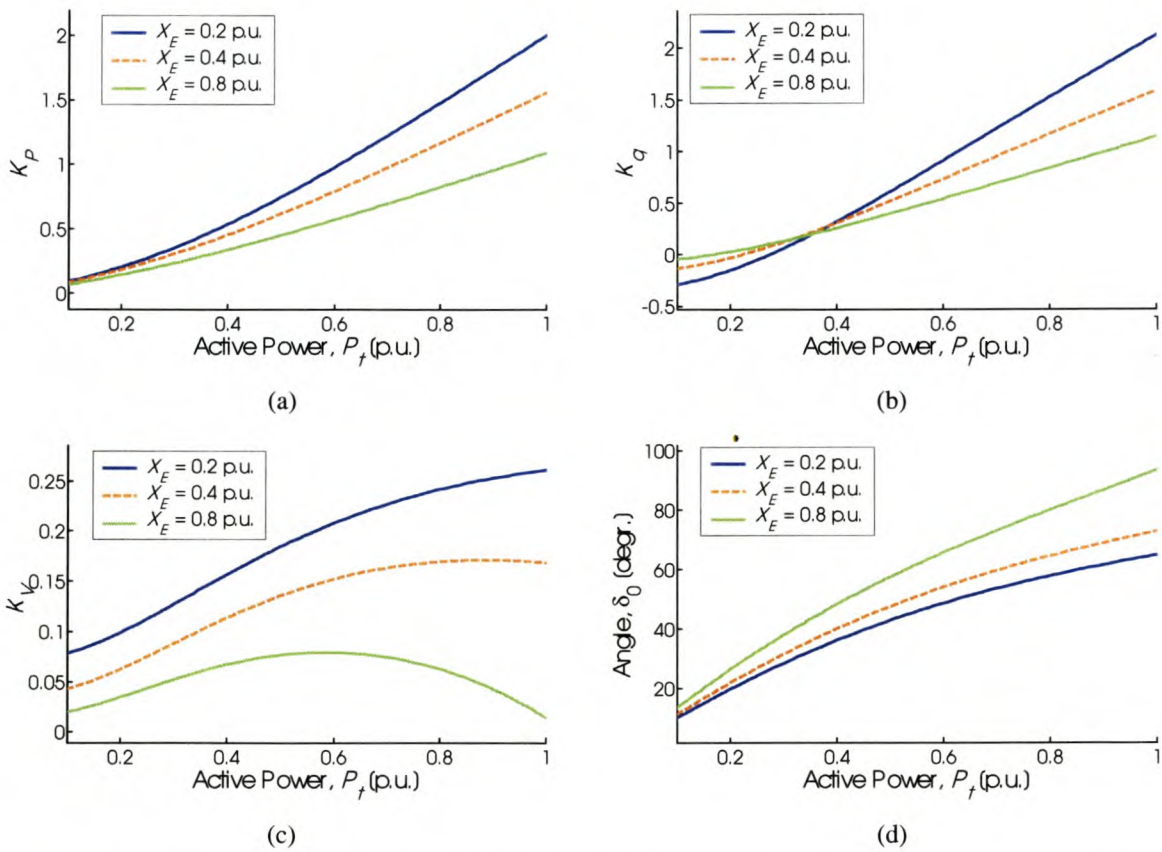

Fig. 5.6: Parameters K_P, K_q, K_V and rotor angle δ_0 vs. machine load and external reactance

Fig. 5.6(c): K_V increases as P_t increases, reaches a maximum, and decreases with any further increase in P_t. K_V is also larger in a stronger system. It is possible for K_V to be negative: Fig. 5.7(a) illustrates the scenario of very large X_E (very weak system) with relative high loading.

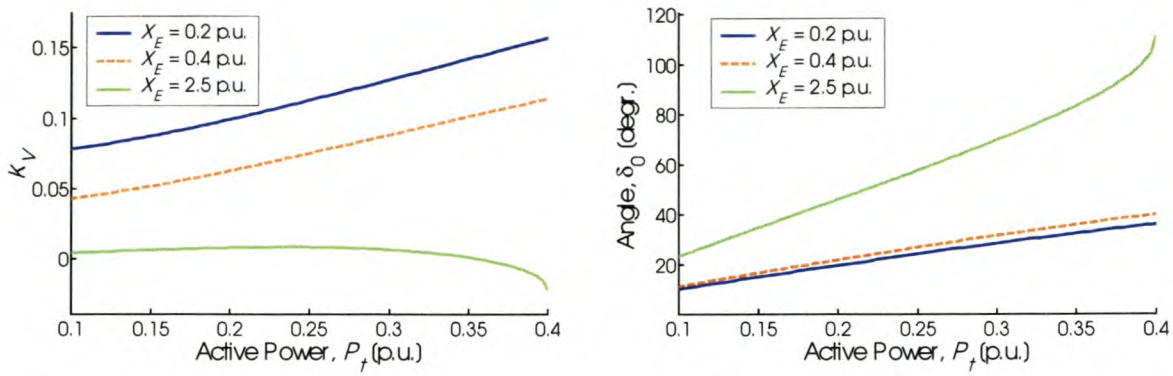

(a) (b)

Fig. 5.7: K_V and rotor angle δ_0 vs. machine load and external reactance – influence of very long ties

With external resistance neglected and noticing that the per unit armature resistance R_a is significantly smaller than machine per unit reactances (Table B.1), the expression for K_V (Eq. (5.40)) reduces to

$$K_V = \frac{E_B \sin\delta_0}{D} X_{qs} \frac{e_{d0}}{E_{t0}} \left(-1 + X_{Td} \frac{(X_{Td} + X_{Tq})}{D} \right) - \frac{M}{D} X'_{ds} \frac{e_{q0}}{E_{t0}} \left(-1 + X_{Tq} \frac{(X_{Td} + X_{Tq})}{D} \right), \tag{5.52}$$

where

$$M = \frac{L_{ads}}{L_{ads} + L_{fd}} \psi_{fd0} - E_B \cos\delta_0 .$$

When X_E is very large and machine load relatively high, the steady-state rotor angle approaches and possibly exceeds 90°. Fig. 5.7(b) shows this angle. Now, $\cos\delta_0 \approx 0.0$ at high δ_0, and is negative with $\delta_0 > 90°$. As a result, M increases with increase in δ_0 and even exceeds unity when δ_0 is high. The second term in Eq. (5.52) then dominates the first term, and K_V is negative.

This situation of negative K_V is of academic rather than practical importance; it is impractical to operate the system at such high values of δ_0. Another example of this occurrence is the parameter K_1 discussed in section 3.6.2.

This section presented the parameters K_P, K_q and K_V for the system without external resistance. Section 5.6 discusses the "plant" transfer function and its role in the CSC torque expressions. For the system without external resistance, section 5.8.2 shows K_P approximates the "plant" transfer function; the indirect component (see section 5.6.1 for definition) is negligible.

For the system with external resistance, however, the indirect component of the "plant" transfer function cannot be ignored. Sections 5.8.3 and 5.8.4 shows why. The damping and synchronizing torques by the CSC controller is then a complex function of the parameters K_P, K_q and K_V, other K-parameters, as well as the system eigenvalue. There is no direct relation between the CSC torques and any of K_P, K_q and K_V. The following sections thus only discuss the trends of these parameters briefly. The focus is more on comparison of results to previous research on this subject.

5.5.3 Line resistance

Section 5.5.2 neglected system external resistance to simplify analysis and obtain results typical of the case where a power source is connected to a large system through high voltage transmission line(s), with no or negligible local load. This section focuses on the influence of line resistance on K_P, K_q and K_V. Appendix G.1 contains the results. It is observed that the influence of external resistance on the K-parameters in some cases affect the trends described in section 5.5.2. Where appropriate reference to this fact will be made.

K_P decreases as R_E/X_E increases when the generator operates at light load and/or into a weak system. This tendency reverses at moderate to high loading in the case of a strong system.

Fig. 5.8(a) shows the parameter K_P in the very low P_t region, with $X_E = 0.4$ p.u. Results for other X_E indicate that, regardless of system strength, K_P is negative when the generator operates at light load into a system with large R_E/X_E.

In the expression for K_P, Eq. (5.26), terms containing R_T are separated from the rest of the expression to give

$$K_P = \frac{R_T}{D^2}\left(M\left(X_{Td}+X_{Tq}\right)E_{q0} - E_B \sin\delta_0\left(X_{Td}+X_{Tq}\right)\left(X_q - X'_d\right)_{q0}\right)$$
$$+\frac{E_{q0}}{D}E_B \sin\delta_0\left(-1+\frac{X_{Td}}{D}\left(X_{Td}+X_{Tq}\right)\right) \qquad (5.53)$$
$$+\frac{M}{D}\left(X_q - X'_d\right)_{q0}\left(-1+\frac{X_{Tq}}{D}\left(X_{Td}+X_{Tq}\right)\right),$$

where $M = \dfrac{L_{ads}}{L_{ads}+L_{fd}}\psi_{fd0} - E_B\cos\delta_0$.

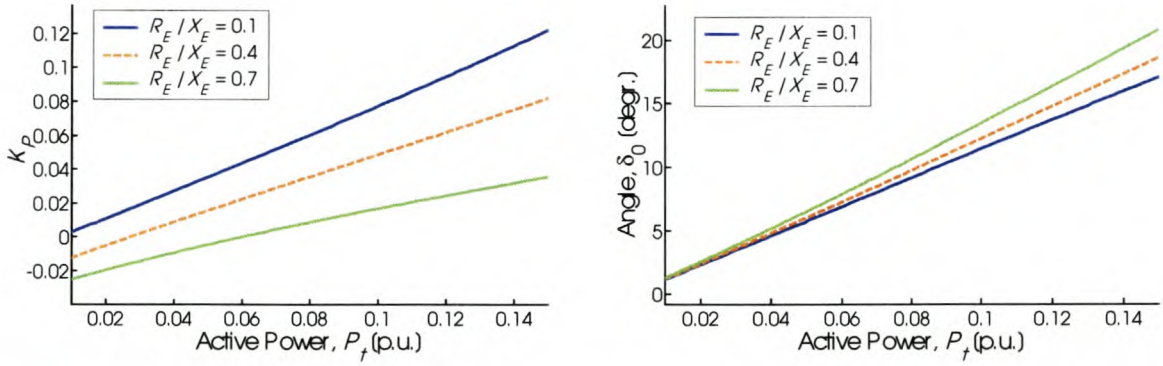

(a) (b)

Fig. 5.8: K_P and rotor angle δ_0 at low P_t, with X_E = 0.4 p.u.

When P_t is low, the rotor angle δ_0 is small and $\cos\delta_0 \approx 1.0$. Then

$$E_B\cos\delta_0 > L_{ads}\psi_{fd0}/\left(L_{ads}+L_{fd}\right),$$

and a negative M result. As a result, the first and third terms in Eq. (5.53) are negative. An increase in R_T causes the first term to dominate the remaining terms, and K_P is negative when the generator operates at low P_t.

Theoretically this has significance for the CSC damping torque contribution. However, results of section 5.8.3 show that despite negative K_P a CSC controller is still able to introduce positive damping torque to the system. This can be attributed to the indirect component to the "plant" transfer function (section 5.6.1).

Previous research ([5], [15]) showed mathematically that K_P is always positive. The discussion above proves this is not always the case for a system with significant external resistance.

K_q behaves similar to K_P discussed above. With significant R_E/X_E K_q slightly decreases as P_t increases from zero, reach a minimum, and increase with any further increase in P_t. Compare Fig. 5.6(b).

K_V increases with increase in R_E/X_E.

5.5.4 Local load

This section discusses on the influence of local load on K_P, K_q and K_V. Appendix G.2 contains the results for this section.

A resistance R_{load} models the local load (section 3.4.1). Table 3.1 gives the X_{line} and R_{load} value combinations used in the investigation, and the resulting X_E, R_E and E_B values from which the system parameters are determined.

K_P increases with increase in local load.

K_q increases with increase in local load when the machine operates at low P_t. This trend reverses with increase in P_t, so that K_q decreases with increase in local load for a constant line reactance. As is the case with significant R_E/X_E (section 5.5.3), in a system with large local load K_q decreases as P_t increases from zero, reaches a minimum, and increases with any further increase in P_t.

Observation: the increase in K_q with increase in local load under low P_t conditions is significant, even so that K_q is positive when that is not the case for a system without local load (Fig. 5.6(b)).

K_V decreases with increase in local load when the machine operates at low to medium P_t. With significant local load K_V changes sign from positive to negative. When the generator operates at high P_t, K_V increases with increase in local load for a constant line reactance.

5.5.5 Influence of saturation

Synchronous machine saturation was modelled to obtain the results for the previous sections. This section considers the influence of neglecting saturation, often the assumption in literature. Results for the previous sections were regenerated for the system of Appendix B

with machine saturation neglected (constant machine inductances/reactances). Appendix G.3 contains the results.

Neglecting machine saturation influences the results of *machine load and line reactance* (section 5.5.2), *line resistance* (section 5.5.3) and *local load* (section 5.5.4) as follows:

1. K_P and K_V values are lower when machine saturation is not modelled.
2. The parameter K_q is larger in value.

Neglecting to model saturation of the machine inductances does, in some cases, influence the trends of K_P, K_q and K_V described in the previous sections. An elaborate discussion on this topic is beyond the scope of this research. It will suffice to mention that in some cases (K_q at low P_t is an example) a parameter is positive when it would not be if saturation were modelled, or vice versa. Consequently it is necessary to model machine saturation to obtain the correct trends of K_P, K_q and K_V, and a correct impression of the signs of the constants. Section 5.8.6 considers whether the effect of saturation is as significant on the CSC torques.

5.5.6 Summary of results

The trends of the system model *K*-parameters, with respect to *machine load and line reactance* (section 5.5.2), *line resistance* (section 5.5.3) and *local load* (section 5.5.4) were examined. The influence of *saturation modelling* on the results was also considered (section 5.5.5).

A summary of the results follows. The trends are compared to results from previous investigations on the *K*-parameters of the SMIB system model.

$\boldsymbol{K_P}$ increases as P_t increases and/or system strength increases. This result is also obtained in Refs [5] and [15]. The variation of K_P with respect to R_E/X_E depends on both P_t and X_E. K_P increases with increase in local load.

In the case of large R_E/X_E, K_P can be negative when the generator operates at light load. This disproves the statement in [5] that K_P is always positive. Ref. [5] does not consider external resistance in the SMIB system.

The parameter K_P has significant influence on the "plant" transfer function in a system without any external resistance. Sections 5.6.1 and 5.8.2 discuss the concept of the "plant" transfer function and its influence on CSC performance in more depth.

$\boldsymbol{K_q}$ is negative for low-medium generator loading, and increases as P_t increases form zero, becoming positive for moderate to high P_t. How K_q varies with respect to both line reactance and local load depends on P_t. With significant local load it is possible to have K_q positive at low-medium P_t. Also, the variation of K_q with respect to R_E/X_E varies with machine load and system strength. Both line resistance to reactance ratio and local load affects the trend of K_q with respect to P_t when the generator operates at low load.

$\boldsymbol{K_V}$ increases as P_t increases, reaches a maximum, and decreases with any further increase in P_t. K_V is also larger in a stronger system. K_V can become negative in the unusual case of very long ties and relative high loading. This scenario is of academic rather than practical interest (see discussion on K_1, section 3.6.6).

K_V increases as R_E/X_E increases for a constant X_E. The variation of K_V with respect to changes in local load depends on the machine load P_t. With significant local load K_V changes its sign from positive to negative when the generator operates at light load into a weak system.

Both K_q and K_V influence the indirect component of the "plant" transfer function, discussed in section 5.6.1. Combined with the trends of K_2, K_3 and K_6, and the system eigenvalue, K_q and K_V cause the "plant" transfer function to deviate from the mostly dominant K_P. This is most prominent in a system with significant R_E/X_E or local load. Sections 5.8.3 and 5.8.4 describe this in more detail.

Sections 5.6 and 5.8 discuss the CSC damping and synchronizing torques. These torques are complex functions of the system *K*-parameters, eigenvalue, and CSC controller parameters. Results are interpreted in terms of the results of the *K*-parameters of sections 3.6 and 5.5.

5.6 CSC Torque Coefficients

In section 5.2.3 the influence of a CSC on the stability of a classical model SMIB system is discussed. It is seen that a CSC can enhance the damping of electromechanical oscillations. The damping effect increases with increase in transmission line loading and the amount of fixed capacitive compensation implemented.

In this and subsequent sections, the analysis is extended to the system represented by Fig. 5.5 and Eq. (5.50). Refs [5] and [15] presents similar work, but for a simple gain controller. This work extends on the concepts and methodology introduced in [5], by considering the conventional CSC controller of section 5.3.

Section 2.3 discusses the concepts of synchronizing and damping torques. Based on these concepts, the air-gap torque as a result of CSC action can be decomposed into the following components:

$$\Delta T_e\big|_{\text{CSC}} = K_{S(\text{CSC})}\Delta\delta + K_{D(\text{CSC})}\Delta\omega_r \tag{5.54}$$

$K_{D(\text{CSC})}\Delta\omega_r$ is the damping torque component of the air-gap torque due to CSC action, with $K_{D(\text{CSC})}$ the *CSC damping torque coefficient*. $K_{S(\text{CSC})}\Delta\delta$ is the synchronising torque the CSC controller introduces into the system, with *CSC synchronizing torque coefficient* $K_{S(\text{CSC})}$. This section derives expressions for $K_{D(\text{CSC})}$ and $K_{S(\text{CSC})}$ for use in the investigation.

5.6.1 "Plant" transfer function

Let $GEP(s)\big|_{\text{CSC}}$ denote the transfer function from the stabilizer output ΔX_C to the component of electrical air-gap torque ΔT_e that can be modulated via reactance control. Fig. 5.9 illustrates the transfer function. Variation of $GEP(s)\big|_{\text{CSC}}$ with voltage regulator gain, generator power level and ac system strength plays an important role in CSC performance, as will be seen.

$GEP(s)\big|_{\text{CSC}}$ has a direct component in the coefficient K_P, and an indirect component through variation of the field flux linkage by changes in ΔX_C [5][15]. Fig. 5.9 shows this latter component to be

$$\Delta\psi_{fd}\big|_{\text{CSC}} = \frac{K_3}{1+sT_{3fd}}\left(-K_q\Delta X_C + \frac{K_A}{1+sT_A}\left(-K_V\Delta X_C - K_6\Delta\psi_{fd}\big|_{\text{CSC}}\right)\right). \tag{5.55}$$

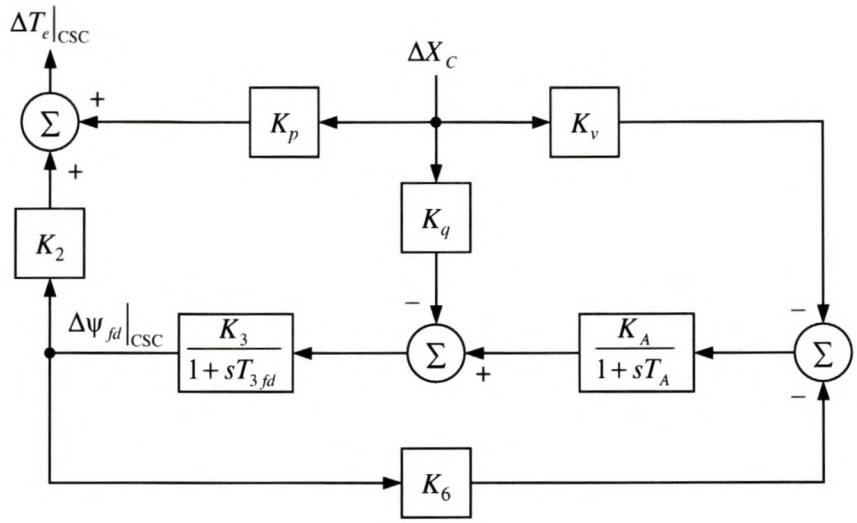

Fig. 5.9: CSC forward path

The field flux linkage variation is fed back through the parameter K_6 to the exciter block input; hence $\Delta\psi_{fd}\big|_{CSC}$ appears also on the right hand side of Eq. (5.55). This expression is rearranged to give

$$\frac{\Delta\psi_{fd}\big|_{CSC}}{\Delta X_C} = \frac{-K_3\left(K_q\left(1+sT_A\right)+K_V K_A\right)}{\left(1+sT_{3fd}\right)\left(1+sT_A\right)+K_3 K_6 K_A}. \tag{5.56}$$

This, together with the direct component $K_P \Delta X_C$, is used to express the transfer function $GEP(s)\big|_{CSC}$ as

$$\begin{aligned} GEP(s)\big|_{CSC} &= \frac{\Delta T_e\big|_{CSC}}{\Delta X_C} \\ &= K_P + K_2 \frac{\Delta\psi_{fd}\big|_{CSC}}{\Delta X_C} = K_P - \frac{K_2 K_3\left(K_q\left(1+sT_A\right)+K_V K_A\right)}{\left(1+sT_{3fd}\right)\left(1+sT_A\right)+K_3 K_6 K_A} \end{aligned}. \tag{5.57}$$

Section 5.7.2 discusses the phase characteristic of $GEP(s)\big|_{CSC}$ and the compensation thereof by the CSC controller.

Eq. (5.57) shows the transfer function through which the CSC controller operates can be considered as a sum of two components:

- One component applies directly into the electromechanical oscillation loop of the generator, and is termed the *direct component*. Its sensitivity is determined by the coefficient K_P.
- The other component, dubbed the *indirect component*, is the component that adds torque through variations in the field flux linkage.

Typically, the direct component dominates over the indirect component, so that the influence of the indirect component in analysis may be assumed negligible [5][15]. As will be seen in the investigation of section 5.8 this is not always the case, particularly in the system with external resistance. The generalization $GEP(s)\big|_{\text{CSC}} \approx K_P$ is therefore not made in this investigation.

5.6.2 Torque expressions

Fig. 5.3 and Eq. (5.12) describe the conventional CSC controller configuration used in the investigation. Combining (5.12) with the expression for $GEP(s)\big|_{\text{CSC}}$ gives the torque contribution due to the CSC controller as

$$\begin{aligned}\Delta T_e\big|_{\text{CSC}} &= \frac{\Delta T_e\big|_{\text{CSC}}}{\Delta X_C}\frac{\Delta X_C}{\Delta \omega_r}\Delta\omega_r \\ &= \left(K_P - \frac{K_2K_3\left(K_q(1+sT_A)+K_VK_A\right)}{(1+sT_{3fd})(1+sT_A)+K_3K_6K_A}\right)\left(\frac{K_C(sT_W)(1+sT_1)(1+sT_3)}{(1+sT_W)(1+sT_2)(1+sT_4)}\right)\Delta\omega_r\end{aligned} \tag{5.58}$$

This is the air-gap torque exerted by CSC action. To evaluate $\Delta T_e\big|_{\text{CSC}}$, the eigenvalue $\lambda = \sigma + j\omega$ corresponding to the rotor angle mode is substituted for s. λ is obtained from the state matrix $\mathbf{A}$ of Eq. (5.50).

Since $\Delta T_e\big|_{\text{CSC}}$ is proportional to $\Delta\omega_r$, the expressions for K_D and K_S derived in Appendix A.3 are used to evaluate the CSC damping and synchronizing torque coefficients:

$$K_{D(\text{CSC})} = \text{Re}\left(\frac{\Delta T_e\big|_{\text{CSC}}}{\Delta\omega_r}\right) + \left(\frac{\sigma}{\omega}\right)\text{Im}\left(\frac{\Delta T_e\big|_{\text{CSC}}}{\Delta\omega_r}\right) \tag{5.59}$$

$$K_{S(\text{CSC})} = -\left(\frac{\sigma^2}{\omega_0\omega} + \frac{\omega}{\omega_0}\right)\text{Im}\left(\frac{\Delta T_e\big|_{\text{CSC}}}{\Delta\omega_r}\right) \tag{5.60}$$

These expressions for $K_{D(\text{CSC})}$ and $K_{S(\text{CSC})}$ are used in the investigation of section 5.8.

5.7 Controller Optimisation Using ISE Technique

Eq. (5.58) shows the CSC damping and synchronizing torques are a complex function of the system K-parameters, eigenvalue, and CSC controller parameters. Sections 3.6 and 5.5 discuss the K-parameters. To obtain the eigenvalue from the state matrix of Eq. (5.50), and evaluate the CSC torques, values for the CSC controller parameters are needed.

Section 4.5 discusses the integral of the square of the error technique used to evaluate the parameters of a PSS conventional controller for optimum performance. This same technique is used to optimise the CSC controller parameters. This section discusses the ISE technique as applied to the CSC damping controller.

5.7.1 Performance index and optimisation process

Section 4.5.2 derives an expression for the ISE performance index J in terms of the system state-space model $\dot{\mathbf{x}} = \mathbf{A}\mathbf{x} + \mathbf{\Gamma}\mathbf{p}$. Eq. (5.50) gives the state-space model for the SMIB system with CSC. To evaluate J is to evaluate the expression

$$J = \hat{\mathbf{x}}(0)^T \mathbf{P}\hat{\mathbf{x}}(0), \tag{5.61}$$

where $\hat{\mathbf{x}}(0) = \mathbf{A}^{-1}\mathbf{\Gamma}\mathbf{p}$ and $\mathbf{P}$ is a symmetric matrix obtained by solving the Lyapunov equation $\mathbf{A}^T\mathbf{P} + \mathbf{P}\mathbf{A} = -\mathbf{Q}$. A diagonal matrix with main diagonal $[0 \;\; 1 \;\; 0 \;\; 0 \;\; 0 \;\; 0 \;\; 0]$ defines $\mathbf{Q}$. In other words the error in $\Delta\delta$, $\Delta\hat{\delta}$, is penalized to obtain controller parameters for optimum performance.

Section 4.5.3 describes the procedure to obtain optimal parameters for the PSS case. A similar procedure is used to optimise the CSC controller for a given condition of system load and impedance. The design of an optimal CSC controller differs from that for the PSS in that the time constant $T_2 = T_4$ and gain K_C are optimised. Section 5.7.2 discusses the motivation behind assuming $T_1 = T_3$ constant in the CSC controller design process.

5.7.2 CSC Controller Design

As is the case with the PSS (section 4.5.4), the parameters of the CSC controller to be optimised are the time constants T_W, T_1 . . . T_4 and the gain K_C.

A washout time constant of 10 s is chosen. This is high enough to pass stabilizing signals at the frequencies of interest unchanged, so that the washout block has little impact on the rotor angle mode oscillations.

Also, similar to the PSS controller case of chapter 4, two identical cascade lead-lag networks are considered for the CSC to simplify the problem [4][39][40]. Hence $T_1 = T_3$ and $T_2 = T_4$ in Fig. 5.3. In all ensuing discussions, reference to T_1 implies both the time constants T_1 and T_3; similarly T_2 implies both T_2 and T_4. This is done to facilitate ease of reading.

Eq. (5.57) gives the transfer function of the "plant" through which the CSC controller operates. $GEP(s)\big|_{\text{CSC}}$ has a phase lead over the frequency range of concern. To ensure the CSC controller does not influence the system synchronizing torque negatively, the torque contribution transfer function of Eq. (5.58) ought to exhibit a slight phase lag. Refs [60] pp. 769, [2] and [18] explains this principle for a PSS. The phase compensation of Fig. 5.3 is therefore lag compensation. T_1 is then assumed constant at a predefined value, and T_2 optimised according to the procedure of section 4.5.3.

In the design process of a PSS controller lead compensation, a minimum value of 0.05 s is normally assumed for the lag constant T_2 [2]. This limit can be related to the frequency range under consideration for rotor angle oscillations. The lower limit of 0.05 s corresponds to an oscillation frequency of 20 rad/s, and ensures the PSS controller does not influence torsional oscillation modes outside the desired frequency range.

This same principle can be applied to the CSC controller lag compensation. As $T_1 < T_2$, a minimum value for T_1 of 0.05 s is assumed. Fig. 5.10 illustrates K_D for various T_1 (K_C and T_2 accordingly optimised) for two values of X_E. The minimum value of 0.05 s appears the most appropriate choice, given the fact that damping torque is required more in a weaker system and/or system that is more highly loaded (chapter 3). Appendix G.4 contains results for K_D and K_S for more X_E. The choice of 0.05 s for T_1 also ensures the most synchronizing torque by the CSC controller.

With $T_1 = 0.05\,\text{s}$, the CSC parameters K_C and T_2 are optimised. Fig 5.11 shows the CSC optimised parameters K_C and T_2 for the system without external resistance. The following observations also hold for the system with external line or local load resistance (see results in Appendix G).

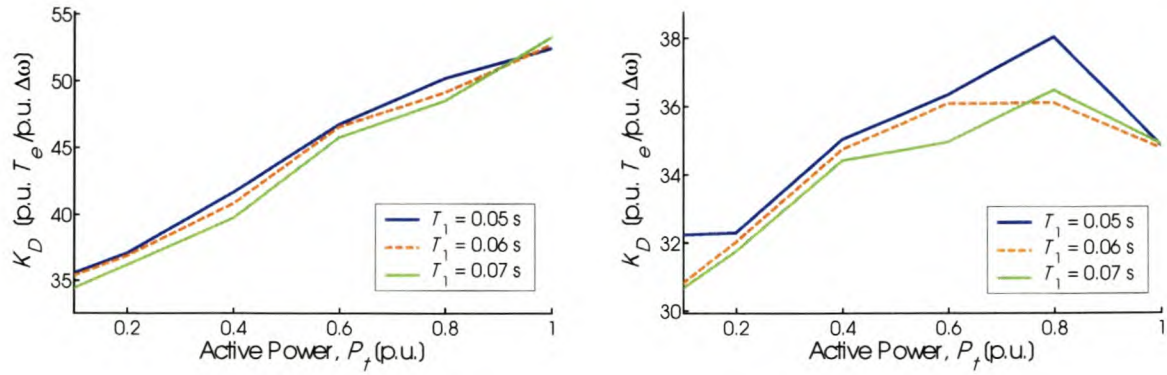

(a) $X_E = 0.4$ p.u. (b) $X_E = 0.8$ p.u.

Fig. 5.10: System damping torque vs. machine load and CSC controller time constant T_1

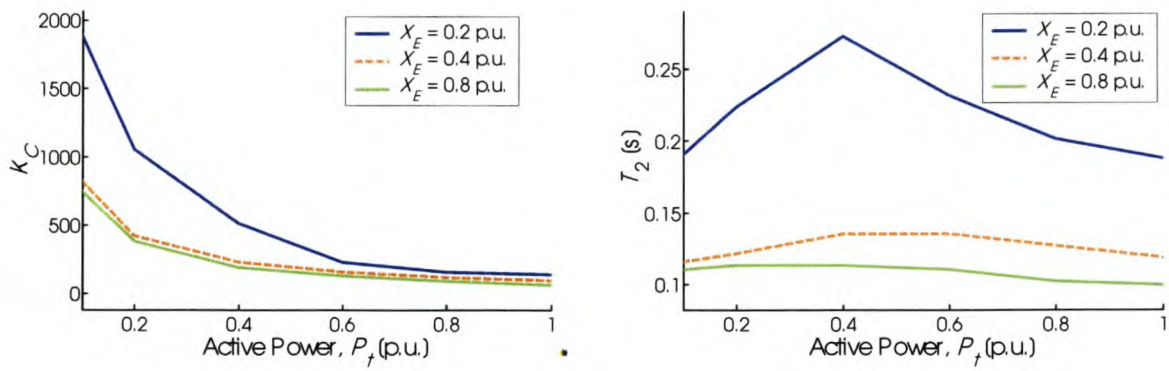

(a) (a)

Fig 5.11: Optimised CSC parameters K_C and T_2 vs. machine load and external reactance

Values for K_C are high at low P_t and reduce with increase in machine load and external reactance. Also, K_C values for the CSC controller optimised by the ISE technique are much higher than the PSS controller gains of Fig 4.6(a). Whether the CSC controller will reach saturation point during system transient oscillation damping depends on the controllable range of the CSC. Prolonged saturation of CSCs can significantly deteriorate their expected performance [33][7]. On the other hand, limiting the values of K_C only serves to reduce the CSC small-signal performance at low P_t. This investigation focuses on small-signal behaviour; transient stability is beyond the scope of this research. As a result, K_C values are not limited to a predefined maximum in the modelling process.

T_2 values increase with increase in generator load, reach a maximum and decrease with further increase in P_t. T_2 is also larger in a stronger system. This is for a system with high AVR gain; an exception to these trends is the system with low K_A – see section 5.8.5.

Investigation shows that under no condition does T_2 obtain values smaller than the minimum threshold of 0.05 s. Hence for all conditions the CSC controller introduces a phase lag to compensate for the phase lead of the "plant" through which it operates.

For the PSS controller it was suggested in [18] that the net phase lag obtain values in the range 0° and 45° to minimize the effect of system changes on stabilizer performance. Results show the CSC controller optimised by the ISE technique exhibits phase lags such that the net phase lag of the CSC controller and "plant" transfer functions, Eq. (5.58), are in the 30° to 45° range for the system without external resistance. Besides damping torque, the CSC controller also enhances the system synchronizing torque, and oscillation frequencies are slightly increased as a result.

5.8 CSC Performance Analysis

This section investigates the ability of a CSC controller to provide damping torque to the system when such damping torque is needed, as determined in chapter 3. Eq. (5.59) gives the expression for the CSC damping torque coefficient used in the investigation. The procedure used is similar to the procedure of section 5.5.

The investigation wishes to compare PSS and CSC capability given a certain condition of system impedance and load. For each condition of system loading and impedance, the controller is optimised for that condition and the torque coefficients reflect such optimum control. The optimisation process requires a significant amount of computations and iterations. To minimize simulation time, solutions are evaluated and plotted for only selected values of system load.

The CSC synchronizing torque coefficient, Eq. (5.60), is also analysed to assess the influence of the CSC controller on the system synchronizing stability whilst improving the damping stability.

The following section discusses the analysis procedure used in this research. Sections 5.8.2 to 5.8.4 investigate the influence of machine loading and system reactance and resistance on the CSC torque coefficients by MATLAB simulation. Machine saturation is modelled and the AVR gain $K_A = 200$. Section 5.8.5 discusses the influence of assuming a lower K_A on CSC performance; section 5.8.6 the effect of neglecting saturation. Section 5.8 ends with a concluding summary.

5.8.1 Analysis procedure

Section 5.5.1 discusses the procedure and parameter values used to obtain plots for the parameters K_P, K_q and K_V. This same procedure and assumptions are used in the investigation of CSC controller performance. Performance is measured in its ability to provide the damping torque needed without negatively affecting the system synchronizing torque. This research assumes both end-point voltages E_t and E_B in Fig. 5.1 constant at unity. Section 3.5 discusses the implications of this. No control is placed on the machine reactive load Q_t; hence Q_t can become negative (machine a sink of reactive power – see Eq. (3.39)), particularly as the external resistance increases.

With E_t and E_B constant at 1.0 p.u., plots of the CSC damping and synchronizing torques, and other parameters, vs. machine load, for various external reactance, external resistance to reactance ratio, and local load resistance, are generated by MATLAB simulation. Section 5.5.1 gives the values of X_E, R_E/X_E, and R_{load} considered in the investigation. Appendix B describes the test system used.

5.8.2 Machine load and line reactance

This section neglects system external resistance. This simplifies analysis and results are typical of the case where a power source is connected to a large system through high voltage transmission line(s), with no or negligible local load.

Fig. 5.12(a) shows the damping torque coefficient for the ISE-optimised CSC controller. For the system with moderate to high external reactance (including the fixed capacitor reactance), the damping ability of the controller increases with increase in system load and strength. In a very strong system the ability of the controller to provide added damping is reduced, compared to the weaker systems.

It is desirable that $K_{D(\mathrm{CSC})}$ increases with generator load; the stability problems for which the CSC is applied also increases with generator load (Fig. 3.23(e)). However, since $K_{D(\mathrm{CSC})}$ at moderate to high X_E decreases as the system becomes weaker, the influence of the CSC controller decreases when the power system requires it most. Fig. 5.12(a) also shows that increasing the amount of fixed compensation (for a system with $X_E = 0.8$ p.u., 50% compensation gives $X_E = 0.4$ p.u.) increases the ability of the CSC to damp oscillations. This is in agreement with results obtained in Ref. [10].

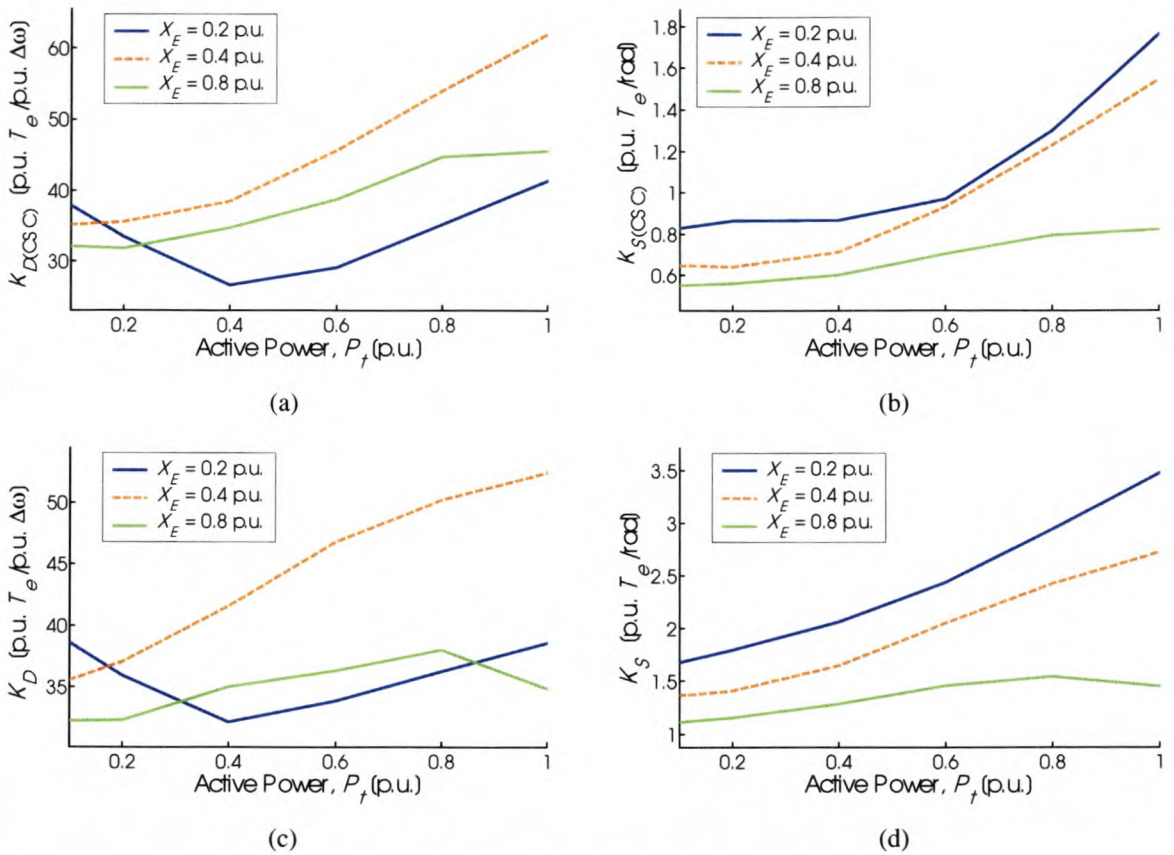

Fig. 5.12: CSC and system torque coefficients vs. machine load and external reactance

The CSC damping performance is reduced at $X_E = 0.2$ p.u., compared to the weaker systems. This appears to indicate there is a limit to the amount of fixed compensation that ensures improved controller performance.

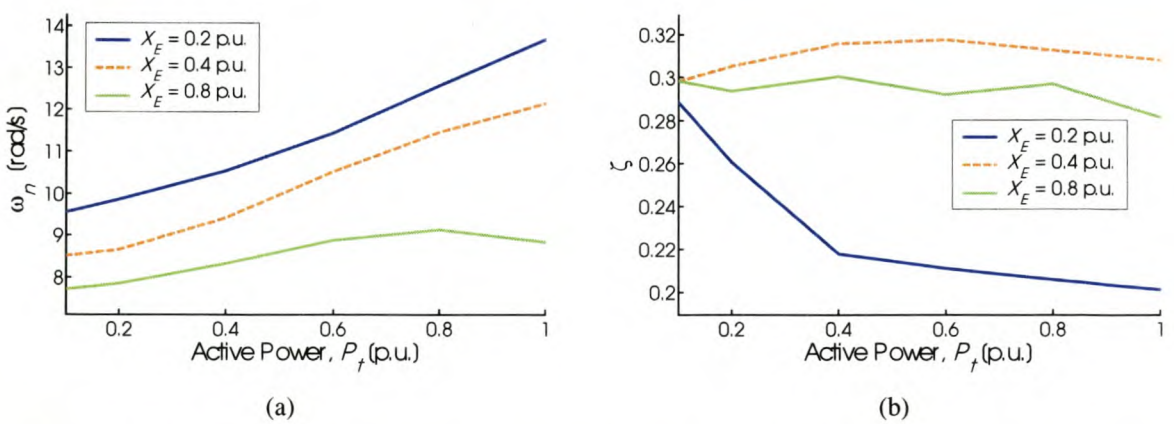

Fig. 5.13: Undamped natural frequency and damping ratio vs. machine load and external reactance

To gain insight into the behaviour of optimal CSC stabilization versus system load and strength, the gains of $GEP(s)|_{CSC}$ and stabilizer transfer function were analysed at the oscillating frequency ω_n. Fig. 5.13(a) shows ω_n for the system conditions considered. Fig. 5.13(b) shows there is little variation in the damping ratio of the stabilized system when X_E is moderate to high; hence considering the transfer function gains at ω_n can give valuable information on the influence certain factors have on CSC performance.

Fig. 5.14 shows the gains of the "plant" and controller transfer functions. Consider the case of $X_E = 0.4\,\text{p.u}$. $|GEP(s)|_{CSC}|$ increases and the controller gain at ω_n decreases with increases in system load. Although the controller gains are significantly larger in value than $|GEP(s)|_{CSC}|$, the increase in $|GEP(s)|_{CSC}|$ exceeds the decrease in $|K_C G_{CSC}(s)|$. The result is a net increase in the gain of the CSC torque transfer function.

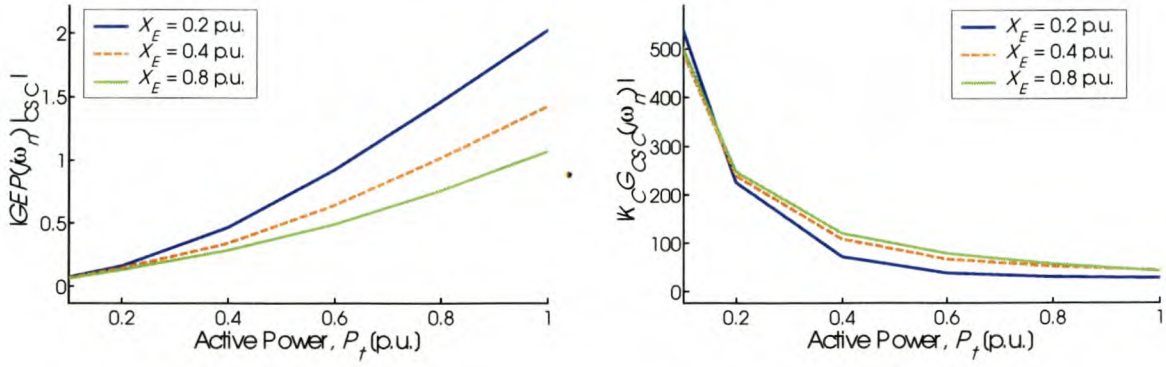

(a) (b)

Fig. 5.14: "Plant" and CSC controller transfer function gains vs. machine load and external reactance

This discussion illustrates that the characteristics of $GEP(s)|_{CSC}$ play a significant role in the behaviour of $\Delta T_e|_{CSC}$. Comparison of Fig. 5.14(a) to Fig. 5.6(a) shows $GEP(s)|_{CSC} \approx K_P$. The influence of the indirect component described in section 5.6.1 is negligible. This agrees with results in Refs [5] and [15].

It is not always appropriate to assume $GEP(s)|_{CSC} \approx K_P$. This is particularly true for the system with significant external resistance. Sections 5.8.3 and 5.8.4 discuss this in more detail.

Fig. 5.12(b) shows the CSC synchronizing torque. The CSC controller optimised by the ISE technique is such that the CSC torque transfer function of Eq. (5.58) exhibits a net phase lag.

As a result, the CSC controller introduces positive synchronizing torque into the system for all conditions [16]. This enhances the synchronous machine transient stability as well as increases the frequencies of oscillation [16].

Fig. 5.12(c) shows the total system damping torque. Values for $K_{D(\mathrm{CSC})}$ are much higher than the damping torque coefficient of the system without oscillation stabilizer (Fig. 3.23(e)). Consequently, K_D follows the trends of $K_{D(\mathrm{CSC})}$ with respect to changes in external reactance and generator loading. At conditions of high loading the slight reduction in K_D with increase in P_t is a result of the AVR damping torque shown in Fig. 3.23(c).

5.8.3 Line resistance

Section 5.8.2 neglected system external resistance. This section focuses on the influence of line resistance on the system model torque coefficients. Appendix G.5 contains results for this section.

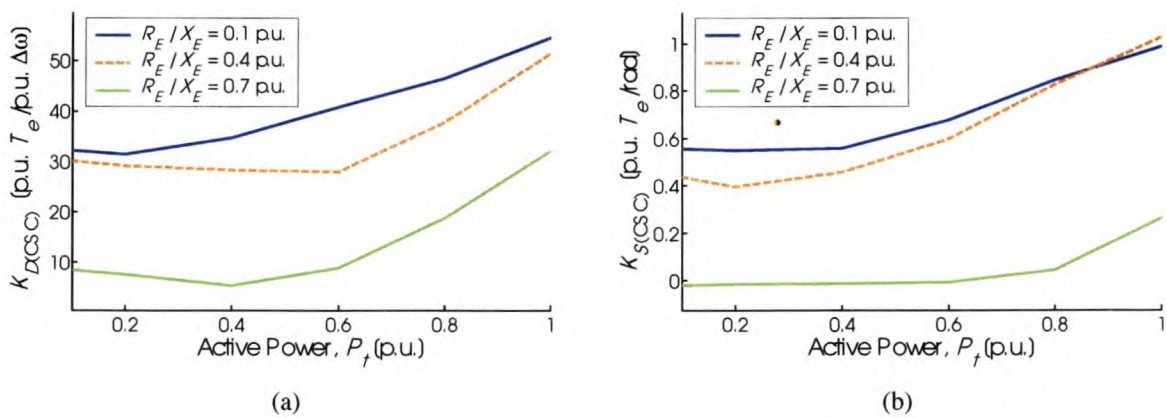

(a) (b)

Fig. 5.15: CSC damping and synchronizing torque coefficients vs. machine load and line resistance, with X_E = 0.8 p.u.

Fig. 5.15(a) shows $K_{D(\mathrm{CSC})}$ for the system with $X_E = 0.8$ p.u. $K_{D(\mathrm{CSC})}$ is higher in a system with lower R_E/X_E. This is a desirable trend; the stability problems for which the stabilizer is applied also increase with reduced R_E/X_E of the external impedance for a constant X_E and P_t (section 3.8.3).

Fig. 5.15(b) shows $K_{S(\mathrm{CSC})}$ for the ISE-optimised CSC controller is negative for high R_E/X_E at low P_t. This is a result of undercompensation of the "plant" phase lead so that $\Delta T_e|_{\mathrm{CSC}}$ has a phase lead at ω_n. Both K_S and ω_n slightly reduce in value [16]. This is of no particular

concern; the system net synchronizing torque is still positive and significantly greater than the negative influence of the CSC controller (see results in Appendix G.5). Transient stability is assured.

For a system with higher R_E/X_E, $GEP(s)|_{CSC}$ deviates some from the generalization $GEP(s)|_{CSC} \approx K_P$ applicable to the scenario of no external resistance (section 5.8.2). Fig. 5.16 shows K_P and $GEP(s)|_{CSC}$ for the system with $X_E = 0.8$ p.u. Comparison between these graphs show the indirect component in Eq. (5.57) becomes more significant with increase in resistance in the external system.

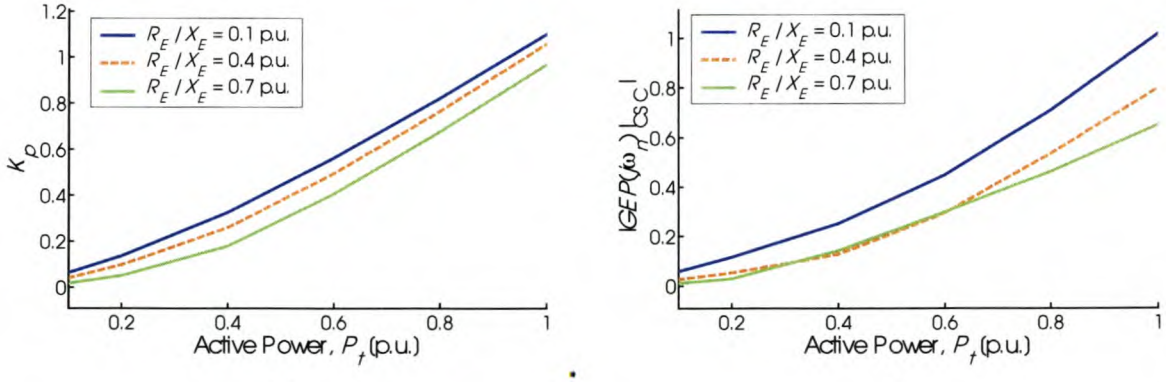

(a) (b)

Fig. 5.16: Parameter K_p and "plant" transfer function vs. machine load and line resistance, with X_E = 0.8 p.u.

5.8.4 Local load

This section focuses on the influence of local load on $K_{D(CSC)}$. Appendix G.6 contains results for this section.

A resistance models the local load. Table 3.1 gives the X_{line} and R_{load} value combinations used in the investigation, and the resulting X_E, R_E and E_B values from which the system parameters are determined (see discussion on Fig. 3.7).

The system damping, as well as the damping by the optimal CSC controller for a given system condition, behaves in a manner similar to the scenario with external line resistance (section 5.8.3). Local load inherently provides damping torque to the system (section 3.8.4), and if sufficient ensures damping stability when otherwise would not be the case (at the expense of synchronizing torque). On the other hand, local load may not be enough to

provide the needed damping (particularly with high external reactance), and added damping is needed.

Fig. 5.17(a) shows $K_{D(\mathrm{CSC})}$ for the system with $X_{line} = 0.8$ p.u . $K_{D(\mathrm{CSC})}$ is higher in a system with lower local load. This is desirable; the stability problem for which the stabilizer is applied also increases with reduced local load (section 3.8.3).

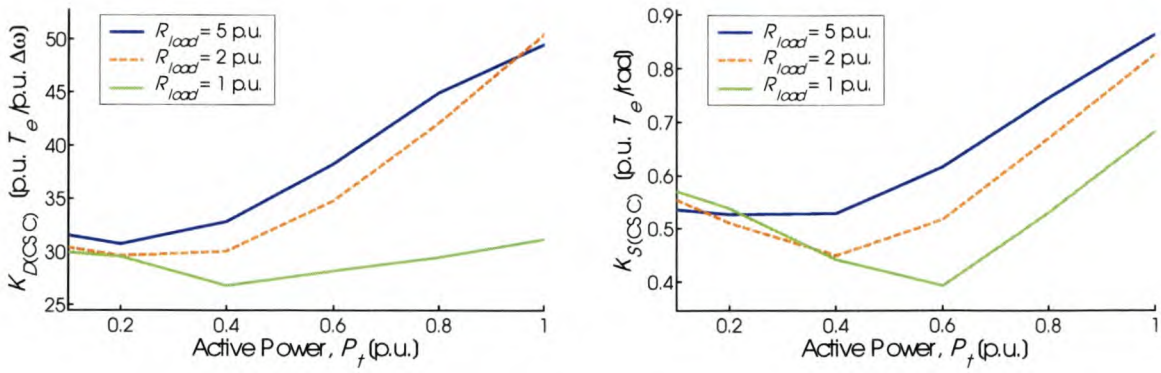

(a) (b)

Fig. 5.17: CSC damping and synchronizing torque coefficients vs. machine load and local load resistance, with X_{line} = 0.8 p.u.

Fig. 5.17(b) shows $K_{S(\mathrm{CSC})}$ for the ISE-optimised CSC controller is positive for all conditions considered. The trend of $K_{S(\mathrm{CSC})}$ with respect to loading of the generator is altered by the addition of local load – now $K_{S(\mathrm{CSC})}$ decreases with increase in P_t, reaches a minimum, then increases with further increase in P_t.

Section 5.8.3 explains how and why $GEP(s)\big|_{\mathrm{CSC}}$ deviates from the generalization $GEP(s)\big|_{\mathrm{CSC}} \approx K_P$. The indirect component becomes significant. This same discussion also applies to the system with local load, particularly in a system with larger external reactance. Appendix G.6 contains graphs of $GEP(s)\big|_{\mathrm{CSC}}$.

5.8.5 Excitation system gain

Results for sections 5.8.2 to 5.8.4 reflect a system with high initial-response excitation system; i.e. with an AVR gain of 200. Section 3.3.2 discusses the motivation behind assuming such a high gain. This section considers the influence of assuming a lower K_A on the CSC performance. Results for the previous sections were regenerated for the system of Appendix B, but with $K_A = 20$. Appendix G.7 contains the results.

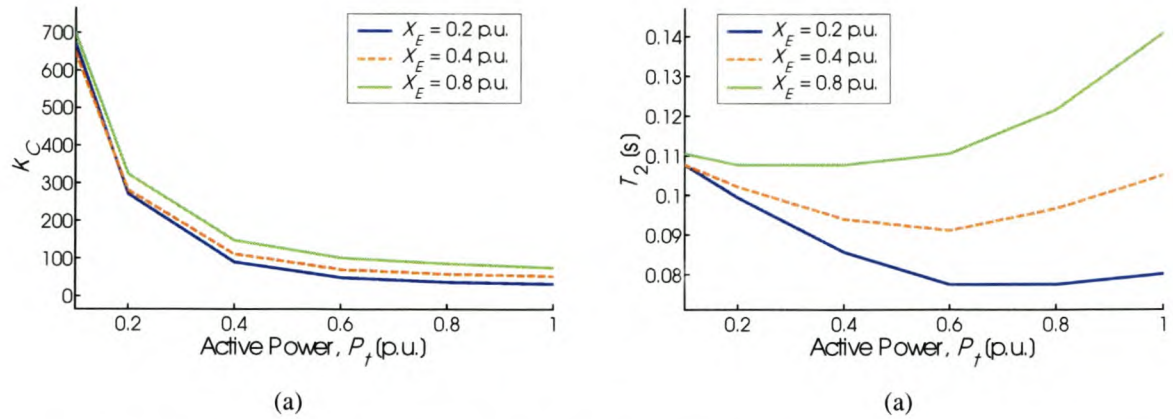

Fig 5.18: Optimised CSC parameters K_C and T_2 vs. machine load and external reactance, with K_A = 20

Results from section 3.8.5 indicate less damping support is needed in a system with lower K_A, compared to a system with a high initial-response excitation system. Yet, under conditions of large external reactance and load K_D is still negative, and there remains a need for stability support.

In a system with lower AVR gain, values for K_C and T_2 are generally lower compared to a system with higher K_A (compare PSS case, section 4.6.5). Fig 5.18 shows the trends of K_C and T_2 are different in the system with lower K_A, compared to the trends in a system with high K_A shown in Fig 5.11.

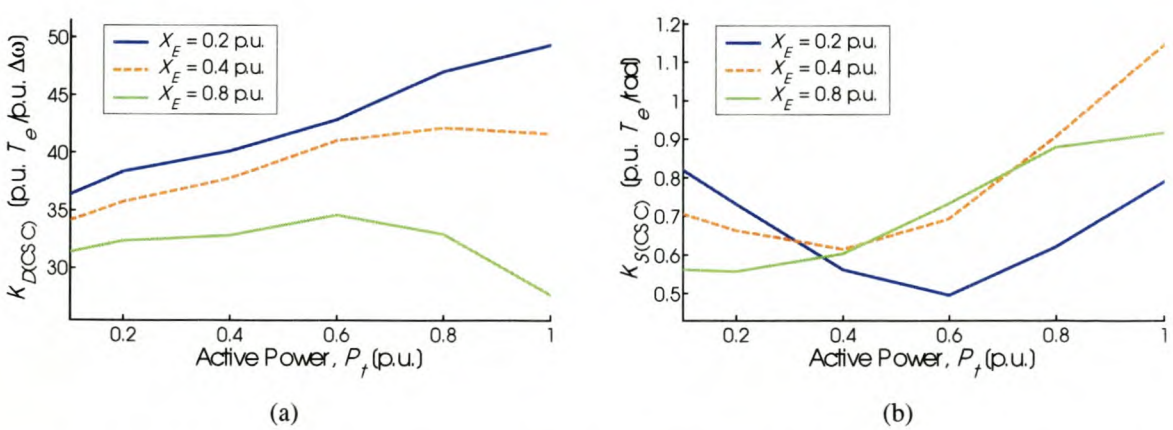

Fig. 5.19: CSC damping and synchronizing torque coefficients vs. machine load and external reactance, when K_A = 20

Fig. 5.19(a) shows the CSC damping torque coefficient for the system with $K_A = 20$. Comparison to Fig. 5.12(a) shows values for $K_{D(\mathrm{CSC})}$ are lower in a system with moderate to high X_E and lower K_A. $K_{D(\mathrm{CSC})}$ also reduces with increased generator load at high values of P_t and X_E (not the case when $K_A = 200$). When $X_E = 0.2$ p.u. $K_{D(\mathrm{CSC})}$ values are higher with lower K_A.

More damping is needed as system load increases. However, when $K_A = 20$ the stabilizer performance decreases as the system load increases, particularly in a weaker system. This is not favourable, even though the stabilizer is able to provide the needed damping torque.

Fig. 5.19(b) shows the synchronizing torque of the CSC controller optimised by the ISE technique, for the system with $K_A = 20$. Comparison to Fig. 5.12(b) shows there is no definite pattern in the variation of $K_{S(\mathrm{CSC})}$ with K_A. Also, the trends of $K_{S(\mathrm{CSC})}$ with respect to P_t and X_E are altered. The synchronizing torque of the CSC remains positive even when K_A is reduced. This is not the case for the PSS, discussed in section 4.6.5.

5.8.6 Influence of saturation

Synchronous machine saturation was modelled to obtain the results of the previous sections. Appendix C describes the modelling of saturation in the synchronous machine. This section considers the influence of neglecting saturation, often the assumption in literature.

The results of section 5.8.2 (system without external resistance, and $K_A = 200$) were regenerated for the system of Appendix B with machine saturation neglected (constant machine inductances/reactances). Appendix G.8 contains the results.

Results show, under most cases, values of K_C and T_2 of the ISE-optimised CSC controller are lower when saturation effect is neglected in a stronger system (T_2 much lower); in a very weak system, values of K_C and T_2 are generally higher. With some exceptions, values of the CSC damping and synchronizing torques are higher in magnitude when $X_E = 0.2$ p.u. (the stronger system), but lower in systems with higher X_E, compared to the model with saturation effect considered.

These results indicate the need to model saturation: (a) to ensure more reliable CSC controller design by the ISE technique, and (b) to more correctly access the influence of such controller on system stability, whether damping or synchronizing.

5.8.7 Summary of results

The trends of the CSC damping torque coefficient, with respect to *machine load and external reactance* (section 5.8.2), *line resistance* (section 5.8.3) and *local load* (section 5.8.4) were examined. The influences of the *AVR gain* (section 5.8.5) and *saturation modelling* (section 5.8.6) on results were also considered.

A summary of the results of section 5.8 follows.

The CSC controller gain, as obtained by the ISE optimisation method, is high at low P_t and decreases with increase in machine load. K_C values are also higher in a stronger system. In a system with lower AVR gain but similar in all other respects, the optimisation process obtains a lower K_C value necessary for optimum performance. Also, when K_A is low K_C is smaller in a stronger system.

Values for T_2 by the ISE optimisation method increase with increase in generator load, reach a maximum, and decrease with further increase in P_t. T_2 is also larger in a stronger system. In a system with lower AVR gain but similar in all other respects, the optimisation process obtains a lower T_2 value necessary for optimum performance. Then the trends with respect to P_t and X_E are also different from those in a system with high K_A.

The CSC optimum damping capability increases with increase in system strength and load, for a system of moderate to high external reactance. In a very strong system the ability of the controller to provide added damping is reduced, compared to the weaker systems. $K_{D(\mathrm{CSC})}$ also increases with decrease in R_E/X_E or local load. The latter characteristic is desirable, since the stability problems for which the stabilizer is needed increases with decrease in R_E/X_E or local load. Values for $K_{D(\mathrm{CSC})}$ are higher in a strong system with lower K_A; the opposite is the case in a weaker system – $K_{D(\mathrm{CSC})}$ is lower if the AVR gain is lower. The latter is favourable – less damping torque is needed in a system with lower K_A.

The CSC controller optimised by the ISE technique introduces positive synchronizing torque into the system that increases with increase in P_t when the generator does not operate into a

local load, and the AVR gain is high. The variation of $K_{S(CSC)}$ with respect to external reactance depends on the gain of the generator AVR. $K_{S(CSC)}$ decreases with increase in R_E/X_E or local load, even to such an extend that $K_{S(CSC)}$ may be negative when R_E/X_E is high. The total system synchronizing torque however remains positive for all system conditions investigated. There is no definite variation of $K_{S(CSC)}$ with respect to changes in K_A.

For K_C and T_2, as well as the CSC synchronizing and damping torque coefficients, the influence of saturation on results varies with system loading and strength.

5.9 Summary

This chapter presented the state-space and block diagram models of the SMIB system with CSC, and determined the ability of a CSC to enhance system stability in situations when such stability support is required, according to results from chapter 3. For purpose of investigation the conventional (classic) CSC controller configuration was assumed.

Both the "plant" transfer function and the CSC controller parameters influence the performance of the stabilizer. In systems without external resistance the constant K_P can approximate the "plant" transfer function. The parameters of the CSC are evaluated for every system condition to give optimum performance at the particular system condition. An optimisation technique based on the integral of the square error performance index is presented and used for that purpose. Some assumptions are made to simplify the optimisation process.

The investigation shows the CSC controller is able to provide both damping and synchronizing torque to the system. The damping support behaves favourably with respect to variation in generator load, R_E/X_E or local load. This is not the case with respect to changes in external system reactance, in the moderate to high reactance range. The variation of CSC damping support with respect to AVR gain varies with system strength.

The influence of the optimised CSC controller on the system synchronizing stability is also investigated. In the case of significant R_E/X_E the controller introduces negative synchronizing torque into the system. The system synchronizing torque however remains positive and the system transiently stable for all conditions.

6 COMPARATIVE SUMMARY

6.1 Introduction

This chapter presents a summary of the results of the previous chapters on system stability and stability enhancement by PSS and CSC. This summary is in the form of a comparison between the damping torque requirements of the SMIB system and the ability of each controller to supply the needed damping torque. The results are compared in two ways:

1. The trends of the damping support. The focus is on the ability of the controller to introduce more damping torque when more is required.
2. The damping torques introduced. Here the discussion focuses on which of an optimised PSS or CSC introduces more damping torque for a given condition of generator loading and network structure (impedance). In other words which controller option is more effective at enhancing the system stability.

6.2 Damping Torque Trends

According to results from chapter 3 and previous research on this subject, damping torque is needed more in a system that is weaker and/or more heavily loaded. In a weak system, added external (line series) resistance does not sufficiently improve the damping stability, so that damping support is still needed. With added local load the air-gap damping torque may be positive (depending on amount of local load), even in a system with high generator load and large external reactance. The system is then oscillatory stable.

Consider now the scenario when a low gain AVR is employed. Then damping support is needed only in the case of a highly loaded generator with large external system reactance. Again increased external system resistance does not sufficiently improve the system stability; damping torque is still needed. However, less local load is needed to ensure stability than in a system with high-response excitation system.

Chapters 4 and 5 discuss the performance of PSS and CSC, and how this performance varies with generator loading and network impedance. The following sections compare the results obtained, in an attempt to determine which controller is more suited to introduce damping when more damping torque is needed.

6.2.1 Generator loading

Consider first the case of a SMIB system with high-response exciter on the generator. *Both the PSS and CSC, with parameters evaluated for optimal performance, are able to introduce more damping torque when the generator is more heavily loaded.* Hence both PSS and CSC behave *favourably* with respect to generator loading.

An exception is CSC performance in a system with (a) large system reactance and (b) low AVR gain. In such a system the synchronizing torque coefficient (before adding controller) is positive but low. Two possible options to increase K_S also alters the unfavourable CSC trend:

1. Employ a high-response excitation system. This increases the synchronizing torque (although only marginally) but at the expense of damping torque. A CSC controller then introduces the damping torque needed, with the trend with respect to generator loading favourable (see above).
2. A more effective (and more costly) alternative is to add fixed series capacitive compensation. 50% fixed compensation is more effective in increasing K_S than a ten-fold increase in AVR gain. The system is stronger and more stable, and with low K_A adding controllable segments to the fixed capacitive compensation may not be necessary. If it is decided to add a controlled segment to the series compensation, in a stronger system the CSC controller introduces more damping torque in a more heavily loaded system. This again is favourable.

6.2.2 External Reactance

Damping torque is needed more in a weaker system. In a strong system stability is generally assured without the need for damping support, except at high values of generator loading and AVR gain.

Neither the PSS nor CSC is able to introduce more damping torque in a weaker system. Exceptions to this rule exist, however, and are considered below.

For the PSS case this is particularly the situation when the generator operates at high load. At lower loading the controller time constant may be fixed to the minimum of 0.05 s. In such a case the PSS introduces more damping torque in a weaker system, which is a favourable

situation. However, damping torque is generally not needed at low values of P_t. This favourable trend is therefore of no concern.

Two more exceptions exist pertaining to the reactance range 0.2 p.u. to 0.4 p.u. These are (a) a CSC controller in a system with high-response excitation system and (b) a PSS controller in a system with low gain AVR. In both cases in the reactance range 0.2 p.u. to 0.4 p.u. the performance increases with increase in external reactance. This is favourable. This indicates there exists a certain value of external reactance at which the performance of the CSC or PSS controller (in a system with high and low gain exciters, respectively) is a maximum.

This also appears to indicate there exists a limit to the amount of fixed compensation that ensures improved CSC controller performance. In the case of a PSS, damping torque is not needed in the range 0.2 p.u. to 0.4 p.u. X_E in a system with low K_A. This favourable trend is, again, therefore of no concern.

6.2.3 External system resistance and local load

This section considers both line resistance and local load. Both the PSS and CSC controllers behave similarly for these two cases.

Whenever the PSS controller time constant T_1 is not fixed at the lower limit of 0.05 s, the ability of the PSS controller to introduce damping torque increases with reduced series resistance or local load. The CSC controller is also more able to introduce damping torque in a system with lower line resistance or local load. These are *favourable* trends.

The PSS controller time constant T_1 is set to the minimum more often in cases of large external reactance and AVR gain, regardless of R_E/X_E or local load. In such cases damping torque is particularly needed at high values of generator load. However, at high values of P_t the controller introduces less damping torque into a system with lower external resistance or local load. This is *not favourable*, and is the result solely of the minimum of 0.05 s set to the time constant T_1.

6.2.4 Excitation system gain

Both the PSS and CSC, with parameters corresponding to optimal performance, are able to provide more damping support in a system with large AVR gain than in a system with low AVR gain. This is a favourable trend.

An exception is the CSC controller operating in a strong system (such as $X_E = 0.2$ p.u.). Then the CSC controller in a system with lower K_A is able to introduce more damping torque than a CSC controller in a system with larger K_A (yet similar in all other respects). This trend is *unfavourable*. This is a disadvantage to implementing too much fixed series compensation to strengthen the system.

6.3 Damping Torque Contribution

This section compares the performance of the PSS and CSC controllers, based on the actual damping torque coefficients of the controllers. *The more damping torque the damping controller contributes to the power system, the more effective is the controller* [42]. The focus here is on which controller is able to provide more damping torque to the system for a given system condition. This section distinguishes between a system with high-response excitation system (such as $K_A = 200$), and a system with low AVR gain ($K_A = 20$).

Consider first the system with $K_A = 200$. Fig. 6.1 shows the PSS and CSC damping torque coefficients for the system without series line resistance or local load. Comparison shows the PSS is able to introduce more damping torque into the system than the CSC. This result holds true even when line resistance or local load is considered. Also, neglecting to model the saturation effect of machine inductances does not influence this result.

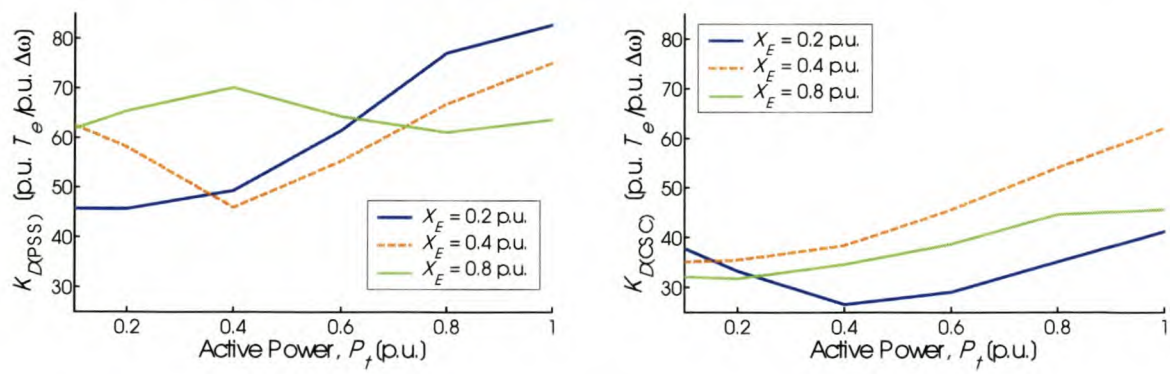

Fig. 6.1: PSS and CSC damping torque coefficients vs. machine load and external reactance

Consider now the system with low exciter gain. Results show in a stronger system (such as $X_E = 0.2$ p.u.), the CSC generally introduces more damping torque than does the PSS. The opposite is true in a weaker system, when the PSS is more effective. In a system with low K_A damping is needed only in the case of a system with large reactance. Although the CSC

is more effective at enhancing stability in a strong system with low K_A, this is of no practical interest.

The PSS controller is more effective to enhance the small-signal stability of the system, compared to the CSC controller. Previous research on this topic ([4], [7]) found the CSC controller is more superior to the PSS in damping the power oscillations. The circumstances of those investigations need, however, to be considered. Ref. [4] considered the damping of inter-area mode oscillations when making the claim. This investigation considers only local mode problems. Also, Ref. [7] states practical reasons to support that claim that was not considered in this research, such as controller saturation during transient behaviour. Transient stability was considered beyond the scope of this research.

This investigation does not negate results from previous research. Instead, results from this investigation simply states the following:

A PSS, with input signal $\Delta\omega_r$ and parameters optimised by the ISE-method, introduces more damping torque than a CSC of similar control topology, also with input signal $\Delta\omega_r$ and parameters optimised using the same methodology.

6.4 Synchronizing Torque

The system has positive synchronizing electrical air-gap torque for all conditions considered. Hence the system is transiently stable. Results show the PSS, optimised by the integral of square error method discussed, introduces negative synchronizing torque into the system only in the case of a strong system with low generator AVR gain. Then the synchronizing torque is more negative with increase in local load or external resistance. In such cases the inherent damping torque of the system (AVR and armature reaction) is positive, and there is no need for added stability support. Hence this is of no particular concern.

The CSC controller introduces negative synchronizing torque into the system only in the case of a system with large line resistance and high-response generator excitation system. However, this is the case only for low values of P_l. A CSC will not be needed in a system with this configuration and loading, and thus this is of no particular concern.

A summary of results of this present chapter is found in the conclusion section of this report.

7 CONCLUSION

7.1 Project Overview

This thesis conducted a study of the small-signal stability of a SMIB system. The need for stability support was presented. Methods considered to enhance the stability of the SMIB system are the power system stabilizer and controlled series capacitor. A technique to optimise the parameters of the PSS or CSC controller was presented. Based on such optimum performance, results for the damping and synchronizing torques by the PSS and CSC controllers were obtained for various combinations of generator loading and system impedance. A comparison of the performance of the PSS and CSC controllers, based on the damping torque contributions by the controllers, was presented.

Chapter 2 performed a background study on the broad issue of system stability, as well as previous research with regards the use of the block diagram approach in small-signal stability analysis. The concepts of generator air-gap damping and synchronizing torques are defined. Several methods of stability enhancement and their performance characteristics were presented. Of these, the PSS and CSC were considered appropriate for investigation.

Chapter 3 presented the Phillips-Heffron block diagram model of the SMIB system. The generator excitation system consists of a thyristor exciter and voltage regulator. From the block diagram expressions for the air-gap torques due to the AVR and field windings were obtained. These expressions are functions of the K-parameters of the block diagram model. It was shown the parameters K_1, K_4 and K_5 have the most dominant influence on the overall small-signal stability of the SMIB system. The stability of the system was determined for various conditions of generator loading and line reactance. The influence of system resistance and local load on system stability was also investigated.

Chapter 4 presented the block diagram model of the SMIB system with PSS, and investigated the ability of a conventional (classic) PSS controller to enhance the system stability. The generator loading and network impedance conditions used in chapter 3 were considered. Performance of the PSS was measured in its ability to provide damping torque to the generator. From the block diagram model expressions for the PSS damping and synchronizing torques were obtained. The PSS performance is a function of the controller parameters, as well as the transfer function of the "plant" through which the controller introduces torque to the generator. The latter is shown to have a significant influence on PSS

performance. Values for the controller parameters were obtained using an ISE-based optimisation method.

Chapter 5 presented the block diagram model of the SMIB system with CSC, and investigated the ability of a conventional (classic) CSC controller to enhance the system stability. The block diagram model to accommodate a CSC differs somewhat from the Phillips-Heffron model as it incorporates additional K-parameters. Expressions for these parameters were developed and their trends investigated. The generator loading and network impedance conditions of chapter 3 were considered. The ability to introduce damping torque was used as a measure of stabilizer performance. From the block diagram model expressions for the CSC damping and synchronizing torques were obtained. The CSC performance is a function of the controller parameters, as well as the transfer function of the "plant" through which the controller introduces torque to the generator. As is the case of the PSS, this "plant" is shown to have a significant influence on CSC performance. Values for the controller parameters were obtained using an ISE-based optimisation method.

Chapter 6 presented a summary of the results of chapters 3 through 5. This summary was in the form of a comparison between the need for damping support and the ability of each controller to supply the needed damping torque. Also, values of the damping torque coefficients of the optimised PSS and CSC controllers were compared. The PSS is able to introduce more damping torque than the CSC.

7.2 Thesis Contribution

The work presented in this report was based on the Phillips-Heffron and the modified Phillips-Heffron models of the SMIB system to describe the small-signal stability of such a system.

In particular, the scenario of remote generation connected to a large system through radial line(s) was considered. This differs from previous research on the parameters and damping torque coefficients of the block diagram model [12][13], as these did not consider the external (remote) system "stiff" and the infinite bus voltage was not a controlled variable set at a pre-determined value.

The following contributions to the field of small-signal stability pertaining to the use of the block diagram approach are made:

- Trends of the parameters $K_1 \ldots K_6$ and the damping and synchronizing torque coefficients of the Phillips-Heffron block diagram are presented, where it is assumed the infinite bus voltage is constant regardless of system loading or impedance.
- Expressions are derived for the parameters K_P, K_q and K_V of the modified Phillips-Heffron model presented in [15].
- Concepts presented in [15] are extended to include a conventional CSC controller scheme, and a system with external resistance or local load.
- Trends of the parameters K_q and K_V versus generator loading and line reactance are presented. Also, trends of K_P, K_q and K_V in systems with external resistance are presented.
- It is shown the indirect component of the "plant" transfer function in the CSC case does play a significant role, particularly in systems with external resistance or local load.
- The influence of the saturation on results is presented. It is shown the methodology of modelling saturation in Ref. [45] is not valid.

Other contributions made to the field of small-signal stability are:

- The ISE optimisation method is applied to the conventional CSC controller and shown to provide substantial damping torque support.
- Trends of the PSS and CSC damping torques, with controllers optimised by the ISE technique, are researched. Results from this investigation are discussed below.
- It is shown that even though significant external (series) resistance improves the system inherent stability, the SMIB system may still be unstable.

7.3 Main Results

The trends investigated are an indication of the ability of a controller to introduce damping torque to the generator when there exists a need for more damping torque to ensure stable operation. The main results emanating from this research are as follows:

1. Both the PSS and CSC, with parameters evaluated for optimal performance, are able to introduce more damping torque when the generator is more heavily loaded. An exception is CSC performance in a system with large reactance and low K_A.

2. Neither the PSS nor CSC is able to introduce more damping torque in a weaker system. An exception is a CSC controller in a system with high-response excitation system, with system reactances in the range 0.2 p.u. to 0.4 p.u.
3. Both the PSS and CSC controllers are able to introduce more damping torque in a system with lower line resistance or local load. An exception is a PSS controller operating in a highly loaded and weak system, with high-response excitation system.
4. Both the PSS and CSC are able to provide more damping support in a system with larger AVR gain. An exception is a CSC controller in a strong system.

Finally, a comparison of the damping torques by the stabilizers optimised for that purpose provides the following main result:

A PSS controller, with input signal $\Delta\omega_r$ and parameters optimised by the ISE-method, introduces more damping torque in the SMIB system than a CSC controller of similar control topology, also with input signal $\Delta\omega_r$ and parameters optimised using the same methodology.

7.4 Suggestions for Future Research

This research considered only small-signal stability, based on the concepts of synchronizing and damping torques. Results were not verified by transient studies of a system disturbance using a non-linear generator model. It is suggested this analysis be performed to validate findings of this report.

How the damping capability of UPFC varies for various system conditions may be investigated. The research performed and presented in this report is based on the Phillips-Heffron and modified Phillips-Heffron block diagram models. The modified Phillips-Heffron block diagram was first presented in [15], to facilitate the inclusion of FACTS devices such as SVC, CSC and PAR. In Ref. [54] it is shown this model also applies to the SMIB system with UPFC.

SMES can also be used to damp power oscillations ([63] pp. 36). Subject of future research may be to extend the block diagram (if the need may be) to facilitate SMES for damping purposes. Using this, the ability of SMES to enhance stability for various conditions of generator loading and system impedance can be evaluated.

Results from section 3.8 appears to indicate there exists a certain system reactance, for a given generator loading, at which the CSC damping controller is most effective. Previous research [9] on this topic does not indicate the existence of such a threshold. Evaluating the

system reactance (including fixed capacitive compensation) for a given generator loading at which the CSC controller is most effective, is probable subject for future research. Knowledge of such a reactance value can aid in evaluating the amount of fixed capacitive compensation to ensure optimum controller performance.

Refs [22] and [29] applied the ISE-technique to optimise the PSS controller parameters. In this investigation, this same technique was also applied to the case of CSC. However, in the development of this technique, the weighting factor α was assumed zero as this gives the best system dynamic performance. This was also assumed for the CSC case. Whether this assumption negatively affects results of CSC damping performance is to be investigated in future research.

This investigation shows that when the time constant T_1 of the PSS controller varies a bit from the value corresponding to optimal damping performance, very different damping torque results and trends are observed. The PSS performance appears sensitive to the controller parameters. Ref. [72] states this fact also. Research in this regard is certainly something to consider.

REFERENCES

Journal and Conference Papers

[1] W.G. Heffron and R.A. Phillips, "Effects of a Modern Amplidyne Voltage Regulator on Underexcited Operation of Large Turbine Generators," *AIEE Trans.*, Vol. PAS-71, pp. 692-697, August 1952.

[2] F.P. deMello and C. Concordia, "Concepts of Synchronous Machine Stability as Affected by Excitation Control," *IEEE Trans.*, Vol. PAS-88, No. 4, pp. 316-329, April 1969.

[3] M.J. Gibbard, D.J. Vowles and P. Pourbeik, "Interactions Between, and Effectiveness of, Power System Stabilizers and FACTS Device Stabilizers in Multimachine Systems," *IEEE Trans.*, Vol. PWRS-15, No. 2, pp. 748-755, May 2000.

[4] M. Noroozian and P. Halvarsson, "Applications of CSCs for Damping of Power Swings," *Vector (Electrical Engineering)*, pp. 2, 4, 6, 8, November 1997.

[5] H.F. Wang, F.J. Swift and M. Li, "Comparison of Modal Controllability between FACTS-based stabilisers and PSS in Increasing the Oscillation Stability of Multimachine Power Systems," *IEE Proceedings: Generation, Transmission and Distribution*, Vol. 143, No. 6, pp. 575-581, November 1996.

[6] D.A. Pastos, N.A. Vovos, G.B. Glannakopoulos and A.D. Lygdis, "Damping Efficiency of SVC and CSC," *IEE Conference Publication*, No. 423, pp. 275-280, 1996.

[7] X.R. Chen, N.C. Pahalawaththa, U.D. Annakkage and C.S. Kumble, "Power System Stability Enhancement by using Controlled Series Compensation," *International Journal of Electrical Power and Energy Systems*, Vol. 16, No. 2, pp. 67-72, 1996.

[8] M. Noroozian and G. Andersson, "Damping of Inter-Area and Local Modes by Use of Controllable Components," *IEEE Trans.*, Vol. PWRD-10, No. 4, pp. 2007-2012, October 1995.

[9] M. Noroozian and G. Andersson, "Damping of Power System Oscillations by Use of Controllable Components," *IEEE Trans.*, Vol. PWRD-9, No. 4, pp. 2046-2054, October 1994.

[10] L. Angquist, B. Lundin and J. Samuelsson, "Power Oscillation Damping using Controlled Reactive Compensation – A Comparison between Series and Shunt Approaches," *IEEE Trans.*, Vol. PWRS-8, No. 2, pp. 687-700, May 1993.

[11] Y.-Y. Hsu, C.-S. Liu, C.J. Lin and C.T. Huang, "Application of Power System Stabilizers and Static VAR Compensators on a Longitudinal Power System," *IEEE Trans.*, Vol. PWRS-3, No. 4, pp. 1464-1470, November 1988.

[12] M.K. El-Sherbiny and D.M. Mehta, "Dynamic System Stability, Part I – Investigation of the Effect of Different Loading and Excitation Systems," *IEEE Trans.*, Vol. PAS-92, No. 5, pp. 1538-1546, September/October 1973.

[13] F.P. deMello and T.F. Laskowski, "Concepts of Power System Dynamic Stability," *IEEE Trans.*, Vol. PAS-94, No. 3, pp. 827-833, May/June 1975.

[14] F.J. Swift, H.F. Wang and M. Li, "Analysis of Controllable Series Compensator to Suppress Power System Oscillations," *IEE Conference Publication*, No. 423, pp. 202-207, 1996.

[15] H.F. Wang, F.J. Swift, "A Unified Model for the Analysis of FACTS Devices in Damping Power System Oscillations Part I: Single-machine Infinite-bus Power Systems," *IEEE Trans.*, Vol. PWRD-12, No. 2, pp. 941-946, April 1997.

[16] E.V. Larsen and D.A. Swann, "Applying Power System Stabilizers, Part I: General Concepts," *IEEE Trans.*, Vol. PAS-100, No. 6, pp. 3017-3024, June 1981.

[17] E.V. Larsen and D.A. Swann, "Applying Power System Stabilizers, Part II: Performance Objectives and Tuning Concepts," *IEEE Trans.*, Vol. PAS-100, No. 6, pp. 3025-3033, June 1981.

[18] E.V. Larsen and D.A. Swann, "Applying Power System Stabilizers, Part III: Practical Considerations," *IEEE Trans.*, Vol. PAS-100, No. 6, pp. 3033-3046, June 1981.

[19] IEEE Committee Report, "Excitation System Models for Power System Stability Studies," *IEEE Trans.*, Vol. PAS-100, No. 2, pp. 494-509, February 1981.

[20] IEEE Committee Report, "Computer Representation of Excitation Systems," *IEEE Trans.*, Vol. PAS-87, No. 6, pp. 1460-1464, June 1968.

[21] Discussion of Ref. [12] by F.P. deMello.

[22] K. Bhattacharya, J. Nanda and M.L. Kothari, "Optimization and Performance Analysis of Conventional Power System Stabilizers," *International Journal of Electrical Power and Energy Systems*, Vol. 19, No. 7, pp. 449-458, 1997.

[23] IEEE Task Force, "Proposed Terms and Definitions for Power System Stability," *IEEE Trans.*, Vol. PAS-101, pp. 1894-1898, July 1982.

[24] Discussion of Ref. [19] by H.H. Chen.

[25] P. Kundur, M Klein, G.J. Rogers and M.S. Zywno, "Application of Power System Stabilizers for Enhancement of Overall System Stability," *IEEE Trans.*, Vol. PWRS-4, No. 2, pp. 614-626, May 1989.

[26] Reply by P. Kundur, *et al.* to comments by C.W. Taylor and others on Ref. [25].

[27] IEEE Task Force, "Load Representation for Dynamic Performance Analysis," *IEEE Trans.*, Vol. PWRS-8, No. 2, pp. 472-482, May 1993.

[28] J.V. Milanović and I.A. Hiskens, "Effects of Load Dynamics on Power System Damping," *IEEE Trans.*, Vol. PWRS-10, No. 2, pp. 1022-1028, May 1995.

[29] M.L. Kothari, J. Nanda and K. Bhattacharya, "Discrete Mode Power System Stabilizers," *IEE Proceedings: Generation, Transmission and Distribution*, Vol. 140, No. 6, pp. 523-531, November 1993.

[30] R.J. Fleming, M.A. Mohan and K. Parvatisam, "Selection of Parameters of Stabilizers in Multimachine Power Systems," *IEEE Trans.*, Vol. PAS-100, No. 5, pp. 2329-2333, May 1981.

[31] P.S. Rao and I. Sen, "Robust Tuning of Power System Stabilizers Using QFT," *IEEE Trans. Control Systems Technology*, Vol. 7, No. 4, pp. 478-486, July 1999.

[32] M. Klein, G.J. Rogers, S. Moorty and P. Kundur, "Analytical Investigation of Factors Influencing Power System Stabilizers Performance," *IEEE Trans. Energy Conversion*, Vol. 7, No. 3, pp. 382-388, September 1992.

[33] X.R. Chen, N.C. Pahalawaththa, U.D. Annakkage and C.S. Kumble, "Enhancement of Power System Stability by using Controlled Series Compensation," *International Journal of Electrical Power and Energy Systems*, Vol. 18, No. 7, pp. 475-481, October 1996.

[34] X. Zhou and J. Liang, "Overview of Control Schemes for TCSC to Enhance the Stability of Power Systems," *IEE Proceedings: Generation, Transmission and Distribution*, Vol. 146, No. 2, pp. 125-130, March 1999.

[35] T.-S. Luor, Y.-Y. Hsu, S.-K. Wang, L.-H. Jeng, T.-Y. Guo, J.-T. Lin, Y.-Y. Chen and C.-Y. Huang, "Application of Thyristor-controlled Series Compensators to Enhance Oscillatory Stability and Transmission Capability of a Longitudinal Power System," *IEEE. Trans.*, Vol. PWRS-14, No. 1, pp. 179-185, February 1999.

[36] H.F. Wang, "Selection of Operating Conditions for the Co-ordinated Setting of Robust Fixed-Parameter Stabilisers," *IEE Proceedings: Generation, Transmission and Distribution*, Vol. 145, No. 2, pp. 111-116, March 1998.

[37] N. Yang, Q. Liu and J.D. McCalley, "TCSC Controller Design for Damping Interarea Oscillations," *IEEE. Trans.*, Vol. PWRS-13, No. 4, pp. 1304-1310, November 1998.

[38] Q. Zhao and J. Jiang, "A TCSC damping controller design using robust control theory," *International Journal of Electrical Power and Energy Systems*, Vol. 20, No. 1, pp. 25-33, January 1998.

[39] G.N. Taranto and D.M. Falcão, "Robust Decentralised Control Design Using Genetic Algorithms in Power System Damping Control," *IEE Proceedings: Generation, Transmission and Distribution*, Vol. 145, No. 1, pp. 1-6, January 1998.

[40] J.M. Ramírez, R.J. Dávalos and A.V. Valenzuela, "Coordination of FACTS-Based Stabilizers for Damping Oscillations," *Power Engineering Review*, Vol. 20, No. 12, pp. 46-49, December 2000.

[41] M.H. Baker, "Transmission Enhancement by FACTS Devices," *Elektron*, Vol. 12, pp. 17-19, October 1995.

[42] H.F. Wang and F.J. Swift, "Application of the Phillips-Heffron Model in the Analysis of the Damping Torque Contribution to Power Systems by SVC Damping Control," *International Journal of Electrical Power and Energy Systems*, Vol. 18, No. 5, pp. 307-313, 1996.

[43] H.F. Wang, F.J. Swift and M. Li, "Oscillation Stabilization of Multi-Machine Power Systems by Controllable Series Compensator," *IEE Conference Publication*, No. 423, pp. 315-320, 1996.

[44] M. Saidy and F.M. Hughes, "An Extended Block Diagram Transfer Function Model of a Synchronous Machine," *International Journal of Electrical Power and Energy Systems*, Vol. 18, No. 2, pp. 139-142, 1996.

[45] M.K. El-Sherbiny, M. Farghally and M.M. Abdel-Hamid, "Dynamic Stability Analysis with Saturation Effect Included," *Modelling, Simulation and Control A*, Vol. 5, No. 3, pp. 27-38, 1985.

[46] F.J. Swift and H.F. Wang, "Application of the Controllable Series Compensator in Damping Power System Oscillations," *IEE Proceedings: Generation, Transmission and Distribution*, Vol. 143, No. 4, pp. 359-364, July 1996.

[47] E.W. Kimbark, "Improvement of System Stability by Switched Series Capacitors," *IEEE Trans.*, Vol. PAS-85, No. 2, pp. 180-188, February 1966.

[48] Reply by M. Noroozian and G. Andersson to comments by S.E.M. de Oliveira and others on Ref. [9].

[49] Discussion of Ref. [10] by C.W. Taylor.

[50] Reply by L. Ängquist et al. to comments by D. Povh and others on Ref. [10].

[51] Discussion of Ref. [10] by D. Povh and H. Tyll.

[52] Discussion of Ref. [10] by J.F. Hauer.

[53] E.A. Leonidaki, N.D. Hatziargyriou and G.J. Georgantzis, "Simulation of Thyristor Controlled Series Capacitors and Subsynchronous Studies," *Proceedings of the Universities Power Engineering Conference*, Vol. 2, pp. 883-886, September 1997.

[54] H.F. Wang, "A Unified Model for the Analysis of FACTS Devices in Damping Power System Oscillations Part III: Unified Power Flow Controller," *IEEE Trans.*, Vol. PWRD-15, No. 3, pp. 978-983, July 2000.

[55] H.F. Wang, "Damping Function of Unified Power Flow Controller," *IEE Proceedings: Generation, Transmission and Distribution*, Vol. 146, No. 1, pp. 81-87, January 1999.

[56] H.F. Wang, Y.S. Hao, B.W. Hogg and Y.H. Yang, "Stabilization of Power Systems by Governor-turbine Control," *International Journal of Electrical Power and Energy Systems*, Vol. 15, No. 6, pp. 351-361, 1993.

[57] H.F. Wang, "Phillips-Heffron Model of Power Systems Installed with STATCOM and Applications," *IEE Proceedings: Generation, Transmission and Distribution*, Vol. 149, No. 6, pp. 521-527, September 1999.

[58] K.V. Patil, J. Senthil, J. Jiang and R.M. Mathur, "Application of STATCOM for Damping Torsional Oscillations in Series Compensated AC Systems," *IEEE Trans. Energy Conversion*, Vol. 13, No. 3, pp. 237-243, September 1998.

[59] N.G. Hingorani, "Flexible AC Transmission," *IEEE Spectrum*, Vol. 30, No. 4, pp. 40-45, April 1993.

Books and Manuals

[60] P. Kundur, Power System Stability and Control, McGraw-Hill, 1994.

[61] Y.-N. Yu, *Electric Power System Dynamics*, Academic Press, 1983.

[62] T.J.E. Miller (editor), *Reactive Power Control in Electric Systems*, John Wiley & Sons, 1982.

[63] J. Machowski, J.W. Bialek and J.R. Bumby, *Power System Dynamics and Stability*, John Wiley & Sons, 1997.

[64] P.M. Anderson and A.A. Fouad, *Power System Control and Stability*, The Iowa State University Press, 1977.

[65] J.D. Glover and M.S. Sarma, *Power System Analysis and Design*, Second Edition, PWS Publishing, 1994.

[66] J.J. Grainger and W.D. Stevenson, *Power System Analysis*, McGraw-Hill, 1994.

[67] L.M. Faulkenberry and W. Coffer, *Electrical Power Distribution and Transmission*, Prentice Hall, 1996.

[68] R.C. Dorf, *Modern Control Systems*, Fourth Edition, Addison Wesley, 1987.

[69] C.W. Taylor, *Power System Voltage Stability*, McGraw-Hill, 1994.

[70] N.G. Hingorani and L. Gyugi, *Understanding FACTS*, IEEE Press, NewYork, 2000.

Other References

[71] Conversation with Dr. Vermeulen, Stellenbosch, September 2001.

[72] Conversation with W.-J. Lee, IASTED conference on Power and Energy Systems, Clearwater Beach USA, November 2001.

[73] Africa Grid Planning, *Namibia Power System Database*, NamPower Namibia, June 1999.

A DECOMPOSITION OF TORQUES

A.1 Introduction

To evaluate the stability of a machine connected to an infinite bus or a multi-machine power system, its oscillation modes are determined by eigenvalue analysis, and the synchronizing and damping torque coefficients calculated for the particular mode. The substitution made is

$$s = \lambda = \sigma + j\omega \tag{A.1}$$

where λ is a rotor mode eigenvalue, and a complex frequency. To correctly evaluate the damping and synchronizing torque components at the oscillation mode in which the machine partakes, the eigenvalue of that mode should be used as substitute for s.

It is, however, not always possible to determine the system eigenvalues. Also, the real part of λ is normally much smaller than ω for rotor mechanical modes. In such cases, it is sufficient to evaluate the torque characteristics using $s = j\omega_n$, where ω_n is the undamped natural frequency. This is the approach used in literature to derive at general conclusions regarding torque behaviour at any given frequency, or over a range of frequencies.

It is desired to establish the synchronizing and damping torque coefficients when the air-gap torque in phase with $\Delta\delta$ or $\Delta\omega_r$ is complex. Two scenarios are considered:

- Complex ΔT_e in phase with $\Delta\delta$
- Complex ΔT_e in phase with $\Delta\omega_r$

For each scenario, the use of both the complex frequency and the undamped natural frequency in evaluation of the torque coefficients are discussed.

A.2 ΔT_e in Phase with $\Delta\delta$

Consider

$$\frac{\Delta T_e}{\Delta\delta} = A + jB \tag{A.2}$$

evaluated using the complex frequency given by an eigenvalue. Since $s\Delta\delta = \omega_0\Delta\omega_r$,

$$j\Delta\delta = \frac{\omega_0}{\omega}\Delta\omega_r - \frac{\sigma}{\omega}\Delta\delta \tag{A.3}$$

and

$$\begin{aligned}\Delta T_e &= A\Delta\delta + B(j\Delta\delta)\\ &= A\Delta\delta + B\left(\frac{\omega_0}{\omega}\Delta\omega_r - \frac{\sigma}{\omega}\Delta\delta\right)\\ &= \left(A - B\frac{\sigma}{\omega}\right)\Delta\delta + B\frac{\omega_0}{\omega}\Delta\omega_r\end{aligned} \tag{A.4}$$

Thus, the synchronizing torque coefficient is

$$K_S = \mathrm{Re}\left(\frac{\Delta T_e}{\Delta\delta}\right) - \left(\frac{\sigma}{\omega}\right)\mathrm{Im}\left(\frac{\Delta T_e}{\Delta\delta}\right) \tag{A.5}$$

Similarly, the damping torque coefficient is

$$K_D = \left(\frac{\omega_0}{\omega}\right)\mathrm{Im}\left(\frac{\Delta T_e}{\Delta\delta}\right) \tag{A.6}$$

On the other hand, if $s = j\omega_n$ is used to obtain Eq. (A.2), from $s\Delta\delta = \omega_0\Delta\omega_r$ the expression for $j\Delta\delta$ is

$$j\Delta\delta = \frac{\omega_0}{\omega_n}\Delta\omega_r \tag{A.7}$$

and

$$\begin{aligned}\Delta T_e &= A\Delta\delta + B(j\Delta\delta)\\ &= A\Delta\delta + B\frac{\omega_0}{\omega_n}\Delta\omega_r\\ &= A(\Delta\delta) + B\frac{\omega_0}{\omega_n}(\Delta\omega_r)\end{aligned} \tag{A.8}$$

In this case, the synchronizing torque coefficient is simply the real part of (A.2). ω in Eq. (A.6) is replaced by ω_n to obtain the damping torque coefficient.

A.3 ΔT_e in Phase with $\Delta\omega_r$

A similar procedure to that above is followed. Consider

$$\frac{\Delta T_e}{\Delta\omega_r} = C + jD \tag{A.9}$$

evaluated using the complex frequency given by an eigenvalue. Since $s\Delta\delta = \omega_0\Delta\omega_r$,

$$j\Delta\omega_r = \frac{\sigma}{\omega_0}(j\Delta\delta) - \frac{\omega}{\omega_0}\Delta\delta \tag{A.10}$$

Substituting $j\Delta\delta$ from Eq. (A.3),

$$\begin{aligned} j\Delta\omega_r &= \frac{\sigma}{\omega_0}\left(\frac{\omega_0}{\omega}\Delta\omega_r - \frac{\sigma}{\omega}\Delta\delta\right) - \frac{\omega}{\omega_0}\Delta\delta \\ &= \frac{\sigma}{\omega}\Delta\omega_r - \left(\frac{\sigma^2}{\omega_0\omega} + \frac{\omega}{\omega_0}\right)\Delta\delta \end{aligned} \tag{A.11}$$

Hence,

$$\begin{aligned} \Delta T_e &= C\Delta\omega_r + D(j\Delta\omega_r) \\ &= C\Delta\omega_r + D\left(\frac{\sigma}{\omega}\Delta\omega_r - \left(\frac{\sigma^2}{\omega_0\omega} + \frac{\omega}{\omega_0}\right)\Delta\delta\right) \\ &= -D\left(\frac{\sigma^2}{\omega_0\omega} + \frac{\omega}{\omega_0}\right)\Delta\delta + \left(C + D\frac{\sigma}{\omega}\right)\Delta\omega_r \end{aligned} \tag{A.12}$$

Thus, the synchronizing torque coefficient is

$$K_S = -\left(\frac{\sigma^2}{\omega_0\omega} + \frac{\omega}{\omega_0}\right)\mathrm{Im}\left(\frac{\Delta T_e}{\Delta\omega_r}\right) \tag{A.13}$$

Similarly, the damping torque coefficient is

$$K_D = \mathrm{Re}\left(\frac{\Delta T_e}{\Delta\omega_r}\right) + \left(\frac{\sigma}{\omega}\right)\mathrm{Im}\left(\frac{\Delta T_e}{\Delta\omega_r}\right) \tag{A.14}$$

On the other hand, if $s = j\omega_n$ is used to obtain Eq. (A.9), from $s\Delta\delta = \omega_0\Delta\omega_r$ the expression for $j\Delta\omega_r$ is

$$j\Delta\omega_r = -\frac{\omega_n}{\omega_0}\Delta\delta \tag{A.15}$$

and

$$\begin{aligned} \Delta T_e &= C\Delta\omega_r + D(j\Delta\omega_r) \\ &= C\Delta\omega_r + D\left(-\frac{\omega_n}{\omega_0}\Delta\delta\right) \\ &= -D\frac{\omega_n}{\omega_0}(\Delta\delta) + C(\Delta\omega_r) \end{aligned} \tag{A.16}$$

In this case, the damping torque coefficient is simply the real part of (A.9). The synchronizing torque coefficient is

$$K_S = -\frac{\omega_n}{\omega_0}\,\mathrm{Im}\left(\frac{\Delta T_e}{\Delta \omega_r}\right) \tag{A.17}$$

B SAMPLE TEST SYSTEM DATA

The test synchronous machine data is defined in Table B.1. Reactance values are in per unit on machine rating. Time constants are in seconds. Fig. B.1 depicts the saturation curve.

Table B.1: Sample system machine constants

Parameter		*Value*
Synchronous Reactance	X_d	1.81
	X_q	1.76
Transient Reactance	X'_d	0.3
Transient OC Time Constant	T'_{d0}	8.0 s
Stator Leakage Reactance	X_l	0.16
Stator Resistance	R_a	0.003
Inertia	H	3.5

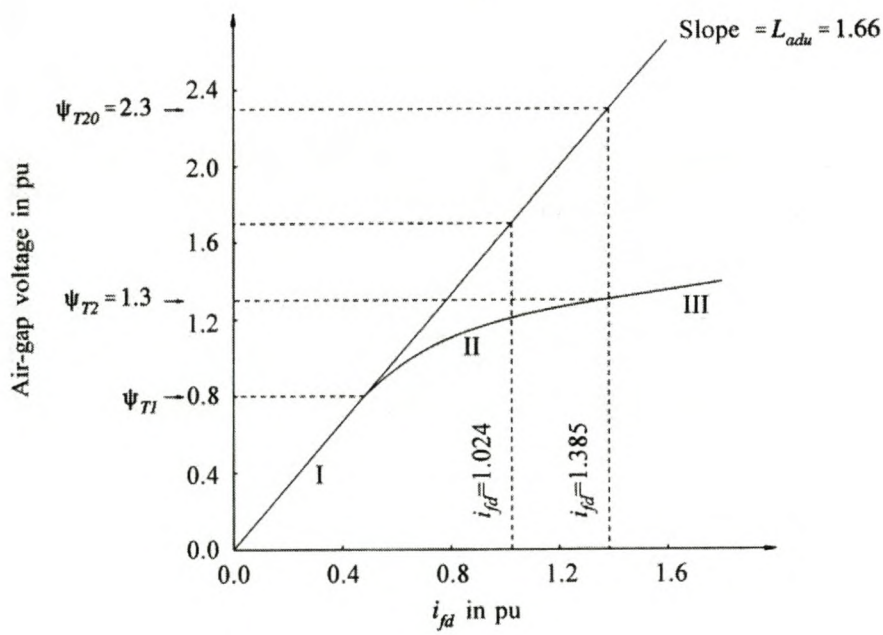

Fig. B.1: Open-circuit saturation curve [60]

The excitation system has a time constant T_A of 0.02 s [20], and a gain K_A of 200.

C MATLAB MODELLING

The following parameters are given:

P_t E_t E_B R_E X_E L_d L_q L'_d T'_{d0} X_l R_a H

For modelling saturation, the following are given, or derived from saturation graphs:

A_{sat} B_{sat} ψ_{TI}

To neglect saturation effect, to investigate the influence saturation has on the results, simply set A_{sat} and B_{sat} equal to zero (0).

Alternatively, instead of L'_d and T'_{d0} given, the field parameters L_{fd} and R_{fd} may be provided. These are related to L'_d and T'_{d0} by

$$L'_d = L_l + \frac{L_{ad}L_{fd}}{L_{ad}+L_{fd}} \tag{C.1}$$

$$T'_{d0} = \frac{L_{ad}+L_{fd}}{R_{fd}} \tag{C.2}$$

where $L_{ad} = L_d - L_l$ (and $L_{aq} = L_q - L_l$ in equations to follow).

In per unit, machine reactances equal machine inductances, and these parameters will be used interchangeably. Thus, $X_d = L_d$, and so forth.

In a system with negligible external resistance ($R_E = 0$) the power angle is derived by the well-known power-angle relationship

$$P_t = \frac{E_t E_B}{X_E}\sin\delta \tag{C.3}$$

In a system with resistance, evaluating the power angle is not as simple a task as without resistance. It can be found that

$$P_t = \frac{E_t(E_t - E_B\cos\delta)R_E}{R_E^2 + X_E^2} + \frac{E_t E_B X_E \sin\delta}{R_E^2 + X_E^2} \tag{C.4}$$

where the relationship

$$I_t = \frac{E_t - E_B e^{-j\delta}}{R_E + jX_E} \tag{C.5}$$

is used for the line current I_t. Notice that with $R_E = 0$, Eq. (C.4) reduces to (C.3).

The power angle δ is obtained by solving for it in Eq. (C.4), making use of a symbolic math software package (such as MAPLE®) to do the task. The following results:

$$\delta = \tan^{-1}\left(\frac{-E_t^2 R_E + R_E N + P_t\left(R_E^2 + X_E^2\right)}{E_t E_B X_E} + j\frac{N}{E_t E_B}\right) \tag{C.6}$$

where

$$N = \frac{E_t^2 R_E^2 - R_E P_t X_E^2 - R_E^3 P_t + U}{R_E^2 + X_E^2}$$

$$U = \sqrt{X_E^2\left(\begin{array}{l} 2E_t^2 R_E^3 P_t - 2R_E^2 P_t^2 X_E^2 - R_E^4 P_t^2 \\ + R_E^2 E_t^2 E_B^2 - E_t^4 R_E^2 - X_E^4 P_t^2 + 2X_E^2 E_t^2 R_E P_t + X_E^2 E_t E_B^2 \end{array}\right)}$$

The reactive power output Q_t at the terminals of the synchronous machine is

$$Q_t = \mathrm{Im}\left(\tilde{E}_t \times \tilde{I}_t^{*}\right) \tag{C.7}$$

and this gives a power factor angle of

$$\varphi = \tan^{-1}\left(\frac{Q_t}{P_t}\right) \tag{C.8}$$

The saturation factors K_{sd} and K_{sq} at a given loading of the machine is determined as

$$K_{sd} = \frac{\psi_{at}}{\psi_{at} + A_{sat} e^{B_{sat}(\psi_{at} - \psi_{T1})}} \tag{C.9}$$

where ψ_{TI} is determined from the saturation characteristic, and ψ_{at} is given by the relation

$$\psi_{at} = \left| E_t + \left(R_a + jX_l\right)\left(\frac{P_t + jQ_t}{E_t}\right)^{*} \right| \tag{C.10}$$

K_{sq} (q-axis saturation factor) is assumed equal to K_{sd}. With the saturation factors evaluated, the saturated values of the inductances L_{ad} and L_{aq} is obtained:

$$\begin{aligned} L_{ads} &= K_{sd} L_{ad} \\ L_{aqs} &= K_{sq} L_{aq} \end{aligned} \tag{C.11}$$

and

$$\begin{aligned} L_{ds} &= L_{ads} + L_l \\ L_{qs} &= L_{aqs} + L_l \end{aligned} \tag{C.12}$$

Having obtained the necessary parameter values, the internal rotor angle can now be evaluated:

$$\delta_i = \tan^{-1}\left(\frac{I_t X_{qs} \cos\varphi - I_t R_a \sin\varphi}{E_t + I_t R_a \cos\varphi + I_t X_{qs} \sin\varphi} \right) \tag{C.13}$$

Then the *d*- and *q*-axis components of the terminal voltage and current are

$$\begin{aligned} e_{d0} &= E_t \sin\delta_i \\ e_{q0} &= E_t \cos\delta_i \\ i_{d0} &= I_t \sin(\delta_i + \varphi) \\ i_{q0} &= I_t \cos(\delta_i + \varphi) \end{aligned} \tag{C.14}$$

Similarly, the *d* and *q*-axis components of the infinite bus voltage $\dot{E}_B$ are

$$\begin{aligned} E_{Bd0} &= e_{d0} - R_E i_{d0} + X_E i_{q0} \\ E_{Bq0} &= e_{q0} - R_E i_{q0} - X_E i_{d0} \end{aligned} \tag{C.15}$$

As a check, the angle δ_0, which equals $\tan^{-1}(E_{Bd0}/E_{Bq0})$, should also equal the sum of the line angle δ and the internal angle δ_i. Also, the voltage E_B is given by $\sqrt{E_{Bd0}^2 + E_{Bq0}^2}$ and should equal E_B defined initially.

The field voltage and current, as well as *d*- and *q*-axis flux linkages, are also used to evaluate the *K*-parameters and subsequently stability, and are given by the following relations:

$$\begin{aligned} i_{fd0} &= \frac{e_{q0} + R_a i_{q0} + L_{ds} i_{d0}}{L_{ads}} \\ E_{fd0} &= L_{ad} i_{fd0} \end{aligned} \tag{C.16}$$

$$\begin{aligned} \psi_{ad0} &= L_{ads}(-i_{d0} + i_{fd0}) \\ \psi_{aq0} &= -L_{aqs} i_{q0} \end{aligned} \tag{C.17}$$

The analysis above focused on the initial steady-state values of the system variables (thus the subscript 0), and hence total saturation is used. The concept of incremental saturation is discussed in Kundur ([60] pp. 745). The incremental saturation factor for relating perturbed variables is defined as

$$K_{sd(incr)} = \frac{1}{1 + B_{sat} A_{sat} e^{B_{sat}(\psi_{at0} - \psi_{T1})}} \tag{C.18}$$

and, same as before, the saturated inductance $L_{ads(incr)} = K_{sd(incr)} L_{ad}$. The q-axis saturation is treated similarly. These saturated inductances are used in evaluating X_{Td}, X_{Tq} and D, which are subsequently used to evaluate the K-parameters of the system.

D SMIB SYSTEM STATE-SPACE MODEL

Kundur [60] pp. 737-762 derives the higher order synchronous machine model in a SMIB system. This model is an extension of the classical model to include the effect of field flux linkage variations. The resultant machine equations are used in conjunction with the system equations to give the state-space and block diagram models of the SMIB system. These models and the parameters contained therein are used in the analysis of this report.

Simplifications are made to minimize data requirements and improve simulation efficiency ([60] pp.169-179). The following are neglected from the stator voltage equations:

- The transformer voltage terms (armature $p\psi$ terms)
- The effect of speed variations

Amortisseur (damper windings) effects are also neglected to simplify analysis.

D.1 Synchronous Machine Equations

Fig. D.1 shows the equivalent circuits relating the machine flux linkages and currents. Amortisseurs are neglected.

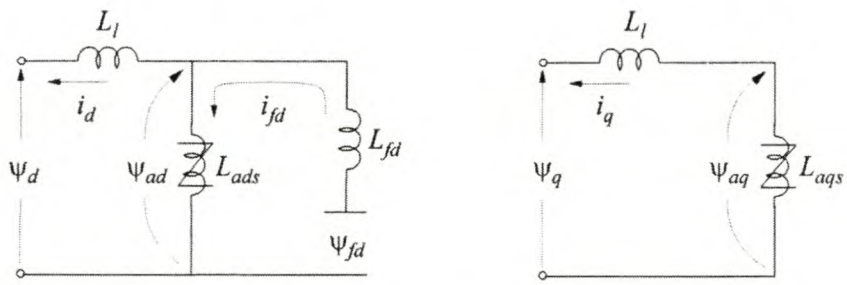

Fig. D.1: *d*- and *q*-axis equivalent circuits [60]

Kundur [60] pp. 174 gives the equations

$$e_d = -\psi_q - R_a i_d, \tag{D.1}$$

$$e_q = \psi_d - R_a i_q \tag{D.2}$$

to describe the *d*- and *q*-axis stator voltages, respectively. R_a is the stator resistance, and ψ_d, ψ_q and i_d, i_q are the *d*- and *q*-axis flux linkages and currents described in Fig. D.1. All parameters are in per unit. The field circuit dynamic equation is

$$p\psi_{fd} = \omega_0\left(e_{fd} - R_{fd}i_{fd}\right), \tag{D.3}$$

where e_{fd} is the per unit rotor voltage, i_{fd} the per unit rotor current and ψ_{fd} the per unit rotor flux linkage described in Fig. D.1. p is the differential operator d/dt, with time t in seconds. The flux linkage equations are

$$\psi_d = -L_d i_d + L_{ad} i_{fd}, \tag{D.4}$$

$$\psi_q = -L_q i_q, \tag{D.5}$$

$$\psi_{fd} = -L_{ad} i_d + L_{ffd} i_{fd}, \tag{D.6}$$

where

$$\begin{aligned} L_d &= L_{ad} + L_l \\ L_q &= L_{aq} + L_l \\ L_{ffd} &= L_{ad} + L_{fd} \end{aligned} \quad . \tag{D.7}$$

The per unit air-gap torque of the synchronous machine is

$$T_e = \psi_d i_q - \psi_q i_d : \tag{D.8}$$

The swing equation ([60], pp. 128-136) is written as

$$p\Delta\omega_r = \frac{1}{2H}\left(T_m - T_e - K_D\Delta\omega_r\right) \tag{D.9}$$

$$p\delta = \omega_0\Delta\omega_r \tag{D.10}$$

where $\omega_0 = 2\pi f_0$ elec. rad/s. $\Delta\omega_r$ is the rotor speed deviation from ω_0, T_m the mechanical input torque, and K_D a damping factor (usually set to zero). The rotor angle δ is the sum of the internal machine angle δ_i and the angle by which E_t leads E_B. Fig. D.2 shows this.

Using Eq. (D.7), Eqs (D.4) and (D.5) are written as

$$\begin{aligned} \psi_d &= -L_l i_d + L_{ads}\left(-i_d + i_{fd}\right) \\ &= -L_l i_d + \psi_{ad} \end{aligned} \tag{D.11}$$

$$\begin{aligned} \psi_q &= -L_l i_q + L_{aqs}\left(-i_q\right) \\ &= -L_l i_q + \psi_{aq} \end{aligned} \tag{D.12}$$

Also, the air-gap torque is changed to

$$\begin{aligned} T_e &= \psi_d i_q - \psi_q i_d \\ &= \psi_{ad} i_q - \psi_{aq} i_d \end{aligned} \tag{D.13}$$

where, from Eqs (D.6), (D.11) and (D.12), the air-gap (mutual) flux linkages are

$$\psi_{ad} = L'_{ads}\left(-i_d + \frac{\psi_{fd}}{L_{fd}}\right) \tag{D.14}$$

$$\psi_{aq} = -L_{aqs} i_q \tag{D.15}$$

The subscript s denotes saturated values, and

$$L'_{ads} = \frac{L_{ads} L_{fd}}{L_{ads} + L_{fd}} \tag{D.16}$$

No rotor circuits are considered in the q-axis. As a result, the stator voltage equations are

$$e_d = -R_a i_d + \left(L_l i_q - \psi_{aq}\right) \tag{D.17}$$

$$e_q = -R_a i_q - \left(L_l i_d - \psi_{ad}\right) \tag{D.18}$$

D.2 Network Equations

The terminal and infinite bus voltages in terms of the d and q components are

$$\tilde{E}_t = e_d + j e_q \tag{D.19}$$

$$\tilde{E}_B = E_{Bd} + j E_{Bq} \tag{D.20}$$

where

$$E_{Bd} = E_B \sin\delta$$

$$E_{Bq} = E_B \cos\delta$$

are the d- and q-axis components of the infinite bus voltage E_B. See Fig. D.2.

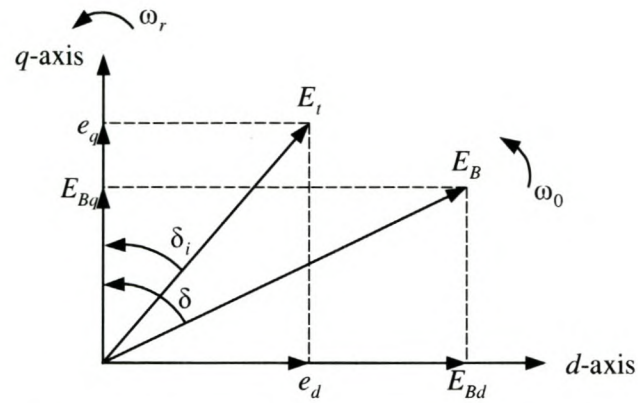

Fig. D.2: Axis representation of system voltages and angles

For a network of equivalent impedance $(R_E + jX_E)$, the machine terminal and infinite bus voltages are related by

$$\begin{aligned} \tilde{E}_t &= \tilde{E}_B + (R_E + jX_E)\tilde{I}_t \\ (e_d + je_q) &= (E_B \sin\delta + E_B \cos\delta) + (R_E + jX_E)(i_d + ji_q) \end{aligned} \tag{D.21}$$

Equating real and imaginary parts in the expression above, give

$$\begin{aligned} e_d &= R_E i_d - X_E i_q + E_B \sin\delta \\ e_q &= R_E i_q + X_E i_d + E_B \cos\delta \end{aligned} \tag{D.22}$$

From the above equations for e_d, e_q, ψ_{ad} and ψ_{aq}, expressions for i_d and i_q in terms of the state variables δ and ψ_{fd} are

$$i_d = \frac{X_{Tq}}{D}\left[\psi_{fd}\left(\frac{L_{ads}}{L_{ads}+L_{fd}}\right) - E_B \cos\delta\right] - \frac{R_T E_B}{D}\sin\delta \tag{D.23}$$

$$i_q = \frac{R_T}{D}\left[\psi_{fd}\left(\frac{L_{ads}}{L_{ads}+L_{fd}}\right) - E_B \cos\delta\right] + \frac{X_{Td} E_B}{D}\sin\delta \tag{D.24}$$

where

$$\begin{aligned} R_T &= R_a + R_E \\ X_{Td} &= (L'_{ads} + L_l) + X_E = X'_{ds} + X_E \\ X_{Tq} &= (L_{aqs} + L_l) + X_E = X_{qs} + X_E \\ D &= R_T^2 + X_{Tq} X_{Td} \end{aligned} \tag{D.25}$$

D.3 Small Perturbation Form of Machine and Network Equations

Eqs (D.23) and (D.24) linearised about the initial condition (defined by $\delta = \delta_0$ and $\psi_{fd} = \psi_{fd0}$) yield

$$\Delta i_d = m_1 \Delta\delta + m_2 \Delta\psi_{fd} \tag{D.26}$$

$$\Delta i_q = n_1 \Delta\delta + n_2 \Delta\psi_{fd} \tag{D.27}$$

where

$$\begin{aligned} m_1 &= \frac{\partial i_d}{\partial \delta} = \frac{E_B}{D}\left(X_{Tq}\sin\delta_0 - R_T\cos\delta_0\right) \\ n_1 &= \frac{\partial i_q}{\partial \delta} = \frac{E_B}{D}\left(R_T\sin\delta_0 + X_{Td}\cos\delta_0\right) \end{aligned} \tag{D.28}$$

$$\begin{aligned} m_2 &= \frac{\partial i_d}{\partial \psi_{fd}} = \frac{X_{Tq}}{D}\frac{L_{ads}}{L_{ads}+L_{fd}} \\ n_2 &= \frac{\partial i_q}{\partial \psi_{fd}} = \frac{R_T}{D}\frac{L_{ads}}{L_{ads}+L_{fd}} \end{aligned} \tag{D.29}$$

Similarly, linearise Eqs (D.14) and (D.15), and substitute the expressions obtained for Δi_d and Δi_q, to get the flux linkages in small oscillation form:

$$\Delta\psi_{ad} = -m_1 L'_{ads}\Delta\delta + \left(\frac{1}{L_{fd}} - m_2\right)\Delta\psi_{fd} \tag{D.30}$$

$$\Delta\psi_{aq} = -n_1 L_{aqs}\Delta\delta - n_2 L_{aqs}\Delta\psi_{fd} \tag{D.31}$$

Eq. (D.13) linearised is

$$\Delta T_e = \psi_{ad0}\Delta i_q + \Delta\psi_{ad} i_{q0} - \psi_{aq0}\Delta i_d - \Delta\psi_{aq} i_{d0} \tag{D.32}$$

By substituting Eqs (D.26), (D.27), (D.30) and (D.31), ΔT_e in terms of the state variables are

$$\Delta T_e = K_1\Delta\delta + K_2\Delta\psi_{fd} \tag{D.33}$$

where

$$K_1 = n_1\left(\psi_{ad0} + L_{aqs} i_{d0}\right) - m_1\left(\psi_{aq0} + L'_{ads} i_{q0}\right) \tag{D.34}$$

$$K_2 = n_2\left(\psi_{ad0} + L_{aqs} i_{d0}\right) - m_2\left(\psi_{aq0} + L'_{ads} i_{q0}\right) + \frac{L'_{ads}}{L_{fd}} i_{q0} \tag{D.35}$$

Linearising Eq. (D.9) and substituting for ΔT_e, yields

$$p\Delta\omega_r = \frac{1}{2H}\left(\Delta T_m - K_1\Delta\delta - K_2\Delta\psi_{fd} - K_D\Delta\omega_r\right) \tag{D.36}$$

This equation solved for $\Delta\omega_r$ gives:

$$\Delta\omega_r = \frac{1}{2Hp + K_D}\left(\Delta T_m - K_1\Delta\delta - K_2\Delta\psi_{fd}\right) \tag{D.37}$$

Finally, Eq. (D.10) in small perturbation form is

$$p\Delta\delta = \omega_0\Delta\omega_r \tag{D.38}$$

D.4 Field Circuit Equations

From Eq. (D.6), keeping in mind that $\psi_{ad} = L_{ads}\left(-i_d + i_{fd}\right)$, the field current may be expressed as

$$i_{fd} = \frac{\psi_{fd} - \psi_{ad}}{L_{fd}} \tag{D.39}$$

Linearising, and substituting for $\Delta\psi_{ad}$ from Eq. (D.30), the field current in terms of perturbed variables is

$$\Delta i_{fd} = m_1\frac{L'_{ads}}{L_{fd}}\Delta\delta + \frac{1}{L_{fd}}\left(1 - \frac{L'_{ads}}{L_{fd}} + m_2 L'_{ads}\right)\Delta\psi_{fd} \tag{D.40}$$

Eq. (D.3) in small perturbation form is

$$p\Delta\psi_{fd} = \frac{\omega_0 R_{fd}}{L_{adu}}\Delta E_{fd} - \omega_0 R_{fd}\Delta i_{fd} \tag{D.41}$$

Substituting the expression for Δi_{fd}:

$$p\Delta\psi_{fd} = \frac{1}{T_{3fd}}\left(-\Delta\psi_{fd} + K_3\left(\Delta E_{fd} - K_4\Delta\delta\right)\right) \tag{D.42}$$

which can be rearranged to give

$$\Delta\psi_{fd} = \frac{K_3}{1+sT_{3fd}}\left(\Delta E_{fd} - K_4\Delta\delta\right) \tag{D.43}$$

where

$$K_3 = \frac{L_{fd}}{L_{adu}}\left(1 - \frac{L'_{ads}}{L_{fd}} + m_2 L'_{ads}\right)^{-1} \tag{D.44}$$

$$K_4 = \frac{L_{adu}}{L_{fd}} m_1 L'_{ads} \tag{D.45}$$

$$T_{3fd} = K_3 T'_{d0} \frac{L_{adu}}{L_{ffd}} \tag{D.46}$$

D.5 Excitation System

For purpose of illustrating the influence of the excitation system on the damping and synchronizing torques of the system, a simple voltage regulator-excitation system is considered (see Fig. D.3).

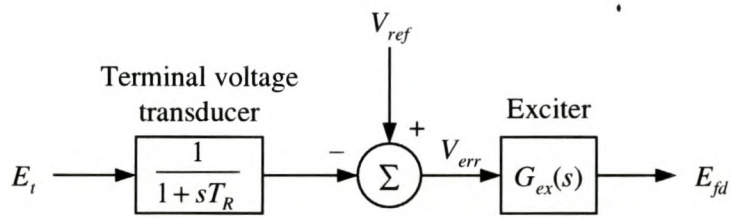

Fig. D.3: Thyristor excitation system with AVR

For simplification, the voltage transducer time constant T_R is set to zero [19]. The regulator is modelled by a single time constant T_A and gain K_A:

$$\begin{aligned} G_{ex}(s) &= \frac{K_A}{1+sT_A} \\ \therefore E_{fd} &= \frac{K_A}{1+sT_A}\left(V_{ref} - E_t\right) \end{aligned} \tag{D.47}$$

With Eq. (D.19) written as $E_t^2 = e_d^2 + e_q^2$, a small perturbation applied, and second-order terms neglected, the following expression is obtained:

$$\Delta E_t = \frac{e_{d0}}{E_{t0}}\Delta e_d + \frac{e_{q0}}{E_{t0}}\Delta e_q \tag{D.48}$$

Eqs (D.17) and (D.18) in small disturbance form are

$$\begin{aligned} \Delta e_d &= -R_a \Delta i_d + L_l \Delta i_q - \Delta \psi_{aq} \\ \Delta e_q &= -R_a \Delta i_q - L_l \Delta i_d + \Delta \psi_{ad} \end{aligned} \tag{D.49}$$

Substituting Eqs (D.26), (D.27), (D.30) and (D.31) into this expression, and the resulting expressions for Δe_d and Δe_q into Eq. (D.48), yields

$$\Delta E_t = K_5 \Delta\delta + K_6 \Delta\psi_{fd} \tag{D.50}$$

where

$$K_5 = \frac{e_{d0}}{E_{t0}}\left(-R_a m_1 + L_l n_1 + L_{aqs} n_1\right) + \frac{e_{q0}}{E_{t0}}\left(-R_a n_1 - L_l m_1 - L'_{ads} m_1\right) \tag{D.51}$$

$$K_6 = \frac{e_{d0}}{E_{t0}}\left(-R_a m_2 + L_l n_2 + L_{aqs} n_2\right) + \frac{e_{q0}}{E_{t0}}\left(-R_a n_2 - L_l m_2 + L'_{ads}\left(\frac{1}{L_{fd}} - m_2\right)\right) \tag{D.52}$$

From Eqs (D.47) and (D.50),

$$\Delta E_{fd} = -\frac{K_A}{1 + sT_A}\left(K_5 \Delta\delta + K_6 \Delta\psi_{fd}\right) \tag{D.53}$$

From this, the expression for $p\Delta E_{fd}$ is as follows:

$$p\Delta E_{fd} = \frac{1}{T_A}\left(-\Delta E_{fd} - K_A\left(K_5 \Delta\delta + K_6 \Delta\psi_{fd}\right)\right) \tag{D.54}$$

D.6 Alternative Form of Equations

In the literature on synchronous machine equations, Eqs (D.3) to (D.6) are often written in terms of the following variables ([60] pp. 180):

$E_I = L_{ad} i_{fd}$ = voltage proportional to i_{fd}

$E'_q = \frac{L_{ad}}{L_{ffd}} \psi_{fd}$ = voltage proportional to ψ_{fd}

$$E_{fd} = \frac{L_{ad}}{R_{fd}} e_{fd} \quad = \text{voltage proportional to } e_{fd}$$

The rotor voltage and flux linkage equations in the alternative form are:

$$\psi_d = -L_d i_d + E_I \tag{D.55}$$

$$\psi_q = -L_q i_q \tag{D.56}$$

$$E'_q = E_I - (L_d - L'_d) i_d \tag{D.57}$$

$$pE'_q = \frac{1}{T'_{d0}} (E_{fd} - E_I) \tag{D.58}$$

The parameters L_d, L_q, L'_d and T'_{d0} are functions of saturation.

In terms of voltages instead of flux linkages, the per-unit air-gap torque (Eq. (D.8)) is

$$T_e = e_d i_d + e_q i_q + R_a (i_d^2 + i_q^2) \tag{D.59}$$

Using these relations, the *K*-parameters are expressed as follows.

$$K_1 = \frac{E_B E_{q0}}{D} (R_T \sin\delta_0 + X_{Td} \cos\delta_0) + \frac{E_B i_{q0}}{D} (X_q - X'_d)(X_{Tq} \sin\delta_0 - R_T \cos\delta_0) \tag{D.60}$$

$$K_2 = \frac{L_{ads}}{L_{ads} + L_{fd}} \left(\frac{R_T}{D} E_{q0} + \left(\frac{X_{Tq}(X_q - X'_d)}{D} + 1 \right) i_{q0} \right) \tag{D.61}$$

$$K_3 = \frac{L_{ads} + L_{fd}}{L_{adu}} \frac{1}{1 + \frac{X_{Tq}}{D}(X_d - X'_d)} \tag{D.62}$$

$$T_{3fd} = \frac{T'_{d0s}}{1 + \frac{X_{Tq}}{D}(X_d - X'_d)} \tag{D.63}$$

$$K_4 = L_{adu} \frac{L_{ads}}{L_{ads} + L_{fd}} \frac{E_B}{D} (X_{Tq} \sin\delta_0 - R_T \cos\delta_0) \tag{D.64}$$

K_5 with R_a neglected – very small:

$$K_5 = \frac{e_{d0}}{E_{t0}}\left(X_q \frac{R_T E_B \sin\delta_0 + X_{Td} E_B \cos\delta_0}{D} \right) + \frac{e_{q0}}{E_{t0}}\left(+ X'_d \frac{R_T E_B \cos\delta_0 - X_{Tq} E_B \sin\delta_0}{D} \right) \tag{D.65}$$

$$K_6 = \frac{L_{ads}}{L_{ads} + L_{fd}}\left(\frac{e_{q0}}{E_{t0}}\left(1 - \frac{R_a R_T + X'_d X_{Tq}}{D} \right) + \frac{e_{d0}}{E_{t0}}\left(\frac{R_T X_q - R_a X_{Tq}}{D} \right) \right) \tag{D.66}$$

K_6 with R_a neglected – very small:

$$K_6 = \frac{L_{ads}}{L_{ads} + L_{fd}}\left(\frac{e_{q0}}{E_{t0}}\left(1 - \frac{X'_d X_{Tq}}{D} \right) + \frac{e_{d0}}{E_{t0}} X_q \frac{R_T}{D} \right) \tag{D.67}$$

E SIMULATION RESULTS OF CHAPTER 3

E.1 Results of Section 3.6.3 – Line Resistance

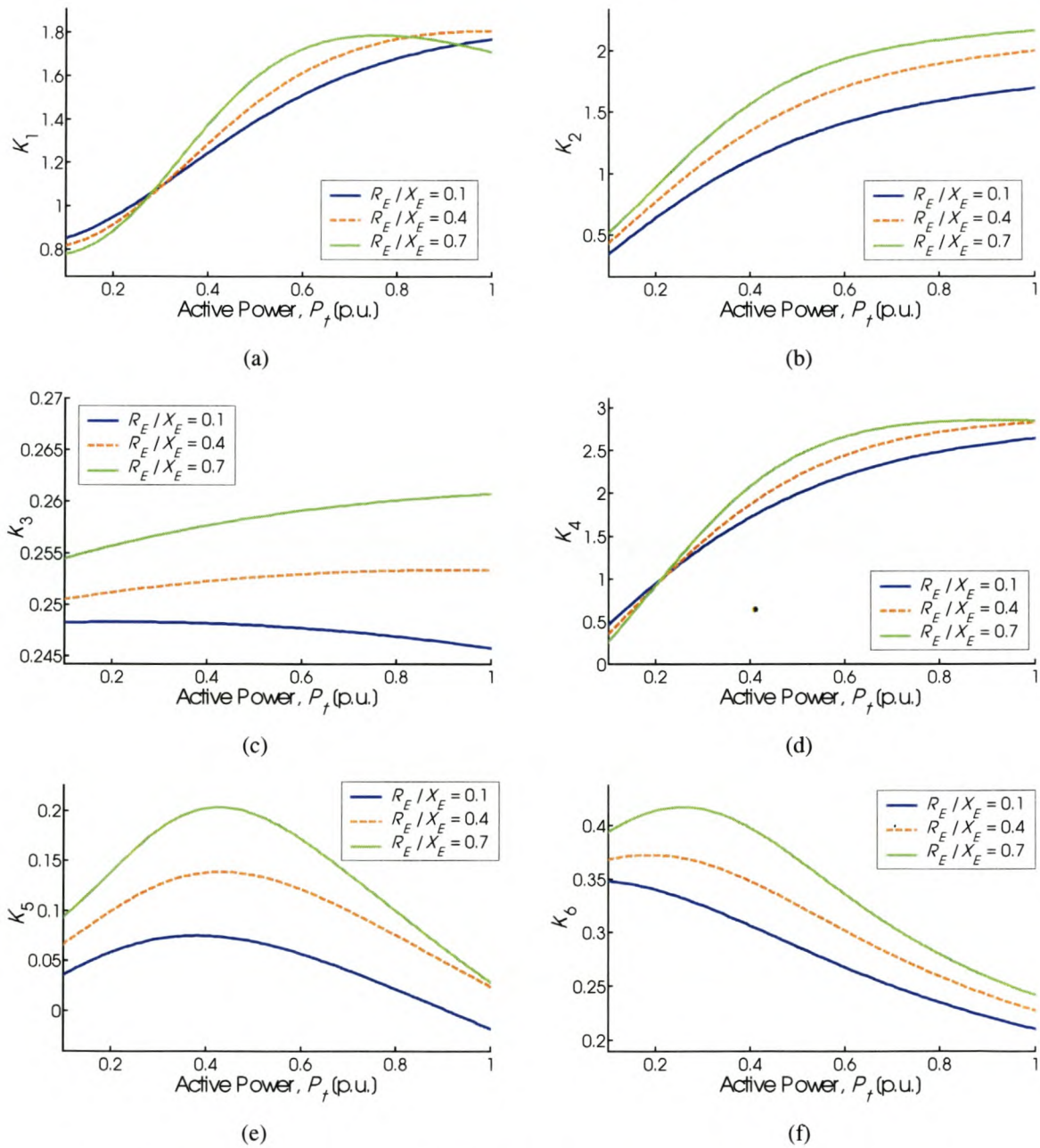

Fig. E.1: Parameters $K_1 \ldots K_6$ vs. machine load and line resistance, with $X_E = 0.2$ p.u.

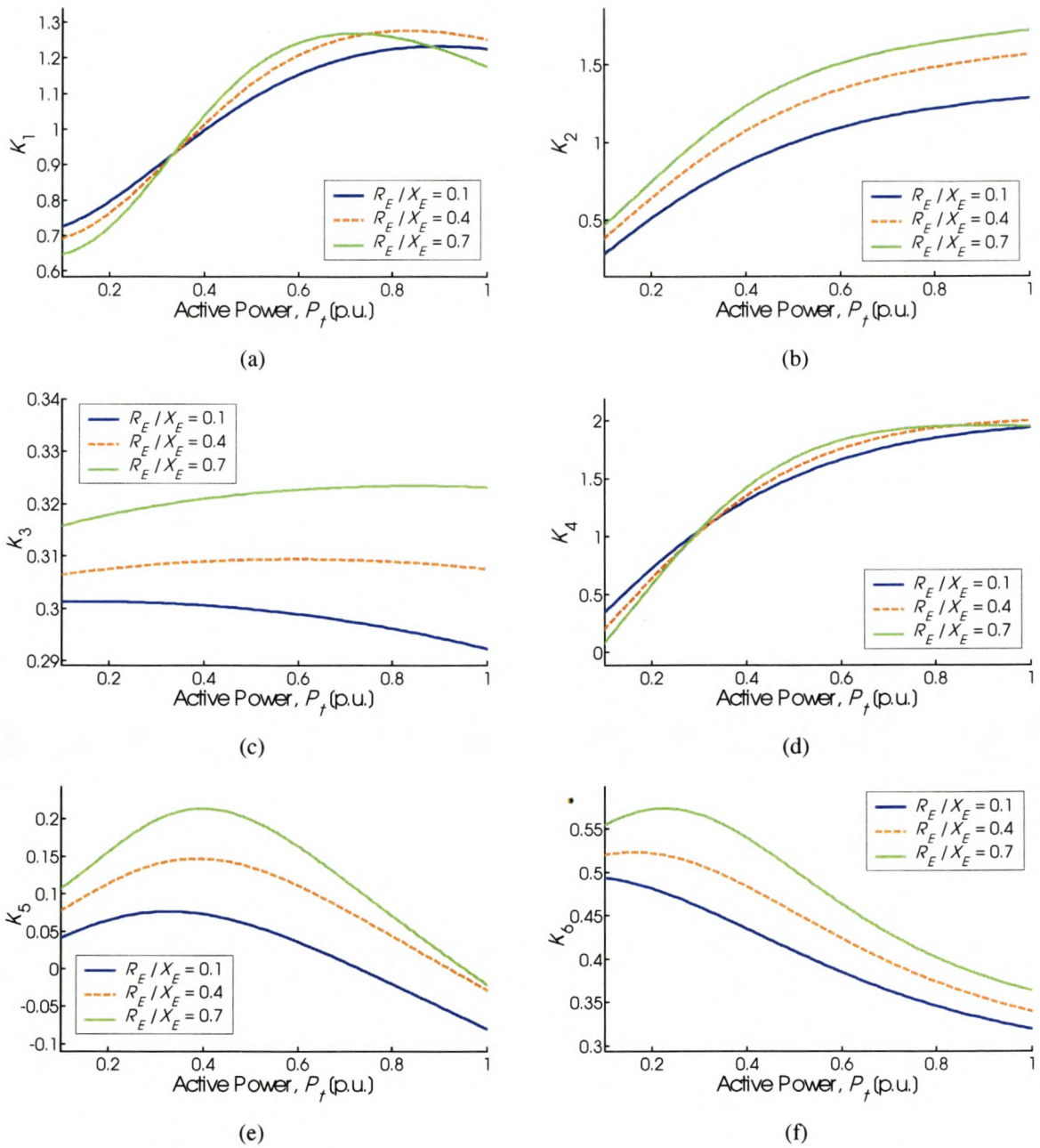

Fig. E.2: Parameters $K_1 \ldots K_6$ vs. machine load and line resistance, with $X_E = 0.4$ p.u.

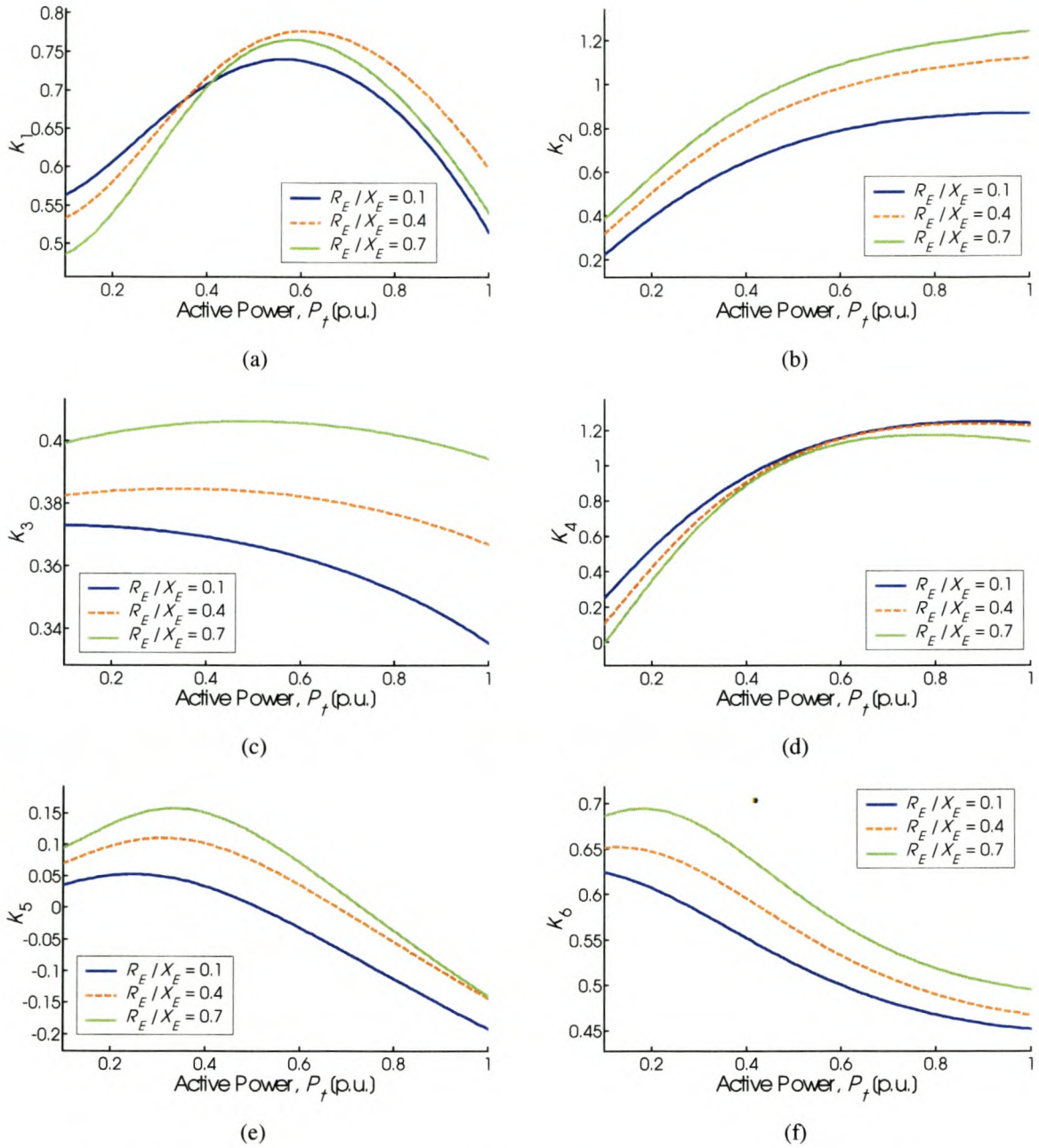

Fig. E.3: Parameters $K_1 \ldots K_6$ vs. machine load and line resistance, with $X_E = 0.8$ p.u.

E.2 Results of Section 3.6.4 – Local Load

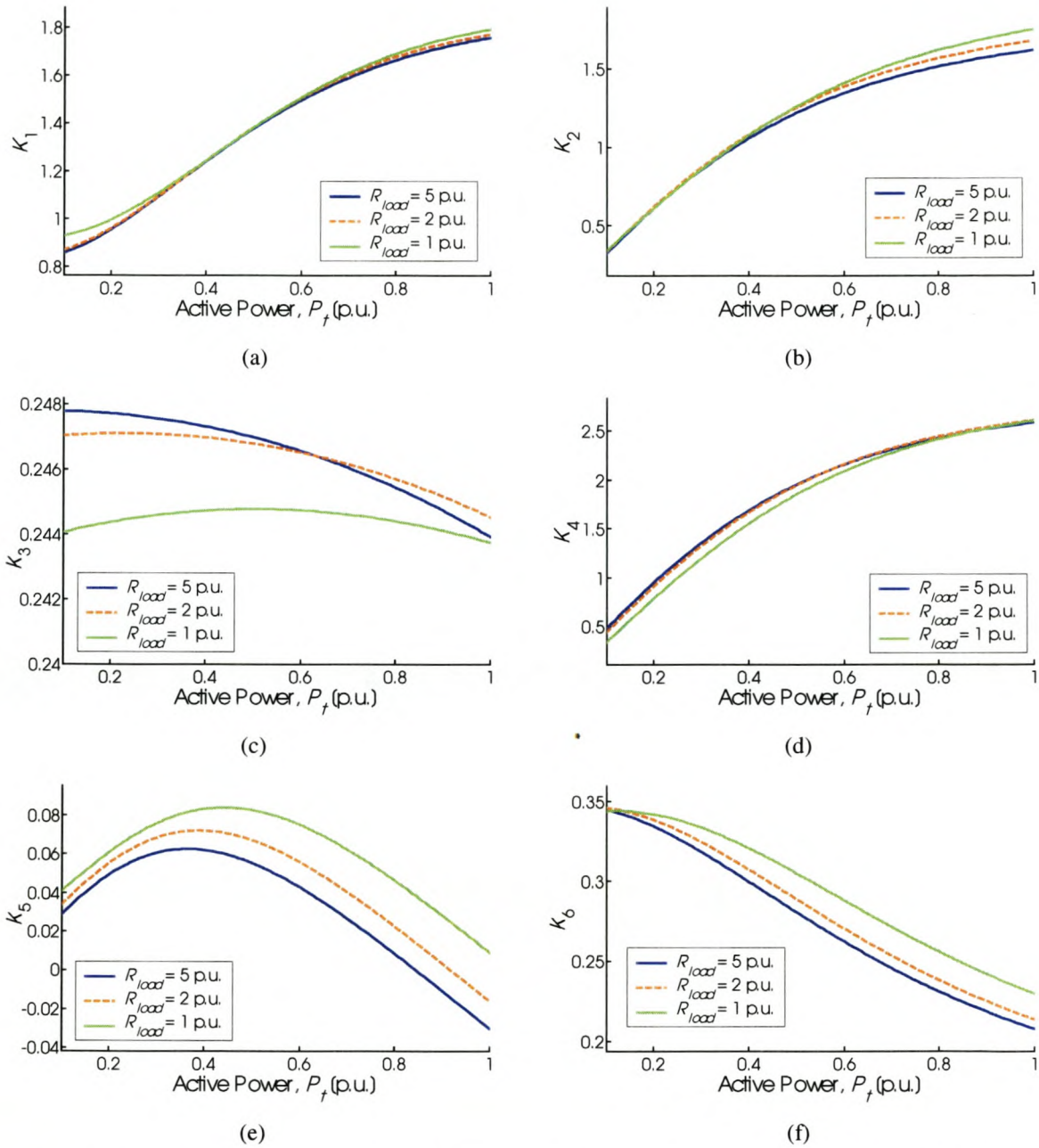

Fig. E.4: Parameters $K_1 \ldots K_6$ vs. machine load and local load resistance, with X_{line} = 0.2 p.u.

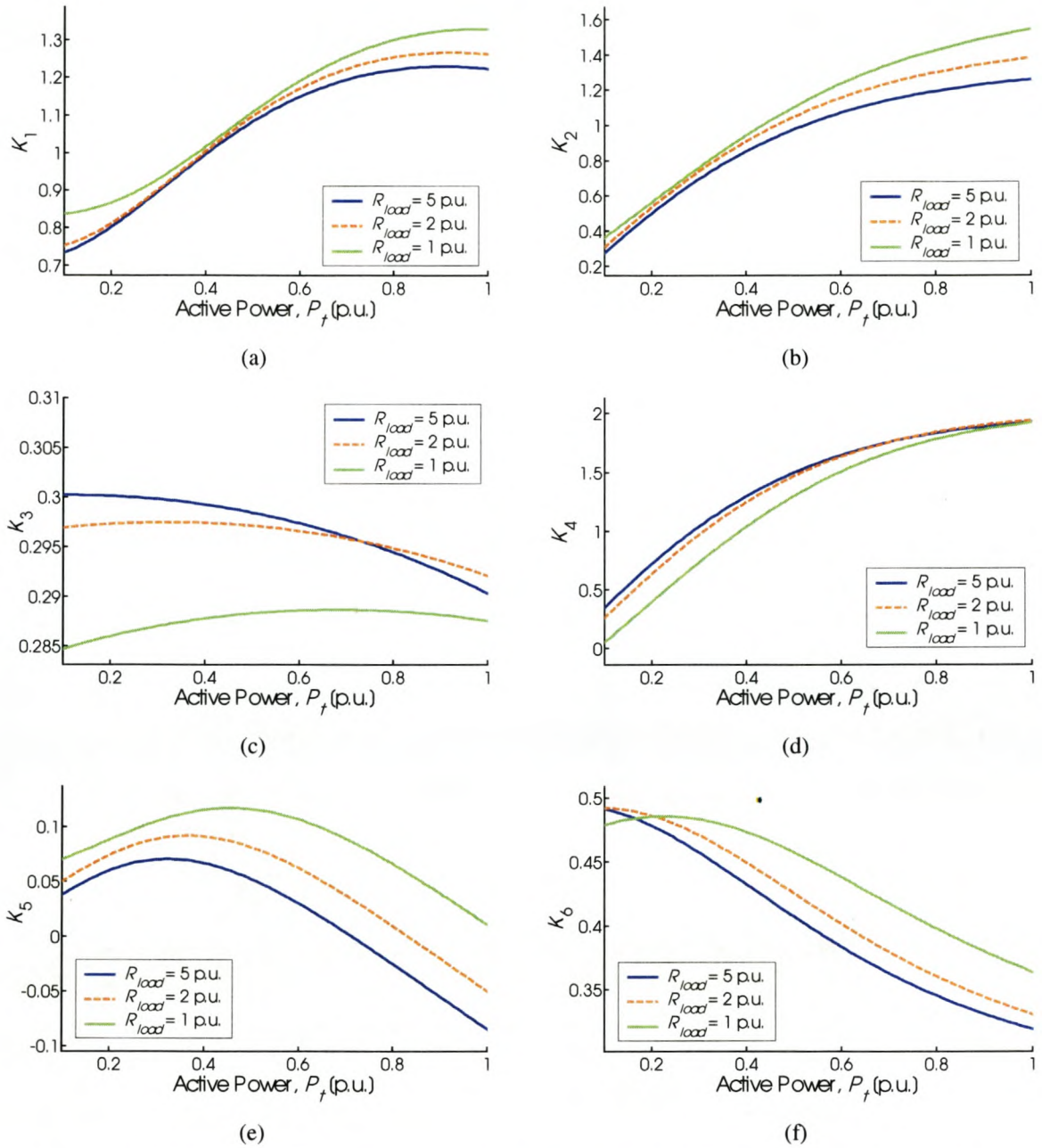

Fig. E.5: Parameters $K_1 \ldots K_6$ vs. machine load and local load resistance, with X_{line} = 0.4 p.u.

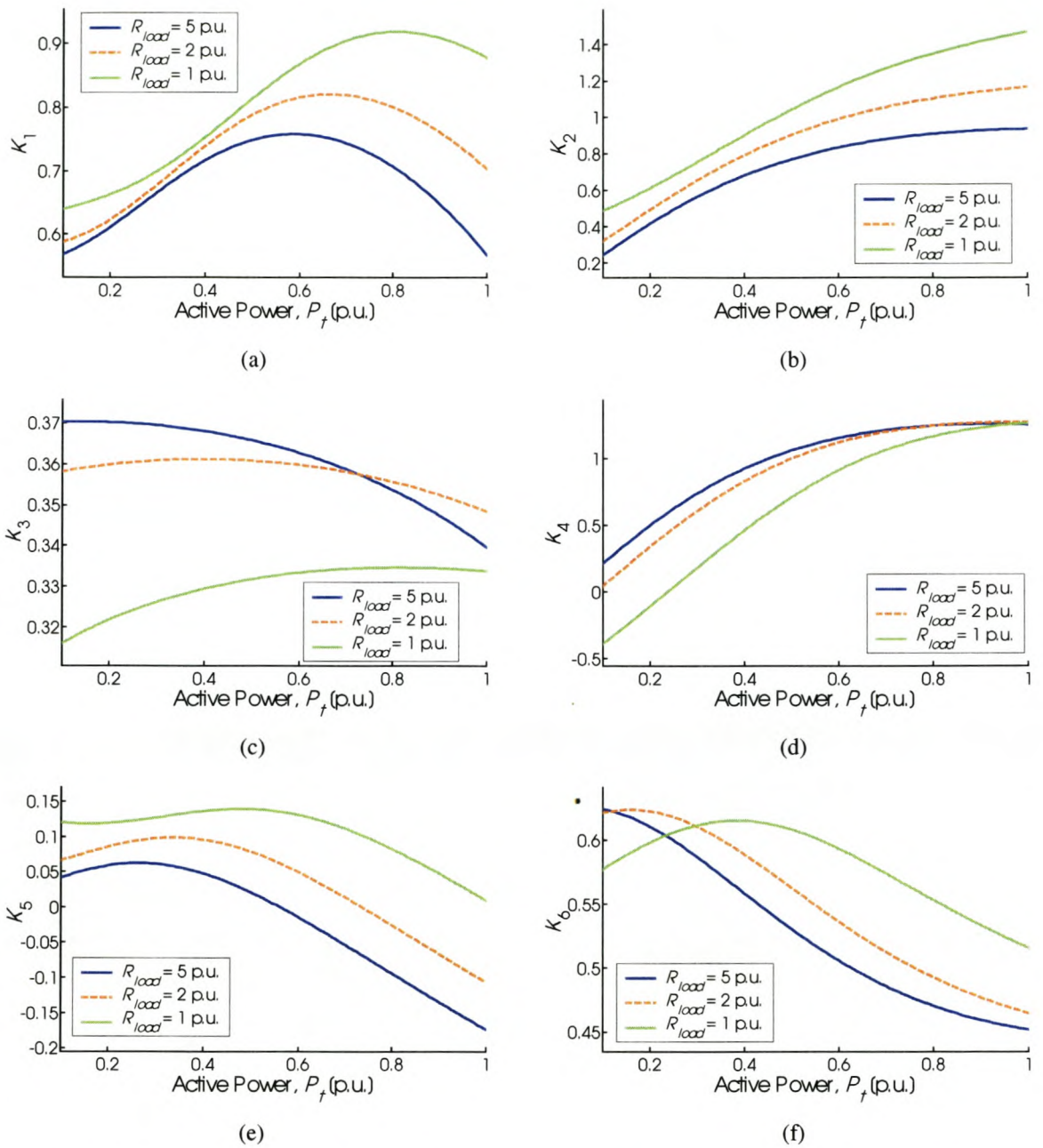

Fig. E.6: Parameters $K_1 \ldots K_6$ vs. machine load and local load resistance, with X_{line} = 0.8 p.u.

E.3 Results of Section 3.6.5 – Influence of Saturation

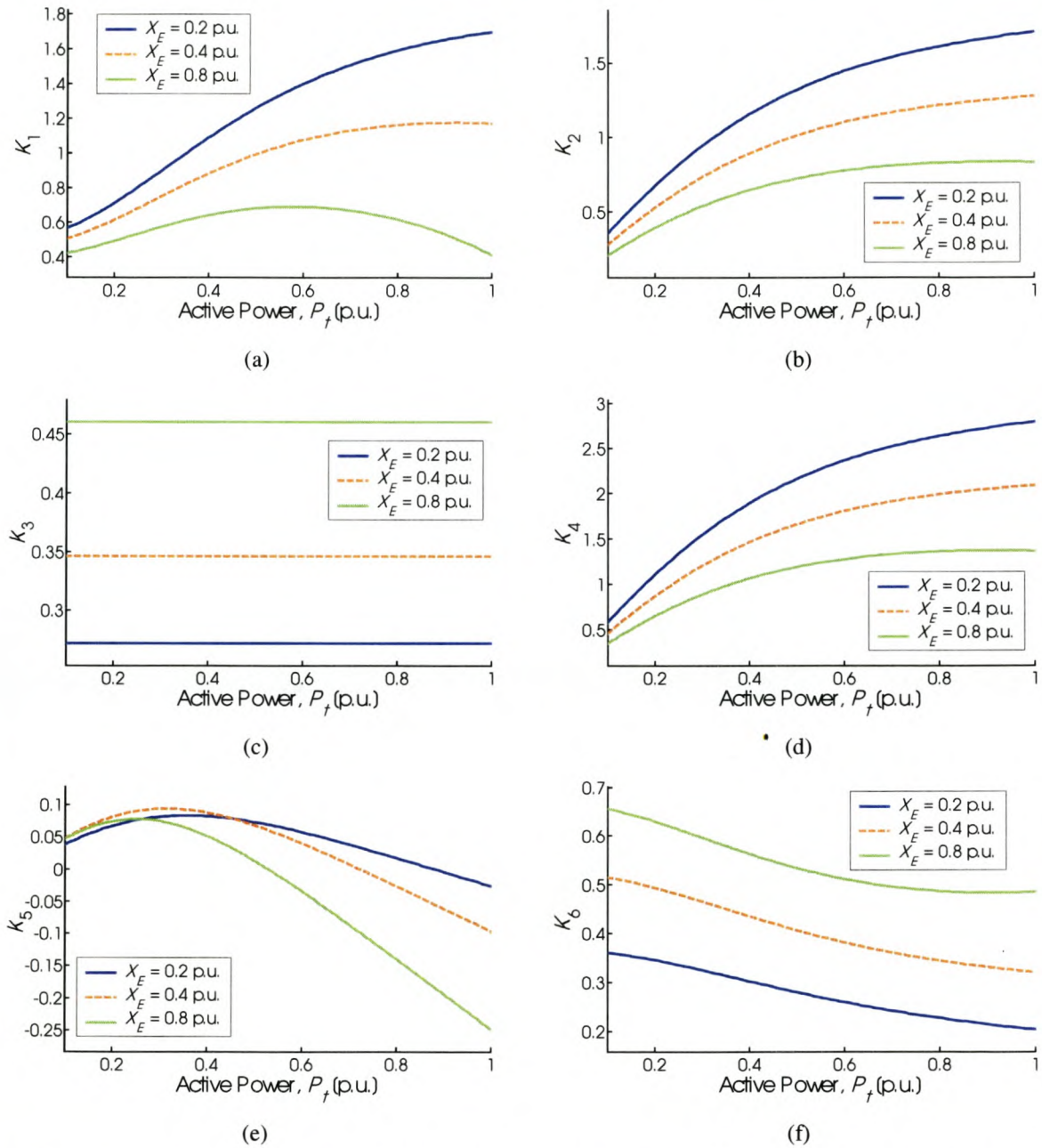

Fig. E.7: Parameters K_1 . . . K_6 vs. machine load and external reactance; saturation not modelled

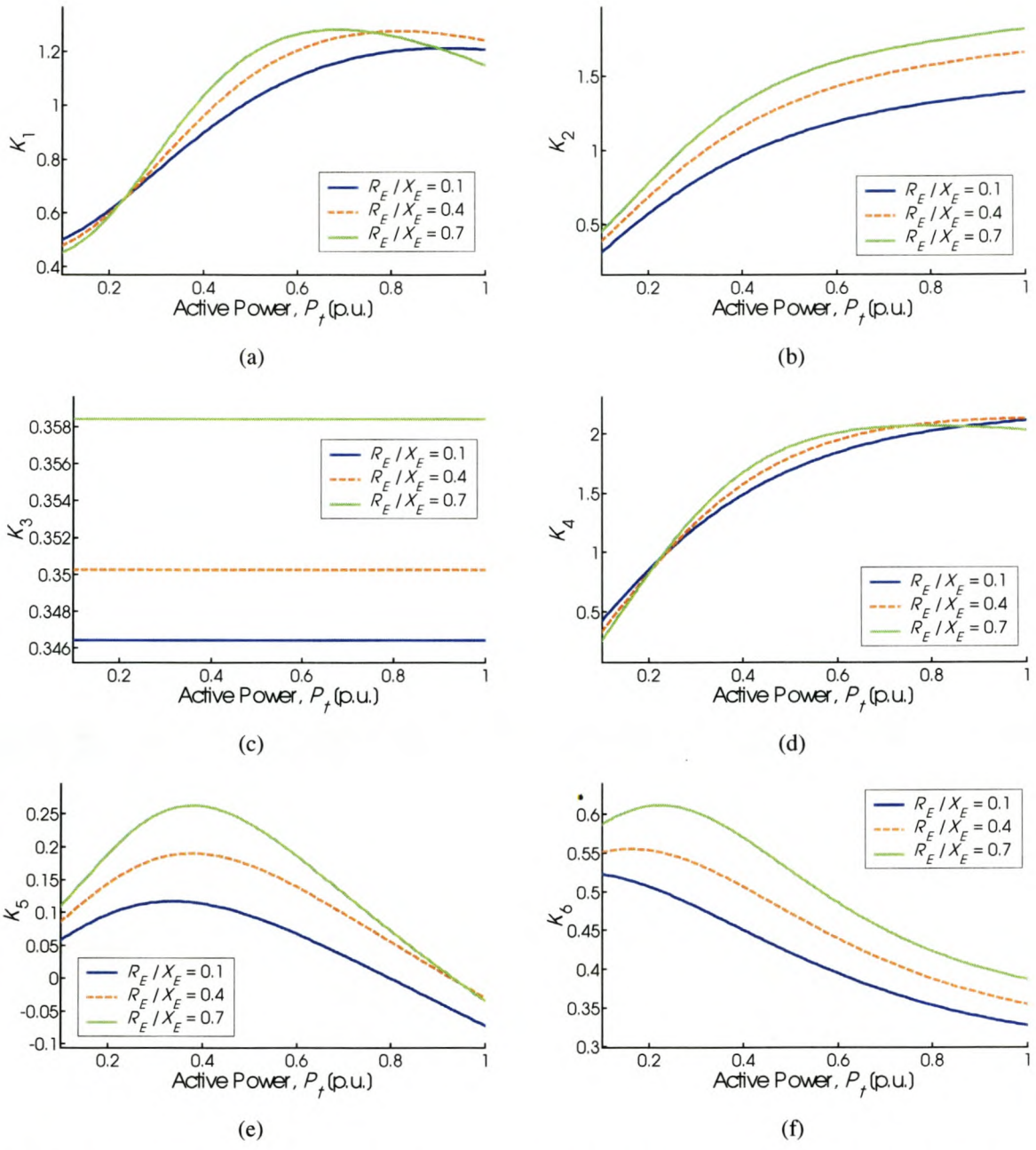

Fig. E.8: Parameters $K_1 \ldots K_6$ vs. machine load and line resistance, with $X_E = 0.4$ p.u.; saturation not modelled

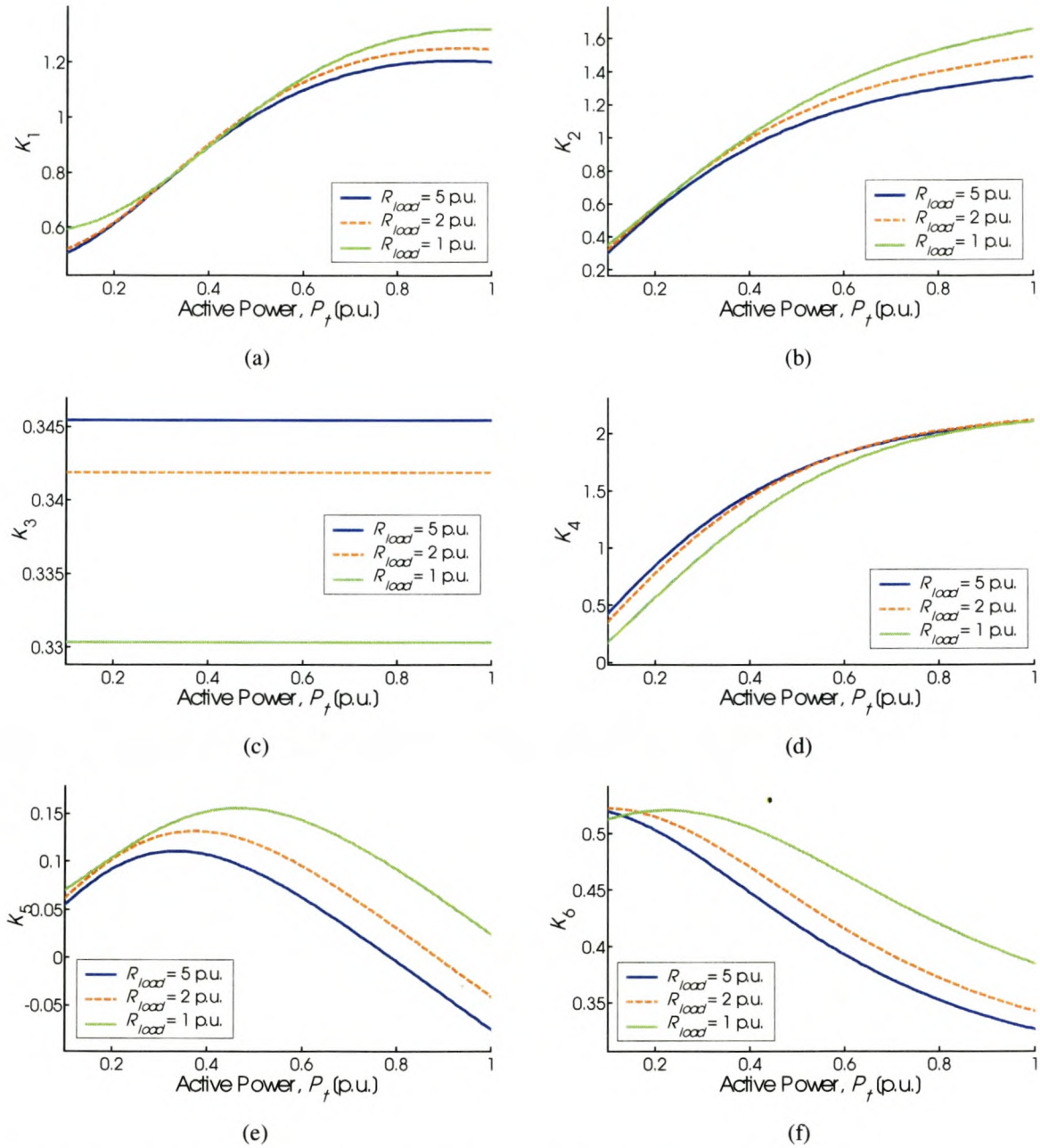

Fig. E.9: Parameters K_1 . . . K_6 vs. machine load and local load resistance, with X_{line} = 0.4 p.u.; saturation not modelled

E.4 Results of Section 3.8.3 – Line Resistance

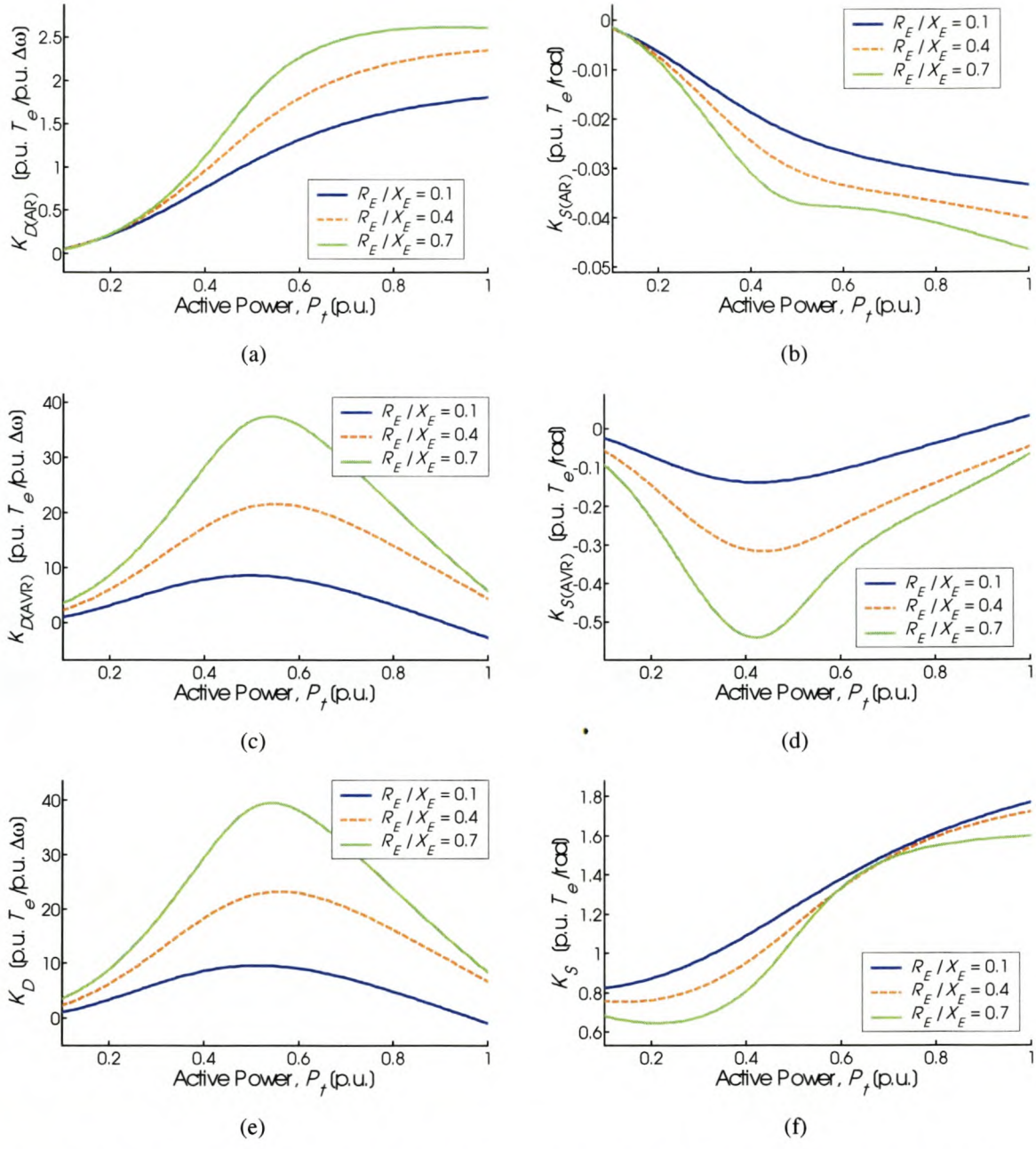

Fig. E.10: Damping and synchronizing torques vs. machine load and line resistance, with $X_E = 0.2$ p.u.

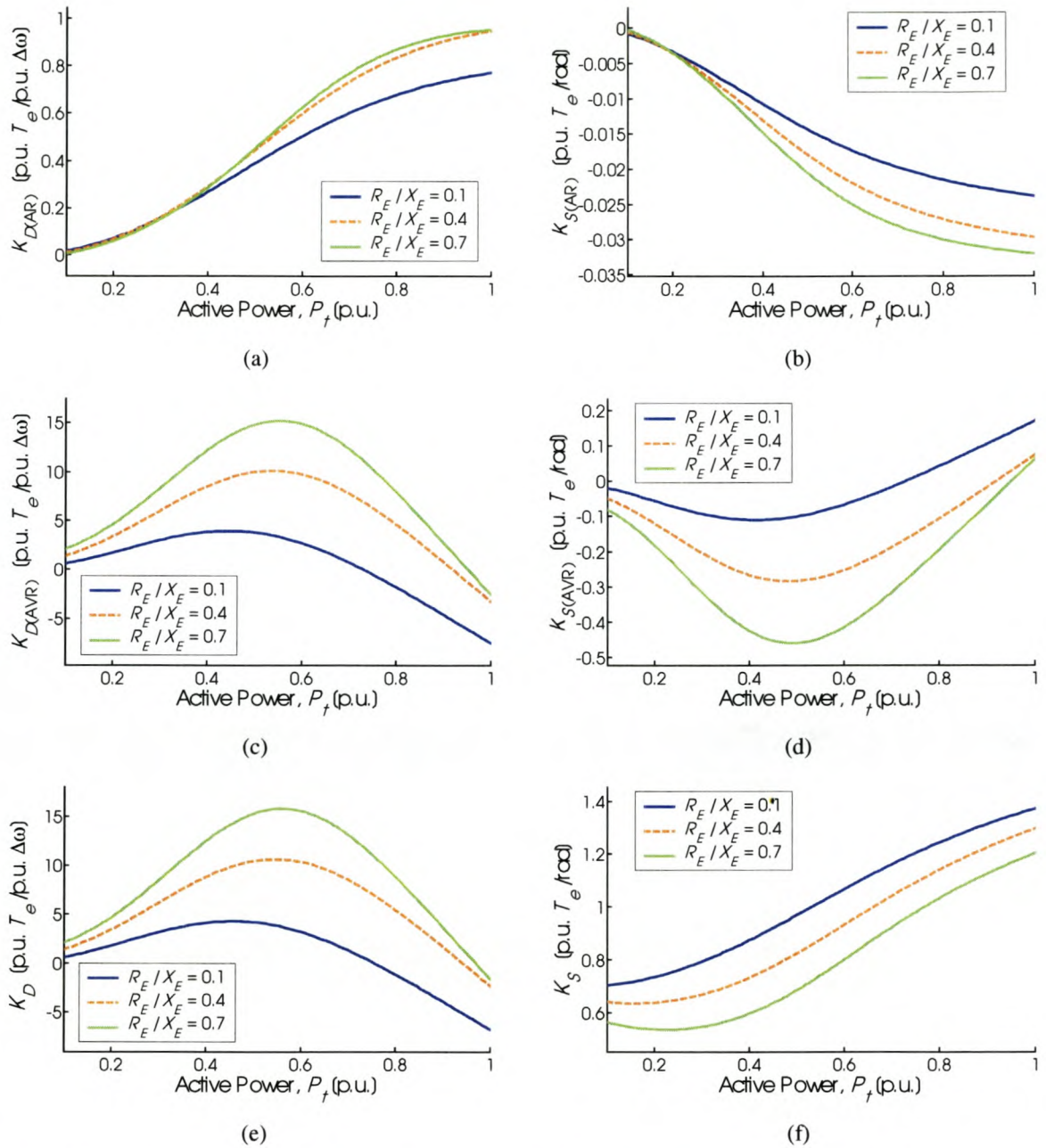

Fig. E.11: Damping and synchronizing torques vs. machine load and line resistance, with $X_E = 0.4$ p.u.

E.5 Results of Section 3.8.4 – Local Load

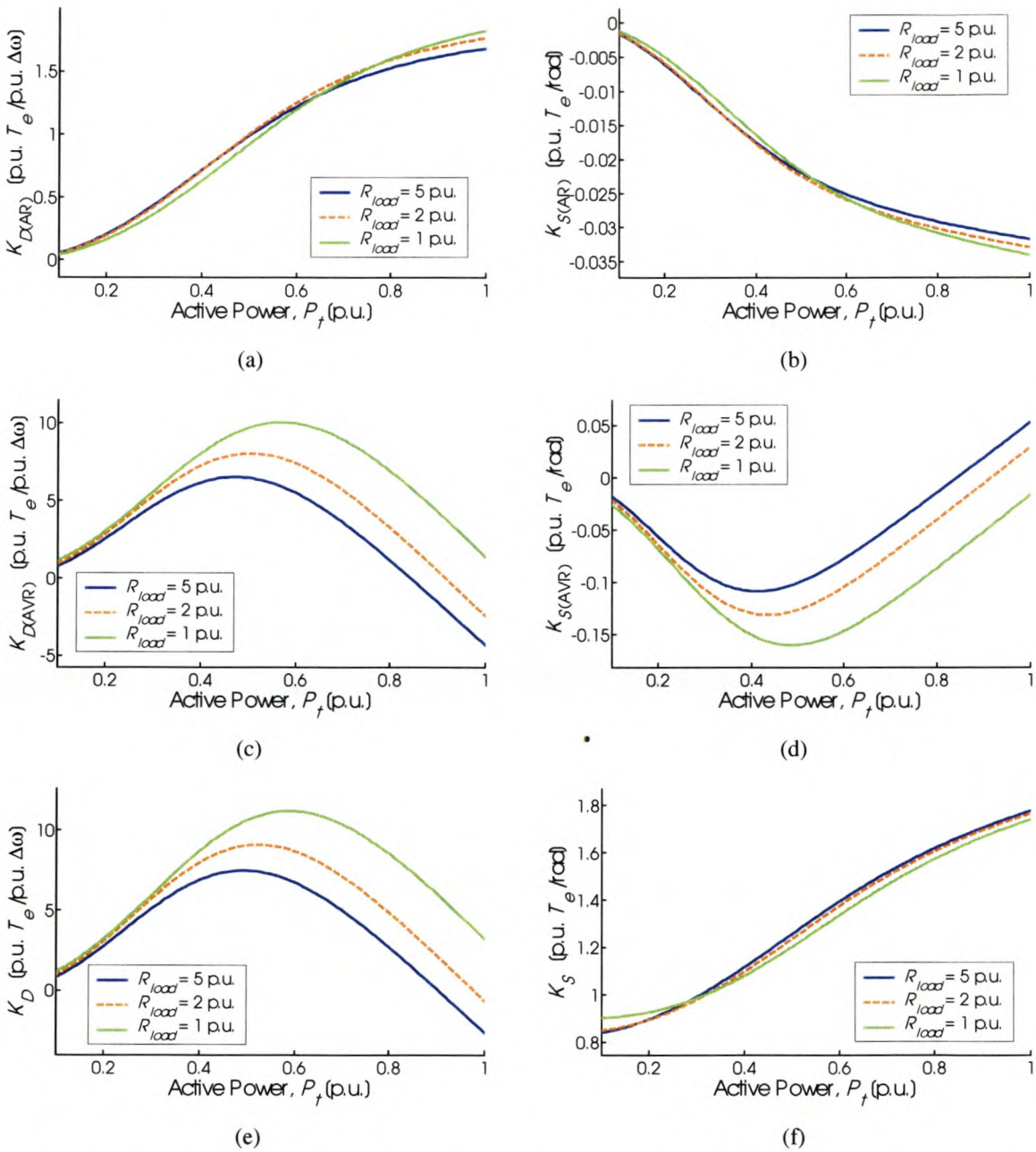

Fig. E.12: Damping and synchronizing torques vs. machine load and local load resistance, with X_{line} = 0.2 p.u.

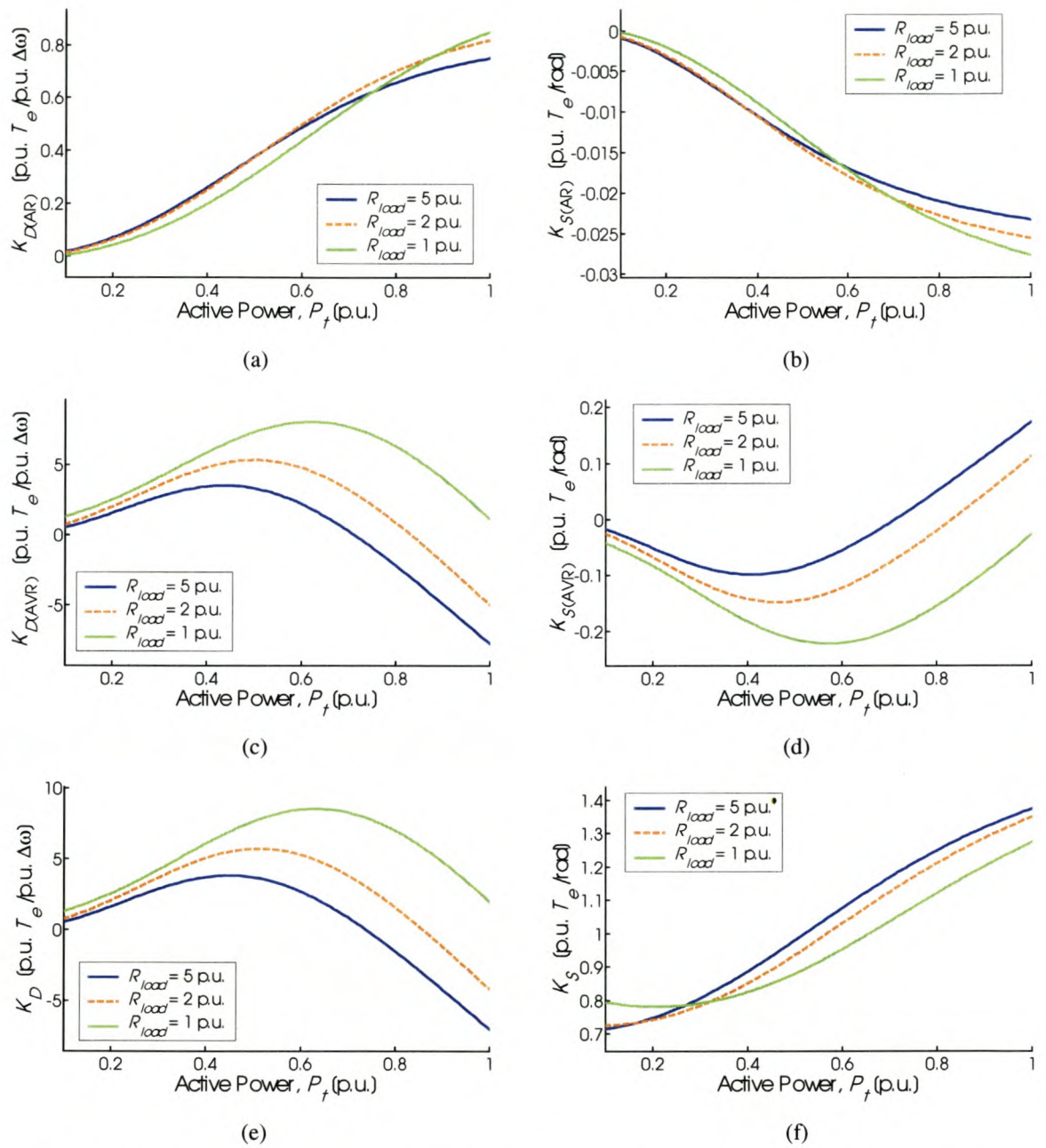

Fig. E.13: Damping and synchronizing torques vs. machine load and local load resistance, with X_{line} = 0.4 p.u.

E.6 Results of Section 3.8.5 – AVR Gain

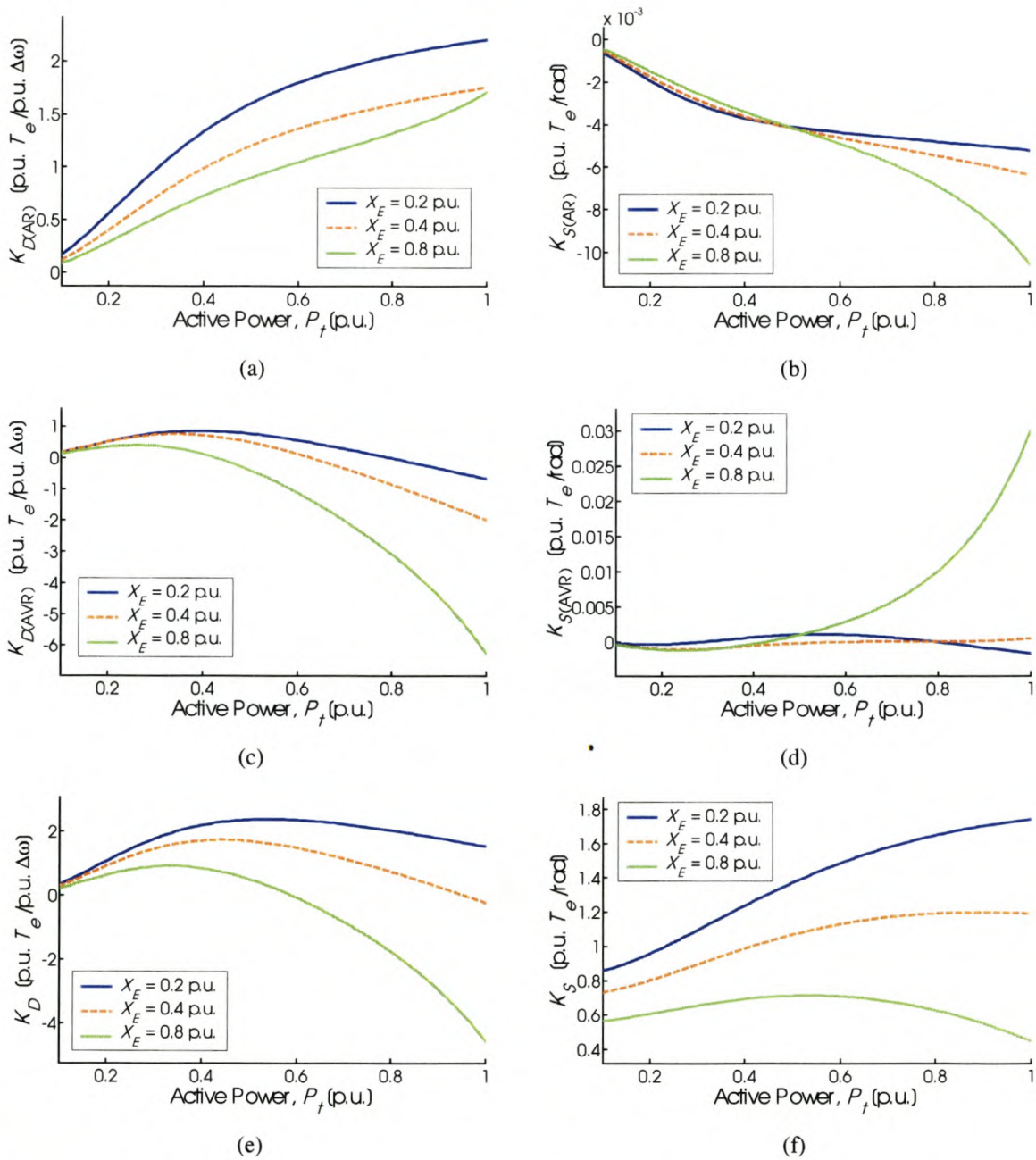

Fig. E.14: Damping and synchronizing torques vs. machine load and external reactance, with K_A = 20

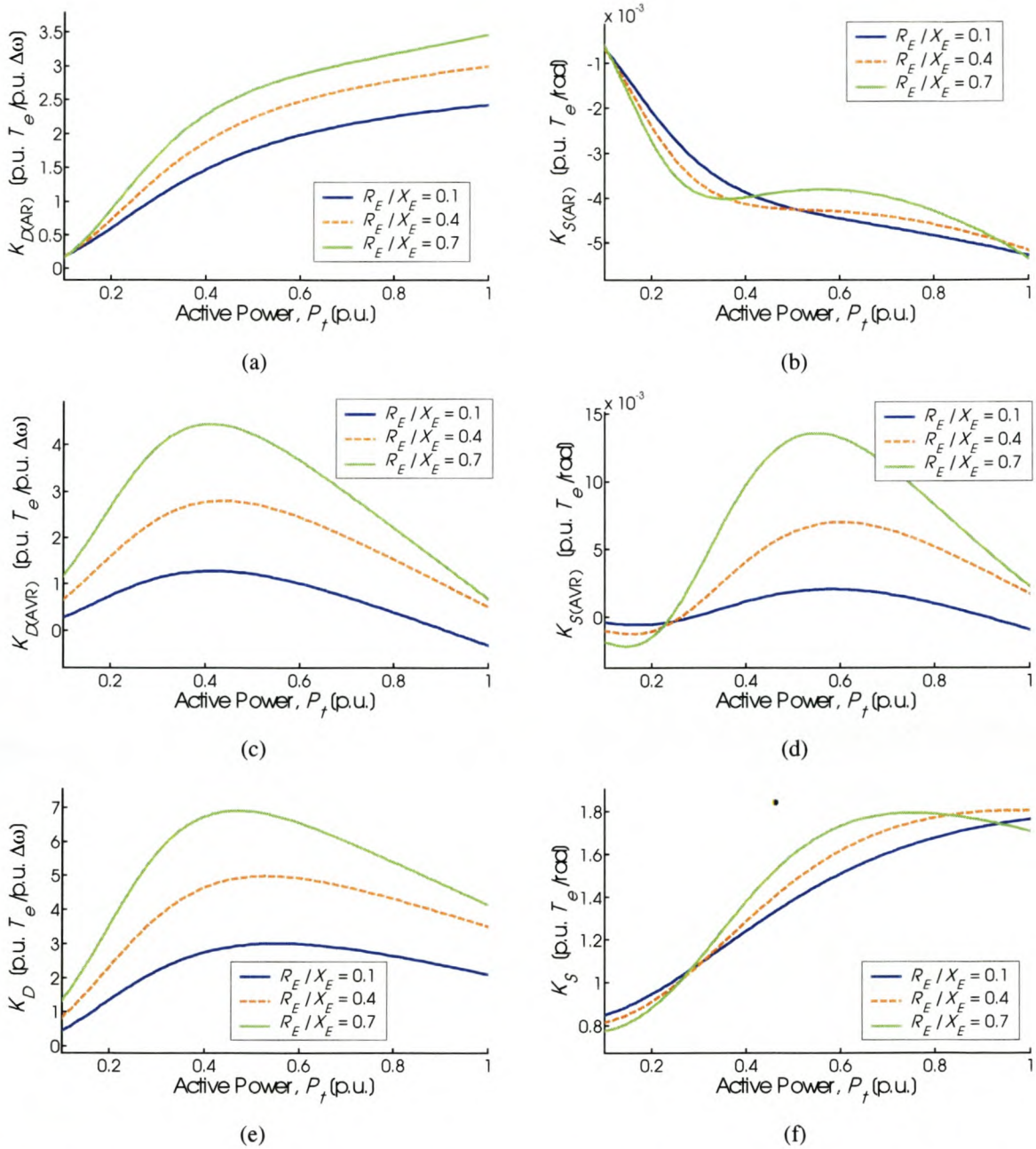

Fig. E.15: Damping and synchronizing torques vs. machine load and line resistance, with $X_E = 0.2$ p.u. and $K_A = 20$

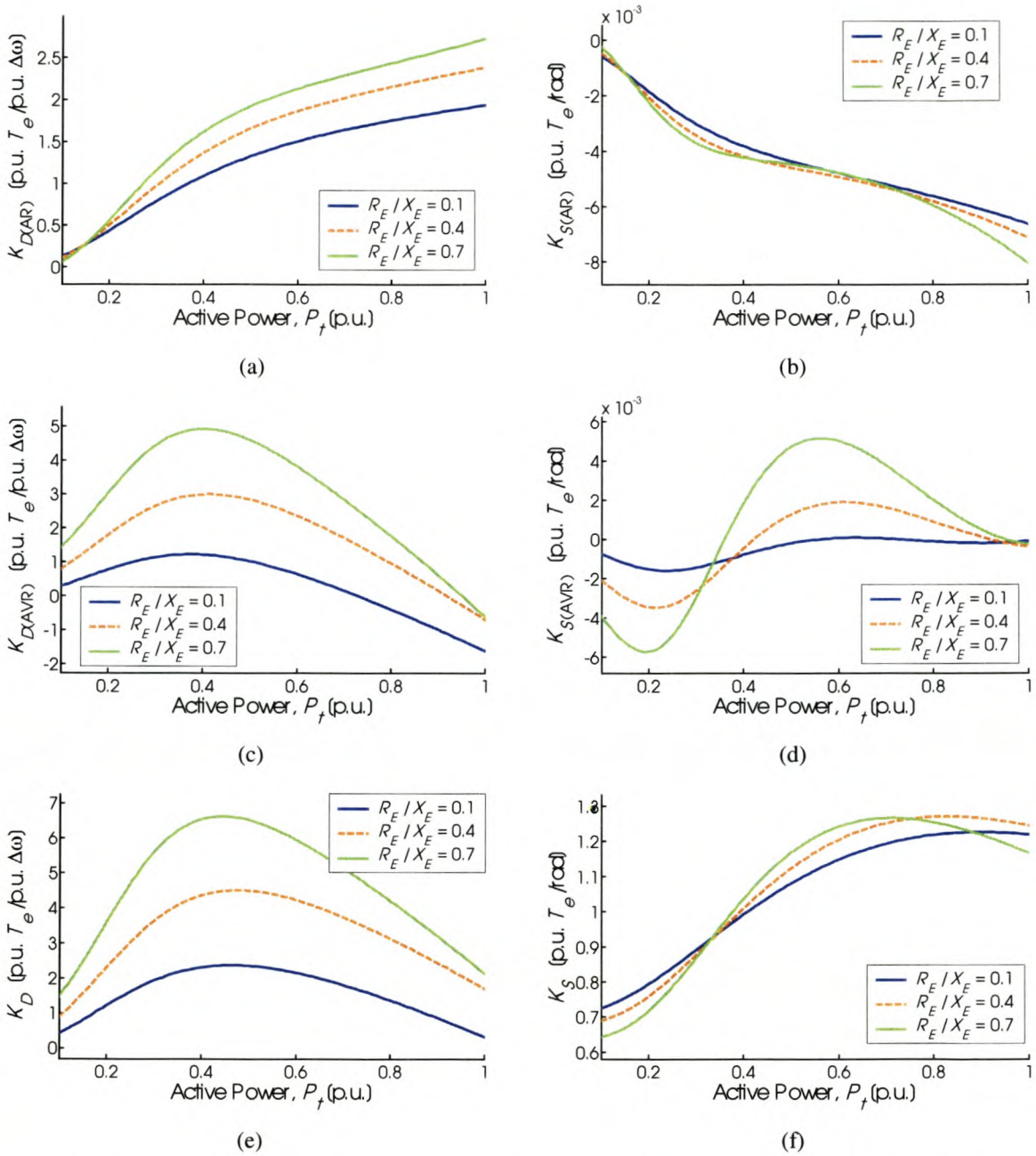

Fig. E.16: Damping and synchronizing torques vs. machine load and line resistance, with X_E = 0.4 p.u. and K_A = 20

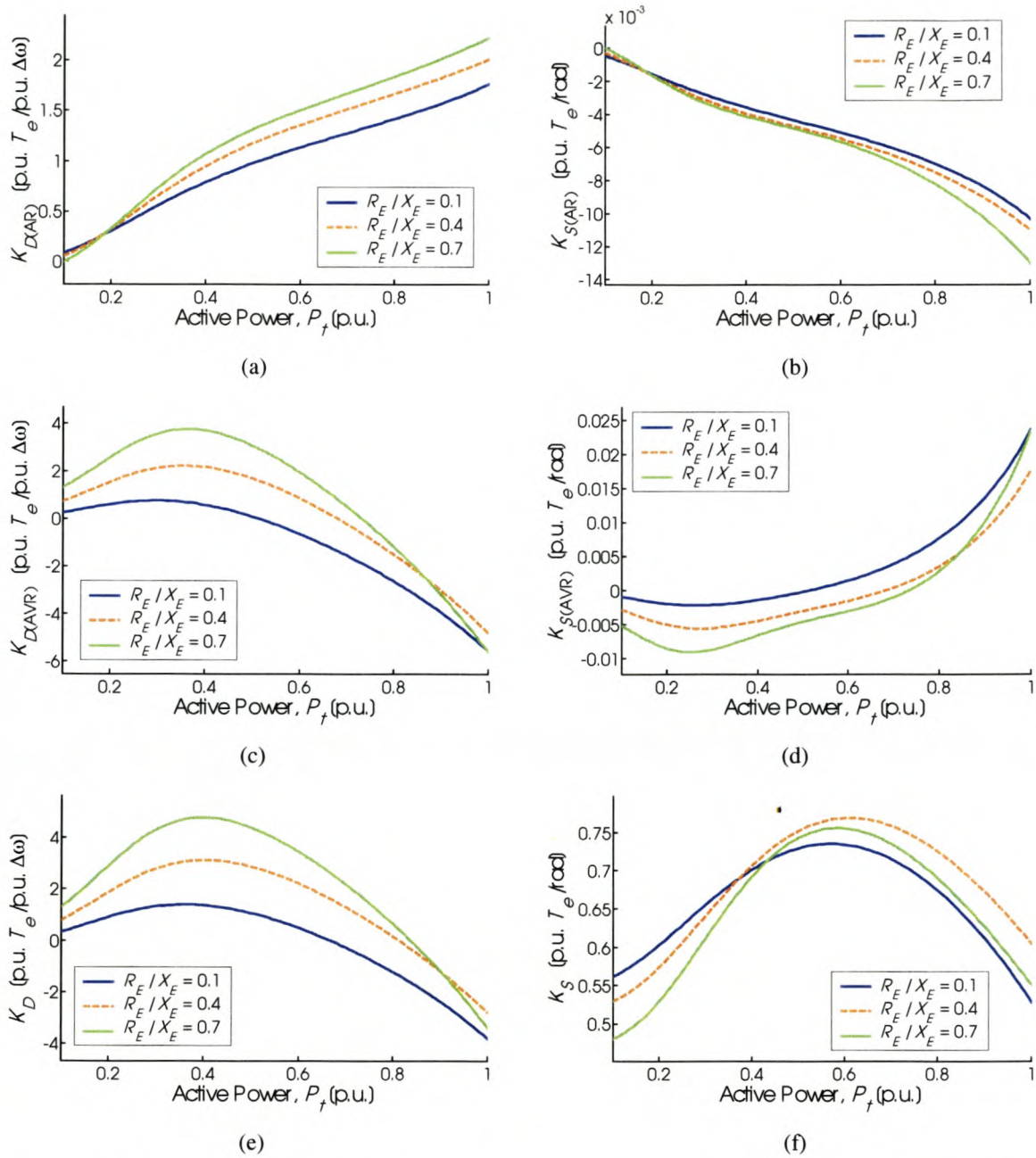

Fig. E.17: Damping and synchronizing torques vs. machine load and line resistance, with $X_E = 0.8$ p.u. and $K_A = 20$

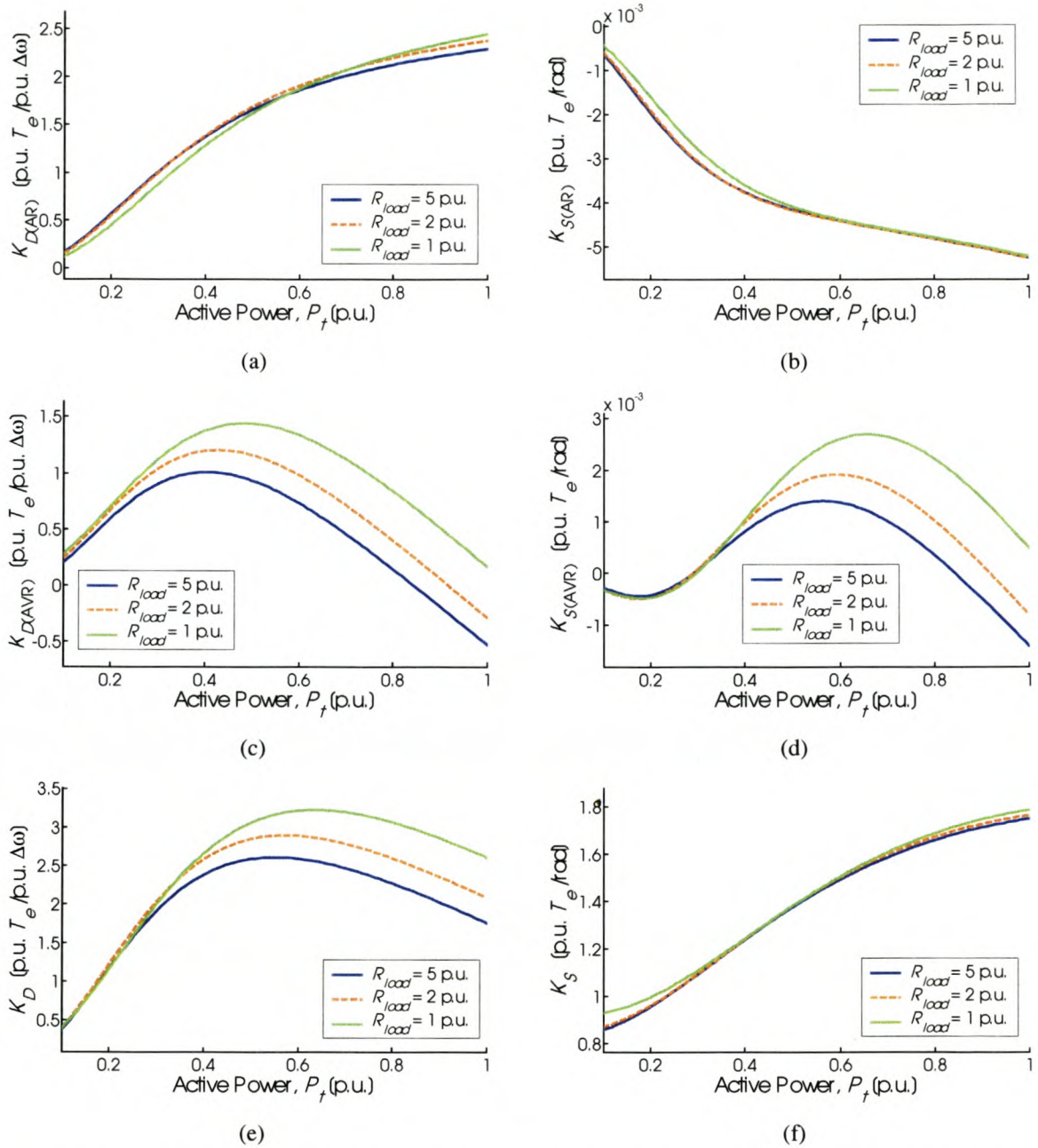

Fig. E.18: Damping and synchronizing torques vs. machine load and local load resistance, with X_{line} = 0.2 p.u. and K_A = 20

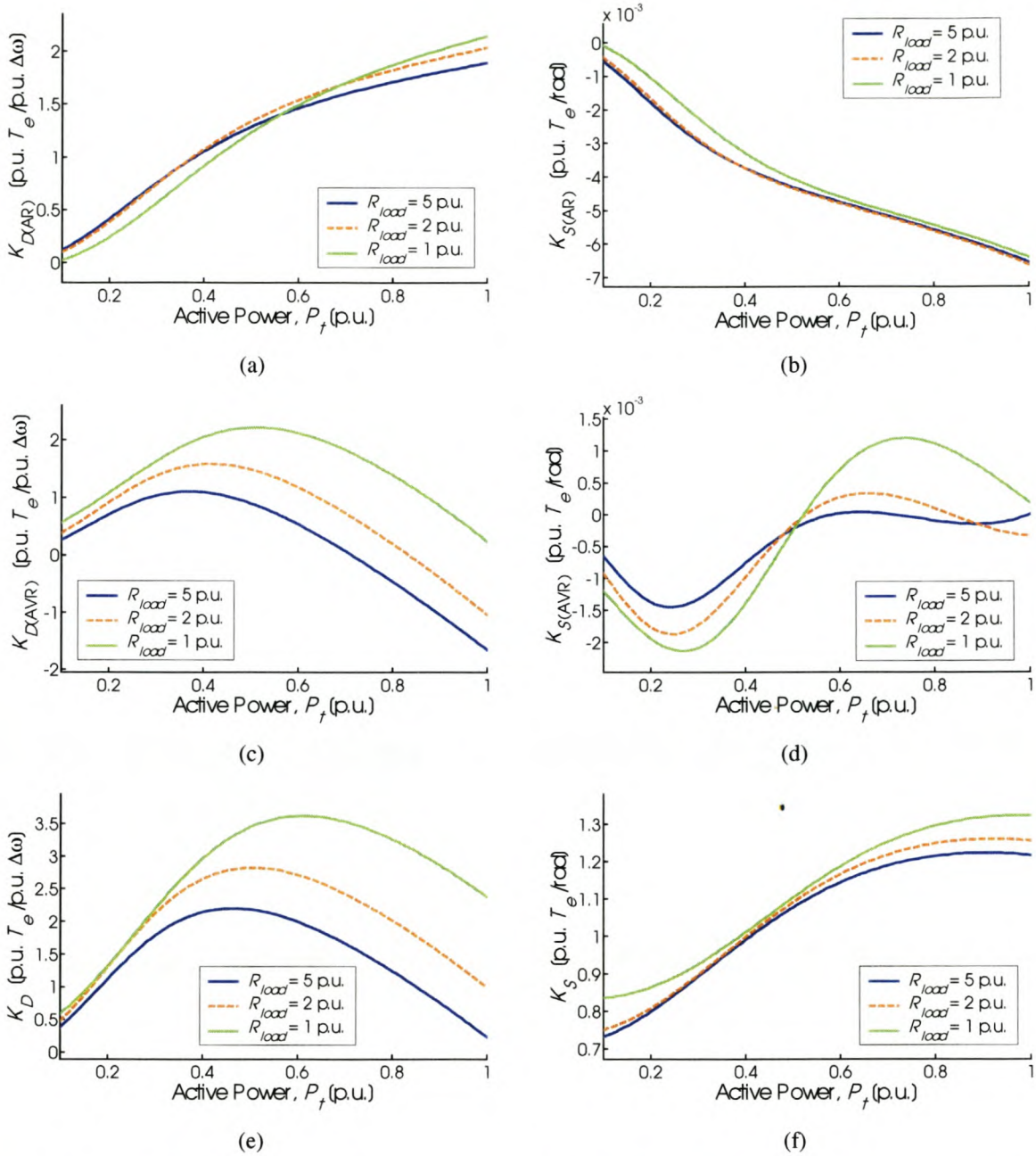

Fig. E.19: Damping and synchronizing torques vs. machine load and local load resistance, with X_{line} = 0.4 p.u. and K_A = 20

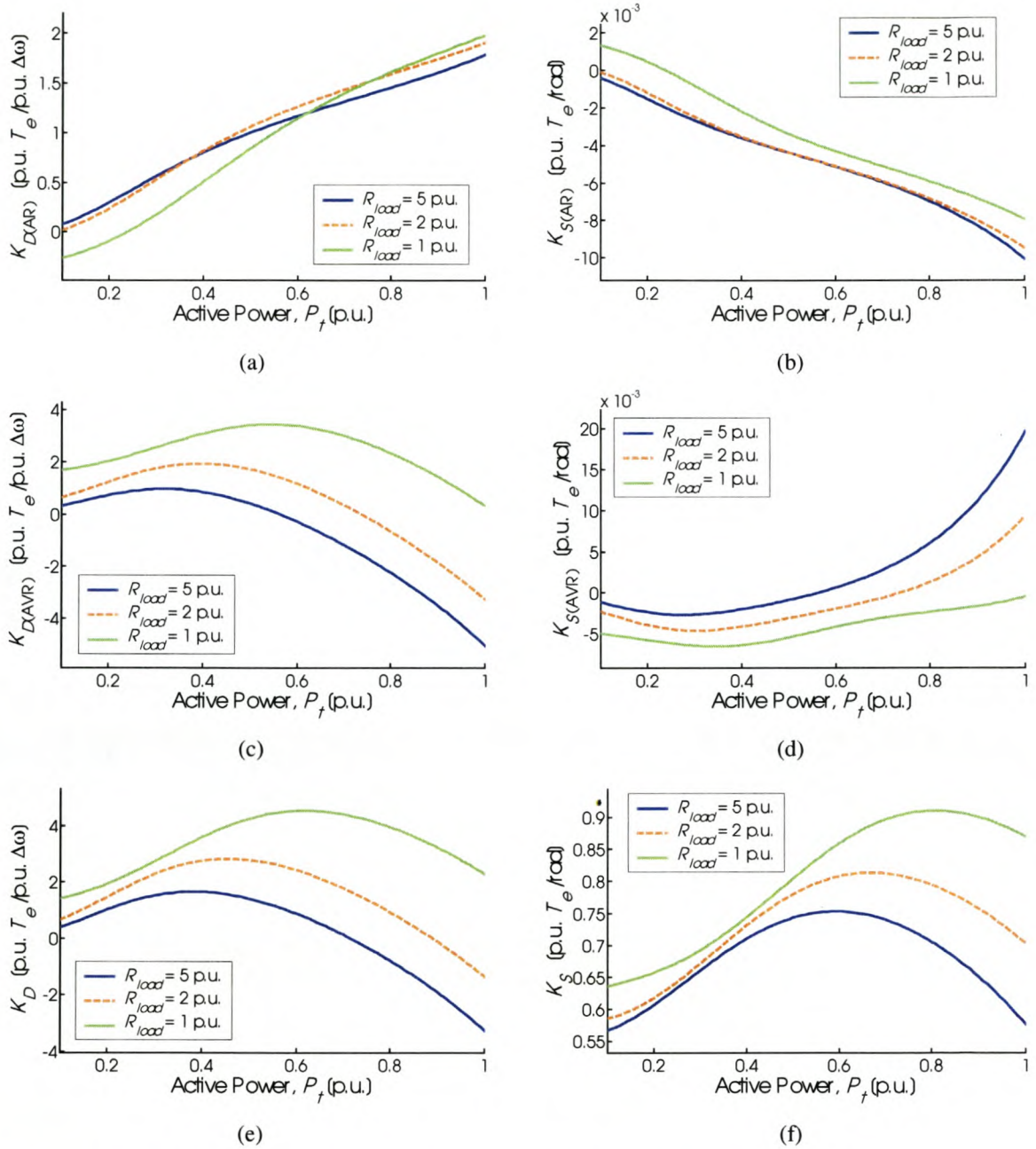

Fig. E.20: Damping and synchronizing torques vs. machine load and local load resistance, with X_{line} = 0.8 p.u. and K_A = 20

E.7 Results of Section 3.8.6 – Influence of Saturation

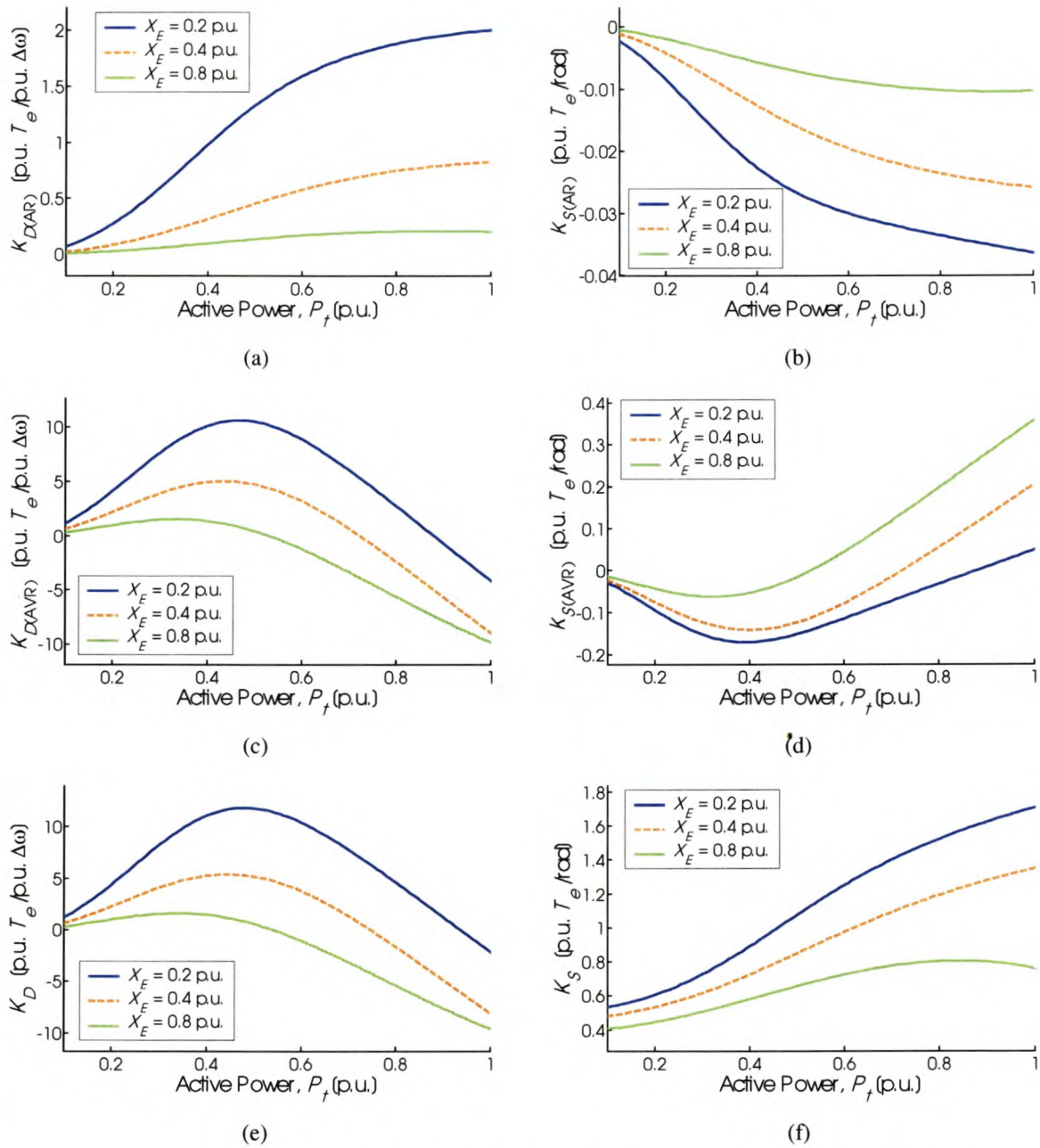

Fig. E.21: Damping and synchronizing torques vs. machine load and external reactance; saturation not modelled

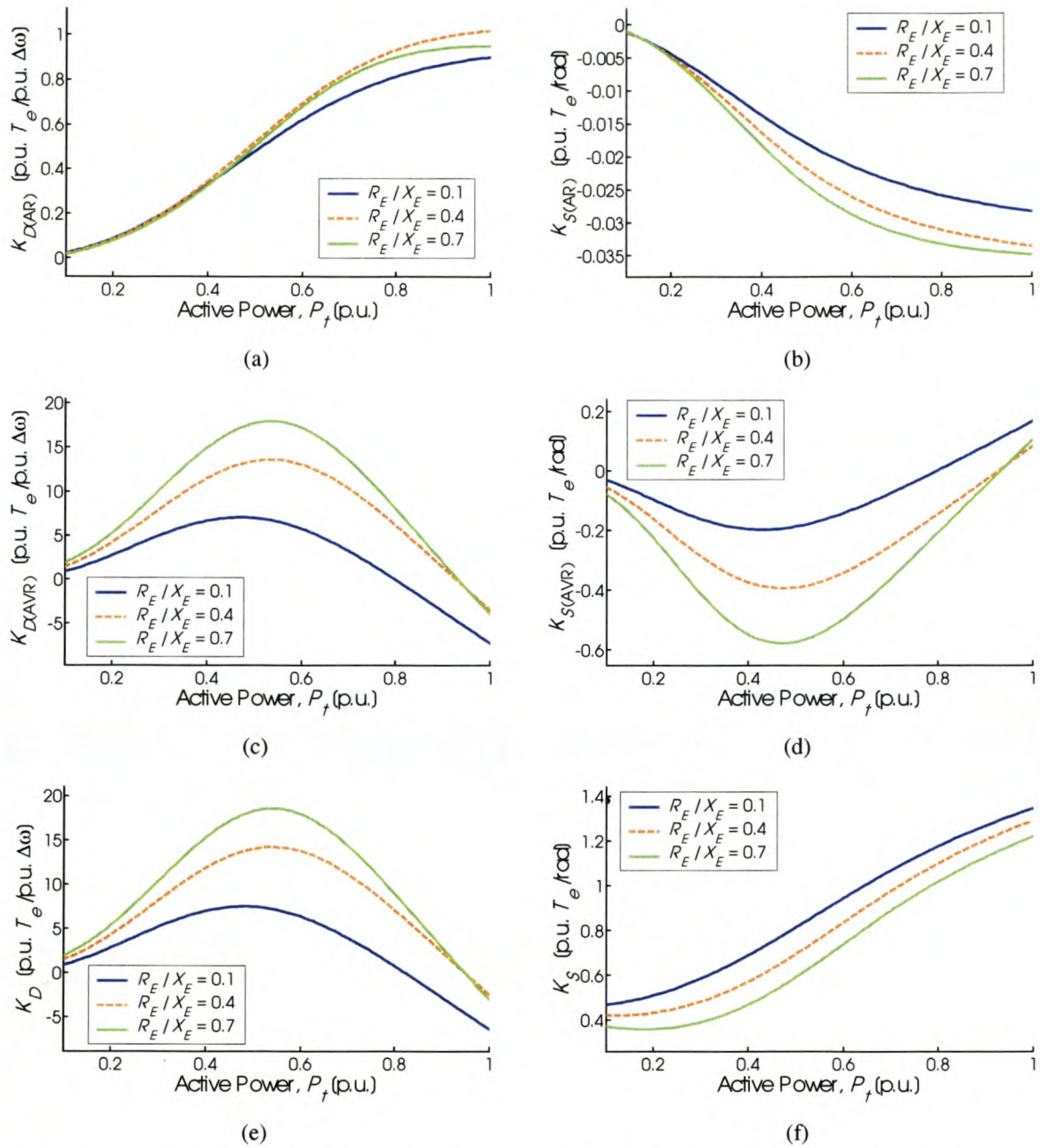

Fig. E.22: Damping and synchronizing torques vs. machine load and line resistance, with $X_E = 0.4$ p.u.; saturation not modelled

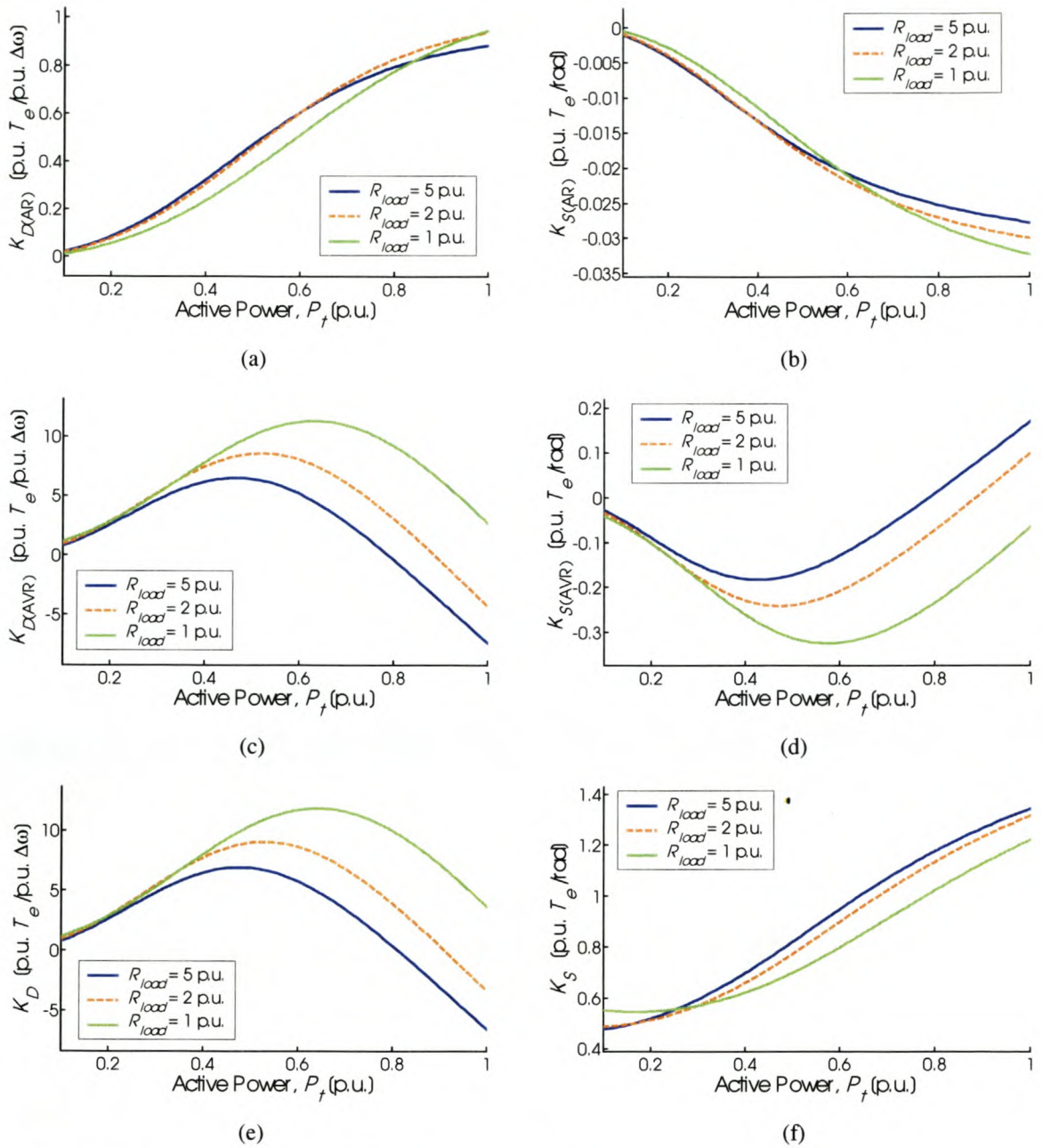

Fig. E.23: Damping and synchronizing torques vs. machine load and local load resistance, with X_{line} = 0.4 p.u.; saturation not modelled

F SIMULATION RESULTS OF CHAPTER 4 – PSS

F.1 Results of Section 4.5.4 – PSS Controller Design

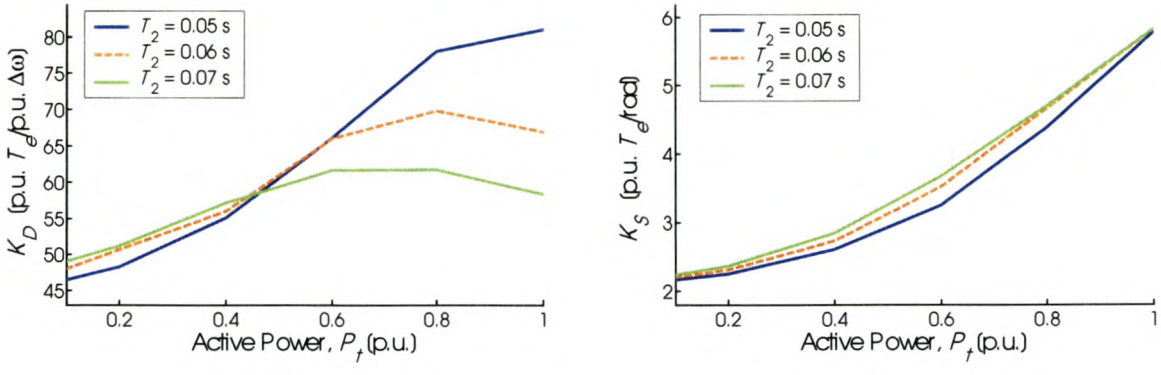

Fig. F.1: System torques vs. machine load and PSS controller time constant T_2, with X_E = 0.2 p.u.

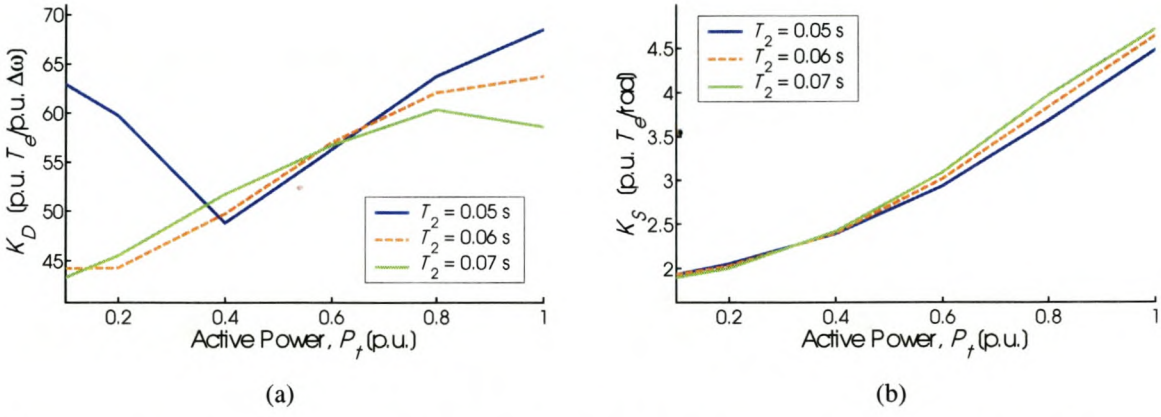

Fig. F.2: System torques vs. machine load and PSS controller time constant T_2, with X_E = 0.4 p.u.

F.2 Results of Section 4.6.3 – Line Resistance

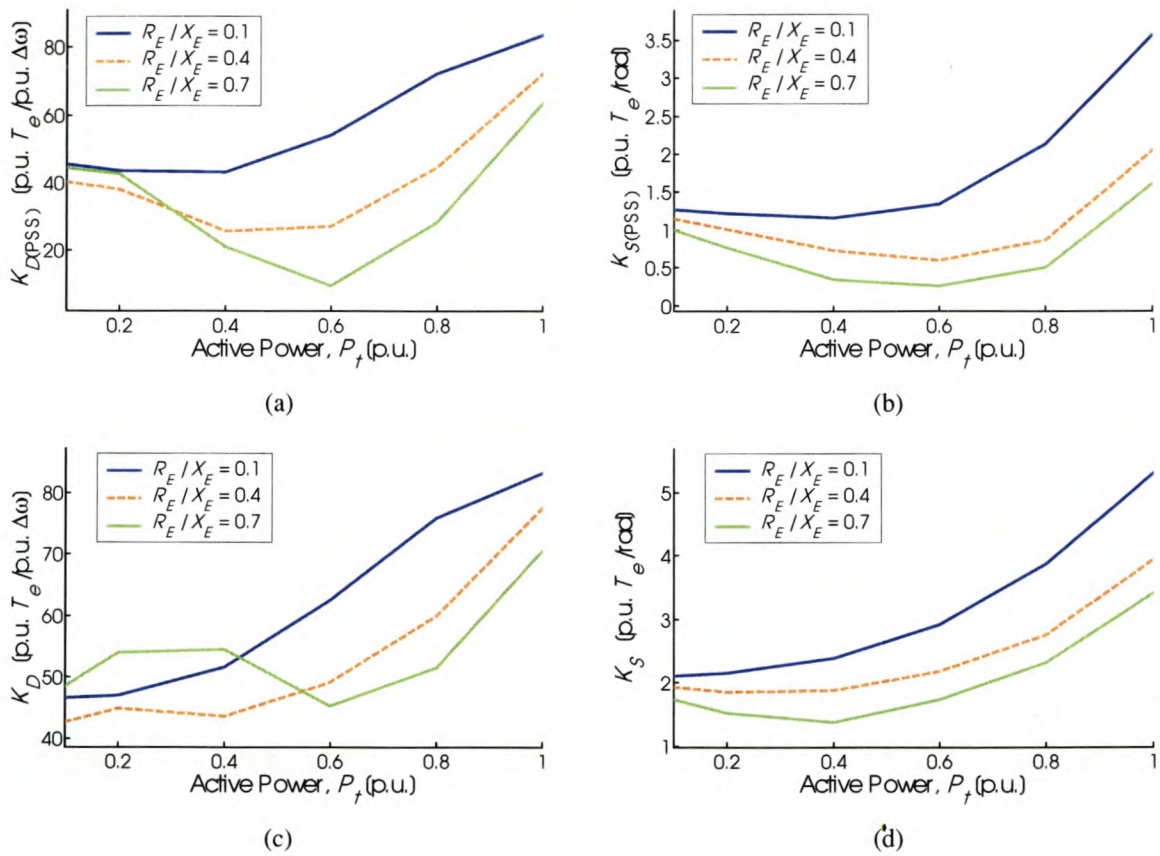

Fig. F.3: PSS and system torque coefficients vs. machine load and line resistance, with $X_E = 0.2$ p.u.

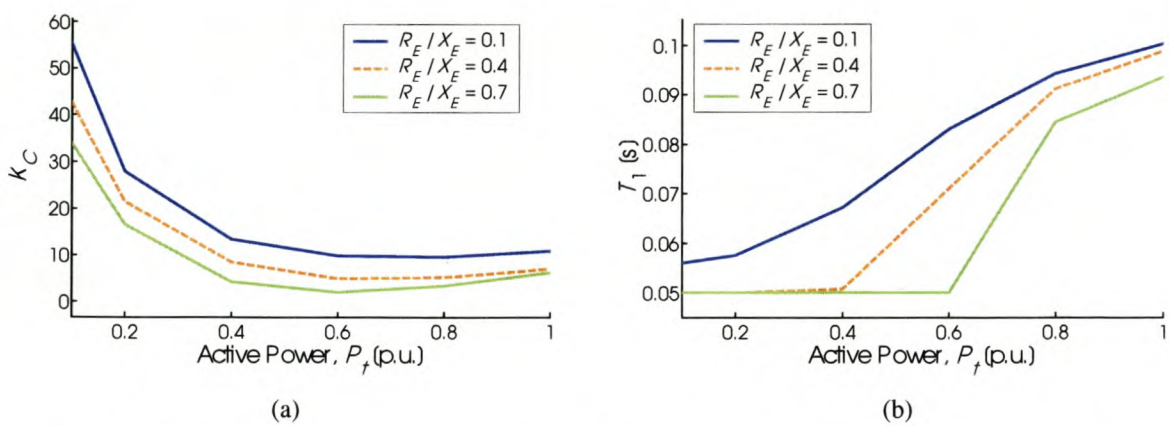

Fig. F.4: PSS gain and time constant T_1 vs. machine load and line resistance, with $X_E = 0.2$ p.u.

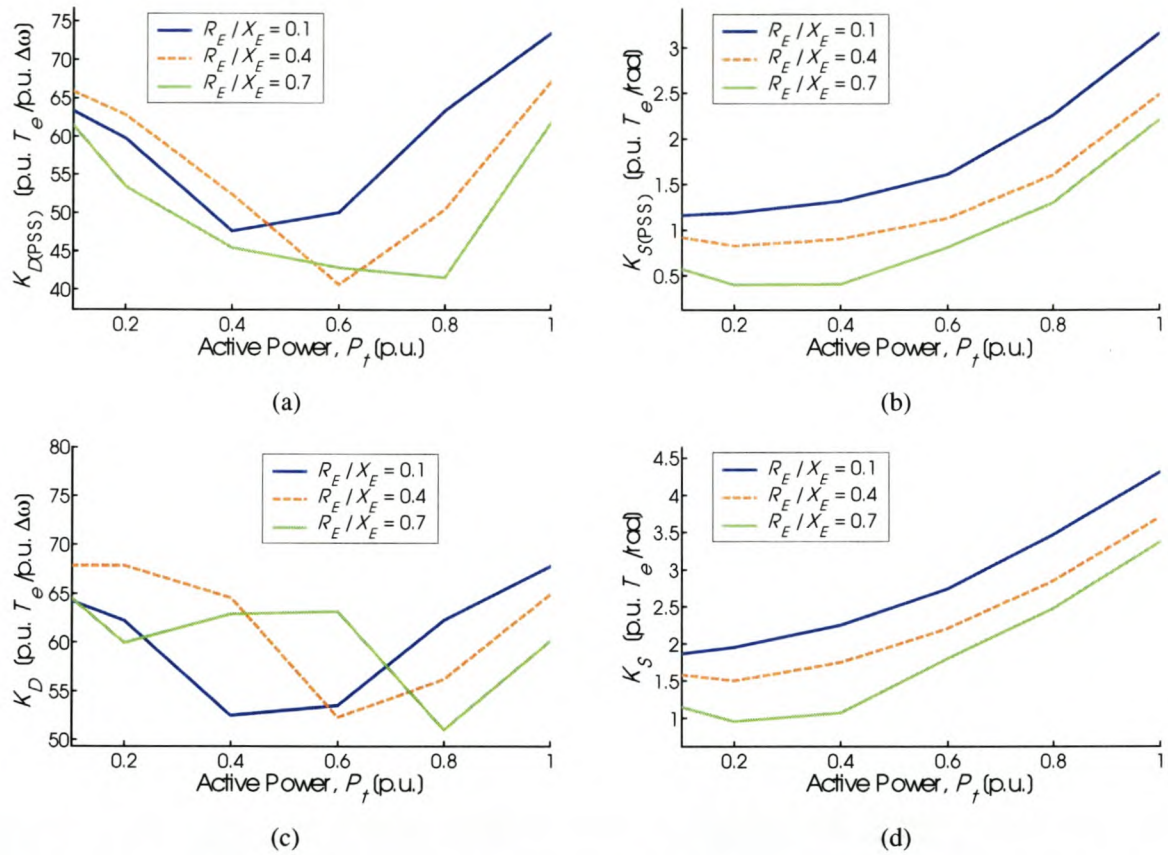

Fig. F.5: PSS and system torque coefficients vs. machine load and line resistance, with $X_E = 0.4$ p.u.

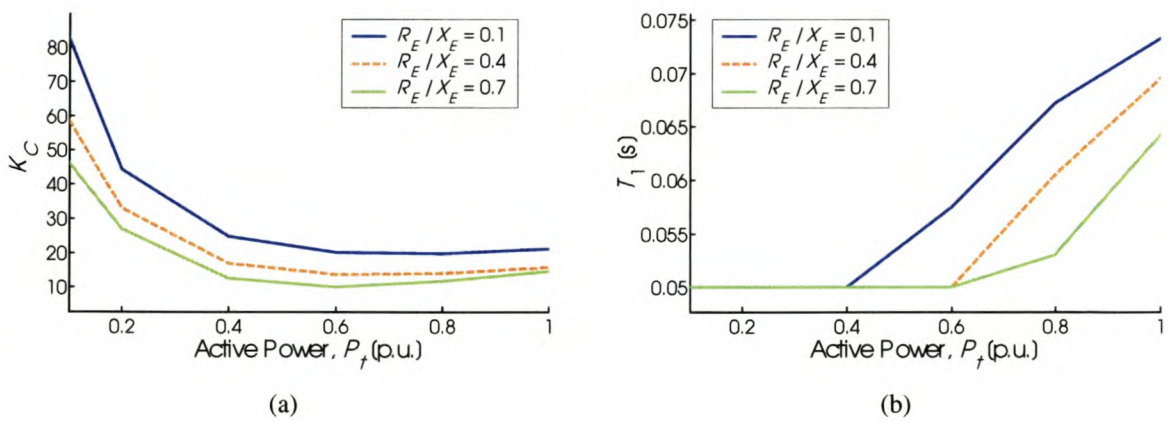

Fig. F.6: PSS gain and time constant T_1 vs. machine load and line resistance, with $X_E = 0.4$ p.u.

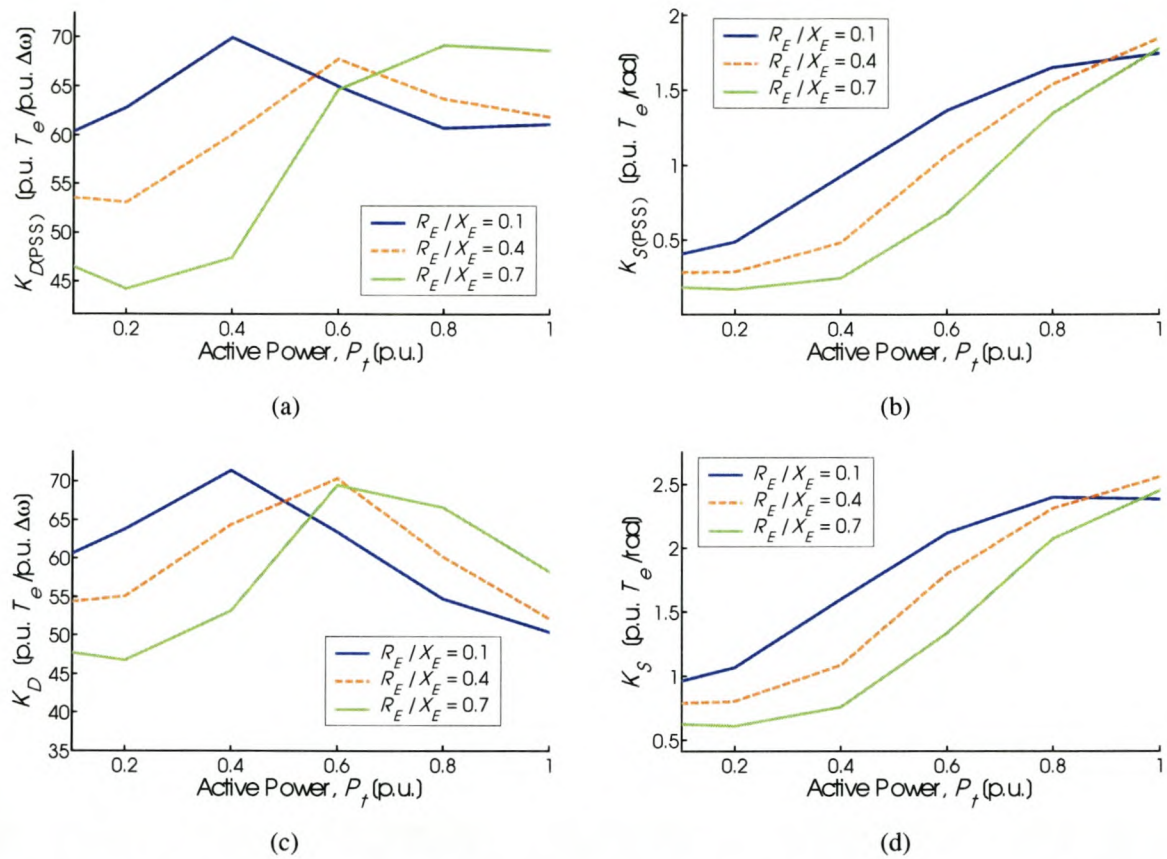

Fig. F.7: PSS and system torque coefficients vs. machine load and line resistance, with $X_E = 0.8$ p.u.

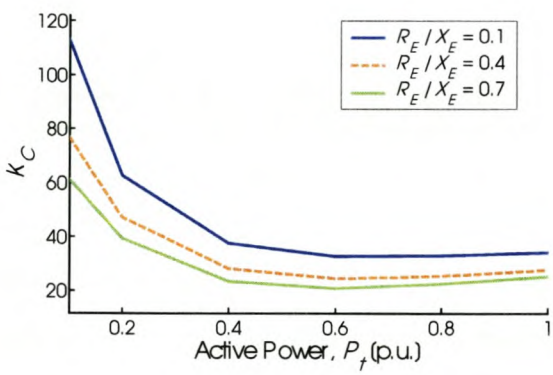

T_1 values all 0.05 p.u.

(b)

Fig. F.8: PSS gain and time constant T_1 vs. machine load and line resistance, with $X_E = 0.8$ p.u.

F.3 Results of Section 4.6.4 – Local Load

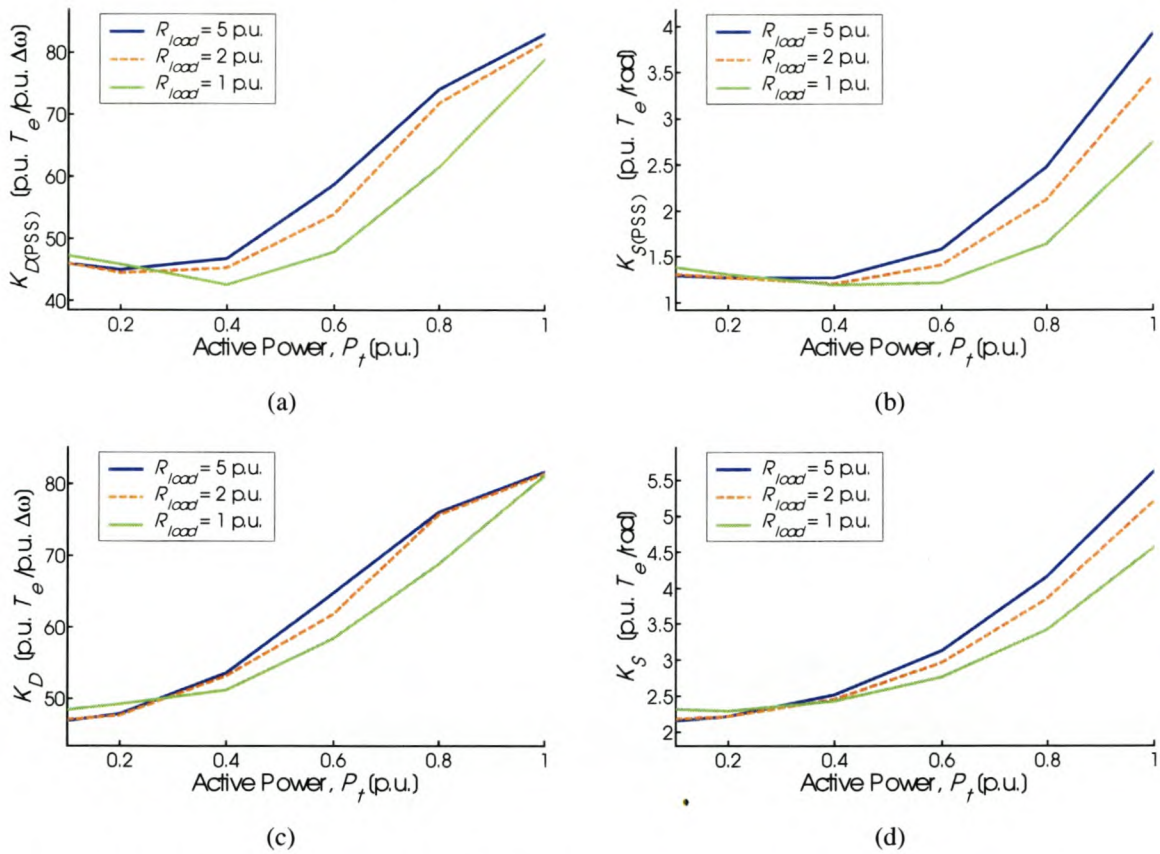

Fig. F.9: PSS and system torque coefficients vs. machine load and local load resistance, with X_{line} = 0.2 p.u.

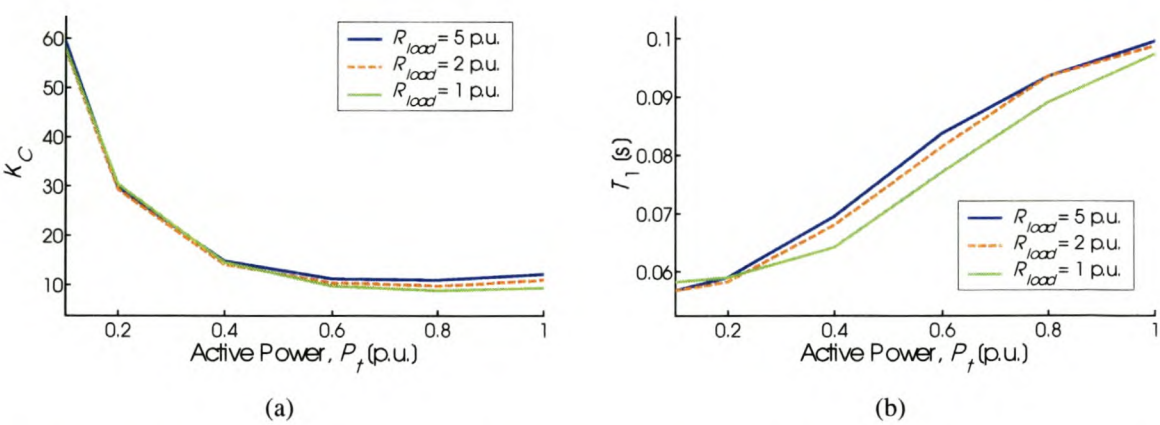

Fig. F.10: PSS gain and time constant T_1 vs. machine load and local load resistance, with X_{line} = 0.2 p.u.

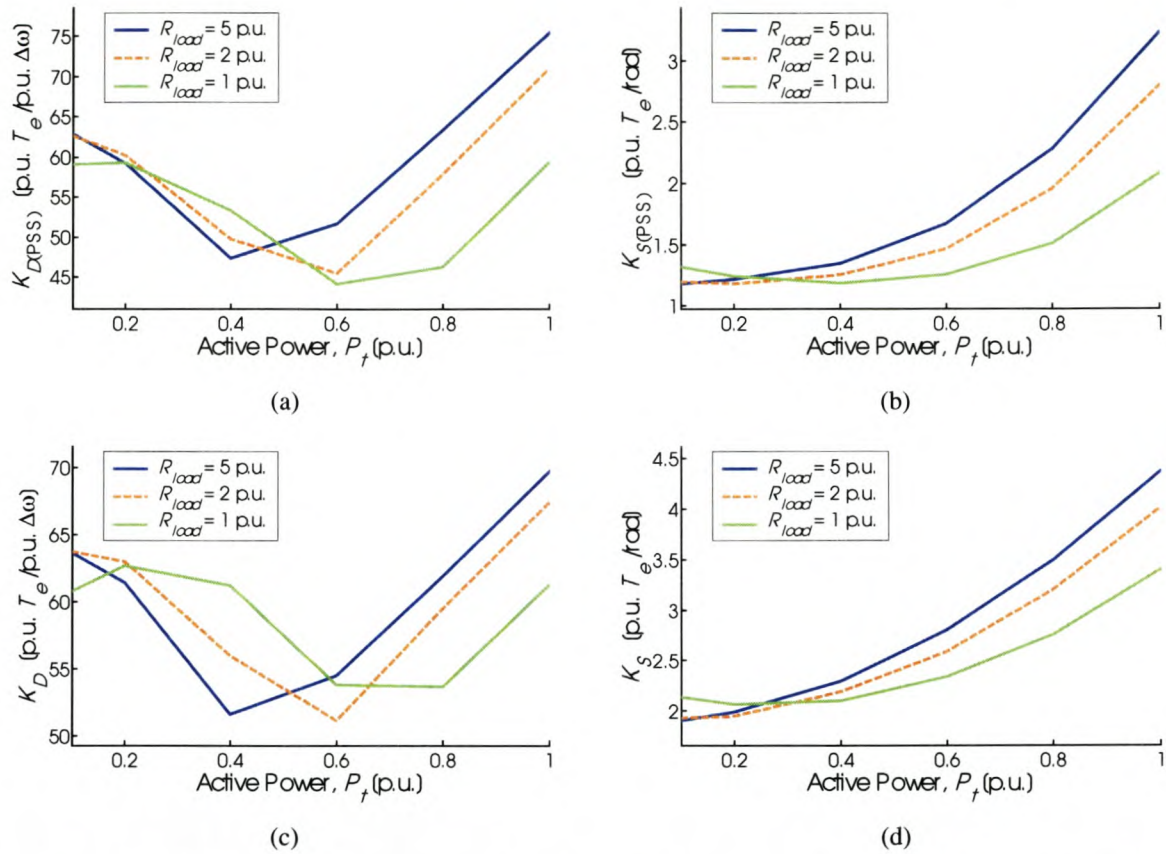

Fig. F.11: PSS and system torque coefficients vs. machine load and local load resistance, with X_{line} = 0.4 p.u.

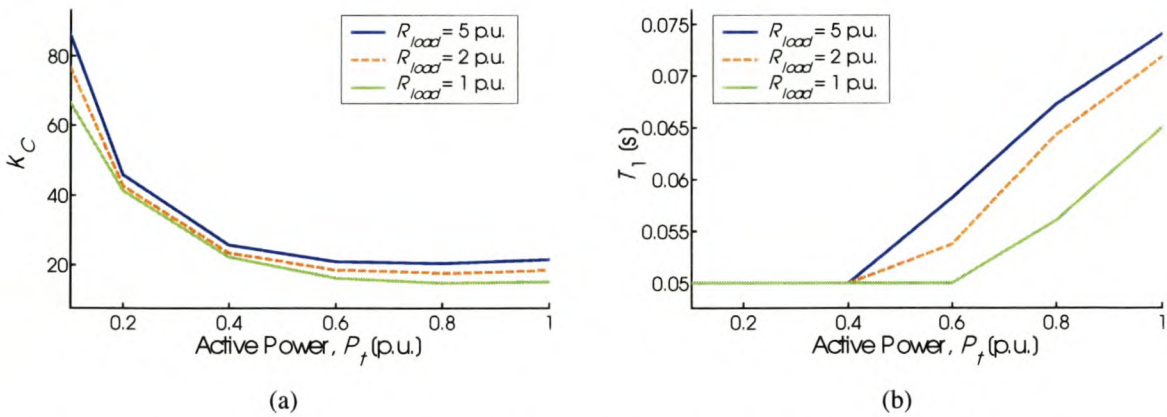

Fig. F.12: PSS gain and time constant T_1 vs. machine load and local load resistance, with X_{line} = 0.4 p.u.

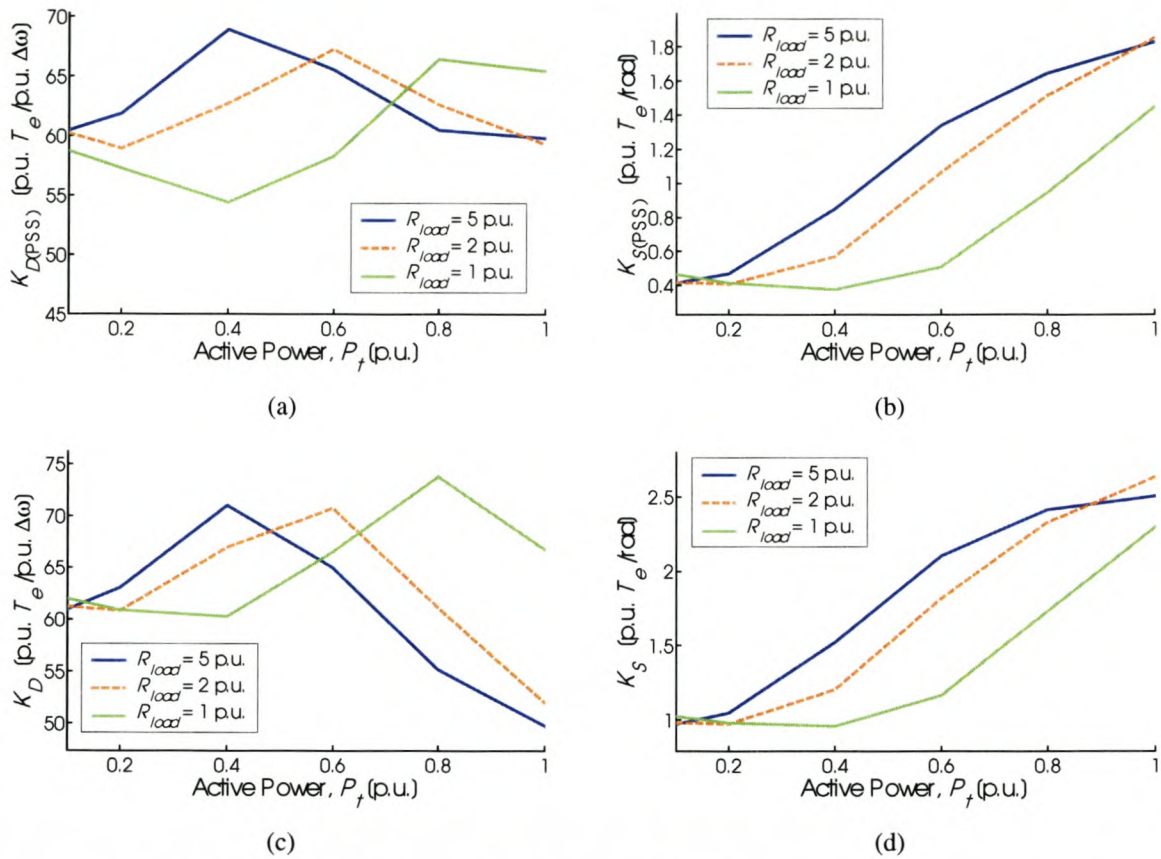

Fig. F.13: PSS and system torque coefficients vs. machine load and local load resistance, with X_{line} = 0.8 p.u.

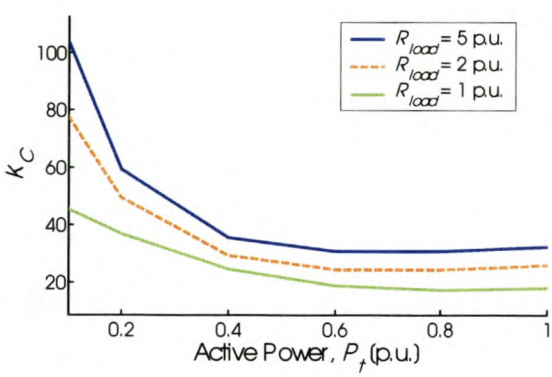

T_1 values all 0.05 p.u.

(b)

Fig. F.14: PSS gain and time constant T_1 vs. machine load and local load resistance, with X_{line} = 0.8 p.u.

F.4 Results of Section 4.6.5 – AVR Gain

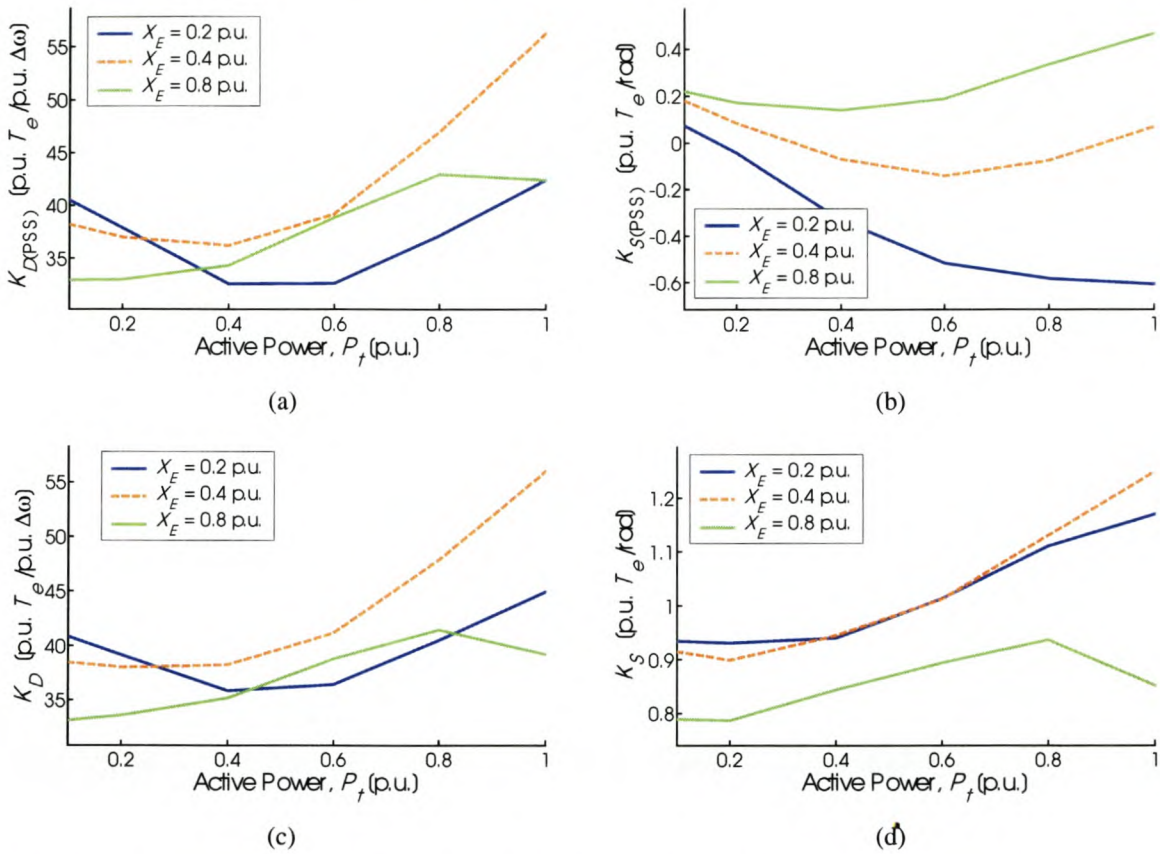

Fig. F.15: PSS and system torque coefficients vs. machine load and external reactance, with K_A = 20

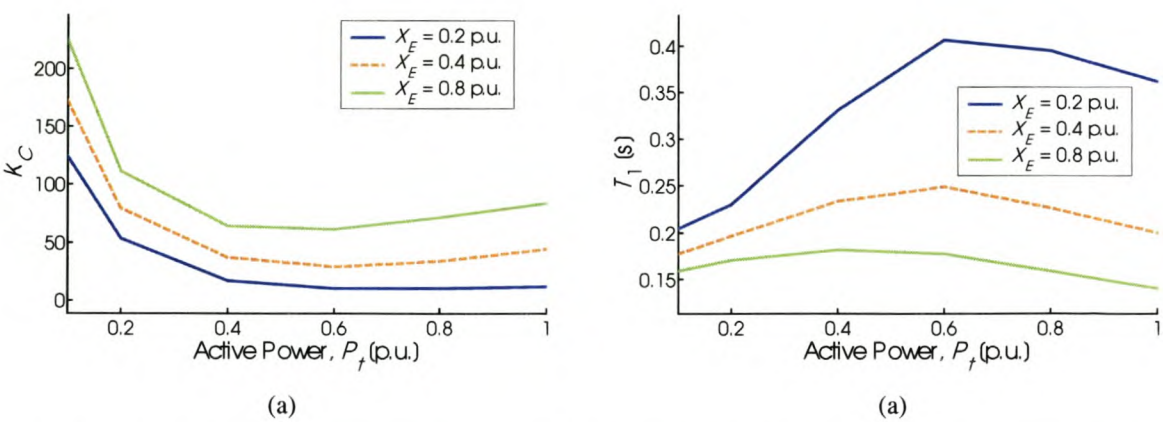

Fig F.16: Optimised PSS parameters K_C and T_1 vs. machine load and external reactance, with K_A = 20

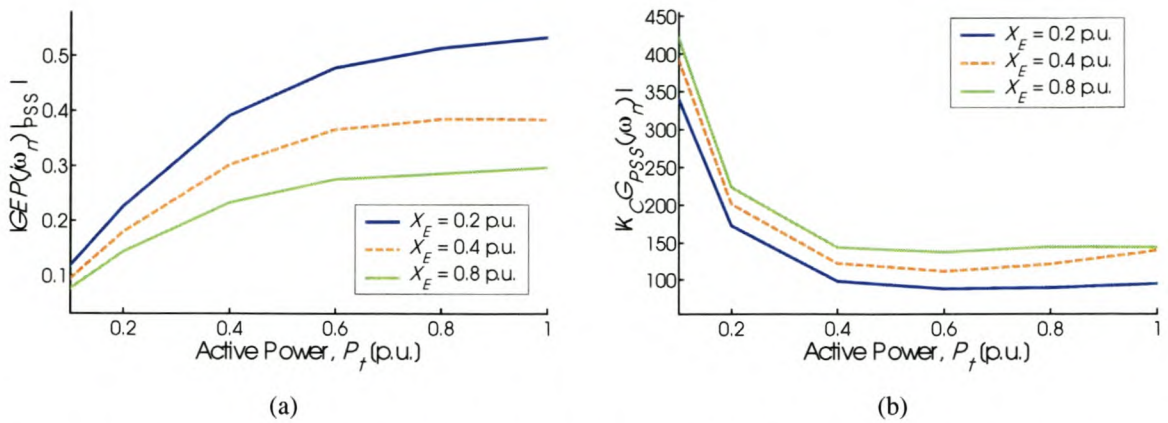

(a) (b)

Fig. F.17: "Plant" and PSS controller transfer function gains vs. machine load and external reactance, with $K_A = 20$

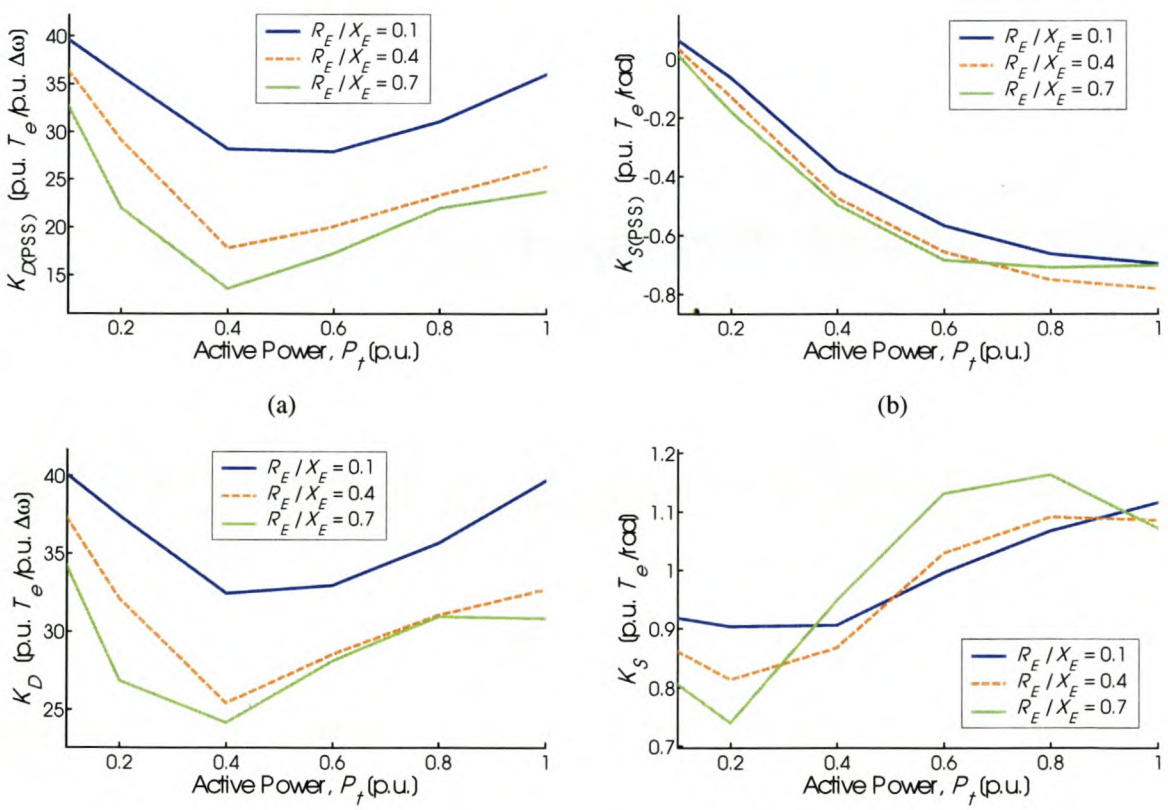

(a) (b)

(c) (d)

Fig. F.18: PSS and system torque coefficients vs. machine load and line resistance, with $X_E = 0.2$ p.u. and $K_A = 20$

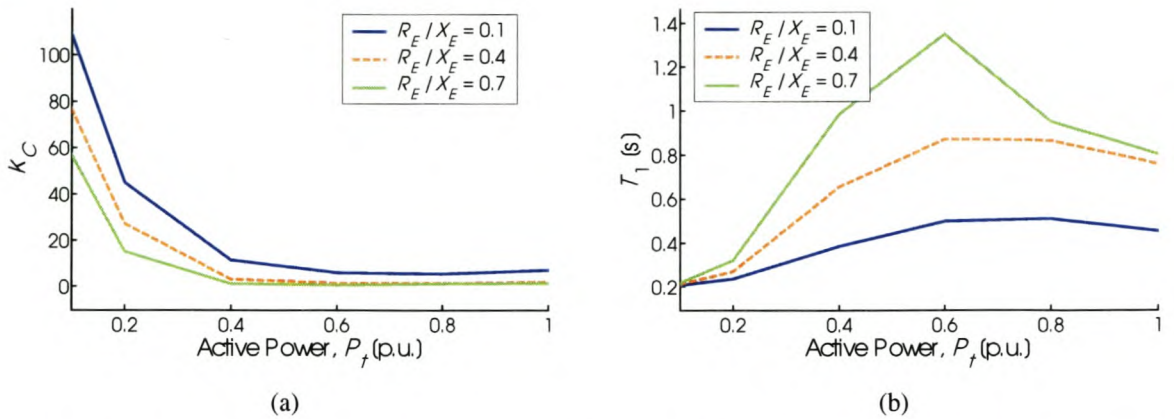

Fig. F.19: PSS gain and time constant T_1 vs. machine load and line resistance, with $X_E = 0.2$ p.u. and $K_A = 20$

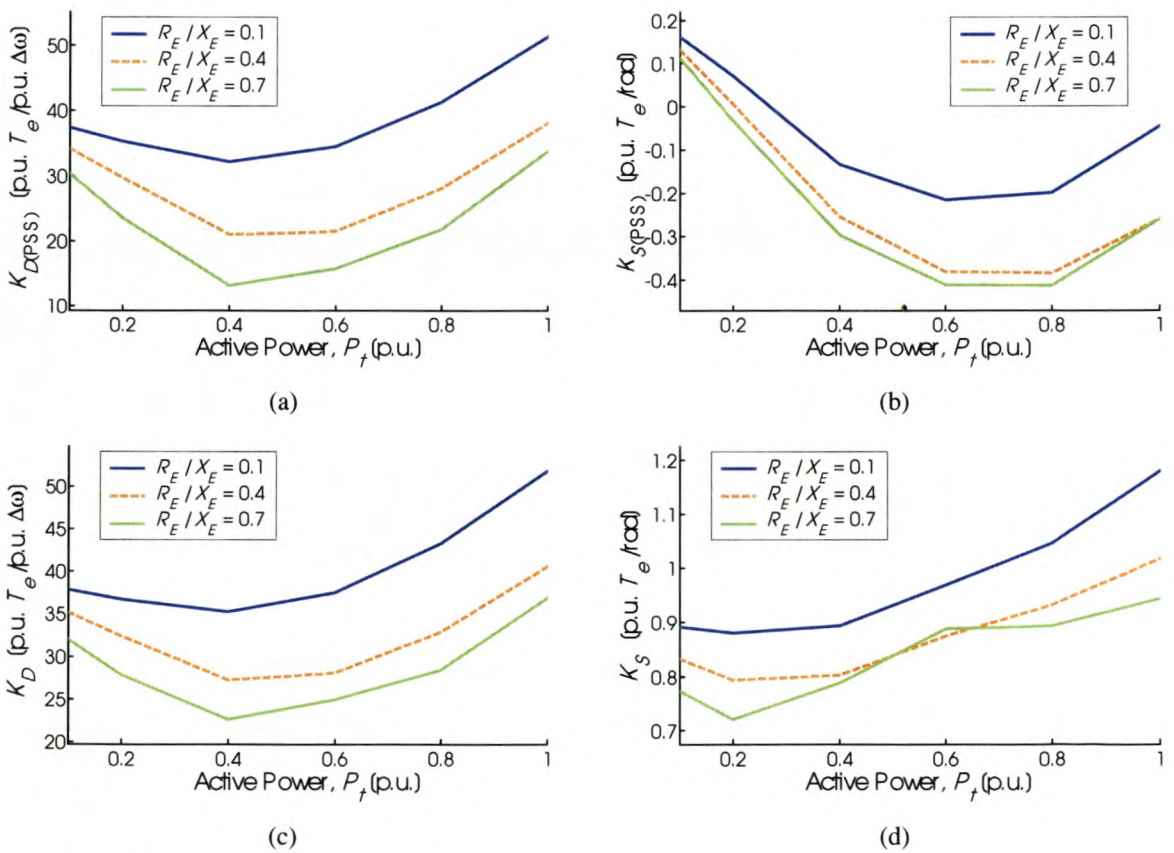

Fig. F.20: PSS and system torque coefficients vs. machine load and line resistance, with $X_E = 0.4$ p.u. and $K_A = 20$

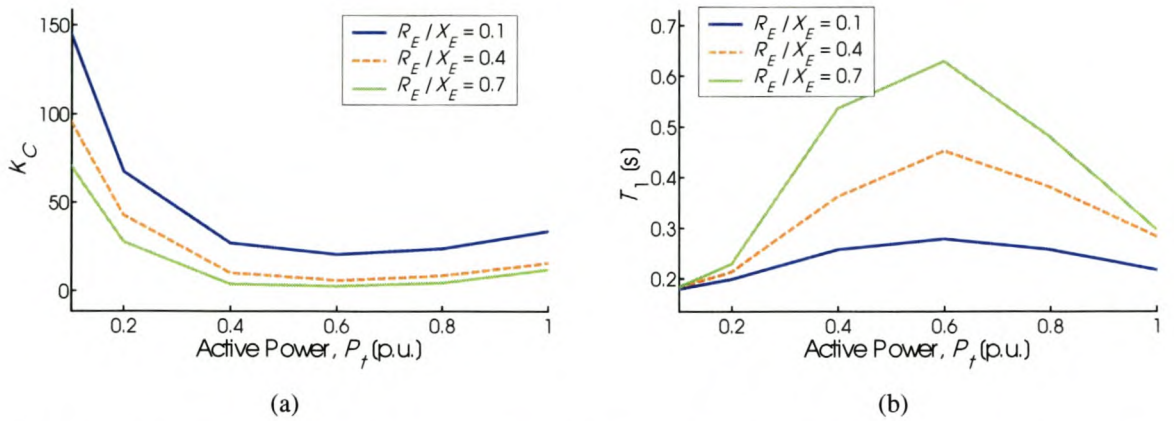

Fig. F.21: PSS gain and time constant T_1 vs. machine load and line resistance, with $X_E = 0.4$ p.u. and $K_A = 20$

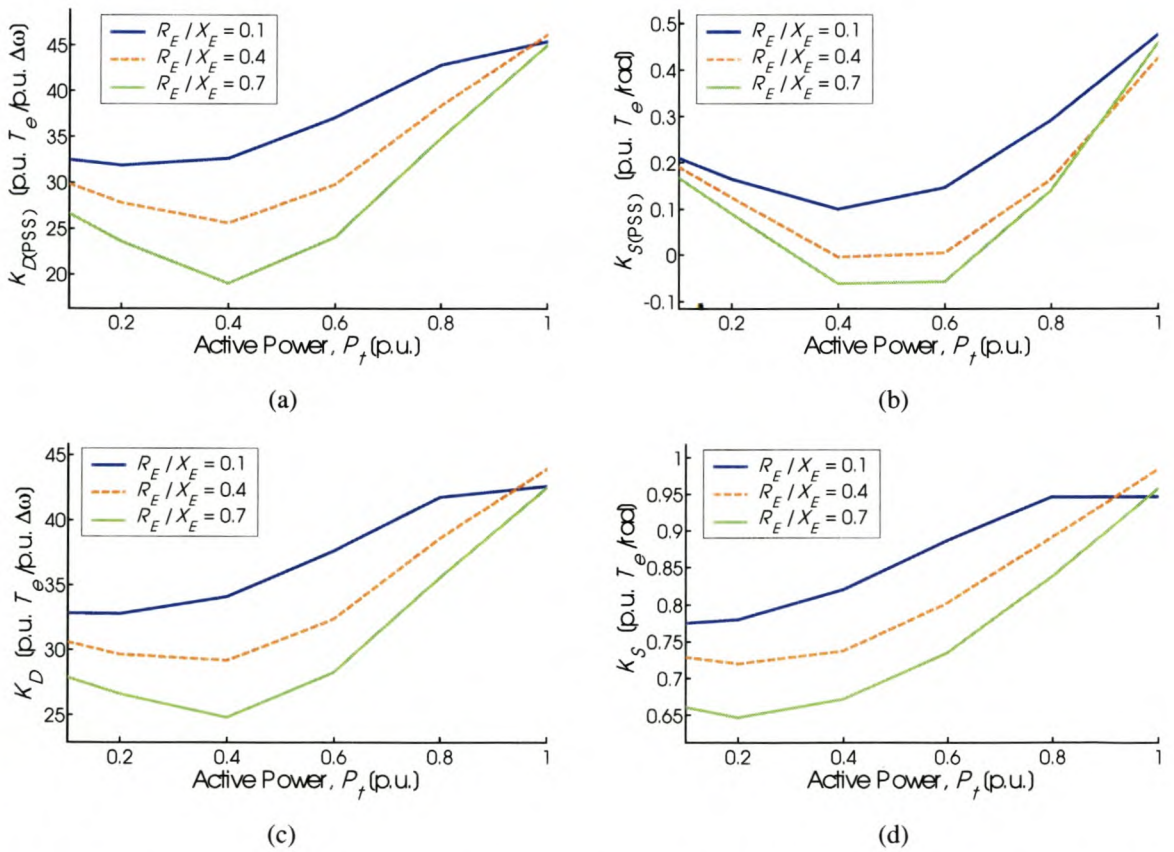

Fig. F.22: PSS and system torque coefficients vs. machine load and line resistance, with $X_E = 0.8$ p.u. and $K_A = 20$

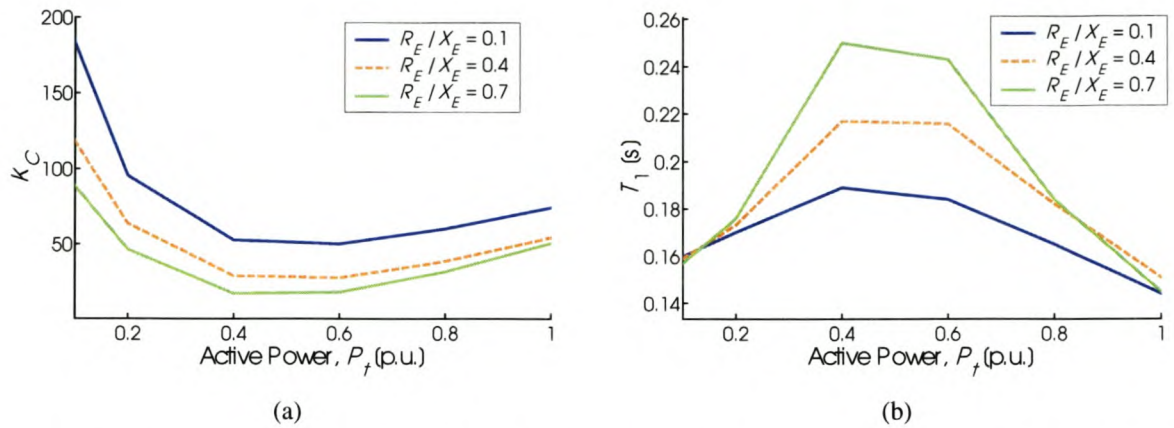

Fig. F.23: PSS gain and time constant T_1 vs. machine load and line resistance, with X_E = 0.8 p.u. and K_A = 20

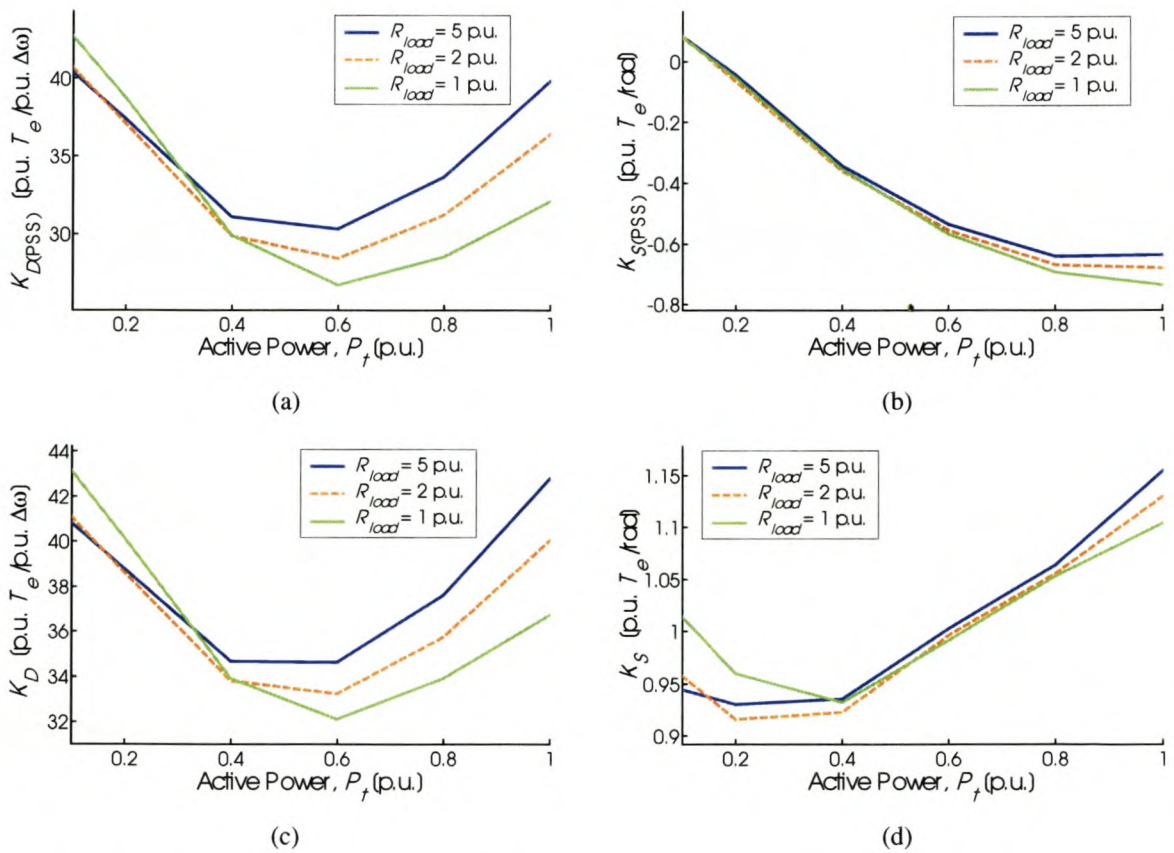

Fig. F.24: PSS and system torque coefficients vs. machine load and local load resistance, with X_{line} = 0.2 p.u. and K_A = 20

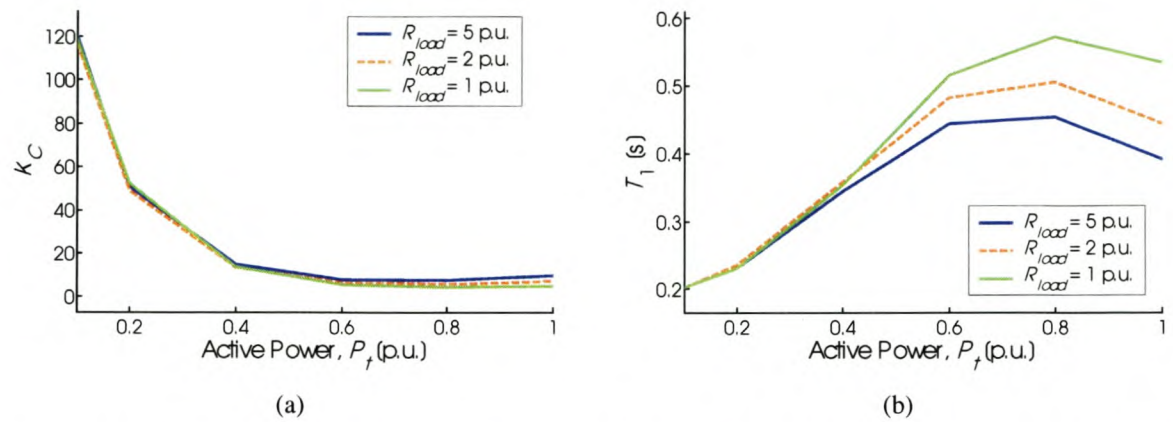

Fig. F.25: PSS gain and time constant T_1 vs. machine load and local load resistance, with X_{line} = 0.2 p.u. and K_A = 20

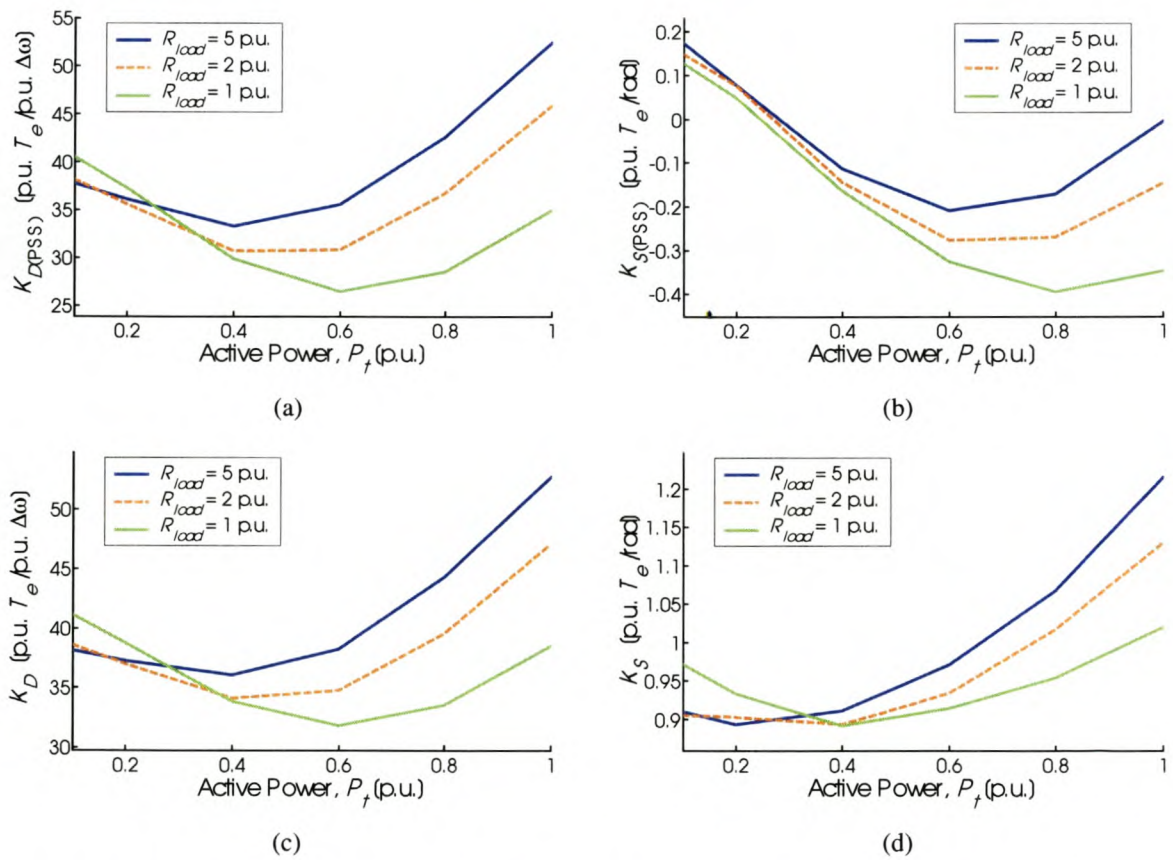

Fig. F.26: PSS and system torque coefficients vs. machine load and local load resistance, with X_{line} = 0.4 p.u. and K_A = 20

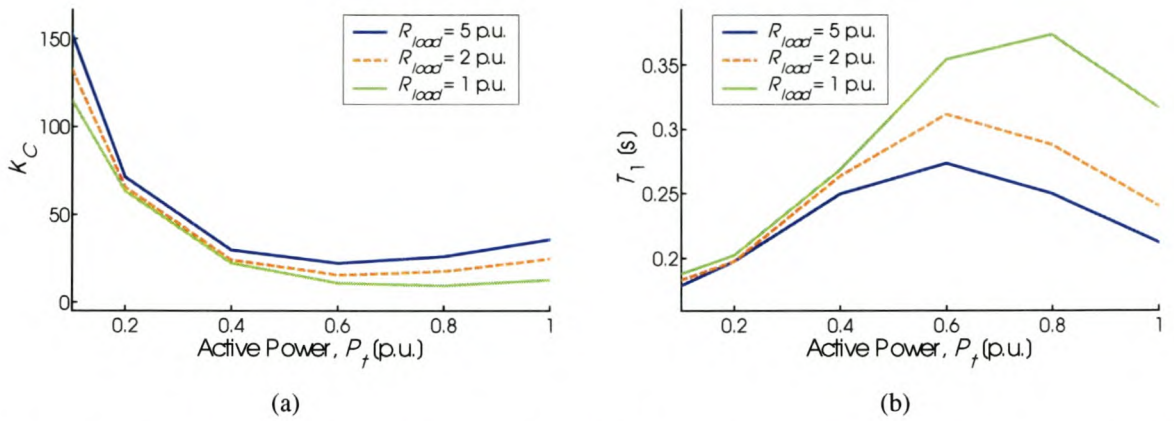

Fig. F.27: PSS gain and time constant T_1 vs. machine load and local load resistance, with X_{line} = 0.4 p.u. and K_A = 20

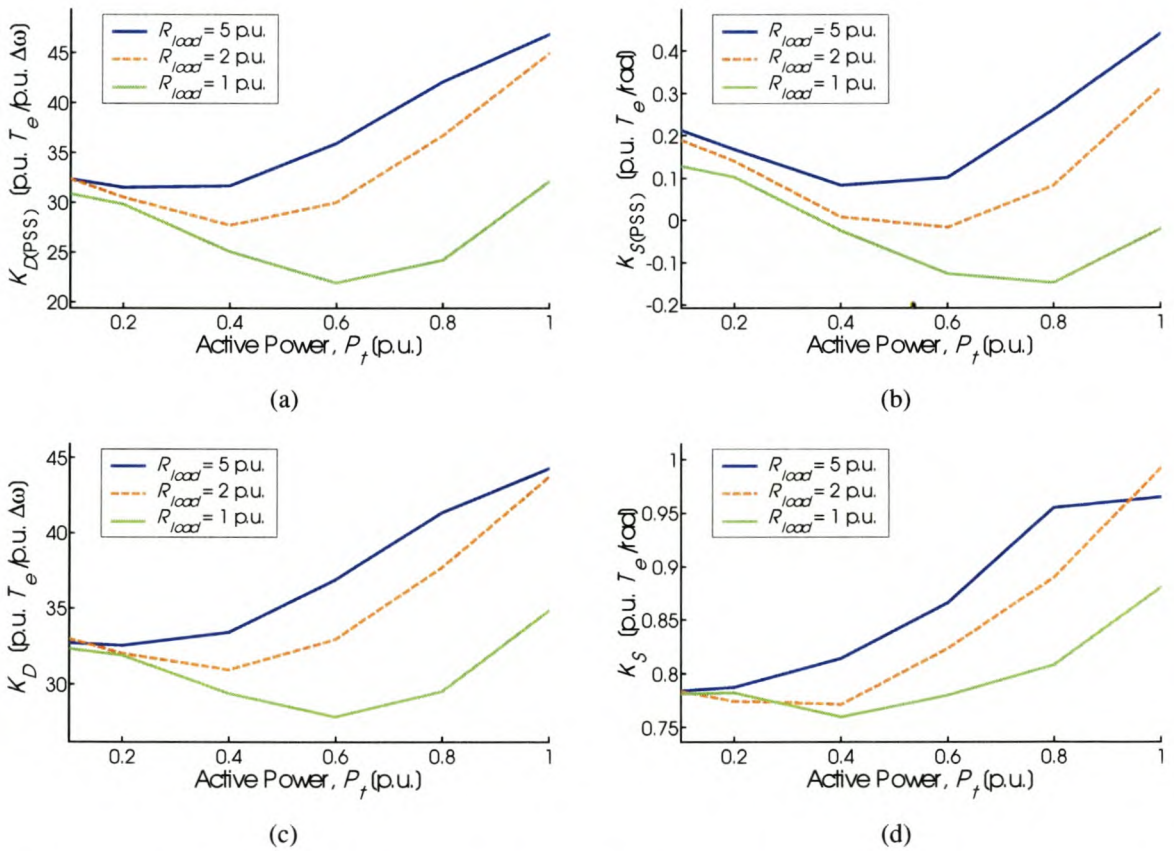

Fig. F.28: PSS and system torque coefficients vs. machine load and local load resistance, with X_{line} = 0.8 p.u. and K_A = 20

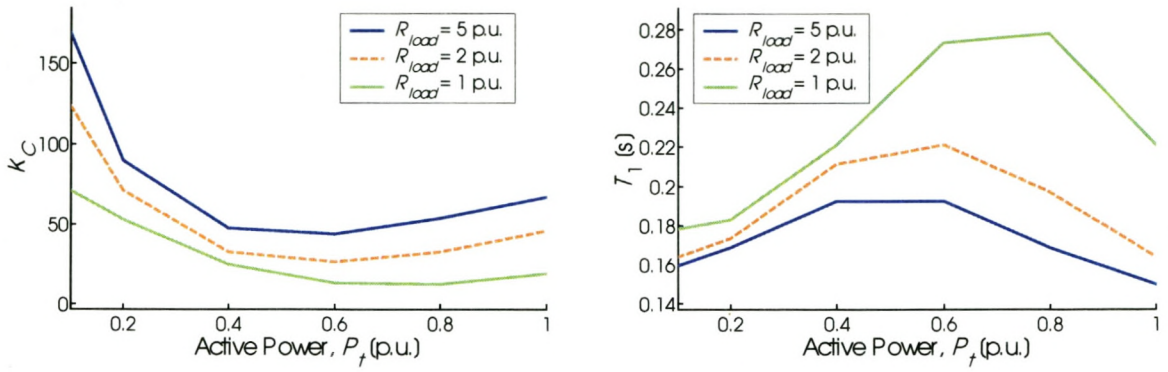

Fig. F.29: PSS gain and time constant T_1 vs. machine load and local load resistance, with X_{line} = 0.8 p.u. and K_A = 20

F.5 Results of Section 4.6.6 – Influence of Saturation

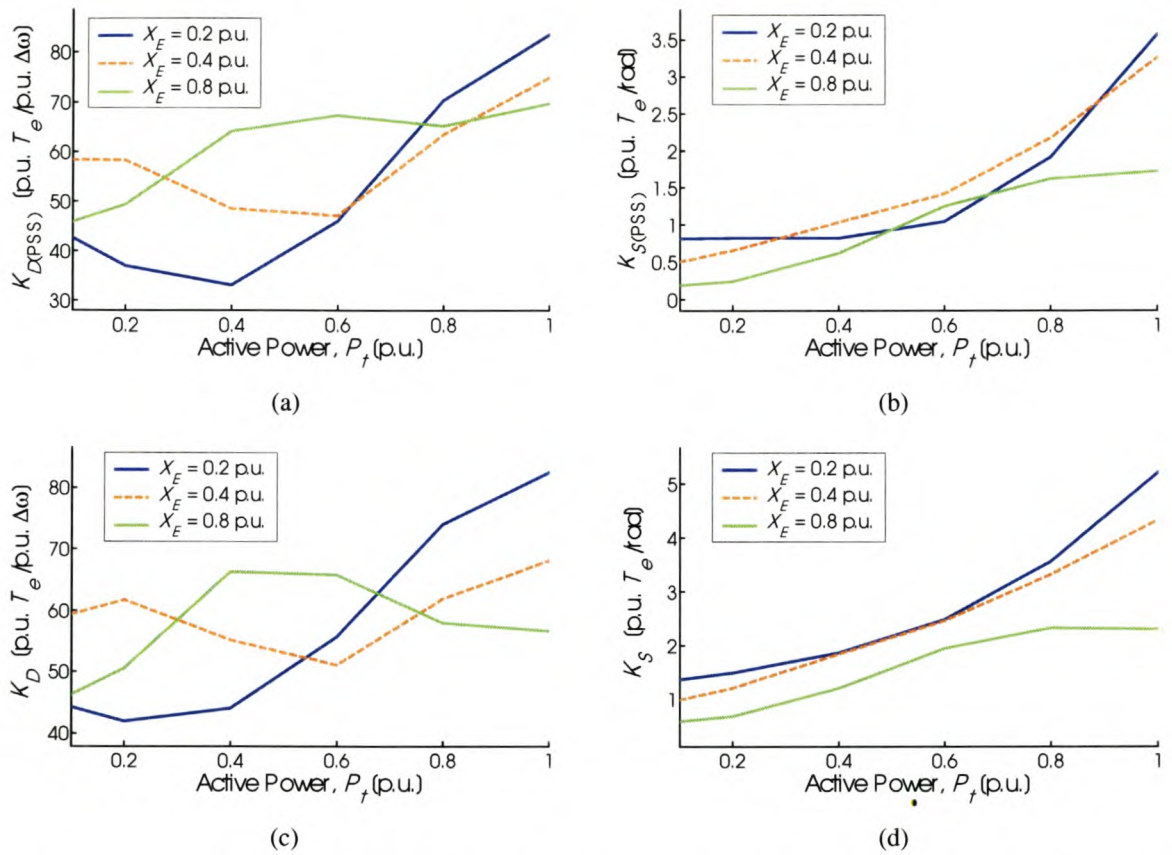

Fig. F.30: PSS and system torque coefficients vs. machine load and external reactance; saturation effect neglected

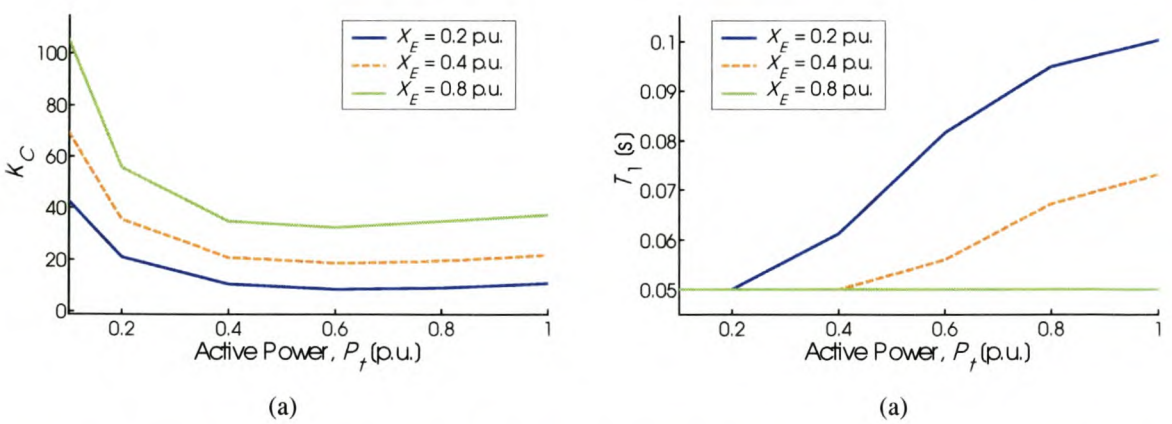

Fig F.31: Optimised PSS parameters K_C and T_1 vs. machine load and external reactance; saturation effect neglected

G SIMULATION RESULTS OF CHAPTER 5 – CSC

G.1 Results of Section 5.5.3 – Line Resistance

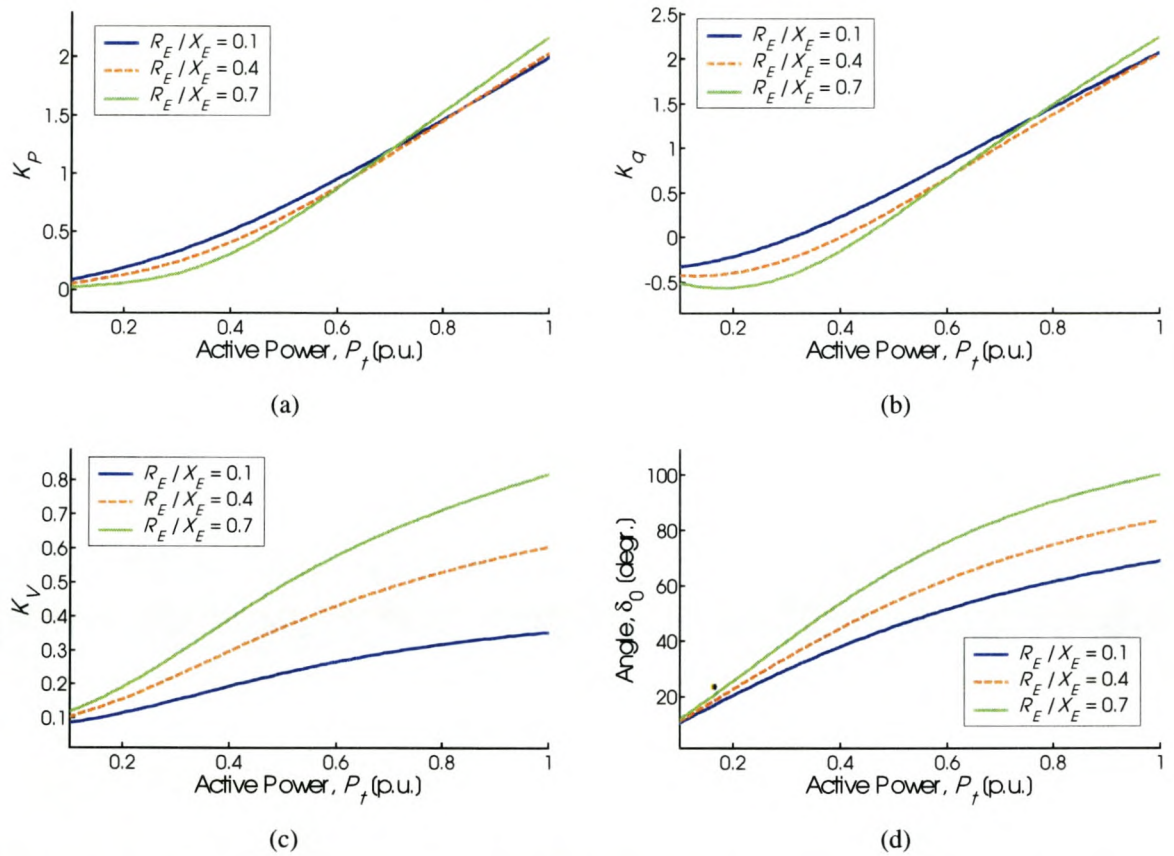

Fig. G.1: Parameters K_P, K_q, K_V and rotor angle δ_0 vs. machine load and line resistance, with $X_E = 0.2$ p.u.

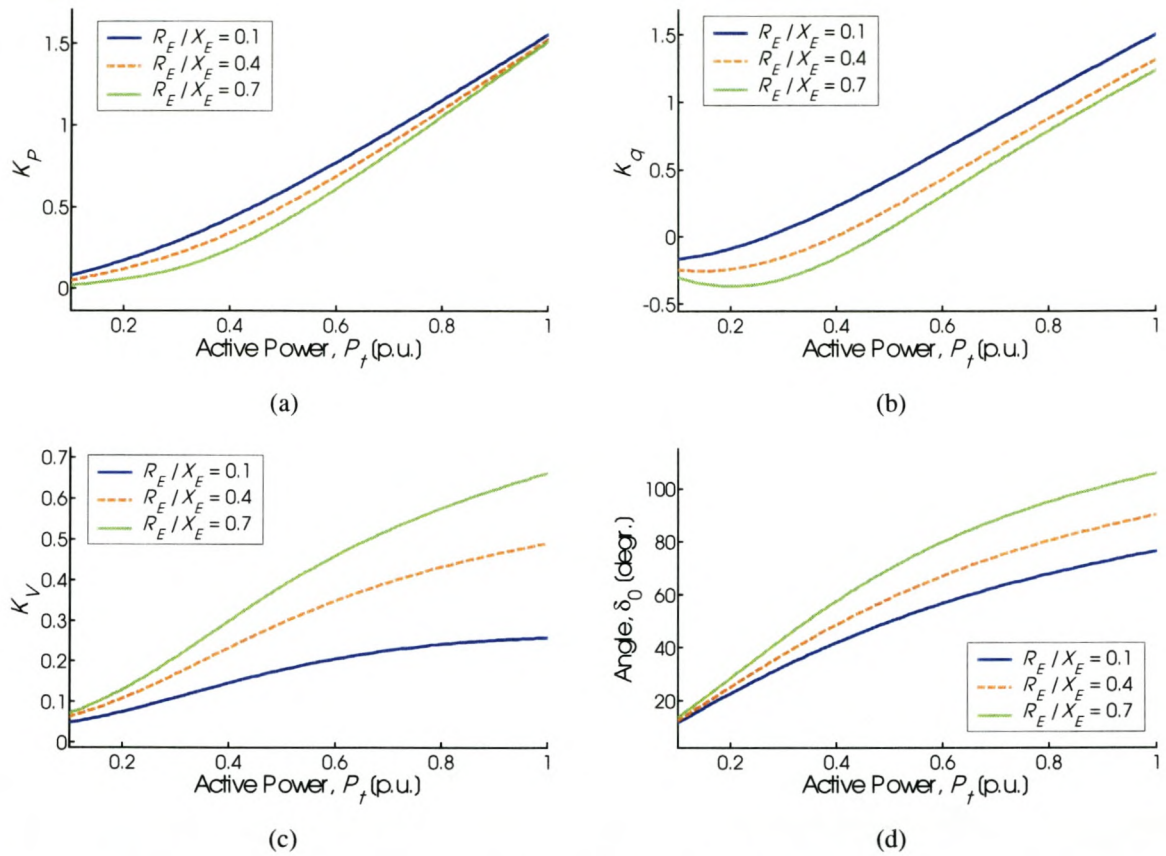

Fig. G.2: Parameters K_P, K_q, K_V and rotor angle δ_0 vs. machine load and line resistance, with $X_E = 0.4$ p.u.

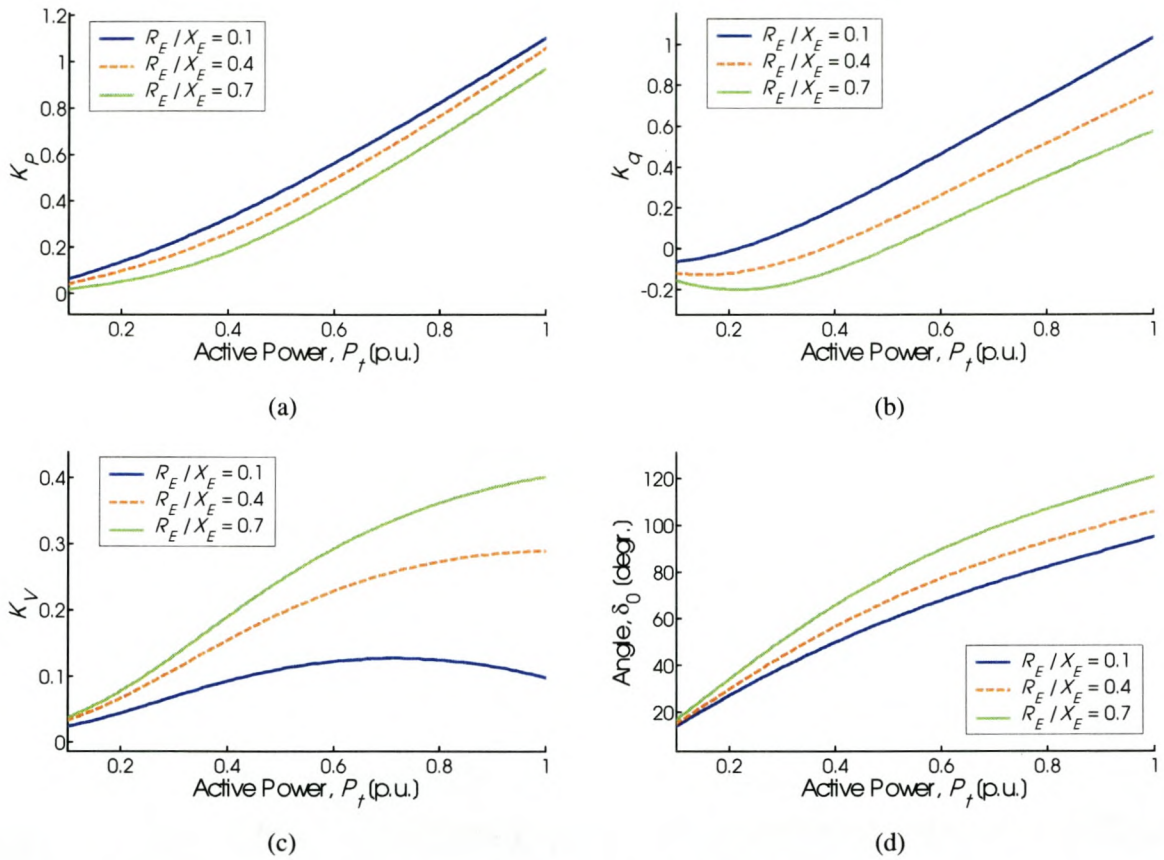

Fig. G.3: Parameters K_P, K_q, K_V and rotor angle δ_0 vs. machine load and line resistance, with $X_E = 0.8$ p.u.

G.2 Results of Section 5.5.4 –Local Load

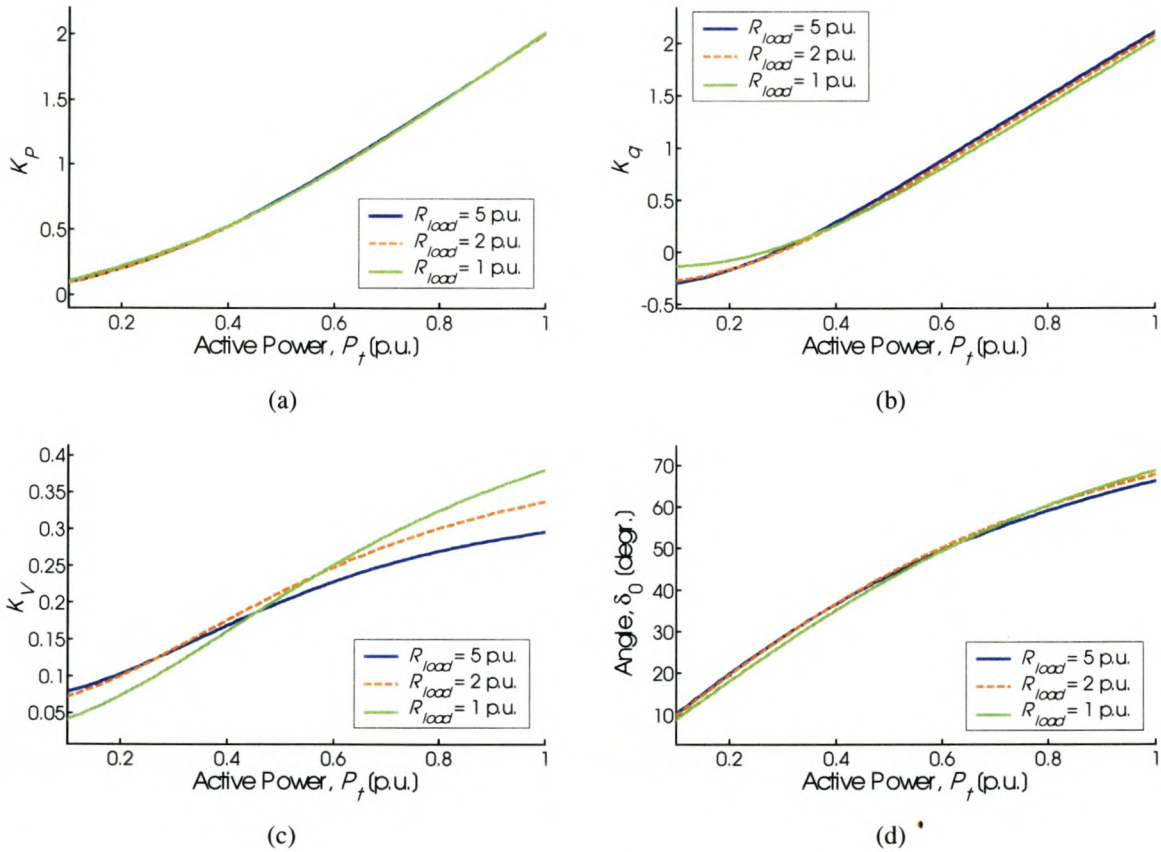

Fig. G.4: Parameters K_P, K_q, K_V and rotor angle δ_0 vs. machine load and local load resistance, with X_{line} = 0.2 p.u.

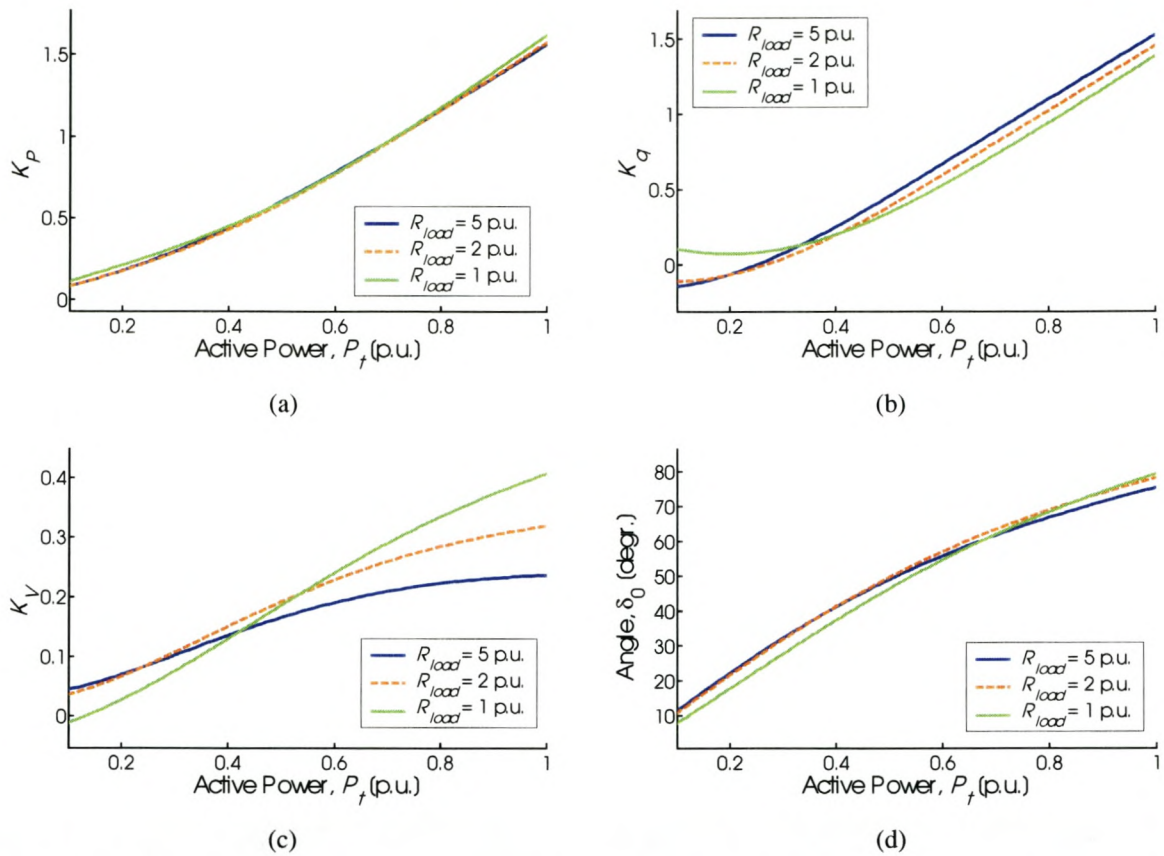

Fig. G.5: Parameters K_P, K_q, K_V and rotor angle δ_0 vs. machine load and local load resistance, with X_{line} = 0.4 p.u.

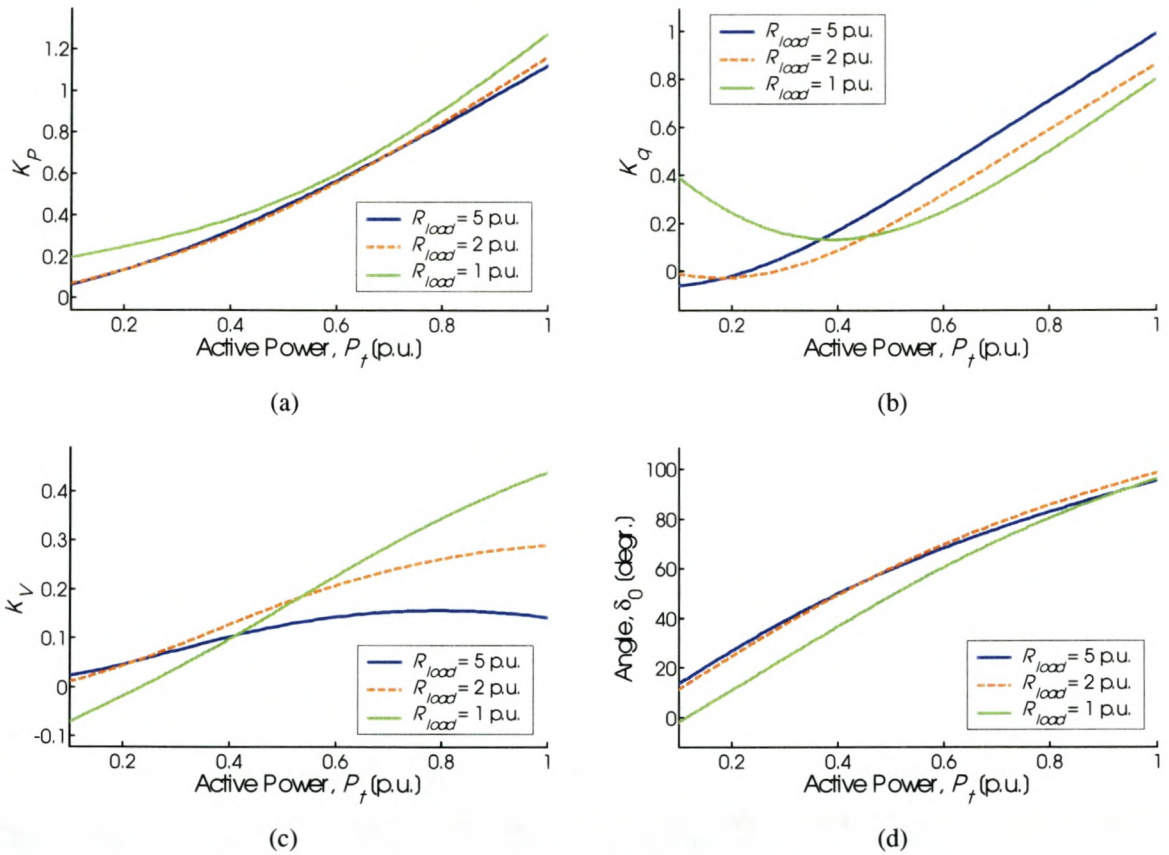

Fig. G.6: Parameters K_P, K_q, K_V and rotor angle δ_0 vs. machine load and local load resistance, with X_{line} = 0.8 p.u.

G.3 Results of Section 5.5.5 – Influence of Saturation

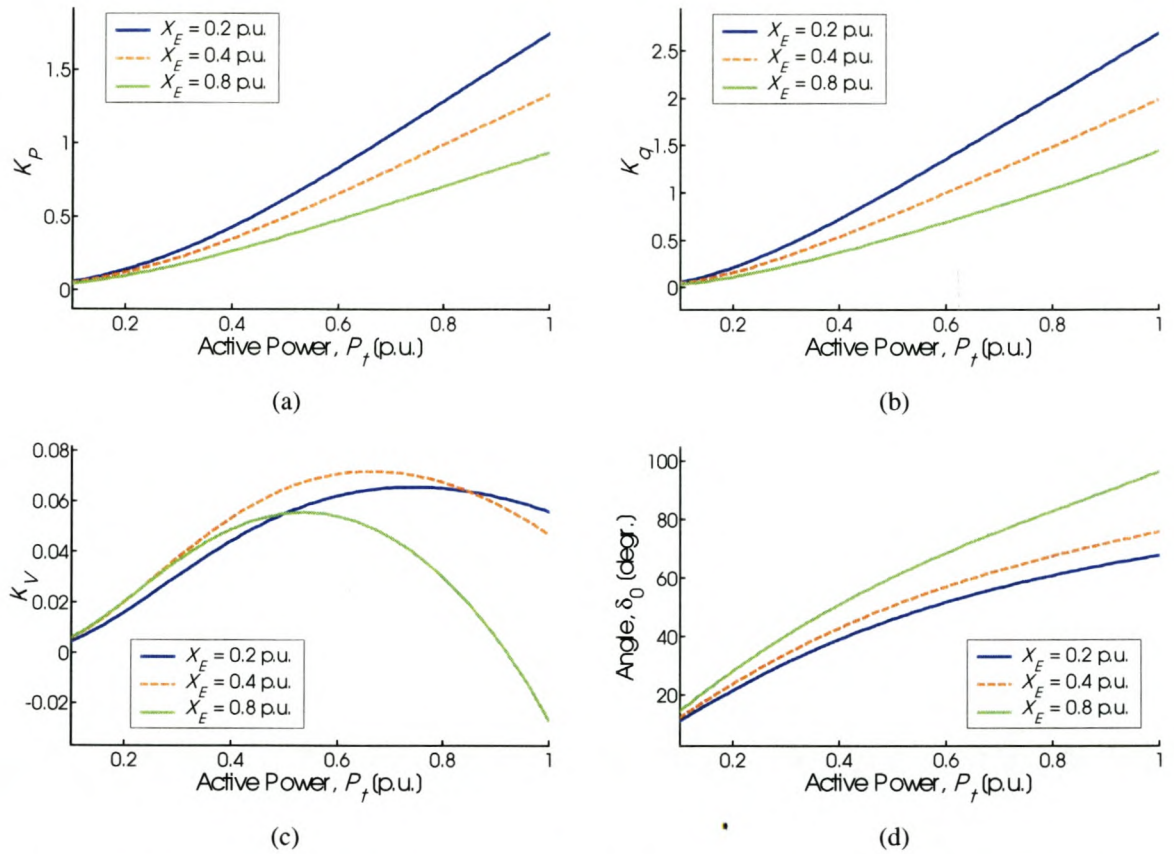

Fig. G.7: Parameters K_P, K_q, K_V and rotor angle δ_0 vs. machine load and external reactance; saturation not modelled

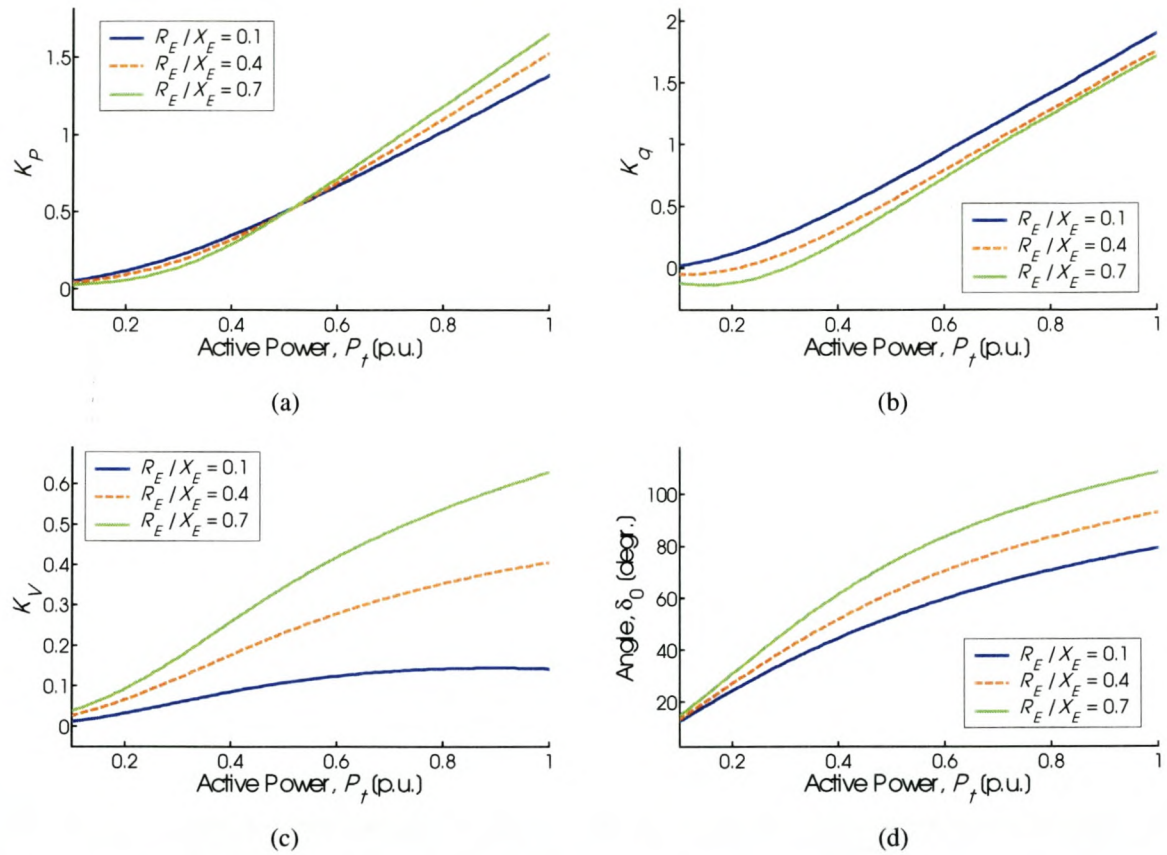

Fig. G.8: Parameters K_P, K_q, K_V and rotor angle δ_0 vs. machine load and line resistance, with $X_E = 0.4$ p.u.; saturation not modelled

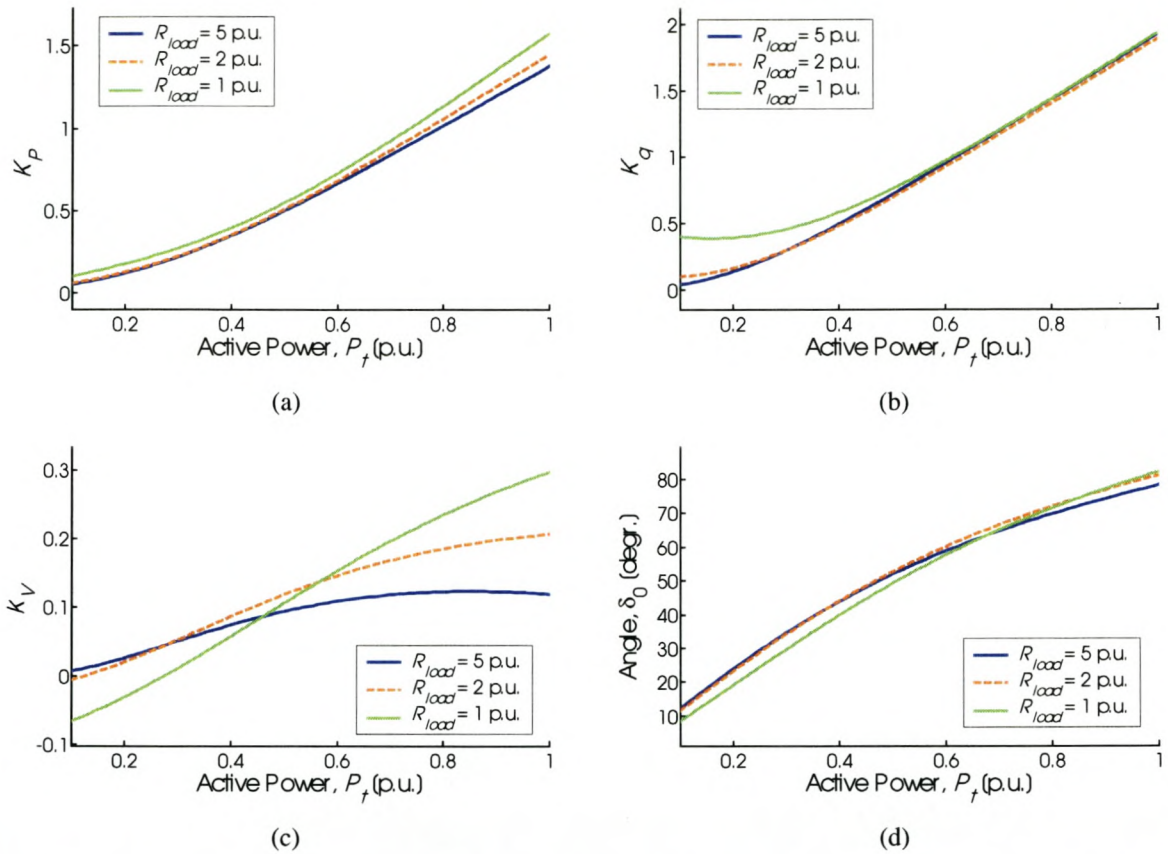

Fig. G.9: Parameters K_P, K_q, K_V and rotor angle δ_0 vs. machine load and local load resistance, with X_{line} = 0.4 p.u.; saturation not modelled

G.4 Results of Section 5.7.2 – CSC Controller Design

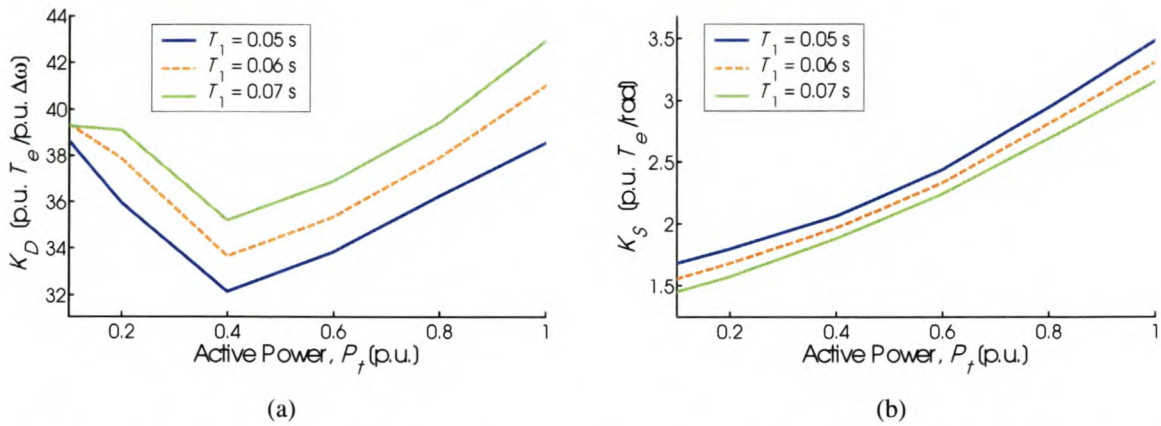

Fig. G.10: System torques vs. machine load and CSC controller time constant T_1, with X_E = 0.2 p.u.

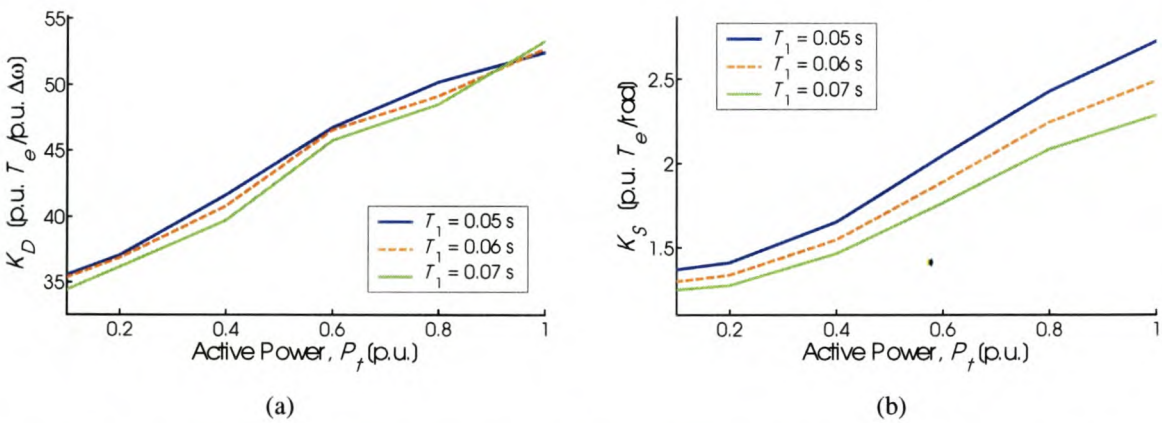

Fig. G.11: System torques vs. machine load and CSC controller time constant T_1, with X_E = 0.4 p.u.

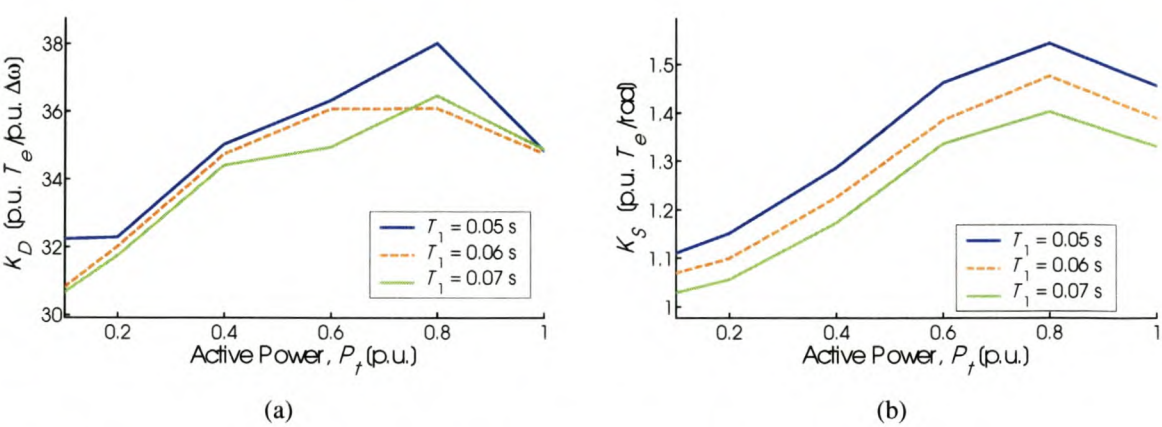

Fig. G.12: System torques vs. machine load and CSC controller time constant T_1, with X_E = 0.8 p.u.

G.5 Results of Section 5.8.3 – Line Resistance

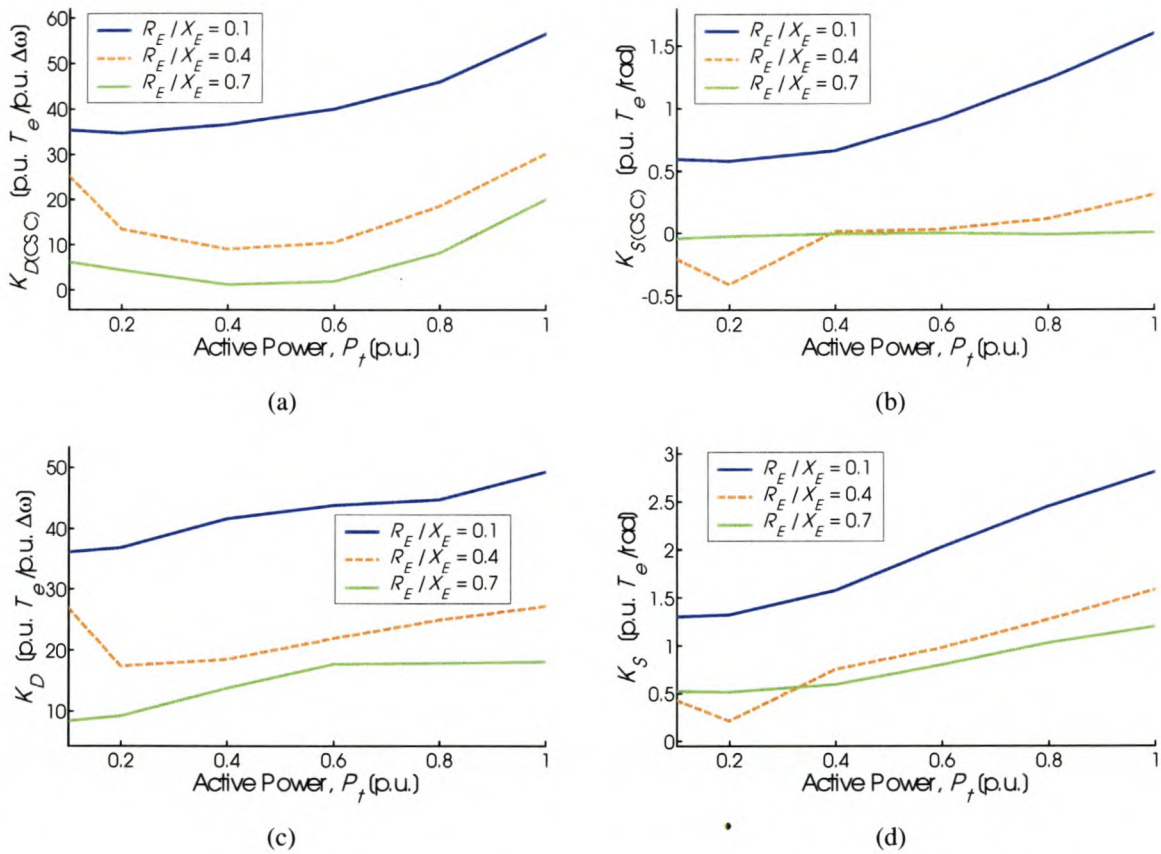

Fig. G.13: CSC and system torque coefficients vs. machine load and line resistance, with $X_E = 0.4$ p.u.

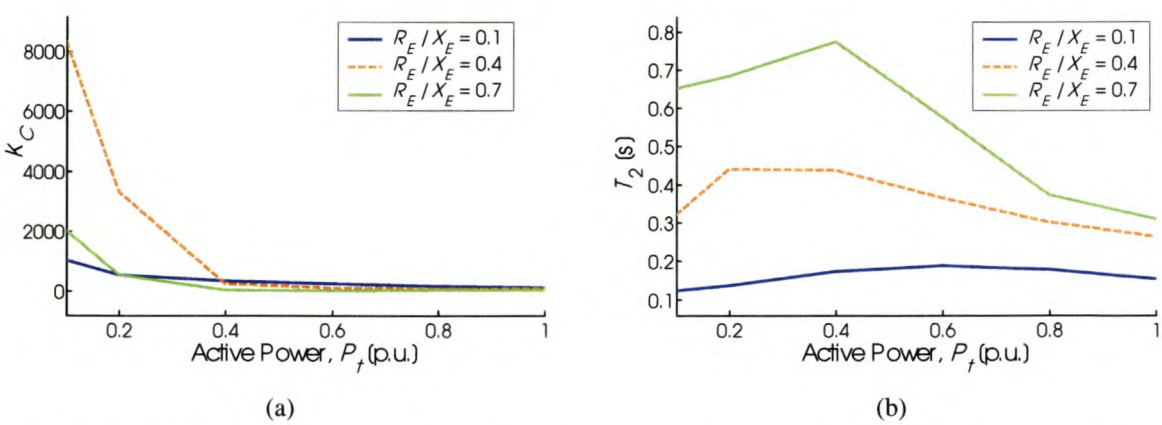

Fig. G.14: CSC gain and time constant T_2 vs. machine load and line resistance, with $X_E = 0.4$ p.u.

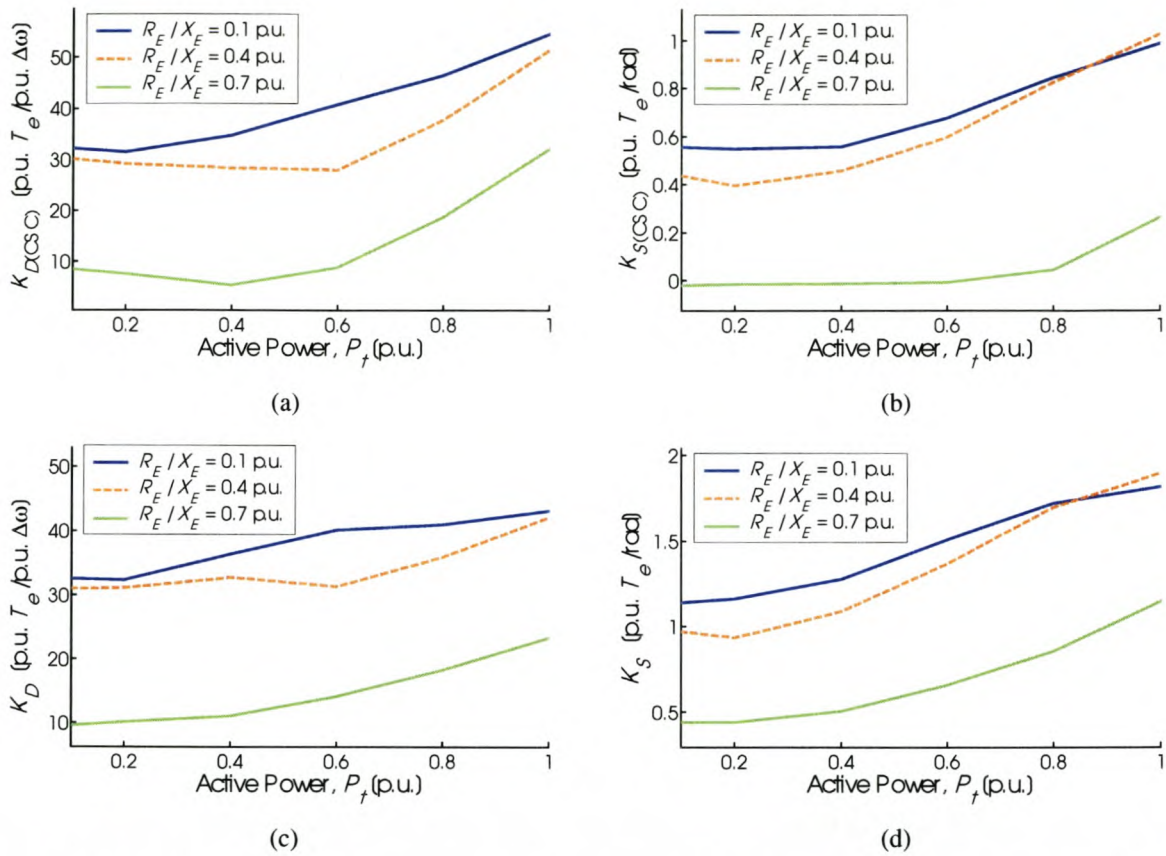

Fig. G.15: CSC and system torque coefficients vs. machine load and line resistance, with X_E = 0.8 p.u.

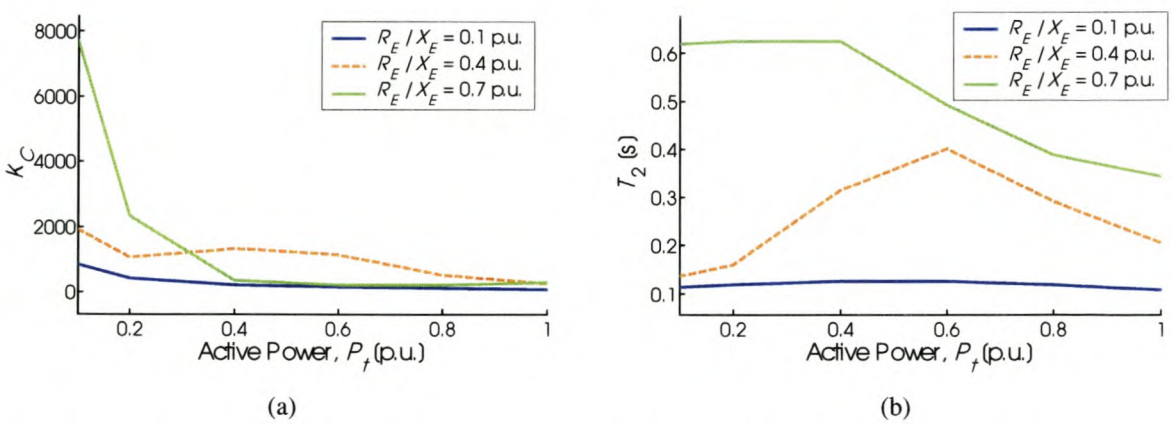

Fig. G.16: CSC gain and time constant T_2 vs. machine load and line resistance, with X_E = 0.8 p.u.

G.6 Results of Section 5.8.4 – Local Load

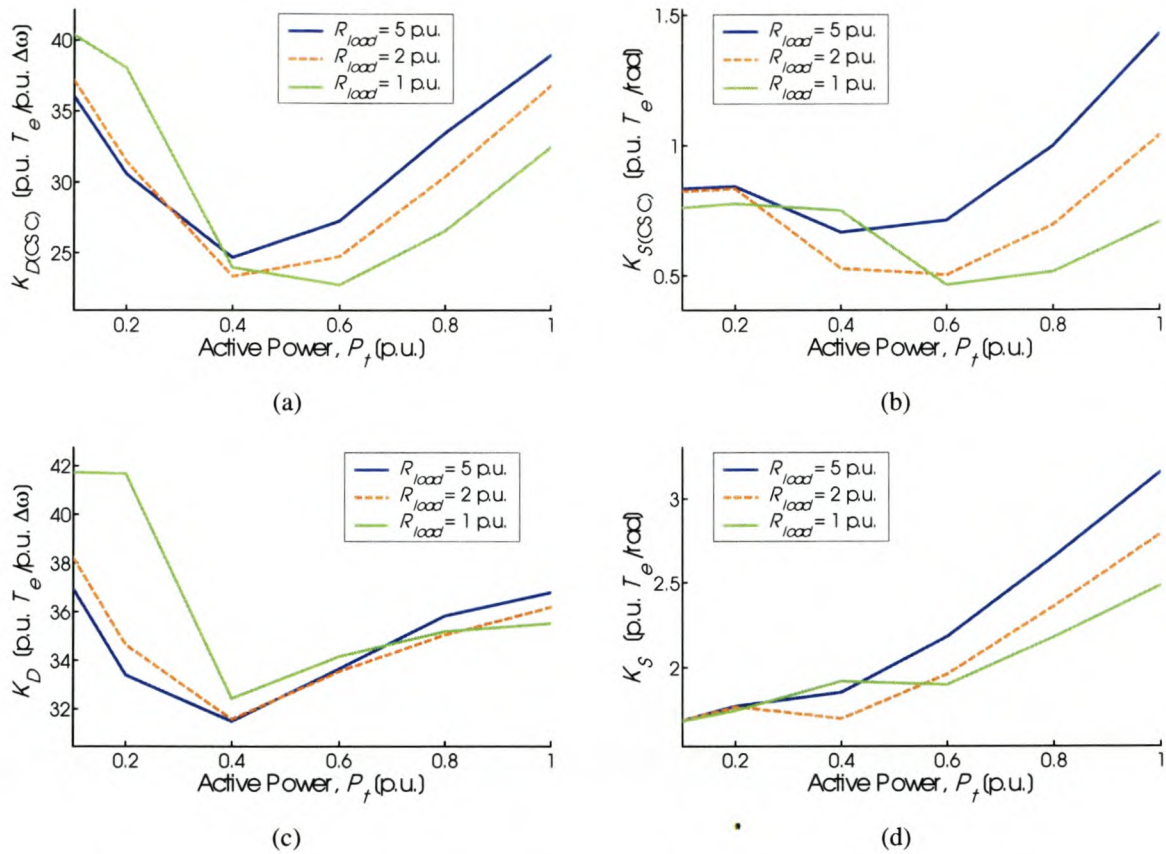

Fig. G.17: CSC and system torque coefficients vs. machine load and local load resistance, with X_{line} = 0.2 p.u.

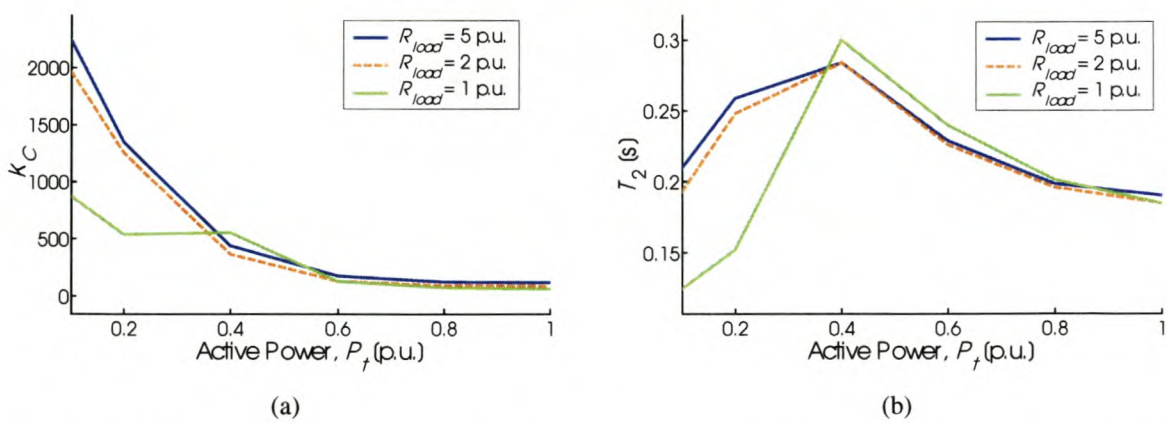

Fig. G.18: CSC gain and time constant T_2 vs. machine load and local load resistance, with X_{line} = 0.2 p.u.

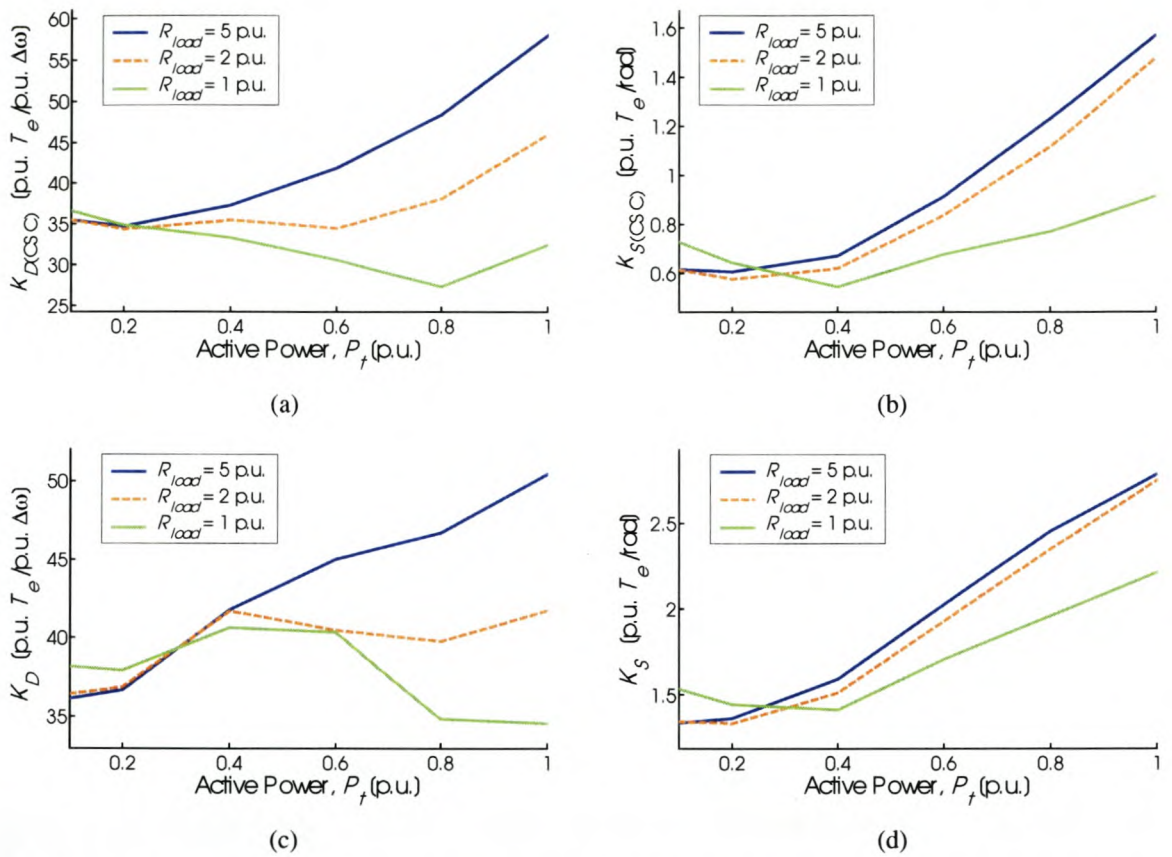

Fig. G.19: CSC and system torque coefficients vs. machine load and local load resistance, with X_{line} = 0.4 p.u.

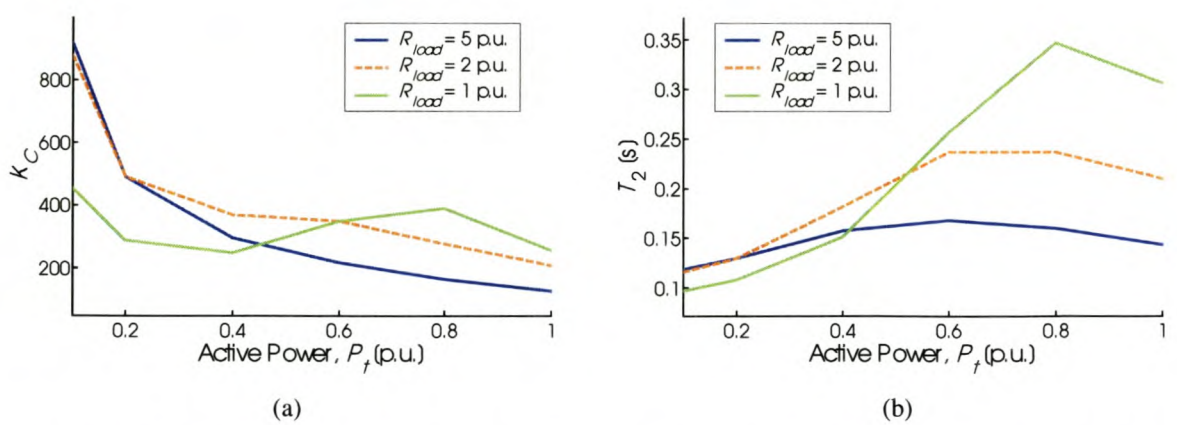

Fig. G.20: CSC gain and time constant T_2 vs. machine load and local load resistance, with X_{line} = 0.4 p.u.

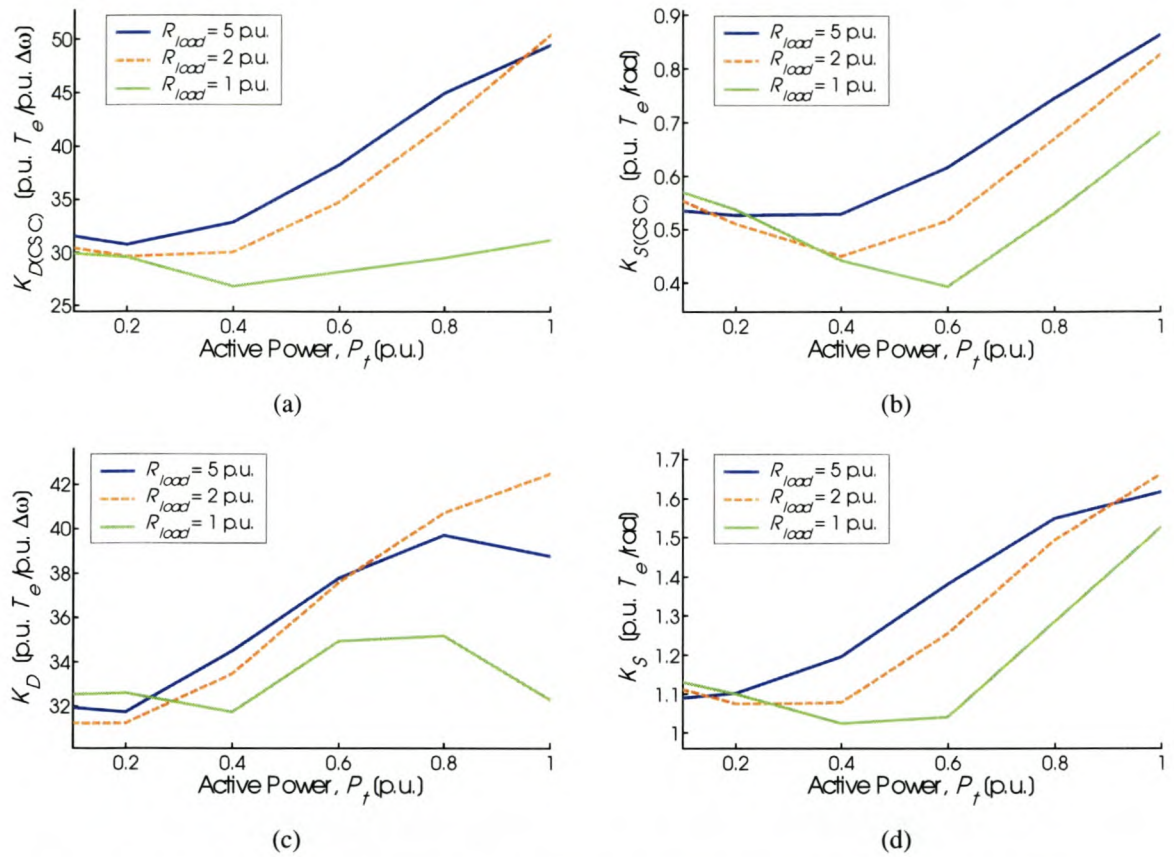

Fig. G.21: CSC and system torque coefficients vs. machine load and local load resistance, with X_{line} = 0.8 p.u.

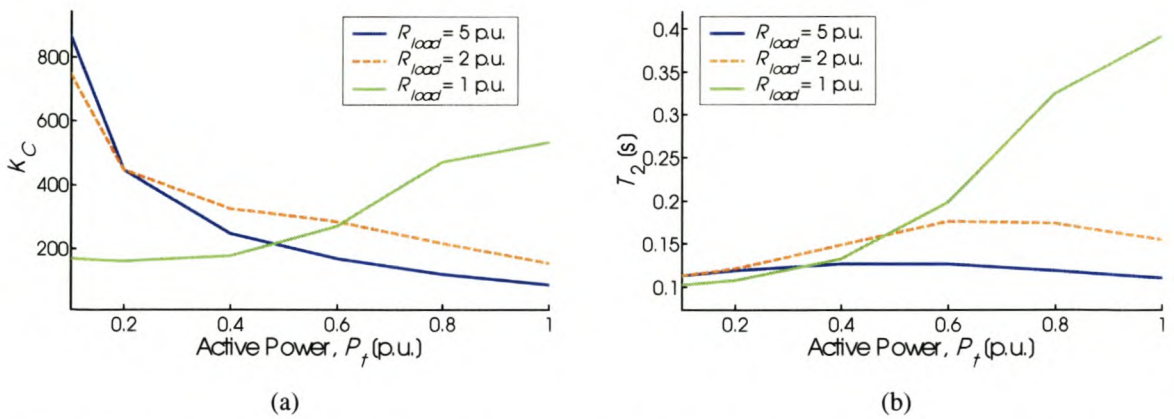

Fig. G.22: CSC gain and time constant T_2 vs. machine load and local load resistance, with X_{line} = 0.8 p.u.

G.7 Results of Section 5.8.5 – AVR Gain

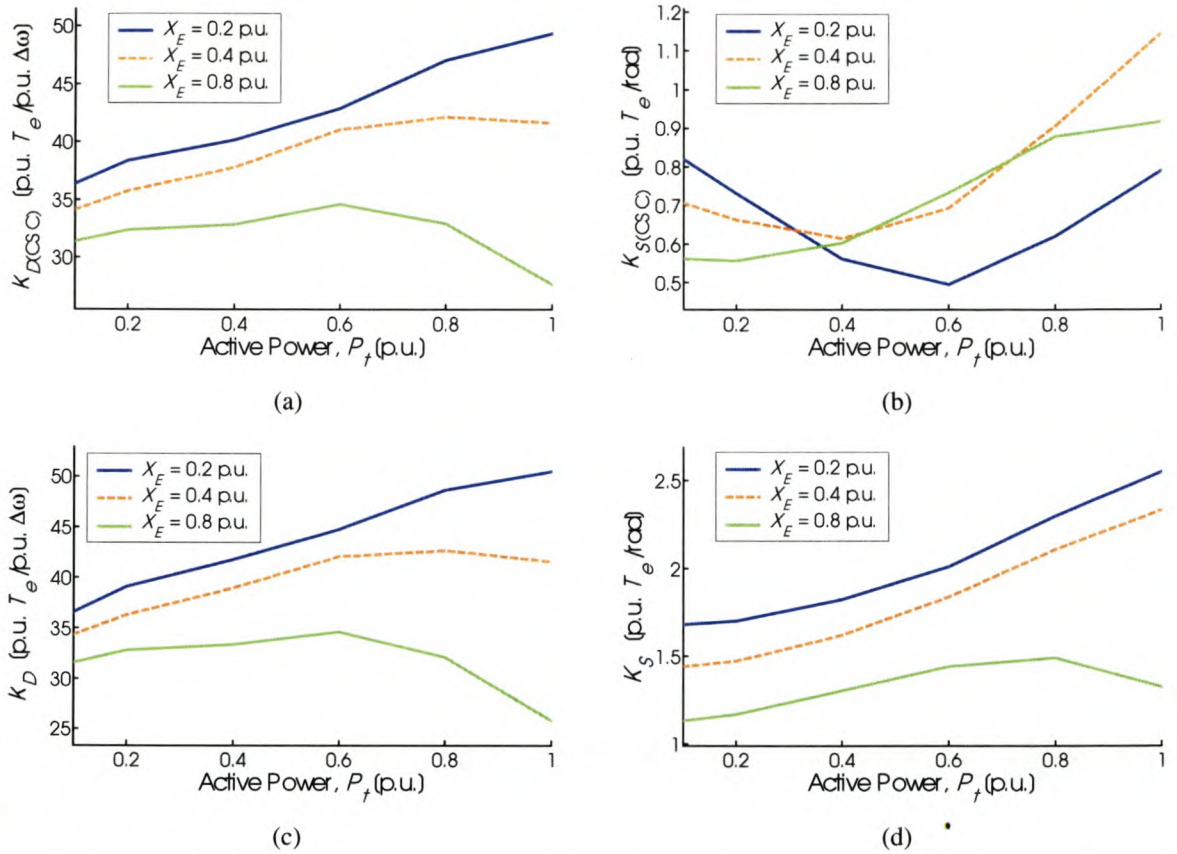

Fig. G.23: CSC and system torque coefficients vs. machine load and external reactance, with K_A = 20

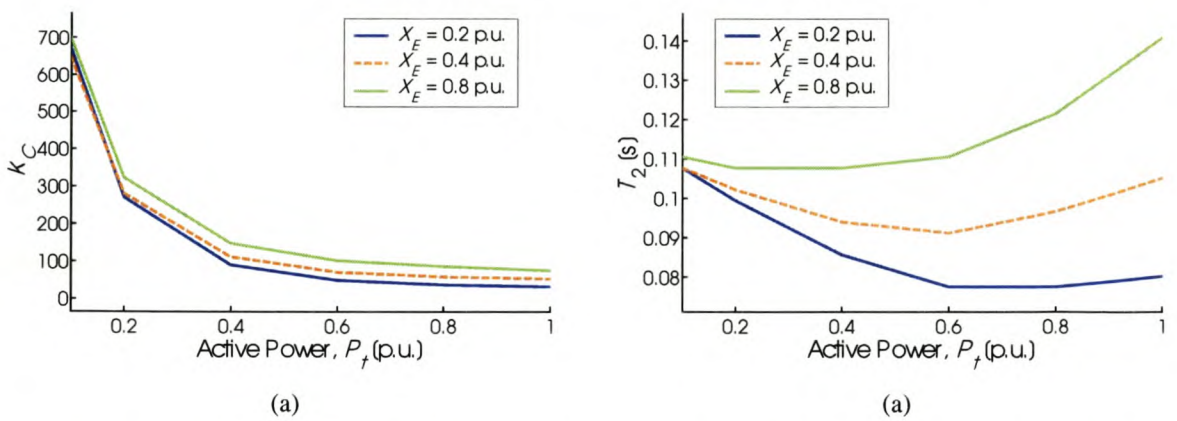

Fig G.24: Optimised CSC parameters K_C and T_2 vs. machine load and external reactance, with K_A = 20

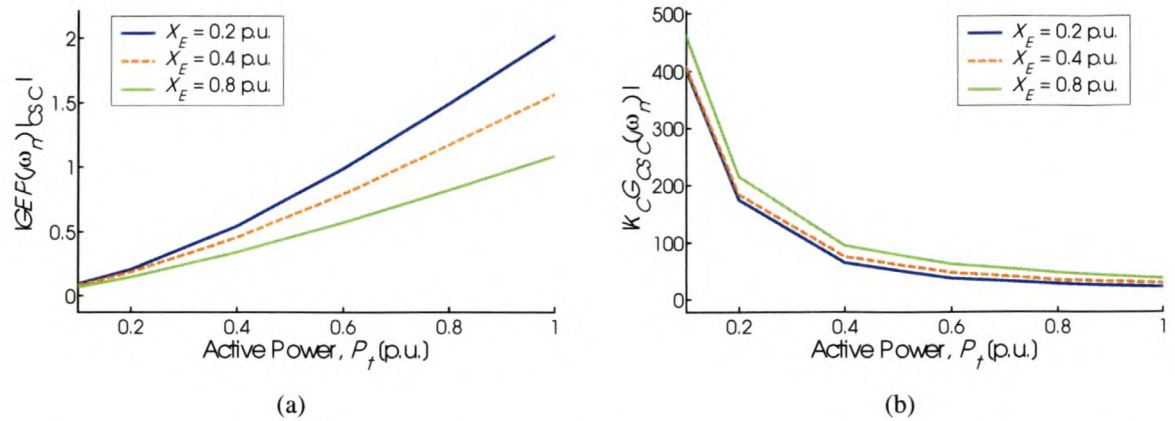

(a) (b)

Fig. G.25: "Plant" and CSC controller transfer function gains vs. machine load and external reactance, with K_A = 20

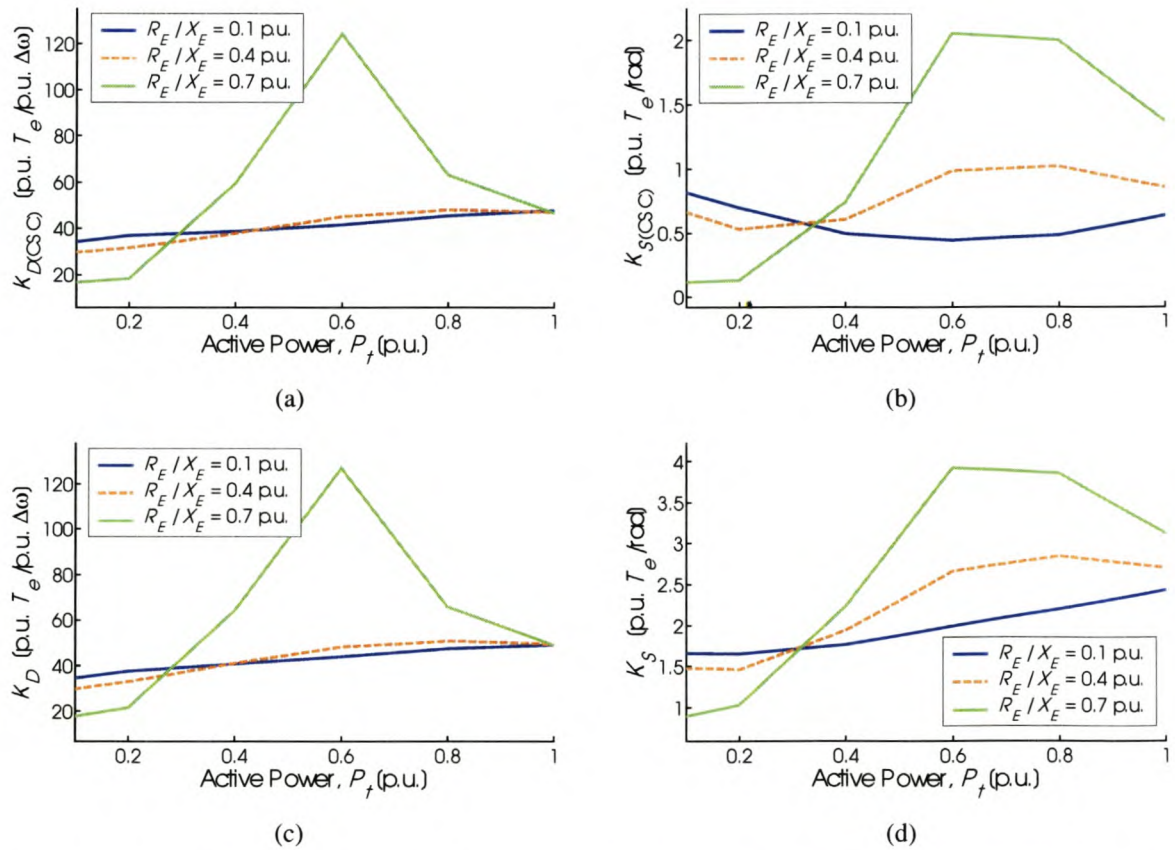

(a) (b)

(c) (d)

Fig. G.26: CSC and system torque coefficients vs. machine load and line resistance, with X_E = 0.2 p.u. and K_A = 20

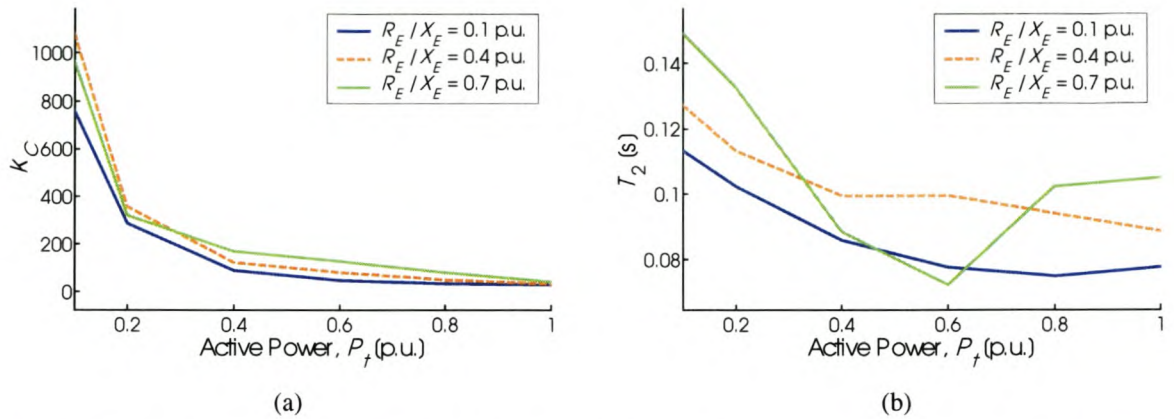

Fig. G.27: CSC gain and time constant T_2 vs. machine load and line resistance, with X_E = 0.2 p.u. and K_A = 20

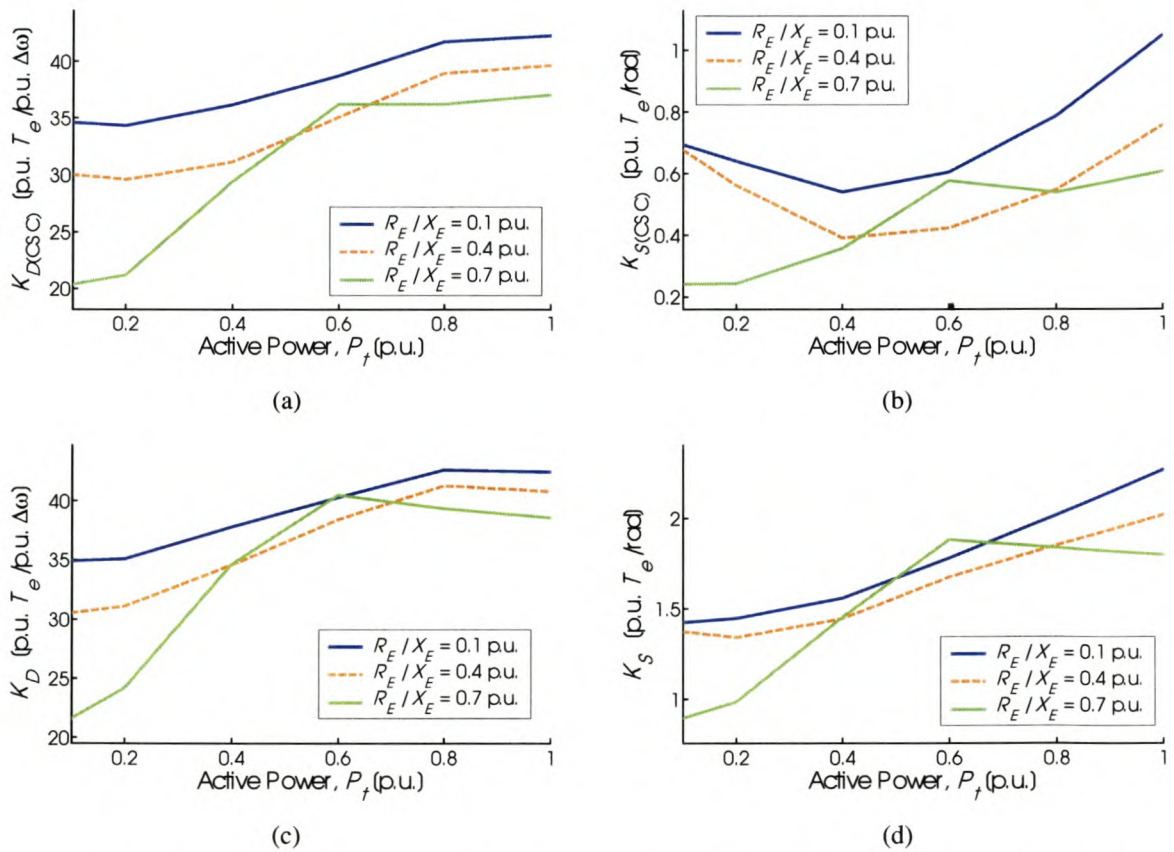

Fig. G.28: CSC and system torque coefficients vs. machine load and line resistance, with X_E = 0.4 p.u. and K_A = 20

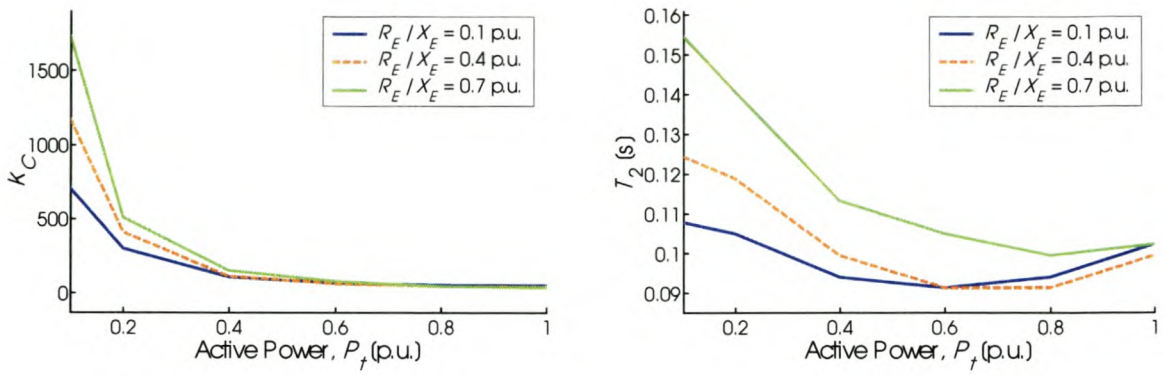

Fig. G.29: CSC gain and time constant T_2 vs. machine load and line resistance, with X_E = 0.4 p.u. and K_A = 20

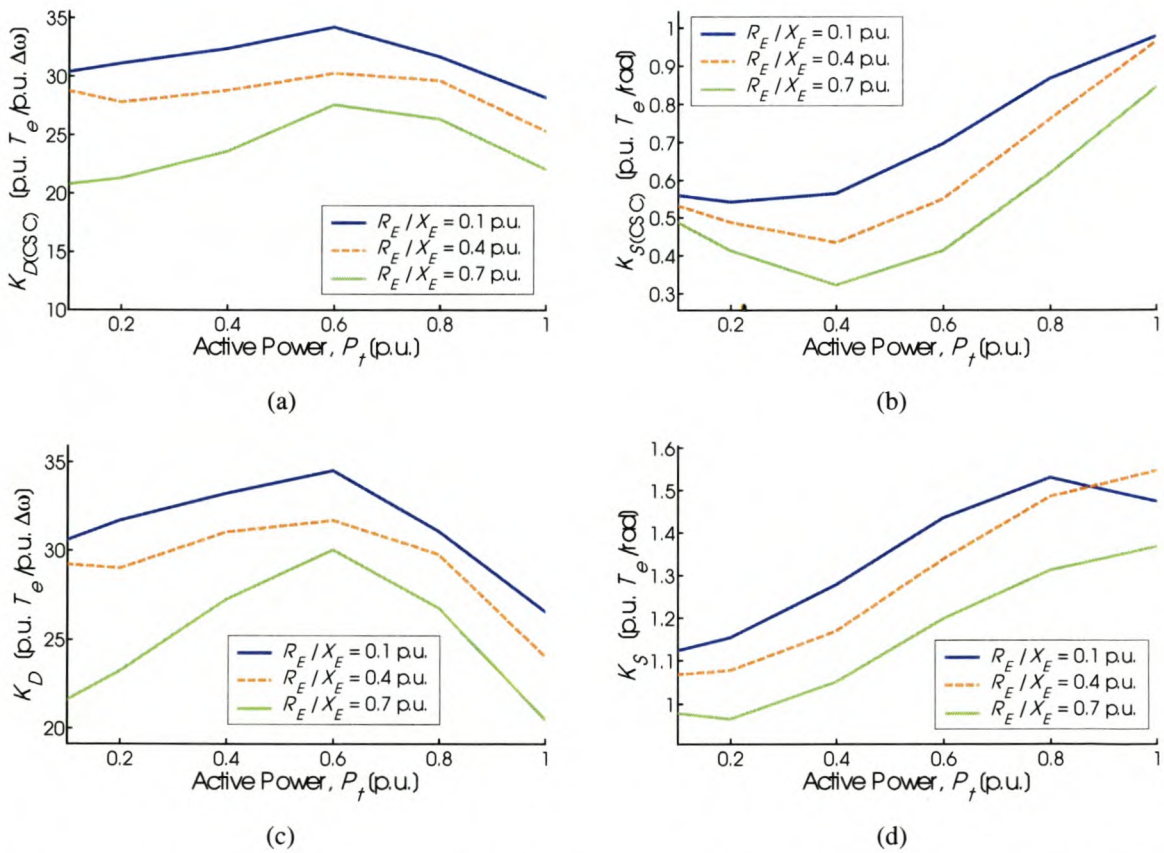

Fig. G.30: CSC and system torque coefficients vs. machine load and line resistance, with X_E = 0.8 p.u. and K_A = 20

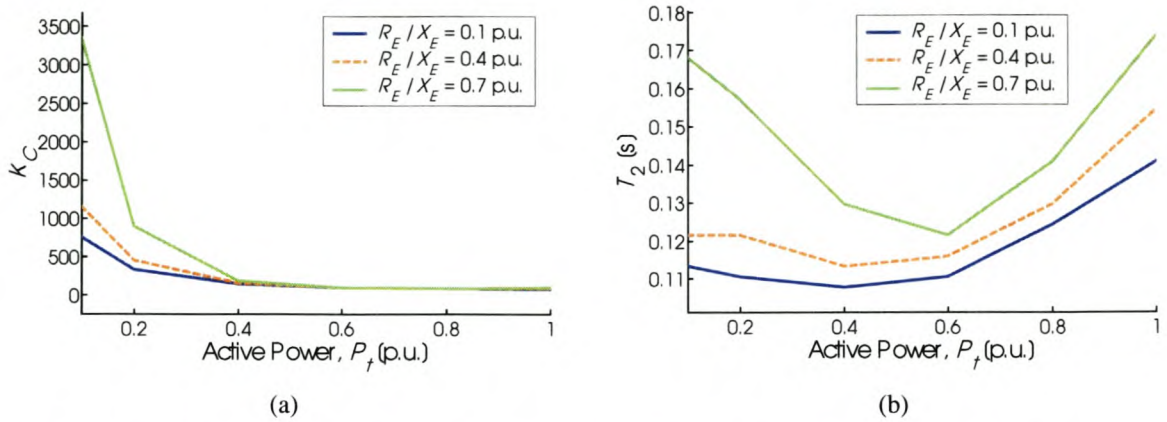

Fig. G.31: CSC gain and time constant T_2 vs. machine load and line resistance, with X_E = 0.8 p.u. and K_A = 20

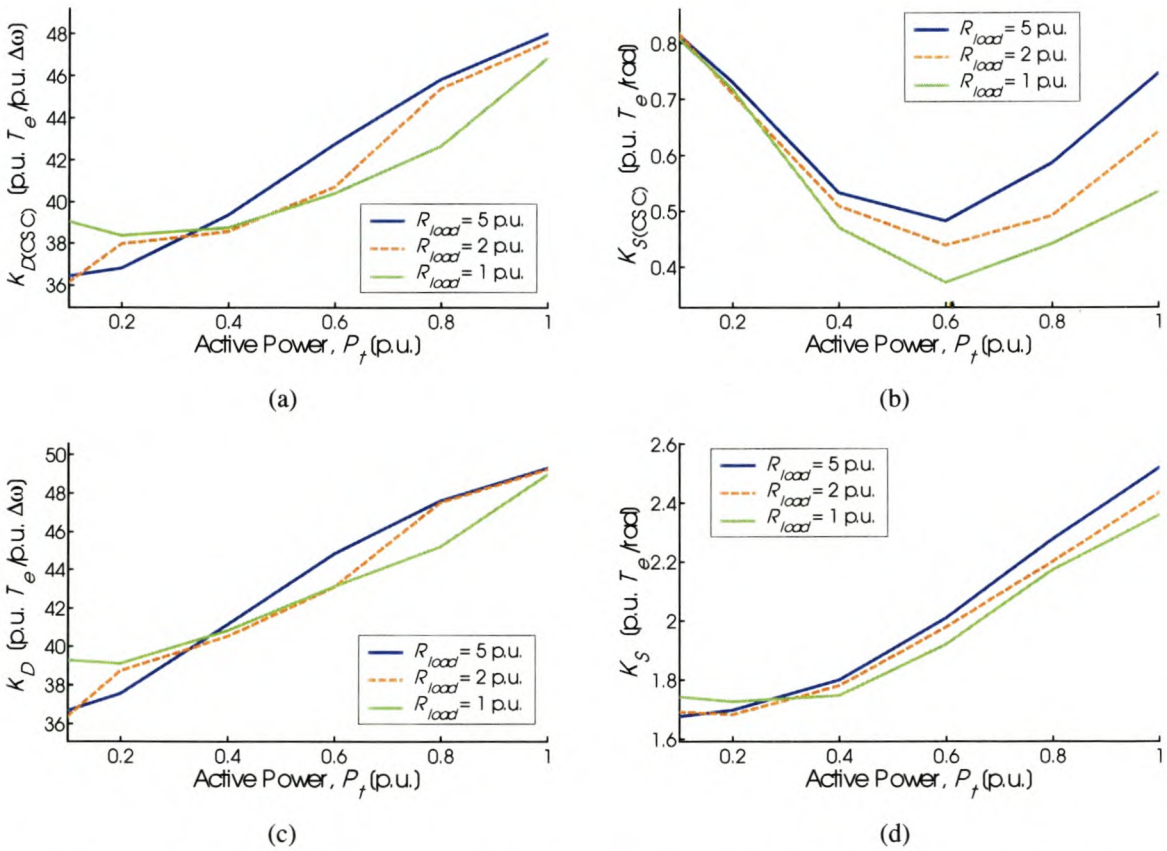

Fig. G.32: CSC and system torque coefficients vs. machine load and local load resistance, with X_{line} = 0.2 p.u. and K_A = 20

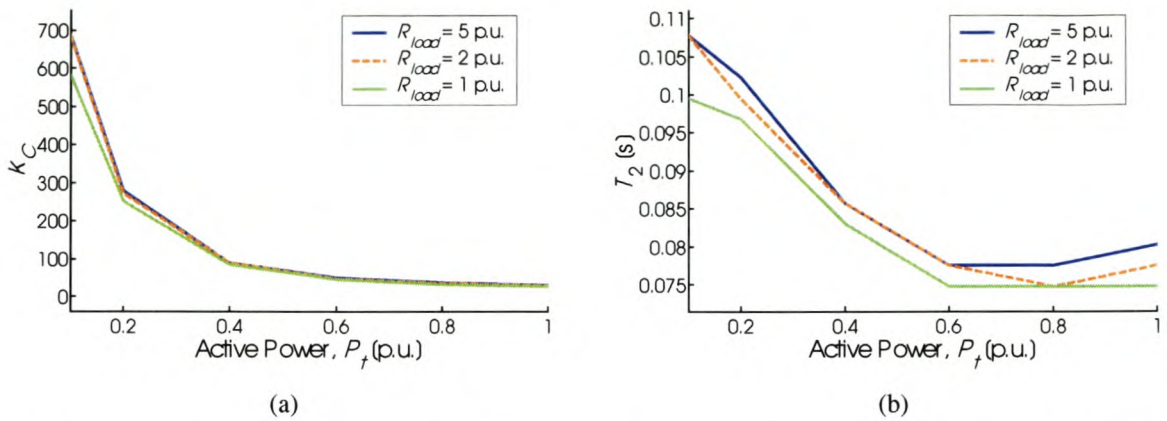

Fig. G.33: CSC gain and time constant T_2 vs. machine load and local load resistance, with X_{line} = 0.2 p.u. and K_A = 20

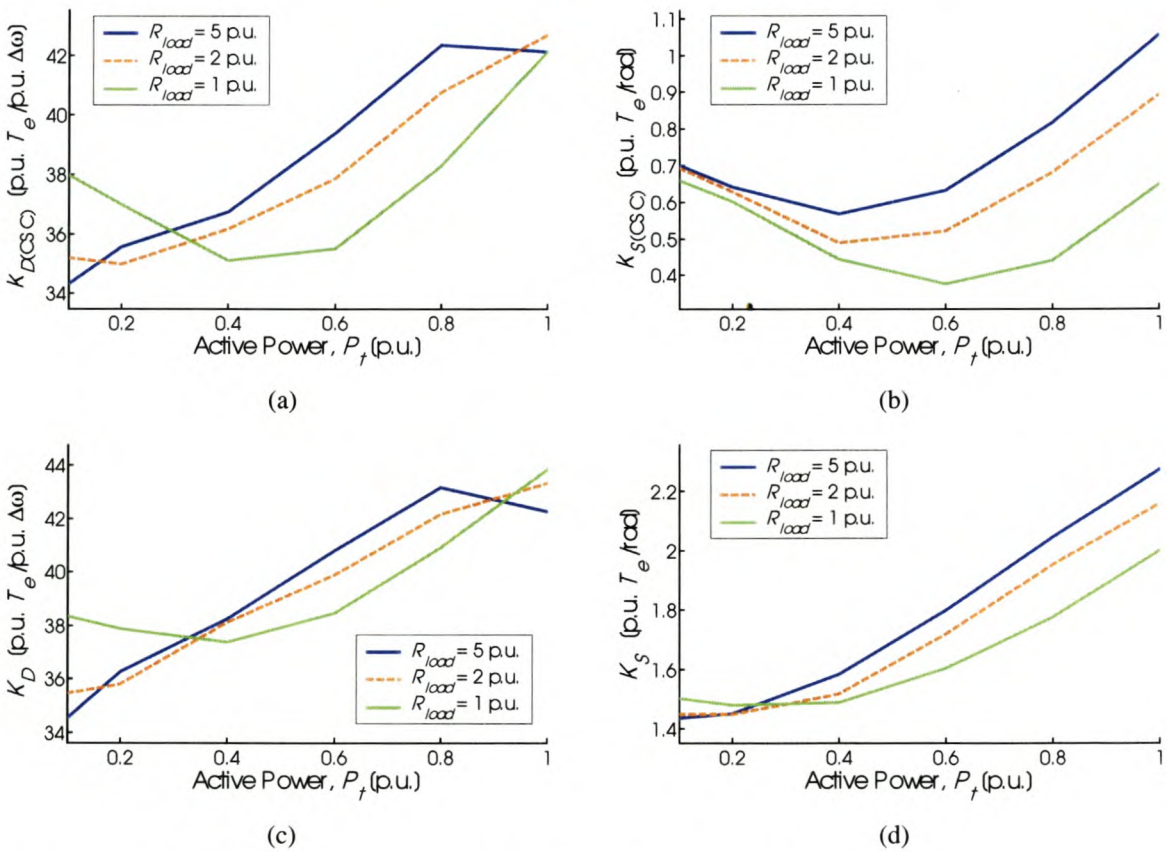

Fig. G.34: CSC and system torque coefficients vs. machine load and local load resistance, with X_{line} = 0.4 p.u. and K_A = 20

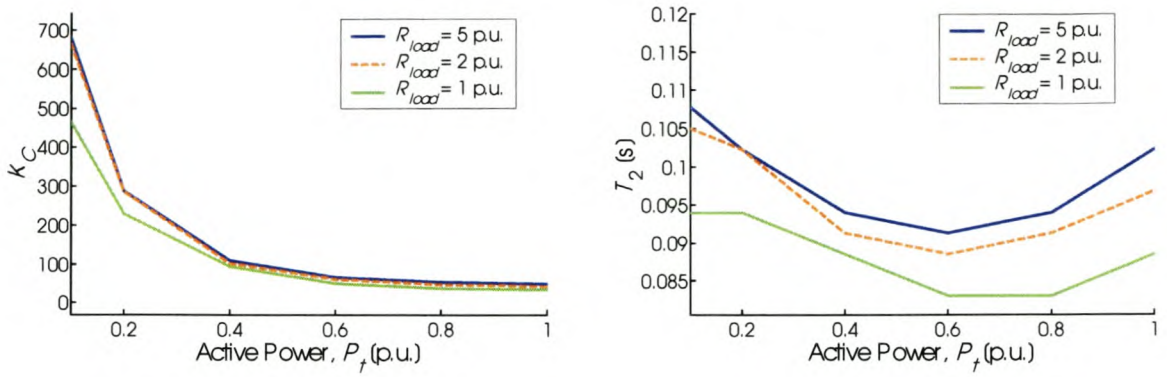

Fig. G.35: CSC gain and time constant T_2 vs. machine load and local load resistance, with X_{line} = 0.4 p.u. and K_A = 20

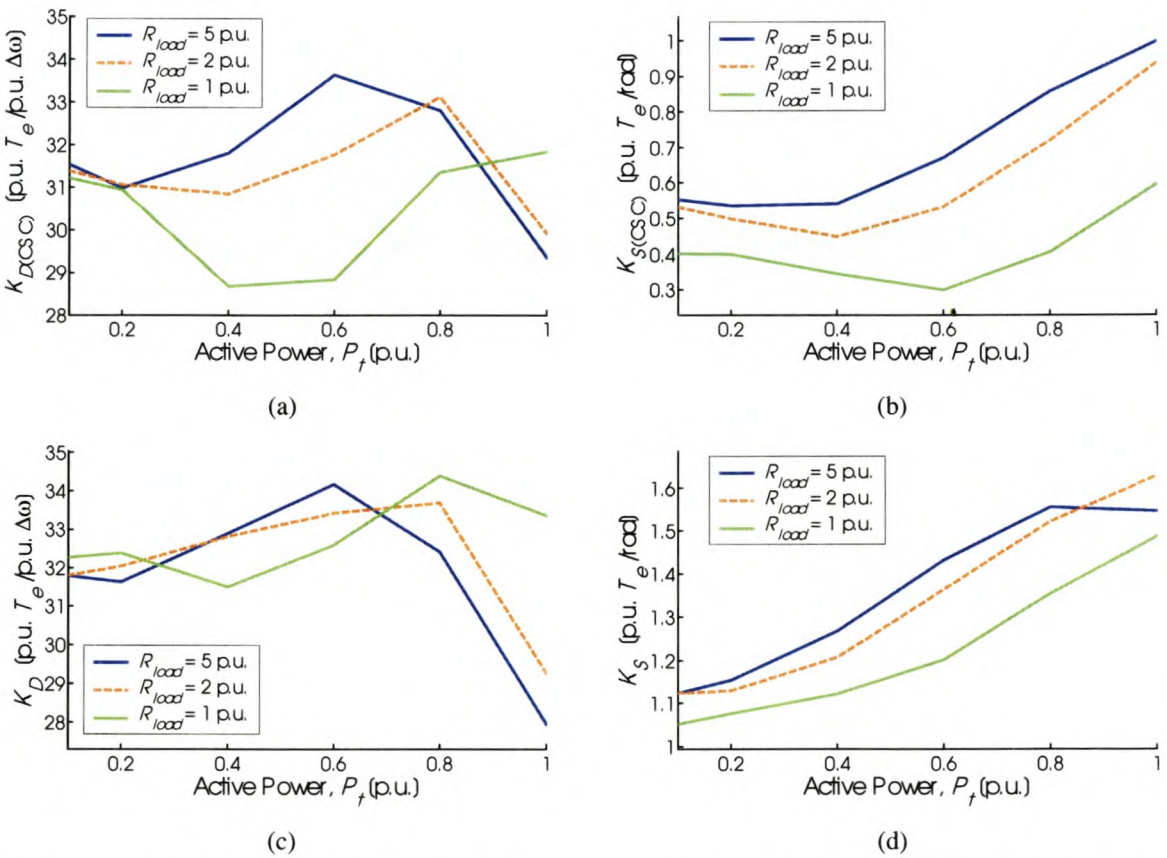

Fig. G.36: CSC and system torque coefficients vs. machine load and local load resistance, with X_{line} = 0.8 p.u. and K_A = 20

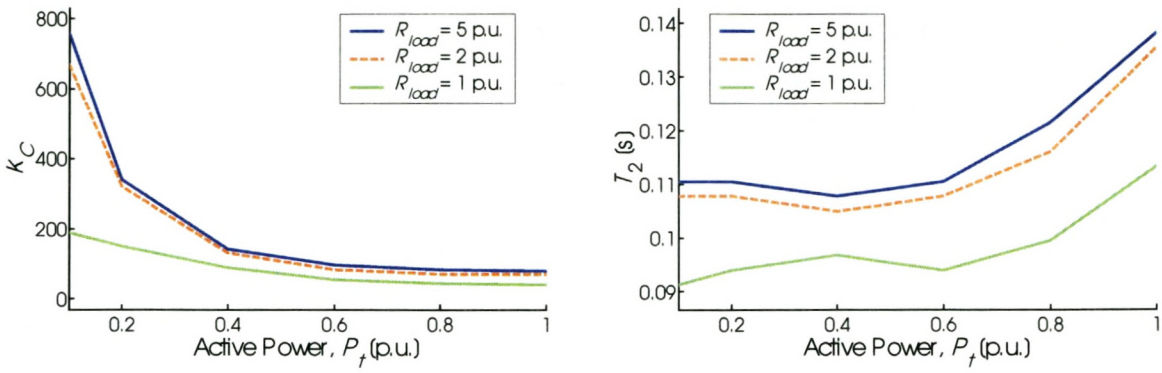

(a) (b)

Fig. G.37: CSC gain and time constant T_2 vs. machine load and local load resistance, with X_{line} = 0.8 p.u. and K_A = 20

G.8 Results of Section 5.8.6 – Influence of Saturation

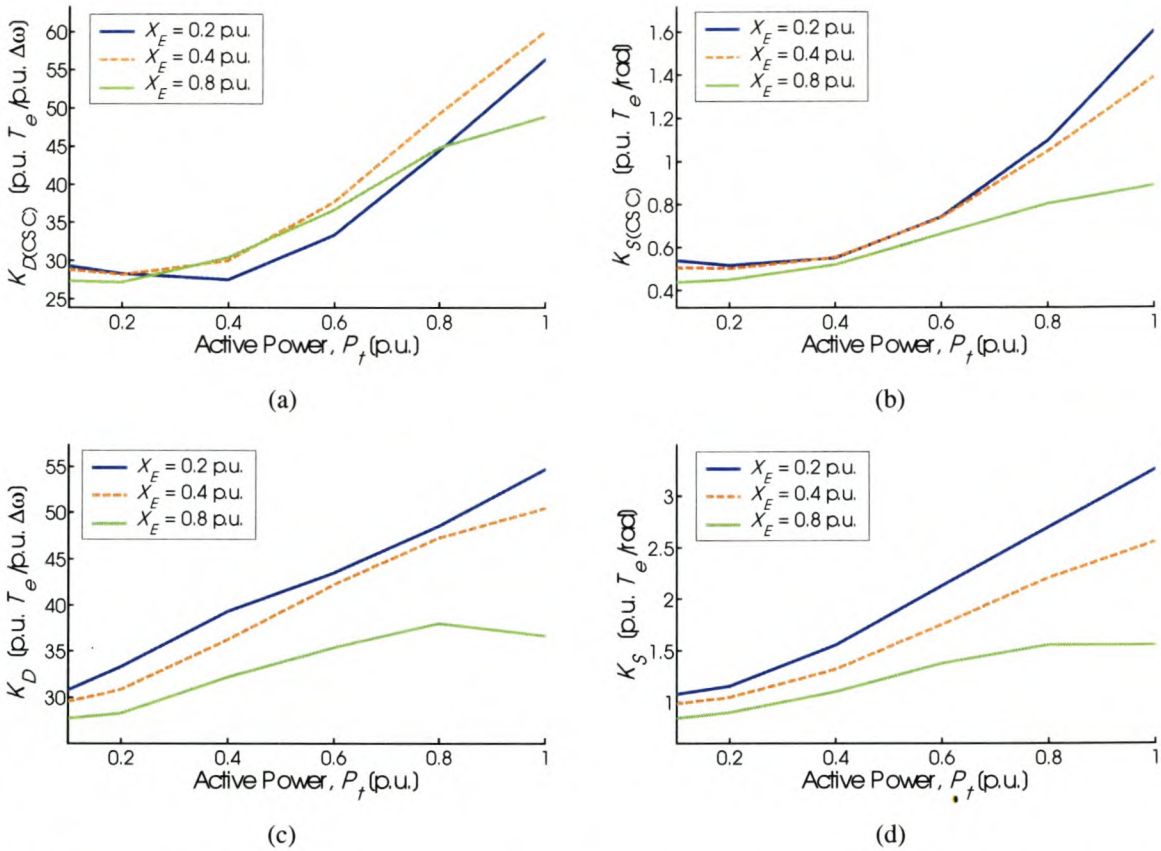

Fig. G.38: CSC and system torque coefficients vs. machine load and external reactance; saturation effect neglected

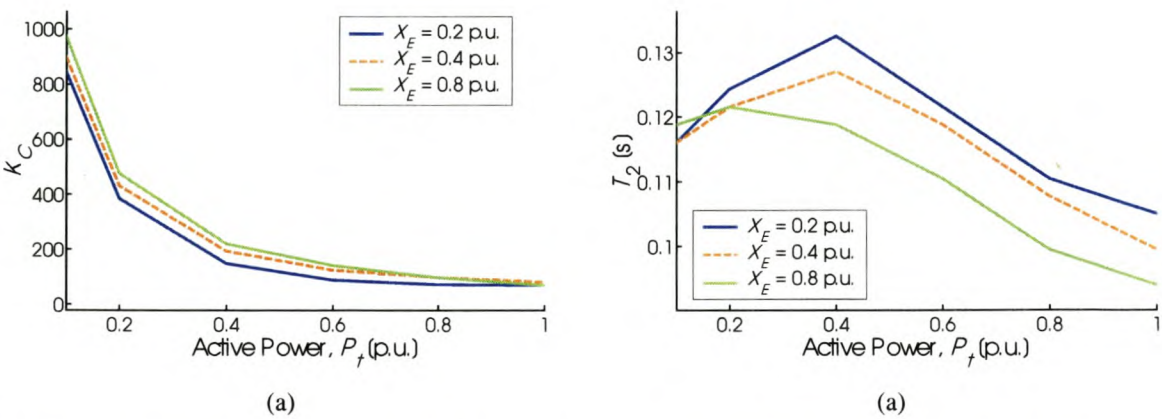

Fig G.39: Optimised CSC parameters K_C and T_2 vs. machine load and external reactance; saturation effect neglected